MEASURING AND VALIDATING NEUTRON CAPTURE CROSS SECTIONS USING A LEAD SLOWING-DOWN SPECTROMETER

By

Nicholas Thompson

A Dissertation Submitted to the Graduate

Faculty of Rensselaer Polytechnic Institute

in Partial Fulfillment of the

Requirements for the Degree of

DOCTOR OF PHILOSOPHY

Major Subject: NUCLEAR ENGINEERING AND SCIENCE

Approved by the
Examining Committee:

_____
Dr. Yaron Danon, Dissertation Adviser

_____
Dr. Li (Emily) Liu, Member

_____
Dr. Wei Ji, Member

_____
Dr. Rachel Slaybaugh, University of California, Berkeley, Member

Rensselaer Polytechnic Institute
Troy, New York

July 2017
(For Graduation August 2017)

© Copyright 2017
by
Nicholas Thompson
All Rights Reserved

CONTENTS

LIST OF TABLES vi

LIST OF FIGURES vii

ACKNOWLEDGMENT xii

ABSTRACT xiv

1. INTRODUCTION 1

1.1 Neutron Capture Interactions 2

1.2 Measuring Neutron Capture Cross Sections 6

1.3 The Gaerttner Linear Accelerator Center and Lead Slowing-Down Spectrometer 7

1.3.1 Reaction Rates 11

1.4 Motivation and Objectives 14

2. DETECTOR DEVELOPMENT 15

2.1 Simulations 15

2.1.1 Effects of Lead Libraries 18

2.2 Detector Selection 20

2.2.1 Detector Selection Measurements 22

2.3 Refining the Method 23

3. MEASUREMENTS & DATA ANALYSIS 25

3.1 Experimental Setup 25

3.1.1 Optimizing the Experimental Setup 27

3.2 Data Acquisition 28

3.3 Data Analysis 31

3.3.1 Comparison Between Data Acquisition Systems 33

3.3.2 Impacts of Changing the Discriminator Level 34

3.3.3 Generating Cross Sections 35

3.3.4 Pulse Shape Analysis and Pulse Height Weighting 37

4. RESULTS . . . 43
4.1 Validating Nuclear Data . . . 43
4.1.1 Tantalum Measurements . . . 44
4.1.2 Nickel Measurements . . . 46
4.1.3 Silver Measurements . . . 48
4.1.4 Gold Measurements . . . 52
4.1.5 Niobium Measurements . . . 54
4.1.6 Tin Measurements . . . 56
4.1.7 Zirconium Measurements . . . 57
4.1.8 Indium Measurements . . . 58
4.1.9 Iron Measurements . . . 62
4.1.10 Cobalt Measurements . . . 63
4.1.11 Molybdenum Measurements . . . 64
4.1.12 Carbon Measurements . . . 65
4.2 Coincidence Measurements . . . 66
4.3 Cross Section Results . . . 70
4.3.1 Minimum Cross Section . . . 70
4.3.2 Limitations . . . 73
4.4 Pulse Height Weighting Results . . . 74
5. CONCLUSIONS AND FUTURE WORK . . . 78
5.1 Conclusions . . . 78
5.2 Future Work . . . 79
REFERENCES . . . 81
APPENDICES . . . 87
A. Material Impurities . . . 87
A.1 LSDS Impurities . . . 87
A.2 Sample Materials . . . 87
A.2.1 Silver Sample . . . 87
A.2.2 Gold Sample . . . 88
A.2.3 Cobalt Sample . . . 88
A.2.4 Iron Sample . . . 89
A.2.5 Indium Sample . . . 90

A.2.6 Niobium Sample 91
A.2.7 Nickel Sample 91
A.2.8 Molybdenum Sample 91
A.2.9 Tin Sample 92
A.2.10 Tantalum Sample 92
A.2.11 Zirconium Sample 93
B. Event by Event Analysis Code 94
C. Example MCNP6 Simulation Input 108
D. Measurement Results Tables 121
E. Simulation Results Tables 148

LIST OF TABLES

4.1 Sample Information. 44

4.2 ^{107}Ag Resonance Parameters, 202.5 eV, T=300 K. 50

4.3 ^{107}Ag Resonance Parameters, 173.7 eV, T=300 K. 51

A.1 LSDS Impurities Table. 87

D.1 Measurement Results: Ta, Ag, Au. 121

D.2 Measurement Results: Nb, In, Mo. 127

D.3 Measurement Results: Sn, Zr. 134

D.4 Measurement Results: Fe, Co. 140

E.1 Simulation Results: Ta, Ag. 148

E.2 Simulation Results: Au, Nb. 152

E.3 Simulation Results: In, Mo. 156

E.4 Simulation Results: Sn, Zr. 160

E.5 Simulation Results: Fe, Co. 163

LIST OF FIGURES

1.1 ^{238}U Neutron Capture Cross Section (ENDF/B-VII.1), separating the thermal, resolved resonance, unresolved resonance, and fast region. . . . 4

1.2 ^{238}U Neutron Capture Cross Section (ENDF/B-VII.1) at the boundary between the resolved resonance region and the unresolved resonance region. 5

1.3 Photograph of the RPI LSDS showing some of the Measurement Ports and the Electron Beam Tube. 8

1.4 Neutron flux in the LSDS per eV (from Equation 1.3), compared to simulation. 9

1.5 Left: Neutron flux in the LSDS per μs, MCNP simulation. Right: Heatmap of the neutron flux in the LSDS, MCNP simulation. Note that at short and very long slowing down times, the energy distribution is widest. 10

1.6 Neutron energy resolution of the RPI LSDS, comparing the Fisher equation to an MCNP simulation. Note that the energy resolution is best between 10 eV and 1 keV. 11

1.7 Capture rate based on the broadened capture yield using ENDF/B-VII.1 data, compared to a 10 mil Ta measurement. 13

2.1 MCNPX Visual Editor image of the LSDS. On the left, the image is colored by material, with green representing the LSDS, and blue representing air. On the right, the image is colored by neutron/photon importance, where the areas of highest importance are red and lowest importance are blue. The view is cross sectional and the orientation is from the top (X-Y plane). The neutron source is in the center of the LSDS. For scale, the LSDS is a 1.8 meter cube. 16

2.2 Comparison between simulation results using an F4/FM capture rate tally, an F6 gamma energy deposition tally, and PoliMi. 18

2.3 Comparison between simulation results ENDF/B-VII.1, JEFF 3.2, and JENDL 4.0 nuclear data libraries for lead cross sections compared to measurement results for a 10 mil tantalum sample. 19

2.4 Comparison between simulation results ENDF/B-VII.1, JEFF 3.2, and JENDL 4.0 nuclear data libraries for lead cross sections compared to measurement results for a 10 mil tantalum sample, zoomed to highlight discrepancies. Left: Low energy region. Right: High energy region. . . . 19

2.5 Comparison between the simulated detector responses with and without a 4.9 gram silver sample made with a C_6D_6, LYSO, and a YAP detector. Note difference in signal to background ratio for the three detectors. MCNP simulation. 21

2.6 Comparison between the measurements of a 40 mil tantalum sample made with a C_6D_6 and a YAP detector. Measurements are background subtracted. Note the difference in resolution. 23

2.7 Left: Simulation and experimental data from a measurement with a tantalum sample plotted as a function of time. Right: The same results plotted as a function of average neutron energy. The detector experienced significant dead-time before 30 μs (above 200 eV) and the experimental count rate does not match the simulated results before this point. The sample was a 40 mil, 1.7 gram foil of tantalum, LINAC current was 0.5μA, detector radius was 0.75 inches, detector length was 1.5 cm, measurement time was 30 minutes. 24

3.1 MCNPX Visual Editor image of the experimental setup. The view is cross sectional and the orientation is from the top (X-Y plane). For scale, the scintillator is 2 mm thick with a 0.75 inch radius. 26

3.2 Diagram of the electronic setup for the measurement and data acquisition systems. Lines in black represent cables carrying signals, lines in red represent high voltage cables, and lines in blue represent the LINAC pre-trigger cables, which start the data acquisition on both systems. . . 29

3.3 Raw data from a measurement of a 10 mil tantalum sample, one 2mm YAP detector, one 600 second (ten minute) run. 30

3.4 Comparison between the measurement results between the analog and digital data acquisition systems. 33

3.5 Left: Comparison between MCNP-PoliMi generate spectra using different discriminator setpoints. Right: Same data, normalized to a simulated 150 keV discriminator setpoint. 34

3.6 Left: Comparison between measurement data using different discriminator setpoints. Right: Same data, normalized to the 125 keV discriminator setpoint used in the experiment. 35

3.7 Plot of the detector efficiency, based on MCNP simulations. 37

3.8 Plot of detector responses to various energy gammas, generated by MCNP. The large spread in energies is due to the Gaussian Energy Broadening card used with the F8 tally. 39

3.9 Plot of weighting function as a function of energy. Note that the Y axis is a log scale; large pulses are weighted much more than small pulses. . 40

3.10 Plot of Time-of-Flight/Energy matrix. 41

3.11 Plot of Time-of-Flight/Energy matrix after weighting. 42

4.1 Measurement and Simulation of a 10 mil tantalum sample, one 2mm YAP detector (Second round of measurements). 45

4.2 Left: Measurement of 10 mil tantalum sample, compared to MCNP simulations using ENDF/B-VII.1, JEFF 3.2, and JENDL 4.0 libraries. Right: Same data, zoomed in, with a linear y-axis. Note that above 330 eV, the ENDF/B-VII.1 result becomes linear, missing features present in the measurement, JEFF 3.2, and JENDL 4.0 results. 46

4.3 Left: Experimental results from a measurement with nickel and without a sample, as a function of time. Right: Simulations and experimental data from a measurement with a nickel sample plotted as a function of energy. One simulation simulated a pure natural nickel sample, the other simulated the nickel sample and all impurities. 47

4.4 Left: Measurement of a 0.6 mm silver sample, one 2mm YAP detector and MCNP simulations using ENDF/B-VII.1, JEFF 3.2, and JENDL 4.0 libraries. Right: Same data, zoomed in to better show discrepancies between 100 eV to 10 keV. 48

4.5 Neutron capture cross section from the ENDF/B-VII.1, JEFF 3.2, and JENDL 4.0 libraries for ^{107}Ag, 202.5 eV resonance. 49

4.6 Left: Neutron capture cross section from the ENDF/B-VII.1, JEFF 3.2, and JENDL 4.0 libraries for ^{107}Ag from 1 keV to 1.5 keV. Right: Neutron capture cross section from the ENDF/B-VII.1, JEFF 3.2, and JENDL 4.0 libraries for ^{109}Ag from 1.5 keV to 2 keV. 52

4.7 Left: Measurement of a 0.4 mm gold sample, one 2mm YAP detector and MCNP simulations using ENDF/B-VII.1, JEFF 3.2, and JENDL 4.0 libraries. Right: Same data, zoomed in to highlight discrepancies. . 53

4.8 Neutron capture cross section from the ENDF/B-VII.1, JEFF 3.2, and JENDL 4.0 libraries for ^{197}Au. 53

4.9 Left: Measurement of a 1.27 mm niobium sample, one 2mm YAP detector and MCNP simulations using ENDF/B-VII.1, JEFF 3.2, and JENDL 4.0 libraries. Right: Same data, zoomed in. Note: ENDF/B-VII.1 and JEFF 3.2 are identical. 54

4.10 Left: ENDF/B-VII.1 and JENDL 4.0 capture cross section libraries for ^{93}Nb. Right: ENDF/B-VII.1 and JENDL 4.0 capture and scattering neutron cross section libraries at the 378.47 eV resonance of ^{93}Nb. . . . 55

4.11 Left: Measurement of 1.0 mm tin sample compared to MCNP simulations using ENDF/B-VII.1, JEFF 3.2, and JENDL 4.0 libraries. Right: Zoomed in to highlight differences. 56

4.12 Left: Measurement of a 1.0 mm zirconium sample, one 2mm YAP detector compared to simulations using ENDF/B-VII.1, JEFF 3.2, and JENDL 4.0 libraries. Right: Zoomed in to highlight differences. 58

4.13 Measurement of a 0.6 mm indium sample, one 2mm YAP detector, compared to MCNP simulations using ENDF/B-VII.1, JEFF 3.2, and JENDL 4.0 libraries. 59

4.14 Measurement of 0.6 mm indium sample compared to MCNP simulations using ENDF/B-VII.1, JEFF 3.2, and JENDL 4.0 libraries. Left: Zoomed in to show differences in the eV region. Right: Zoomed in to show differences in the keV region. 60

4.15 Comparison between measurement of 0.6 mm indium sample and to MCNP simulations using 1 ppm of hydrogen and 2 ppm of hydrogen in the LSDS. Right: Zoomed in to show differences in the eV region. . . . 61

4.16 Left: Measurement of a 1.0 mm iron sample, one 2mm YAP detector compared to simulations using ENDF/B-VII.1, JEFF 3.2, and JENDL 4.0 libraries. Right: Same data, but more aggressively grouped to smooth out the low energy region. 62

4.17 Measurement of a 0.6 mm cobalt sample, one 2mm YAP detector, compared to MCNP simulations using ENDF/B-VII.1, JEFF 3.2, and JENDL 4.0 libraries. ENDF/B-VII.1 and JEFF 3.2 are nearly identical. 63

4.18 Measurement of a 1.0 mm molybdenum sample, one 2mm YAP detector, compared to MCNP simulations using ENDF/B-VII.1, JEFF 3.2, and JENDL 4.0 libraries. 64

4.19 Measurement of a 1.0 mm molybdenum sample, one 2mm YAP detector compared to simulations using ENDF/B-VII.1, JEFF 3.2, and JENDL 4.0 libraries. Left: Zoomed in on the eV region. Right: Same data, highlighting the keV region. 65

4.20 Measurement of 2.0 mm carbon sample compared to an MCNP simulation using ENDF/B-VII.1. Left: Log-Log plot showing the entire energy region. Note, the capture rate in carbon is so low that the sample and background measurements are nearly identical. Also note that in this figure, if there are no error bars below the data point, that means the error bar is a negative value and can could not be plotted. Right: The same plot, but with a linear Y-axis, to show that most of the data points are near zero. 66

4.21 Comparison between the signal to background ratio for coincidence measurements and single detector measurements (same data as Figure 4.22). 67

4.22 Measurement of a tantalum sample and background, comparing the single detector count rate and coincidence count rate. 68

4.23 Measurement of a tantalum sample and background, comparing the single detector count rate and coincidence count rate. 69

4.24 The minimum cross section from 4.1 compared to broadened ENDF/B-VII.1 cross sections of zirconium (Zr), tin, (Sn), niobium (Nb), nickel (Ni), and iron (Fe). 71

4.25 Broadened capture cross section of tin calculated from measurement of 1.0 mm tin sample compared to ENDF/B-VII.1 natural broadened capture cross section. 72

4.26 Top: Natural silver broadened capture cross section generated from measurement results compared to ENDF/B-VII.1 broadened cross section. Bottom: Plot of transmission through the sample. Note that the first resonance is a "black" resonance, meaning the transmission effectively falls to zero as nearly all neutrons are interacting with the sample. 74

4.27 Measured capture rate, comparing analysis using pulse height weighting to not using pulse height weighting, and comparing against simulated ENDF/B-VII.1 cross section library. 75

4.28 Measured capture rate, Simulations, and the expected percentage of pileup. 76

4.29 Left: 40 pulses from 97.4-99.4 μs, roughly 17 eV. Right: 40 pulses from 1.15-1.40 μs, roughly 60 keV. Note the double pulses in the graph on the right. 76

E.1 Photograph of N. Thompson and A. Weltz setting up a measurement with the RPI LSDS. 168

ACKNOWLEDGMENT

I'd first like to thank Dr. Danon for his tireless support and help keeping me on track. I'd also like to thank the rest of my Committee for their help in this process.

This couldn't have been finished without the help of so many people, but a special thanks goes out to Amanda Youmans, Ezekiel Blain, Adam Daskalakis (Blue on Blue Command Whale), Adam Weltz, Brian McDermott Jesse Brown, Kumar Mohindroo, and Matt Riblett for always being there to talk through an issue or just have a conversation. Amanda Lewis and John Thai also helped enormously by working with me as undergraduate researchers, hopefully they were able to learn something along the way. I'd also like to thank Jason Thompson, Rian Bahran, Dillon Shaver, Spencer Scott, Brian Waite, and Bjorn Becker for their friendship and mentorship during my time at RPI.

The LINAC Staff, past and present also deserve much praise; Matt Gray, Azeddine Kerdoun, Peter Brand, Martin Strock, and Larry Krusieski. Without them, none of the measurements at the LINAC would be possible.

I'd also like to thank the past and present staff and trainees at the Walthousen Reactor Critical Facility, where I learned a great deal and had a lot of fun spending my Wednesday nights with: Glenn Winters, Tim Trumbull, Jason Thompson (again), Peter Caracappa, Sastry Sreepada, Ezekiel Blain (again), Jessica Berry, Emily Frantz, Becca Gazda, Brian McDermott (again), Walter Pfuntner, Chris Morrison, Jaron Senecal, Alexander Roaldsand, Deborah Lark, Marcus Barbet, Peter Kowal, and Kelly Rowland. Additionally, I'd like to thank all the students who took the Critical Reactor Laboratory while I was a Senior Reactor Operator, getting the opportunity to teach was one of the things that made that facility so special to me.

Marie Dieffenbach deserves an entire page of gratitude.

Everyone who was involved in all of the various clubs and activities outside of my PhD also deserve credit for helping me to learn and grow; some of those activities and people who need special thanks are:

- the American Nuclear Society (Selena Willoughby, Matt Riblett, Lane Carasik,

Sam Brinton, Harsh Desai, Brett Rampal, Kalin Keisling, Margaret Harding, Gene Grecheck, Art Wharton, Alexis Kaplan, Katherine Shield, Alyse Scurlock, Catherine Perego, Tim Crook, Matt Jasica, Matt Wargon, Diego Garcia, Sarah Sarnoski, Kelsey Amundson),

- the Nuclear Engineering Student Delegation (Mark Norsworthy, Matt Gidden, Mark Reed, Sam Brinton, Lane Carasik, Ben Reinke, Samantha Winkle, Dan Curtis, Justin Knowles, Remy DeVoe, Taylor Lane, Jeremy Pearson, Miriam Rathbun),

- the Rensselaer Union (Robyn Marquis, Kristen Lee, Michael Caiola, Jen Church, Erin Amarello, Nick Dvorak, Chaz Goodwine, Martha McElligott, Cameron McLean, Joe Cassidy, Holly Nelson, Shannon Gillespie McComb, Rasika Ekhalikar, Chip Kirchner, Greg Bartell, Jeremy Feldman, Donna Grace Moleta, Conrad Mossl, Nicholas Schlatz, Erica Lane, Matt Rand, Ines Roman, Kirk Bittner, Chris Hoskins, Harrison Kang, Alexandria Pizzola),

- and Rensselaer Student Life (Colleen Smith, Frank Ross).

Thanks also to my friends old and new for their help, especially Kevin Houghtaling, Matt Zimmermann, Sarah Ritter, Erin DeThorne, Justin Nelson, Selena Willoughby, Laura Goulet, Lindsay Obrien, Michael Hughes, Brian Werneke, Andrew Pavlou, Cecily Wilbank, Dan Pollock, Kris Zieb, Tommy Bongiorno, Michelle Smithers, Britnne Eskew, Bryan Eskew, Drew Peiffer, John Hayes, Kate Prussing, Lauren Cooper, Alex Angilella, and Sarah Diehl.

Thank you to Kelly Jenkins, my wonderful girlfriend for her love and support.

And lastly, a huge thanks to my family; my mother Katherine Thompson, my father Bill Thompson, and my brother Peter Thompson for continuing to push me to be my best self.

Sincelery,

Klaus

ABSTRACT

Accurate nuclear data is essential for the modeling, design, and operation of nuclear systems. In this work, the Rensselaer Polytechnic Institute (RPI) Lead Slowing-Down Spectrometer (LSDS) at the Gaerttner Linear Accelerator Center (LINAC) was used to measure neutron capture cross sections and validate capture cross sections in cross section libraries. The RPI LINAC was used to create a fast burst of neutrons in the center of the LSDS, a large cube of high purity lead. A sample and YAP:Ce scintillator were placed in the LSDS, and as neutrons lost energy through scattering interactions with the lead, the scintillator detected capture gammas resulting from neutron capture events in the sample. Samples of silver, gold, cobalt, iron, indium, molybdenum, niobium, nickel, tin, tantalum, and zirconium were measured.

Data was collected as a function of time after neutron pulse, or slowing-down time, which is correlated to average neutron energy. An analog and a digital data acquisition system collected data simultaneously, allowing for collection of pulse shape information as well as timing. Collection of digital data allowed for pulse shape analysis after the experiment. This data was then analyzed and compared to Monte Carlo simulations to validate the accuracy of neutron capture cross section libraries. These measurements represent the first time that neutron capture cross sections have been measured using an LSDS in the United States, and the first time tools such as coincidence measurements and pulse height weighting have been applied to measurements of neutron capture cross sections using an LSDS. Significant differences between measurement results and simulation results were found in multiple materials, and some errors in nuclear data libraries have already been identified due to these measurements.

CHAPTER 1
INTRODUCTION

Nuclear data is required for simulations and design of nuclear reactors and other nuclear applications. The accuracy of this data is crucial, and is increasingly becoming a limiting factor on the accuracy of nuclear simulations. In nearly every nuclear application, the neutron capture cross sections, which can be thought of as the probabilities of a neutron to be captured, are some of the most important values, and can have a large impact on those systems. For example, the distribution of neutrons in a nuclear reactor (or other nuclear application) can be modeled using the neutron transport equation, shown here as Equation 1.1 [2]:

$$\left(\frac{1}{\mathbf{v}(E)}\frac{\delta}{\delta t} + \hat{\mathbf{\Omega}}\cdot\nabla + \Sigma_t(\mathbf{r},E)\right)\psi(\mathbf{r},E,\hat{\mathbf{\Omega}},t) = \int_{4\pi} d\hat{\mathbf{\Omega}}' \int_0^\infty dE'\Sigma_s(\mathbf{r},E'\rightarrow E,\hat{\mathbf{\Omega}}'\rightarrow\hat{\mathbf{\Omega}})\psi(\mathbf{r},E',\hat{\mathbf{\Omega}}',t) + \frac{\chi(E)}{4\pi}\int_{4\pi} d\hat{\mathbf{\Omega}}' \int_0^\infty dE' v(E')\Sigma_f(E')\phi(\mathbf{r},E',\hat{\mathbf{\Omega}})',t) + s(\mathbf{r},E,\hat{\mathbf{\Omega}},t) \quad (1.1)$$

where the Σ_t term is the total cross section of a material, which is made up of the scattering cross section Σ_s, the fission cross section Σ_f, and the capture cross section Σ_γ. The accuracy of simulations of nuclear systems can be directly linked to the quality of the nuclear data, and in particular, the capture cross sections as neutron capture interactions remove neutrons from the system[3],[4].

Additionally, when an atom captures a neutron, it becomes a different isotope of the same element, and its nuclear properties will change (including neutron cross sections and stability). Some isotopes are very radioactive, and some isotopes have large neutron capture cross sections, so accurate capture cross section data is also

---

Portions of this chapter previously appeared as: N.W. Thompson et al. "Progress On Using a Lead Slowing-Down Spectrometer to Measure Neutron Capture Cross Section," in *12th Int. Topical Meeting on Nucl. Applicat. of Accelerators*, Washington D.C., 2015, pp. 351-354[1].

Portions of this chapter are to appear in: N.W. Thompson et al. "Measurements and Analysis of Neutron Capture Cross Sections Using A Lead Slowing-Down Spectrometer," *Nucl. Sci. Eng.*, to be published.

necessary for computing the production of these isotopes and the impacts of those isotopes on the system.

As experiments and demonstration projects have become more expensive and computational tools become cheaper, faster, and more precise, designers of nuclear systems are increasingly relying on simulations[5],[6], making the nuclear data used in those simulations ever more important. Additionally, the increased use of simulations allows for a much shorter design cycle[7]. The list of nuclear applications which require this data is large, and includes nuclear reactors for energy production, medical isotope production facilities, development of nuclear detection systems for national security applications, fusion energy systems, and other national defense applications[8]-[10].

Lastly, specifically for nuclear reactors, neutron capture cross section data is vital for the safety of nuclear systems. Nuclear reactors operate by balancing the creation of neutrons from fission and other sources with the loss of neutrons from leakage and absorption. Capture is a form of absorption, fission is the other primary form of absorption in nuclear reactors, although other interactions such as (n,p), (n,α) and (n,2n) do also occur. In the case of an emergency, the nuclear fission process must be stopped immediately, and so control rods made of neutron absorbing materials (such as boron, silver, indium, and cadmium[11]) are inserted into the core very quickly. In the case of control rods, accurate neutron capture cross sections are crucial for modeling nuclear reactor dynamics as a reactor is being shut down.

Throughout this document, three major nuclear data libraries will be referred to; the US library ENDF/B-VII.1[12], the OECD/NEA (European) library JEFF-3.2[13], and the Japanese library JENDL 4.0[14]. There are other nuclear data libraries from around the world, but this work will mainly focus on these three libraries.

1.1 Neutron Capture Interactions

Neutron capture, also known as radiative capture, is the process whereby a neutron interacts with a nucleus and is physically absorbed by that nucleus, forming

a compound nucleus, which then de-excites by emission of gamma rays (capture gamma rays). The formation of the compound nucleus is similar for all absorption interactions, the difference is how the compound nucleus de-excites; it can emit particles (neutron, proton, alpha etc.), gamma rays (capture), or it can be split apart (as is the case in fission)[15].

Neutron capture cross sections, like most nuclear cross sections, can be highly dependent on neutron energy, and can change drastically over small changes in neutron energy. At low neutron energies (up to 1 eV), neutron cross sections are generally smooth and the cross sections are generally proportional to 1/v; this region is known as the thermal energy region. At high neutron energies (above 0.5 MeV), cross sections also tend to be smooth; this region is known has the fast region. However, between those two ranges, the capture cross sections for most materials used in nuclear systems tends to vary wildly; this region is known as the resonance region. An example of this can be seen in Figure 1.1, which shows the capture cross section for ^{238}U as a function of incident neutron energy.

These spikes in the capture cross section are known as resonances. Resonances occur when an incident neutron has the same amount of energy as a discrete energy level of the compound nucleus which would be formed by the absorption of that neutron [16],[2]. Each of these resonances has a "width" related to the mean lifetime (stability) of that discrete level [17]. As is shown in Figure 1.1, at lower energies, these resonances are widely spaced and easily distinguishable. But at higher incident neutron energies, these resonances seem to appear closer and closer together until they overlap and can no longer be distinguished from one another. In more technical terms, as the incident neutron energy increases, the widths of the levels increases and the spacing between levels stays the same; once the widths are wide enough, the resonances begin to overlap.

As shown in Figure 1.1, between 1 eV and 20 keV, resonances can be distinguished from one another; this is known as the resolved resonance region. This gets more and more difficult at higher energies; above 20 keV, resonances in ^{238}U for radiative capture begin to overlap and only the average cross section can be measured. This denotes the beginning of the unresolved resonance region. There is often some

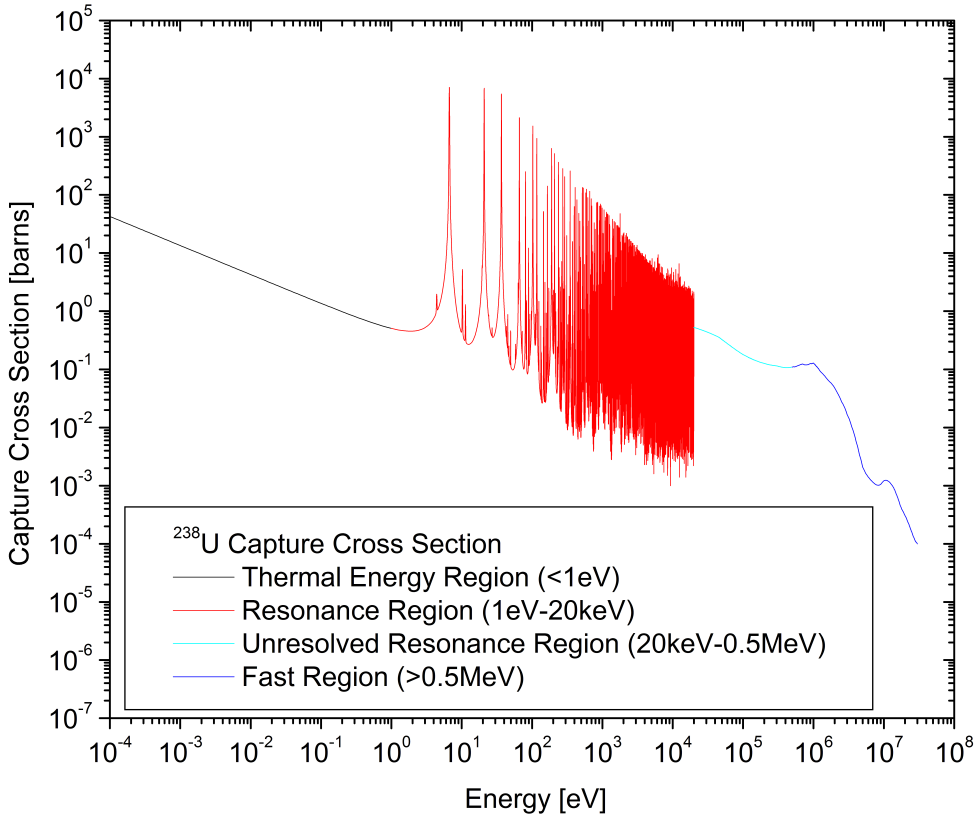

Figure 1.1: ^{238}U Neutron Capture Cross Section (ENDF/B-VII.1), separating the thermal, resolved resonance, unresolved resonance, and fast region.

debate in the nuclear data community about where to start the unresolved resonance region for certain isotopes (as opposed to explicitly resolving each resonance). This can be seen in Figure 1.2, which shows the boundary of the resolved resonance region and unresolved resonance region: to the naked eye, there is no clear boundary on where the cutoff should be, but certain statistical tools (eg. level density stair plots and $\Delta 3(L)$ statistic) can be used to determine where the resolved resonance region should end.

In neutron capture interactions, the compound nucleus deexcites to a more stable state (decays) by emission of a gamma ray cascade. The total energy of the gamma cascade (called the decay energy) is the binding energy of the compound

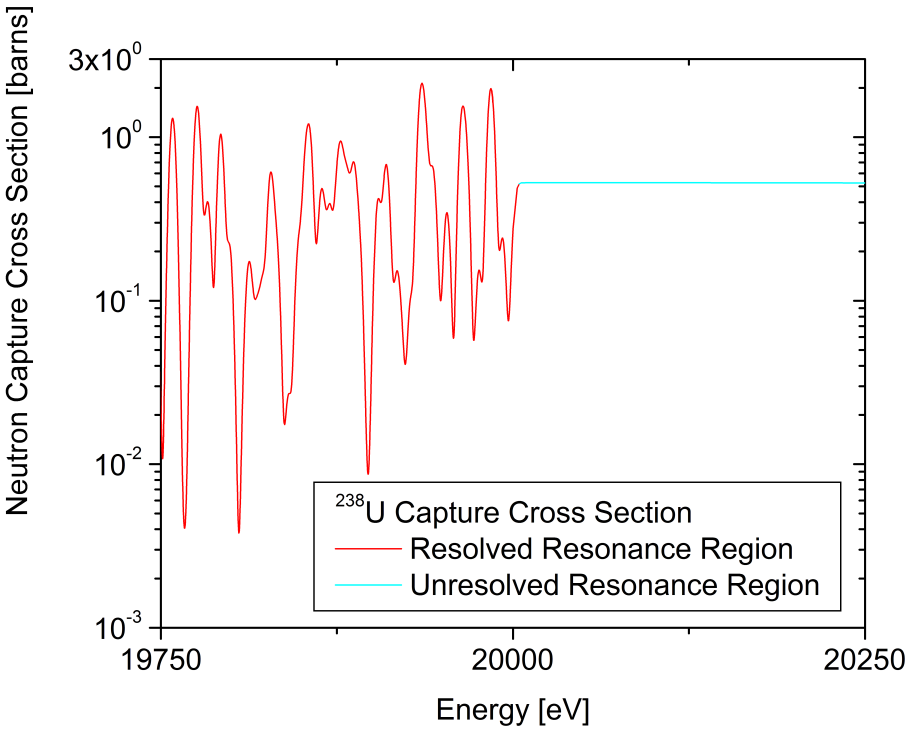

Figure 1.2: ^{238}U Neutron Capture Cross Section (ENDF/B-VII.1) at the boundary between the resolved resonance region and the unresolved resonance region.

nucleus plus the kinetic energy of the incident neutron. The gamma energy distribution of the gamma cascade is dependent on the decay energy of the compound nucleus. The multiplicity of the gammas from a cascade can vary from one to five or more gammas (it may sound obvious, but the average energy of the capture gammas increases as the multiplicity decreases). These distributions can be simulated using codes such as DICEBOX [18]. Gammas emitted in the gamma cascade can be emitted from discrete energy levels to lower discrete energy levels (in which case the gamma will have that discrete energy) or from the continuum, where a range of gamma energies is possible.

A few important notes; for a single isotope, the binding energy will remain constant - but the total excitation energy is also dependent on the kinetic energy of the incident neutron, so when the energy of the incident neutron is high, the total decay energy will be higher, resulting in a different gamma cascade. For low

neutron energies (eg. below 50 keV), this effect can largely be ignored as the total binding energy is on the order of MeV. However, even if the total excitation energy is near constant below 50 keV incident neutron energy, the gamma cascade can vary - resonances that have different spins can have different gamma cascades and multiplicities. If the gamma cascade and/or multiplicity changes, this can result in a different efficiency to detect a capture event. More about this will be explained in Sections 3.3.4 and 4.4.

1.2 Measuring Neutron Capture Cross Sections

While certain modeling codes can predict average cross sections, there is no model that can accurately predict cross sections a priori in the resonance region[19], so experiments are needed to measure these cross sections. There are a number of different ways to measure capture cross sections, but one of the primary methods to make direct measurements of capture cross sections as a function of incident neutron energy is to detect the capture gammas emitted from those capture events.

There are two methods for detecting capture gammas for measuring neutrons capture cross sections, the first being to use a calorimeter (array of gamma detectors completely surrounding the sample) to collect the full energy of all the capture gammas emitted from a capture event. Some examples of systems like this are the DANCE array at LANSCE (LANL) [20], the Total Absorption Calorimeter at n_TOF (CERN) [21] and the RPI Multiplicity Detector at RPI [22]. These systems generally work well for low energy neutrons, but can suffer from false capture at higher energies, where neutrons are scattered off of the sample and are captured in the detector, or scattered off of the sample and back to the sample, resulting in higher detected capture rates, and an overestimation of the capture cross section [23].

The second method is called "Total Energy Detection," in which a gamma detector (or array of gamma detectors) with low efficiency is used. This gamma detector will therefore only detect one gamma ray from a gamma cascade; if the detector efficiency is directly proportional to the energy of the incident gamma, then the efficiency to detect a capture event will be proportional to the sum of the

energies of the incident gammas [24]. Typically, detector efficiency is not directly proportional to the energy of the incident gamma, but the Pulse Height Weighting technique can be used to artificially change the efficiency by "weighting" gammas based on their energy such that the weighted efficiency is proportional to the energy of the gammas. In this method, the experimental setup should be such that only one gamma from a capture event is detected.

Lead Slowing-Down Spectrometers have also been used to measure neutron capture cross sections [25]-[29]. However, in all implementations to date, no measurements of capture cross sections have been made with a Lead Slowing-Down Spectrometer using Pulse Height Weighting to correct for the efficiency to measure gammas. Additionally, based on a thorough review of the literature, this project is the first time measurements of capture cross sections using a Lead Slowing-Down Spectrometer have been made in the US.

1.3 The Gaerttner Linear Accelerator Center and Lead Slowing-Down Spectrometer

The Gaerttner Linear Accelerator Center (LINAC) at Rensselaer Polytechnic Institute (RPI) was specifically designed to measure nuclear data and fine nuclear structure [30]. The LINAC is a 60 MeV electron linear accelerator which is used to create a short pulse of neutrons through (e, γ) and (γ, n) reactions with a tantalum target. In most measurements at the LINAC, detectors are positioned at flight stations, ranging from 15 to 250 meters away from the neutron producing target, and the time-of-flight method is used to determine neutron energy. The LINAC has been used to measure neutron capture, scattering, fission, and total cross sections, as well as prompt fission neutron spectra, fission fragment distributions, and other nuclear data.

At the Gaerttner LINAC Center is also a Lead Slowing-Down Spectrometer (LSDS), a large cube (1.8 m) of high purity lead with a neutron producing target in the center; Figure 1.3 is a photograph of the RPI LSDS. Neutrons lose energy (are slowed down) through successive collisions with the lead nuclei. Due to the low average lethargy gain in each collision, it takes many collisions, and therefore

a relatively large amount of time for the neutrons to thermalize (2 ms). Over that time, neutrons in the lead will have an average neutron energy which is related to time by Equation 1.2 [31]:

$$E = \frac{k}{(t - t_0)^2} \tag{1.2}$$

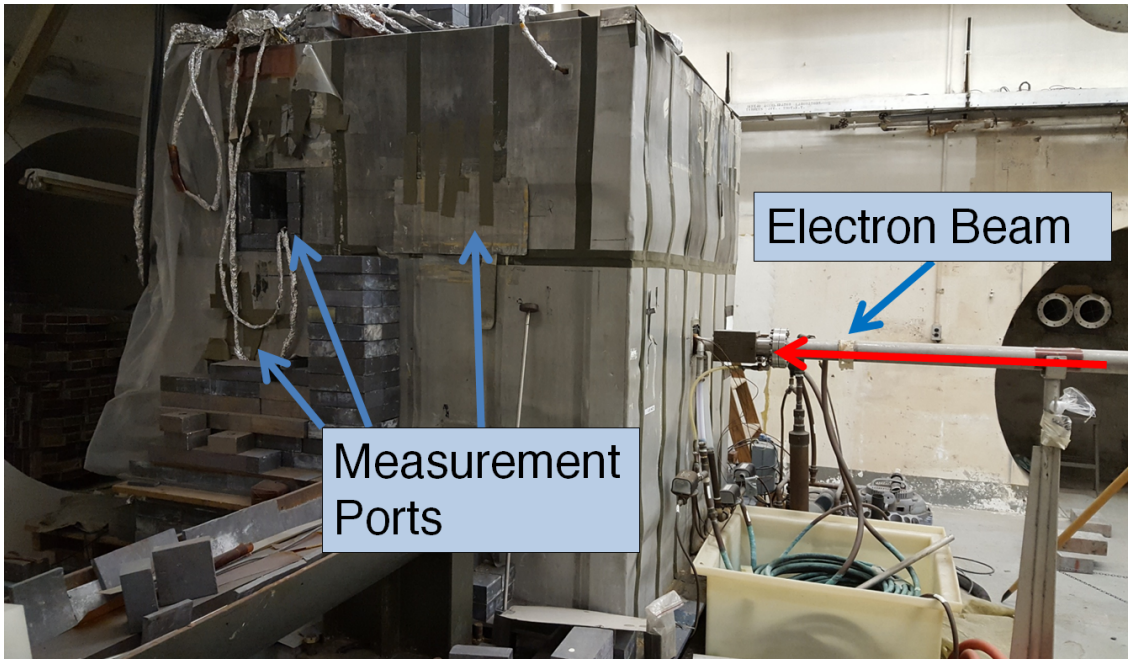

Figure 1.3: Photograph of the RPI LSDS showing some of the Measurement Ports and the Electron Beam Tube.

where E is average neutron energy in eV, t is the slowing down time, k = 165,000 eV*μs^2, and t_0 = 0.3 μs. The relative energy-dependent neutron flux was modeled by Fisher [32] as Equation 1.3:

$$\phi(E) = E^{-0.776} exp\left[- \left(\frac{0.214}{E} \right)^{1/2} \right] \tag{1.3}$$

where ϕ(E) is the neutron flux per eV. Figure 1.4 shows how the time-energy neutron correlation from Fisher closely matches simulations (at least up until 100 keV). After the initial neutron pulse, the neutron population in the LSDS decreases as neutrons are captured or escape; this can be seen in the left plot of Figure 1.5 showing the neutron flux as a function of time. A cadmium sheet surrounds the LSDS to prevent

neutrons from re-entering the system (known as "room return") as this would be deleterious to the neutron energy resolution. For a more visual representation of the energy distribution of the LSDS neutron flux over time, the right plot of Figure 1.5 is a heatmap of the neutron flux, per μs.

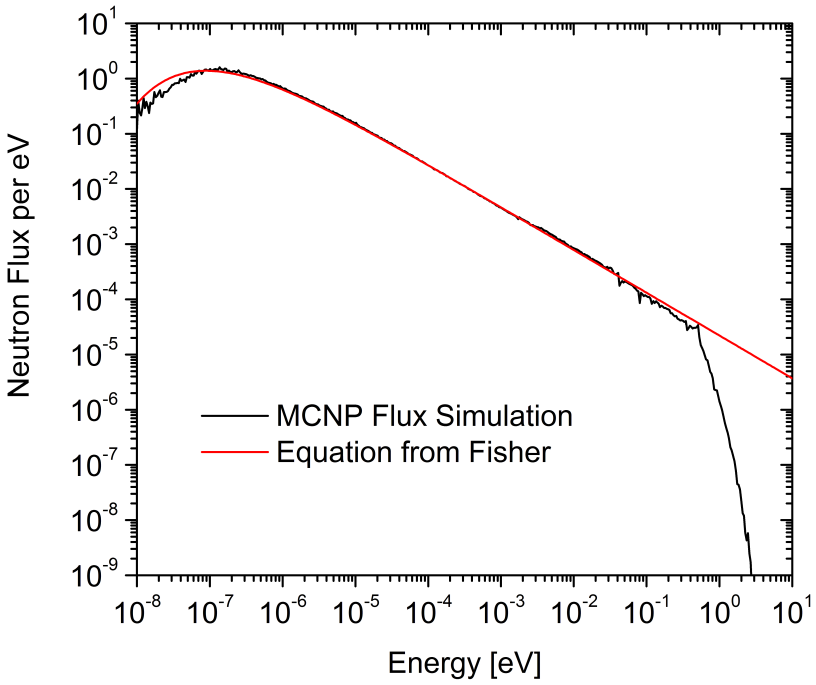

Figure 1.4: Neutron flux in the LSDS per eV (from Equation 1.3), compared to simulation.

The neutron energy resolution of the LSDS is approximately 30% between 1 keV and 10 eV and can be approximated by Equation 1.4 [33]:

$$\left(\frac{\Delta E}{E}\right)_{FWHM} = \sqrt{0.0835 + \frac{0.128}{E} + 3.05 * 10^{-5} E} \tag{1.4}$$

where $(\Delta E/E)_{FWHM}$ is the full width half maximum energy resolution, and E is the average neutron energy in eV. Figure 1.6 shows the neutron energy resolution of the LSDS. It should be noted that this level of resolution is quite poor compared to time-of-flight methods, and so individual resonances can not be resolved with great detail. However, the advantage of the LSDS is the up to 1000 fold increase in neutron flux, allowing for faster measurements and measurements of smaller samples

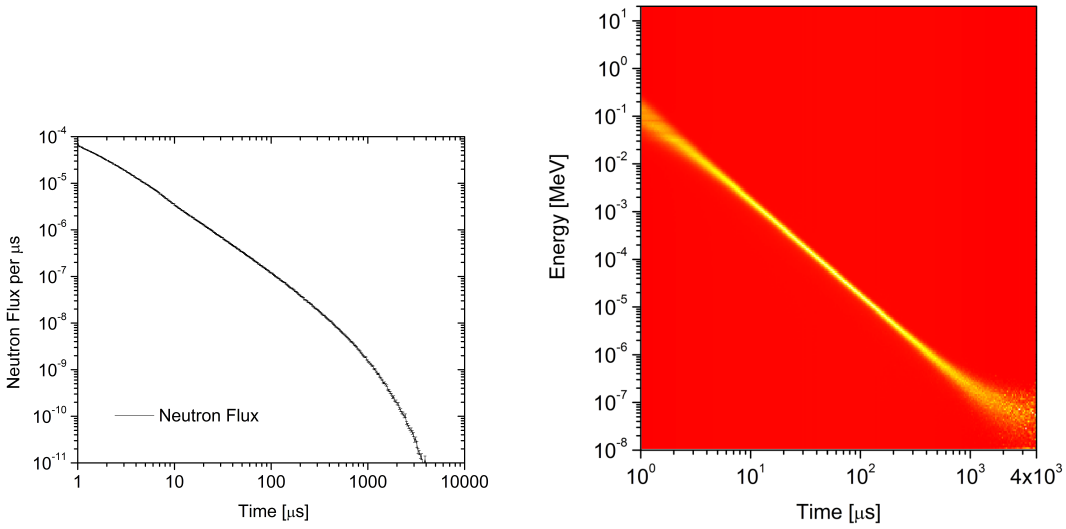

Figure 1.5: Left: Neutron flux in the LSDS per μs, MCNP simulation. Right: Heatmap of the neutron flux in the LSDS, MCNP simulation. Note that at short and very long slowing down times, the energy distribution is widest.

or samples with small cross sections. More detail about the RPI LSDS can be found in Dr. Jason Thompson's thesis [34].

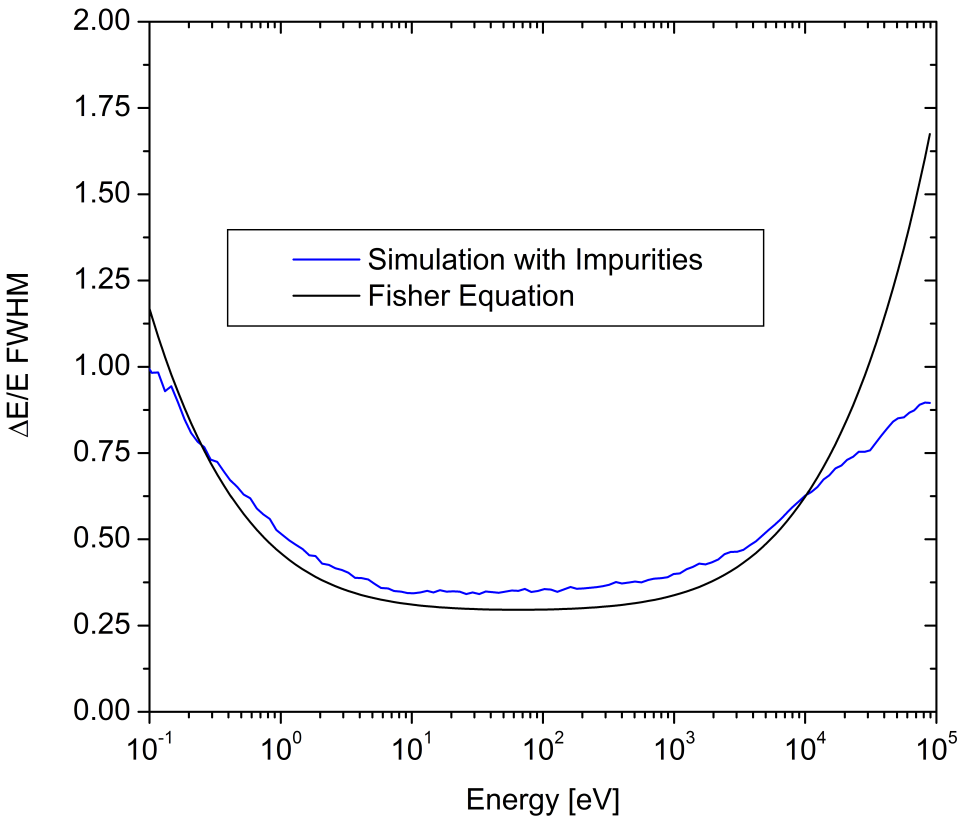

Figure 1.6: Neutron energy resolution of the RPI LSDS, comparing the Fisher equation to an MCNP simulation. Note that the energy resolution is best between 10 eV and 1 keV.

1.3.1 Reaction Rates

In a normal beam Time-of-Flight measurement, the reaction rate could be computed with Equation 1.5:

$$C(E) = \phi(E)\left(1 - e^{-Nx\sigma_t(E)}\right)\frac{\sigma_\gamma(E)}{\sigma_t(E)}\eta_C(E) + Y_{ms}(E)\eta_C(E) \tag{1.5}$$

where C(E) is the reaction rate as a function of energy, σ_γ(E) is the capture cross section as a function of energy, σ_t(E) is the total cross section as a function of energy, ϕ(E) is the flux as a function of energy, N is the number density, x is the thickness of the sample, η_C(E) is the efficiency to detect a capture event as a function of energy,

and Y_{ms}(E) is the correction for multiple scattering as a function of energy. For a very thin sample (where Nxσ_t << 1), a few approximations can be made. The multiple scattering term, Y_{ms}, can be approximated as zero, and the exponential term can also be approximated, as shown in Equation 1.6:

$$\big(1 - Nx\sigma_t(E)\big) \approx e^{-Nx\sigma_t(E)}. \tag{1.6}$$

However, in the case of the LSDS, the cross section is broadened with the LSDS resolution function (shown in Figure 1.6), as is shown in Equation 1.7:

$$BC(E) = \int_0^\infty C(E^{'})R(E, E^{'})dE^{'} \tag{1.7}$$

where BC(E) is the broadened reaction rate and R(E,E$^{'}$) is the LSDS resolution function. After substituting in Equation 1.5, the full reaction rate equation becomes Equation 1.8:

$$BC(E) = Nx\phi(E)\eta_C \int_0^\infty \sigma_\gamma(E^{'})R(E, E^{'})dE^{'}. \tag{1.8}$$

As stated earlier, Equation 1.8 only works if the sample is very thin. If the sample is not very thin, then this thin sample approximation will not be applicable. In this case, the capture yield must be calculated, using Equation 1.9:

$$Y(E) = \phi(E)\Big(1 - e^{-Nx\sigma_t(E)}\Big)\frac{\sigma_\gamma(E)}{\sigma_t(E)} \tag{1.9}$$

where Y(E) is the capture yield. The capture yield can then be broadened with Equation 1.10:

$$BC_Y(E) = Nx\phi(E)\eta_C \int_0^\infty Y(E^{'})R(E, E^{'})dE^{'} \tag{1.10}$$

where BC_Y(E) is the broadened reaction rate based on the capture yield. In calculating the broadened reaction rate, Equation 1.10 was calculated by using Equation 1.11:

$$BC_{Y,i} = Nx\phi(E_i)\eta_C \int_{E_i-3std(E_i)}^{E_i+3std(E_i)} Y(E^{'})G(E^{'}, E_i, std(E_i))dE^{'} \tag{1.11}$$

where $BC_{Y,i}$ is the broadened reaction rate at energy E_i based on the capture yield, std(E_i) is the standard deviation of the Gaussian function used to model the resolution faction (see Equation 1.6), and G($E^{'}$,E_i,std(E_i)) is the value of the Gaussian function with a standard deviation of std(E_i) and a mean of E_i, evaluated at energy $E^{'}$.

Figure 1.7 shows an example of the results of this calculation and how it compares to measurement data. The calculated rate and the measured rate agree quite well, even though this calculation is not taking into account any interactions with the detector or surrounding materials. This is a good indicator that the measurement is actually measuring the capture rate in the sample.

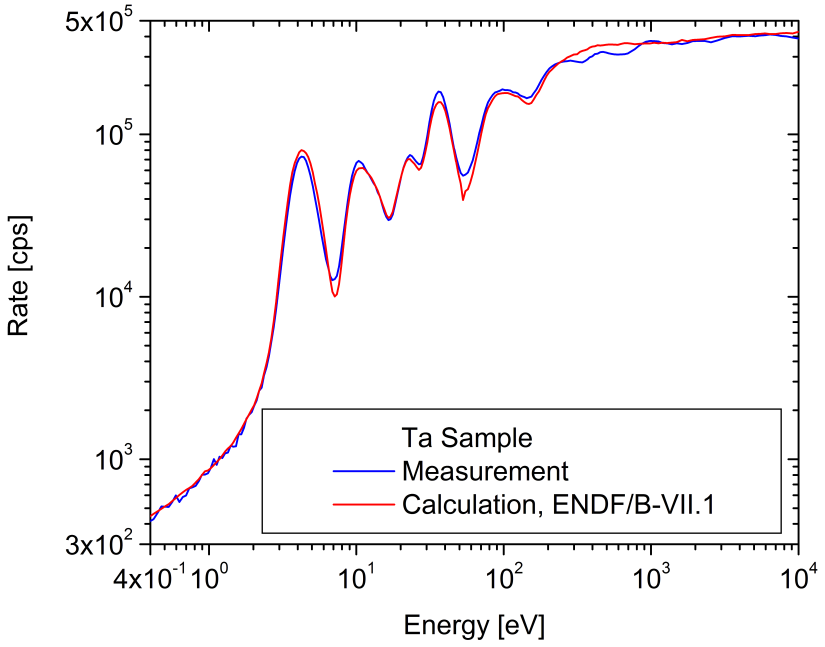

Figure 1.7: Capture rate based on the broadened capture yield using ENDF/B-VII.1 data, compared to a 10 mil Ta measurement.

1.4 Motivation and Objectives

As discussed earlier, accurate nuclear data, and neutron capture cross sections in particular, are required for modeling, designing, and analyzing nuclear systems where neutrons are used. Any improvements that can be made to nuclear data help to make our understanding of those nuclear systems more complete. Perrot et. al.[29] previously found that using an LSDS to benchmark nuclear data libraries was a useful way to find inaccuracies and deficiencies in the nuclear data, and based on the results of those measurements, Perrot et. al. were able to make determinations of which elements and isotopes needed to be studied more carefully.

There are two goals of this work; the first is to develop a measurement system and measure neutron capture cross sections with the RPI LSDS. Measurements of capture cross sections using a LSDS have been performed before, but not at RPI. Setting up such a system requires designing the experiment, designing and assembling detectors, creating a data acquisition system, creating all of the codes for processing that data, testing all of those systems and codes, and iterating on the design to make improvements.

The second goal is to validate and improve existing nuclear data libraries using the experimental results. This can be done by direct measurements of neutron capture cross sections in the thermal and unresolved resonance regions, where cross sections are smooth. This can also be done by benchmarking experimental results against simulated results using different nuclear data evaluations, as has been done previously.

CHAPTER 2
DETECTOR DEVELOPMENT

2.1 Simulations

Throughout this work, simulations were used both aid in the design of the measurements and to compare experimental results with simulated results. For example, these simulations were used to determine the best detectors to use, if the experiments were working properly, and some of the most promising samples to study. The Monte Carlo N-Particle transport code (MCNP)[35],[36] was used for many of the simulations to simulate the entire experiment, including the sample, detector, LSDS, and surrounding room. For most simulations, MCNP6[36] was used, but MCNPX-PoliMi (V2.0)[37], MCNP5[35], and ADVANTG[38] were also used. To speed up the simulations, a number of variance reduction techniques were used, including energy/time/cell splitting and roulette, energy cutoffs, and weight-window cards. For example, the LSDS was modeled as many concentric spheres inside the LSDS cube, with the detector/sample area in the center of the concentric spheres, with the cells having increasing importance as they got closer to the sample, as shown in Figure 2.1. Tallies used included F6 energy deposition tallies, F4 flux tallies (with and without tally multipliers), and F5 point tallies for certain simulations. Appendix C contains an example simulation input file.

For most comparisons to measurements, an F4 tally with an FM flux multiplier was used to simulate the capture rate in the sample. This however is not exactly what is being measured by the detector - the detector is measuring capture gammas emitted from the sample (as well as background gammas). The most accurate way to simulate the experimental setup is by using MCNP-PoliMi, which simulates the

Portions of this chapter previously appeared as: N.W. Thompson et al. "Progress On Using a Lead Slowing-Down Spectrometer to Measure Neutron Capture Cross Section," in *12th Int. Topical Meeting on Nucl. Applicat. of Accelerators*, Washington D.C., 2015, pp. 351-354[1].

Portions of this chapter are to appear in: N.W. Thompson et al. "Measurements and Analysis of Neutron Capture Cross Sections Using A Lead Slowing-Down Spectrometer," *Nucl. Sci. Eng.*, to be published.

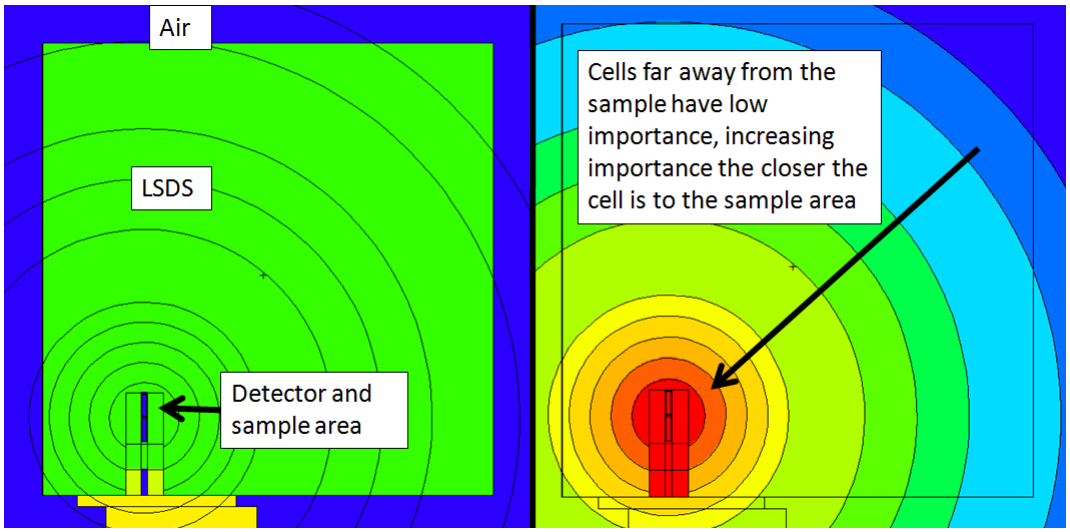

Figure 2.1: MCNPX Visual Editor image of the LSDS. On the left, the image is colored by material, with green representing the LSDS, and blue representing air. On the right, the image is colored by neutron/photon importance, where the areas of highest importance are red and lowest importance are blue. The view is cross sectional and the orientation is from the top (X-Y plane). The neutron source is in the center of the LSDS. For scale, the LSDS is a 1.8 meter cube.

correct gamma cascades[1], and tallying on the scintillator and sample cells, and then using a code to parse the PoliMi output file (which contains information on each event in those cells). The data must then be analyzed to determine when enough energy was deposited in the scintillator to cross the discriminator threshold, when capture events actually occurred in the sample, how much energy was deposited, and from this data, a time of flight spectrum can be built. This process is cumbersome and time consuming, as MCNP-PoliMi can not be run on multiple cores at the same time and processing the resulting files (especially when analyzing for coincidence between two events) can also be a slow process.

One way to speed this up slightly is to accept that MCNP(5/X/6) may not

[1]MCNP5/X/6 simulate gammas based on the average gamma distribution emitted from the sample, independent of the interaction that took place. This means that if a neutron has a probability of elastic scattering and capture interactions with a material and MCNP simulates an interaction, MCNP will randomly sample the gamma emission distribution in both cases, elastic scattering and capture. This works perfectly fine for reactor simulations, but for simulations of particles in coincidence, MCNP will simulate the wrong results. Dr. Sara Pozzi of the University of Michigan developed MCNP-PoliMi to address this issue.

accurately simulate capture gamma cascades correctly, but can simulate gamma energy deposition in the scintillator with an F6 tally. However, MCNP can not add in a detector discriminator as there would be in real life, it just tallies up all the energy deposited in the detector as a function of time[2]. Based on many simulations, it was found that using MCNP-PoliMi, MCNP with a F6 gamma energy deposition tally in the scintillator and MCNP with an F4 neutron capture tally in the sample had very good agreement, only that the F4 tally had better statistics than the F6 and simulations were able to be run many orders of magnitude faster with MCNP than MCNP-PoliMi (see Figure 2.2 for one example comparison). One other advantage of using the F4 tally is that with the F6 or PoliMi approaches, background runs would also need to be subtracted, whereas with the F4 tally, the tally is the capture rate in the sample (so no background subtraction was needed). For coincidence measurements, MCNP-PoliMi simulations were necessary to optimize the system.

[2]Event by event information can be created in MCNP, but again, this data is not accurate (because the gamma cascades are not simulated correctly) and requires a separate code to parse the data.

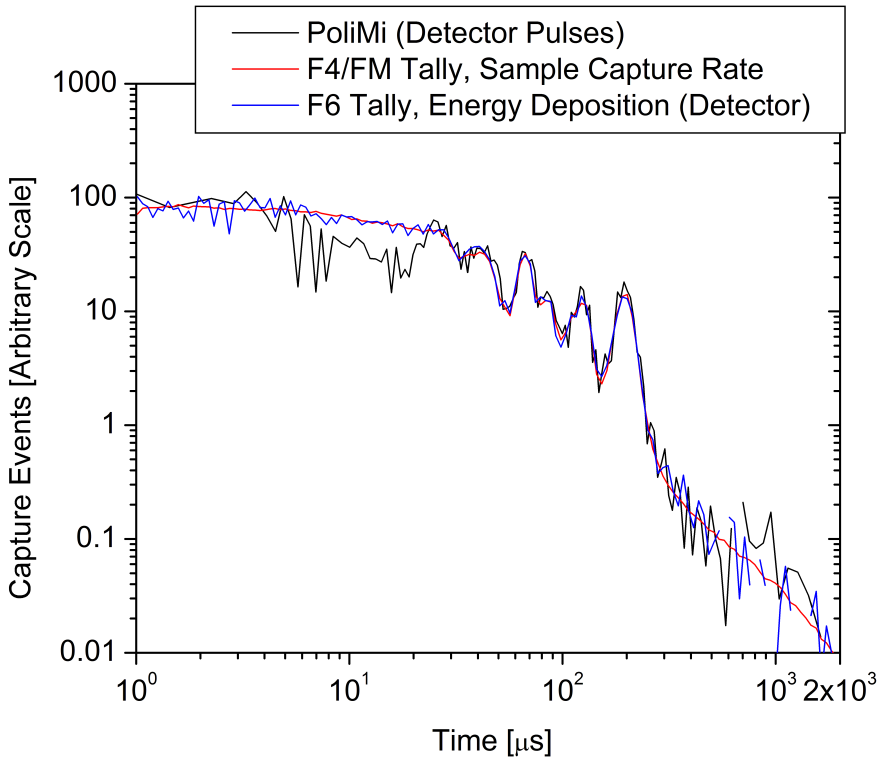

Figure 2.2: Comparison between simulation results using an F4/FM capture rate tally, an F6 gamma energy deposition tally, and PoliMi.

2.1.1 Effects of Lead Libraries

During the initial simulations, it was found that the results varied when different cross section libraries for lead were used. These differences can be seen in Figure 2.3 and Figure 2.4. In these Figures, measurement results were compared against five variations of the same simulation: 1) ENDF/B-VII.1 is used for all cross section libraries for lead and the impurities of lead, 2) JEFF 3.2 libraries are used for lead and, but ENDF/B-VII.1 is used for the impurities of lead, 3) JEFF 3.2 libraries are used for all cross section libraries for lead and the impurities of lead, 4) JENDL 4.0 libraries are used for lead and, but ENDF/B-VII.1 is used for the impurities of lead, and 5) JENDL 4.0 libraries are used for all cross section libraries for lead and the impurities of lead.

As is shown in Figures 2.3 and 2.4, modeling the impurities in lead with different cross section libraries makes virtually no impact on the result of the simulation.

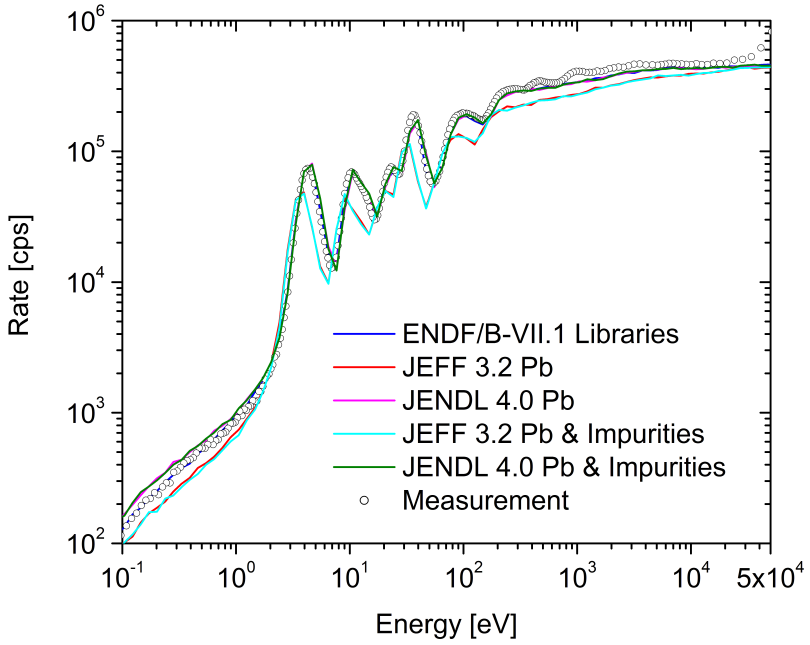

Figure 2.3: Comparison between simulation results ENDF/B-VII.1, JEFF 3.2, and JENDL 4.0 nuclear data libraries for lead cross sections compared to measurement results for a 10 mil tantalum sample.

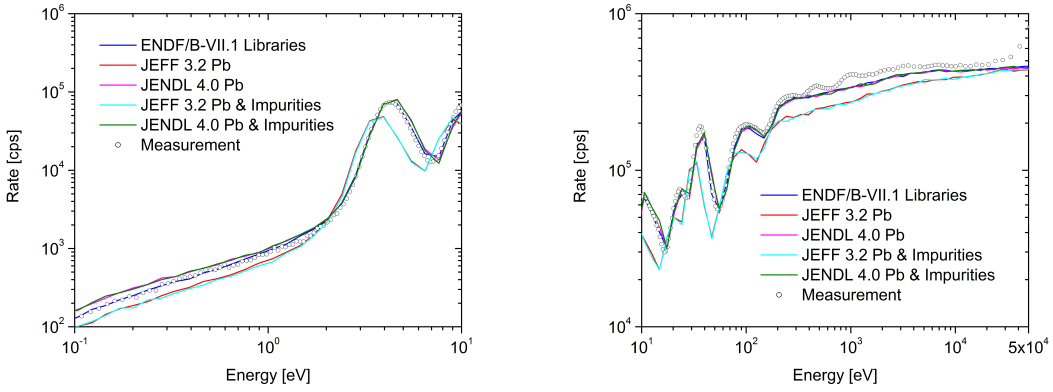

Figure 2.4: Comparison between simulation results ENDF/B-VII.1, JEFF 3.2, and JENDL 4.0 nuclear data libraries for lead cross sections compared to measurement results for a 10 mil tantalum sample, zoomed to highlight discrepancies. Left: Low energy region. Right: High energy region.

However, using different cross section libraries for the lead cross sections makes a large difference. ENDF/B-VII.1 matches well with JENDL 4.0, except at very low energies, but the results using the JEFF 3.2 libraries are completely different. The results seem to be shifted in magnitude and time, indicating that there is a difference in either the capture or scattering (or both) cross sections for lead in JEFF 3.2 compared to ENDF/B-VII.1 and JENDL 4.0. There is a small difference between ENDF and JENDL at low energies, but this difference is minor. These results indicate that the ENDF/B-VII.1 and JENDL 4.0 libraries are very similar and simulate the system well, and the JEFF 3.2 libraries should not be used. Additionally, it is possible that improving the accuracy of the cross section libraries for lead may improve simulations of the LSDS. Since the results of the simulations using ENDF/B-VII.1 libraries for lead agreed with the measurements the best, ENDF/B-VII.1 libraries were used for simulating lead and the impurities in lead in this work.

2.2 Detector Selection

The experimental setup will be explained in more detail later, but for the sake of clarity, in these measurements a detector and sample were placed inside of one of the measurement channels in the LSDS, such that the sample was as close to the detector as possible. During these measurements, there is a high neutron flux in the LSDS, as well as a high gamma flux. Detectors were needed that can not only detect capture gammas, but also have a low neutron capture cross section, and low neutron scattering cross (to not detect neutrons in the LSDS). The detectors also needed to be able to respond quickly and recover quickly, especially from the gamma flash at the beginning of each LINAC pulse.

High light output and high detector efficiency were also considerations, as these would enable smaller detector sizes to minimize the background. In order to get the best possible signal to background ratio, the detector must be as close to the sample as possible and cover as large a solid angle as possible. The further away from the sample, the lower the ratio of capture gammas from the sample to background gammas. Therefore, a detector with a low efficiency would need to be physically larger, and would have a worse signal to background ratio than one which

is smaller and higher efficiency.

Many types of scintillators were simulated, and based on those simulations and the considerations mentioned, a number of detectors were chosen for testing; a deuterated benzene (C_6D_6) liquid scintillator and yttrium aluminium perovskite ($YAlO_3$, YAP), lead tungstate ($PbWO_4$, PWO), lutetium oxyorthosilicate ($Lu_2(SiO_4)O$, LSO), and lutetium-yttrium oxyorthosilicate ($Lu_{2(1-x)}Y_{2x}SiO_5$, LYSO) inorganic crystal scintillators. Inorganic scintillators were bought from Proteus. Figure 2.5 shows an example of one of the simulations performed to determine detector response. Other scintillator materials were ultimately eliminated from consideration, either do to availability, cost, capture cross section, neutron moderation, radioactivity, activation, decay time, or other factors.

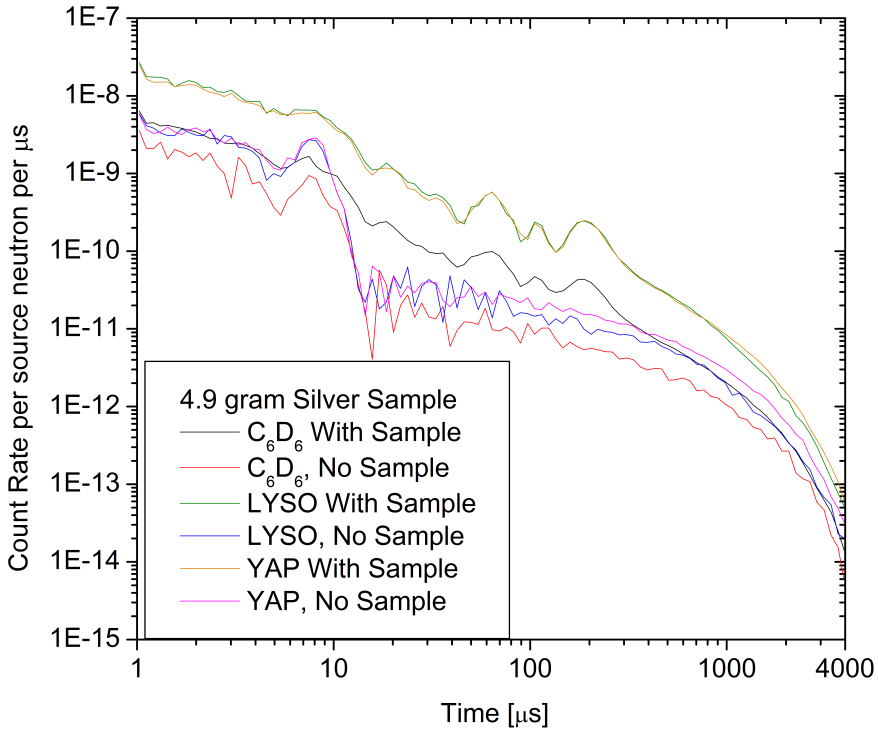

Figure 2.5: Comparison between the simulated detector responses with and without a 4.9 gram silver sample made with a C_6D_6, LYSO, and a YAP detector. Note difference in signal to background ratio for the three detectors. MCNP simulation.

2.2.1 Detector Selection Measurements

A first round of measurements was taken to select the best scintillator for the next measurements. Based on these measurements, it was found that the C_6D_6 detector was impractical due to the significantly increased moderation of neutrons from scattering with the carbon and deuterium in the detector, which greatly reduced the energy resolution of the measurement. Figure 2.6 shows an example of a comparison between a measurement with the C_6D_6 detector and one with the YAP detector with a 40 mil, 1.7 gram tantalum sample. Note that the measurement with the C_6D_6 detector has significantly poorer resolution due to the additional moderation. The PWO scintillator was also not chosen due to neutron capture in the tungsten (which caused an extremely high background). The LYSO and LSO were good candidates, but also suffered from neutron capture in lutetium and higher background counting rates due to beta decay of natural ^{176}Lu. Due to the low neutron capture and scattering cross sections, good light output, and relatively fast timing, YAP scintillators were selected for future measurements.

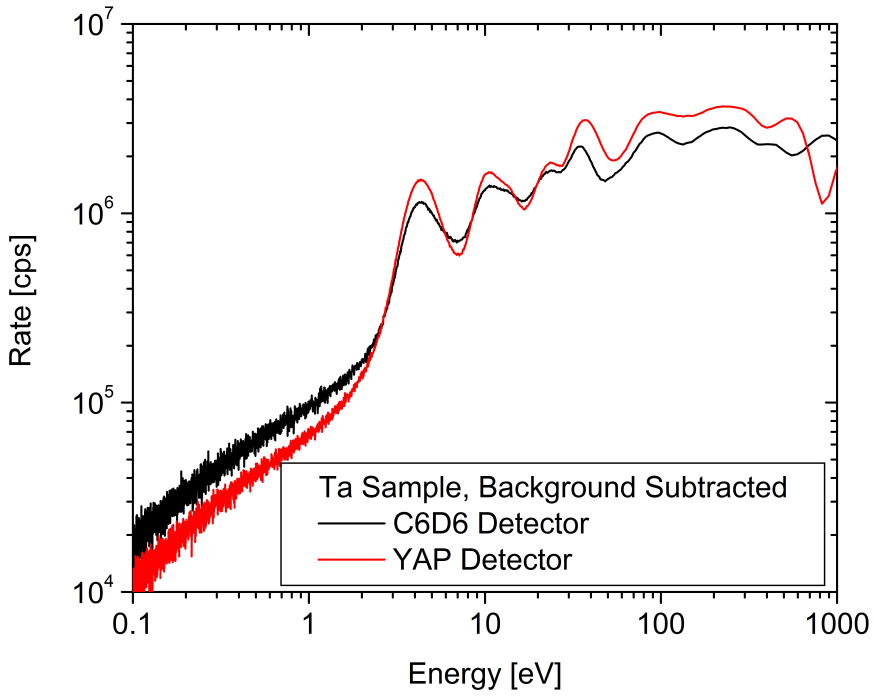

Figure 2.6: Comparison between the measurements of a 40 mil tantalum sample made with a C_6D_6 and a YAP detector. Measurements are background subtracted. Note the difference in resolution.

2.3 Refining the Method

One issue which was found during the first round of measurements was detector deadtime at high count rates. This resulted in the time after LINAC pulse before data could be collected to be much longer than expected, which meant data could not be collected for higher energy neutrons. This can be seen in Figure 2.7, where the measurement and MCNP simulation no longer match above 200 eV (or below 30 μs). This issue was solved in subsequent measurements by operating the LINAC at a lower electron current, and using smaller detectors, both of which lowered the count rate at short slowing-down times (high neutron energies).

Additionally, it became clear that to achieve the best possible neutron energy resolution, all materials containing hydrogen needed to be removed from near the scintillator and sample (or to the best extent possible). Initial measurements were done with electrical tape surrounding the scintillators to eliminate light leaks, however, this tape contained hydrogen and resulted in a poorer neutron energy res-

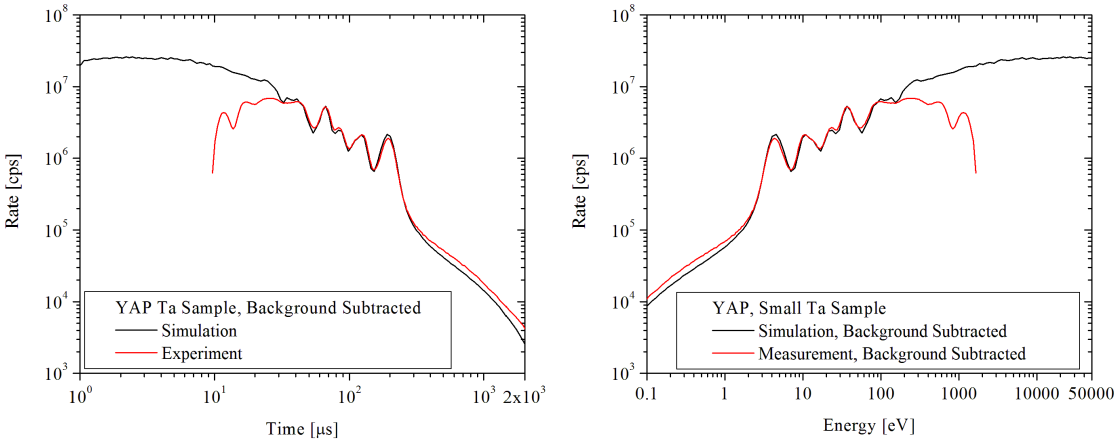

Figure 2.7: Left: Simulation and experimental data from a measurement with a tantalum sample plotted as a function of time. Right: The same results plotted as a function of average neutron energy. The detector experienced significant dead-time before 30 μs (above 200 eV) and the experimental count rate does not match the simulated results before this point. The sample was a 40 mil, 1.7 gram foil of tantalum, LINAC current was 0.5μA, detector radius was 0.75 inches, detector length was 1.5 cm, measurement time was 30 minutes.

olution. Later measurements used Teflon (PTFE) and limited use of Kapton tape instead of electrical tape to reduce the amount of hydrogen.

CHAPTER 3
MEASUREMENTS & DATA ANALYSIS

3.1 Experimental Setup

As detailed in previous publications [1],[39],[40] and the previous chapter, yttrium aluminum perovskite ($YAlO_3$, YAP) scintillators were used to measure capture gammas. Scintillators were cylindrical with a diameter of 0.75 inches, and sizes were varied to determine the optimal size, ranging from 15 mm to 2 mm thick. For each detector, the YAP scintillator was affixed to photomultiplier tube (PMT), in most cases, a Hamamatsu R762 PMT with a quartz window (no boron) and a Hamamatsu E974-17 D-Type Socket Assembly was used. To help in attaching the scintillator to the PMT window, GE Viscasil 12M (Polydimethylsiloxane Fluid) High Viscosity Silicone Fluid was used as an optical grease.

Once the scintillator had been attached to the PMT, the scintillator and PMT were covered with a few (at least six) layers of Teflon (PTFE) tape, and were inserted into the LSDS (most measurements were taken with the sample and detector inserted 40 cm into the LSDS). Figure 3.1 is an MCNPX Visual Editor image of the experimental setup, zoomed in on the sample and scintillator. The LSDS has multiple measurement channels (ports), ranging in size from 4 inches by 4 inches to 12 inches by 12 inches. Lead (and sometimes bismuth) bricks were inserted into these measurement channels to make sure air gaps in the LSDS were as small as possible. For these measurements, specialty bricks were also used which had already been machined to have a 1 inch hole, which the detectors could fit into tightly.

Samples to be measured were wrapped in one layer of aluminum foil, and then attached to the scintillator end of the PMT with kapton tape. The detector[s] where then placed into the LSDS, with a sheet of cadmium covering the entrance of the measurement channel to minimize room return[3]. High voltage and signal cables

Portions of this chapter are to appear in: N.W. Thompson et al. "Measurements and Analysis of Neutron Capture Cross Sections Using A Lead Slowing-Down Spectrometer," *Nucl. Sci. Eng.*, to be published.

[3]Room return occurs when neutrons which have leaked out of the LSDS become thermalized

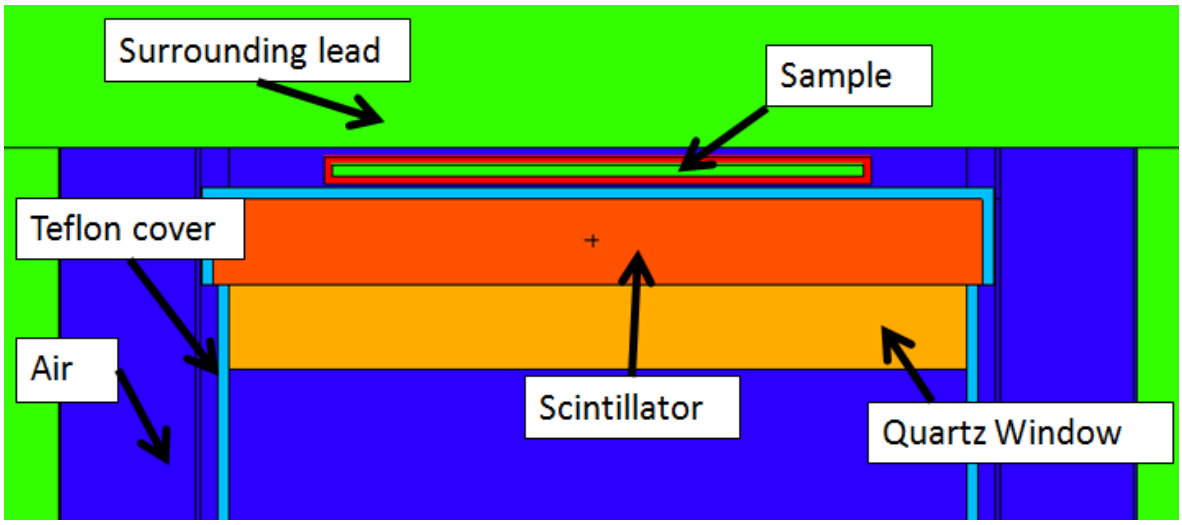

Figure 3.1: MCNPX Visual Editor image of the experimental setup. The view is cross sectional and the orientation is from the top (X-Y plane). For scale, the scintillator is 2 mm thick with a 0.75 inch radius.

were run from the detector[s] out of the target room and into the West Door area of the LINAC, where signals could be recorded. A ^{235}U fission chamber with a ^{235}U mass of approximately 1 mg was used as a flux monitor in a corner of the LSDS away from the other detectors, and measurements were normalized to each other based on the measurement of the flux by the fission chamber[4].

Measurements were normally made for 30 minutes per sample, split into ten minute collections, three times. If the LINAC turned off (tripped) or some other issue arose, that collection would be stopped and a new 'run' would be started. Measurements of background (LINAC operating with no sample) were also taken as well. Normal LINAC operating conditions were an electron pulse width of 250 ns, electron energy of 50-60 MeV, electron current of 0.05 - 0.1 μA, and pulsed at 180 Hz.

---

and are scattered back into the LSDS; this results in an effective broadening in the neutron energy distribution in the LSDS, reducing the energy resolution of the measurement. By surrounding the LSDS in cadmium, these thermalized neutrons will be captured before re-entering the LSDS.

[4]Beam conditions in the LINAC can vary over time and between runs, so it's important to have an independent measurement of the neutron flux in order to correct for this.

3.1.1 Optimizing the Experimental Setup

An important note: sample thicknesses were determined before the measurements by performing simulations of the expected capture rate and comparing that to previous measurements. There is effectively a window of capture rates which will work with this method, and the system can be modified to move that window up or down. This can be done by changing four variables: 1) measurement time/number of measurements, 2) LSDS current/LSDS flux, 3) detector size, 4) sample size.

It should sound pretty obvious, but increasing the measurement time and/or number of measurements will yield more data, and importantly, it has no impact of the quality of the data (eg. resolution, energy region, etc.). So for samples with small cross sections, increasing the measurement time will yield a better result.

Increasing the LSDS current will increase the flux of neutrons in the LSDS, which will allow for more data to be collected quicker, but this is a double edged sword - this also increases the background capture rate, and can effectively 'kill' the detector for a longer period of time (see Figure 2.7 for a measurement with a larger detector and larger neutron flux). This means that increasing the LSDS current limits the minimum time, and therefore maximum neutron energy at which data can be collected. This may be useful for small samples/samples with small cross sections where data in the low energy region is important. In most cases though with this system, reducing the LSDS current allowed for better measurements in the higher energy region.

Increasing the detector size has a similar effect as increasing the LSDS current - more data will be collected, but the maximum neutron energy at which collection can begin will also be impacted. In this work, the YAP scintillator thickness was reduced from 15 mm to 5 mm, and finally 2 mm to collect better data in the high energy region.

Sample size also has a similar effect as increasing LSDS current - a larger sample will capture more neutrons. However, increasing the sample size in particular has some additional drawbacks; if the sample is too large and the transmission of neutrons is too low, self shielding will occur, where many of the neutrons will be captured and the neutron flux will be depressed in the sample. Multiple scattering

may also take place in large samples, where neutrons are effectively moderated by the sample itself and potentially captured, increasing the capture rate. It's normally useful to limit the sample size to minimize these effects. But the sample size also can't be too small, or else the sample will not be seen over the background.

To determine sample thicknesses, the highest capture rate of tantalum and the lowest capture rate of nickel from previous measurements were used as the upper and lower bounds, and simulations of each sample were made and compared to those two capture rates. For some materials, the predicted material thickness was unreasonably large (indicating that an accurate measurement would be very difficult), so more reasonable sample thicknesses were used. For example, for iron, the predicted sample thickness required for an accurate measurement was 12.5 mm, which would have created many problems with self-shielding and multiple scattering, so a 1 mm sample was selected. To get very accurate measurements, in some cases, it might be required that multiple measurements with multiple sample thicknesses and detector thicknesses are required to measure all energy regions of a material.

3.2 Data Acquisition

Detector signals were recorded with two systems, a five channel "analog" Time-of-Flight (TOF) clock (FAST ComTec GmbH MCS6), which can record signal time, and a two channel digital acquisition (DAQ) system (Acqiris U1082A 8-bit High Speed Digitizer), which could record signal time and shape with 1 nanosecond precision. Figure 3.2 is a diagram of the electronic setup. Tests were performed to ensure that both the analog and digital data acquisition systems matched nearly exactly. Data was collected with the default MCS6 software for the analog clock and a custom built data acquisition software which controlled the Acqiris board.

For the analog system, a LINAC pre-trigger signal (which would be sent a few microseconds before the LINAC pulse) would be send to the MCS6 unit, which would begin data collection. The detector signals would be fed into an fast discriminator, which would be calibrated before the measurement. If the voltage of the signal was above the discriminator set point, the discriminator would output a TTL or FAST NIM signal (depending upon the setup), and this signal would be sent to the MCS6

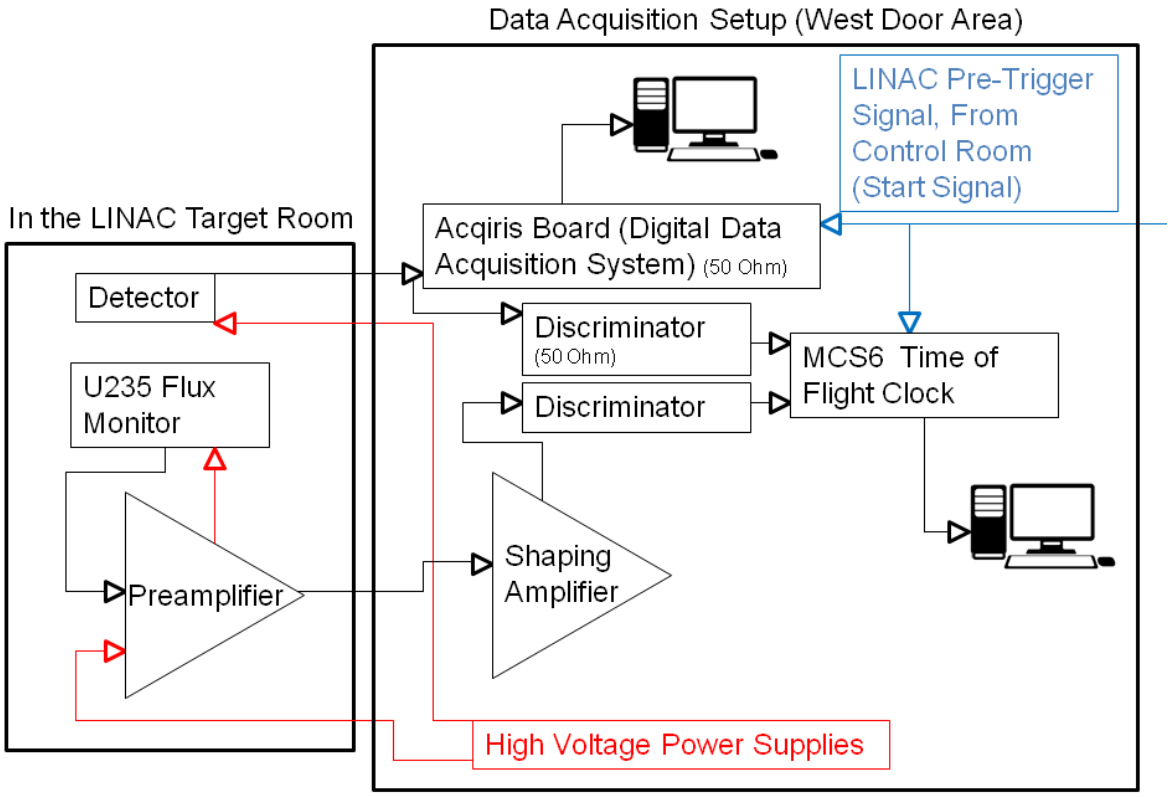

Figure 3.2: Diagram of the electronic setup for the measurement and data acquisition systems. Lines in black represent cables carrying signals, lines in red represent high voltage cables, and lines in blue represent the LINAC pre-trigger cables, which start the data acquisition on both systems.

unit. The MCS6 would then bin the time after the LINAC pre-trigger in 204.8 nanosecond bins. This means that if another signal crossed the discriminator set point in that 204.8 nanosecond window, it would not be counted. The MCS6 was set to collect data for 5 milliseconds, after which it would wait for the next LINAC pre-trigger. Once the run was completed, the data were saved in a simple txt file with the number of pulses collected in each time bin. Figure 3.3 shows a plot of the raw data collected during a typical measurement. As can be seen in the figure, the first few bins (up to 2.3 μs) is data collected before the LINAC pulse, after which is a large peak (Gamma Flash) followed by a period of detector deadtime (the drop at roughly 3 μs) before the detector recovers again. Peaks are easily distinguishable

after the detector recovers. At long slowing-down times, when the count rate is lower, significant noise can be seen, but this is smoothed out by averaging bins.

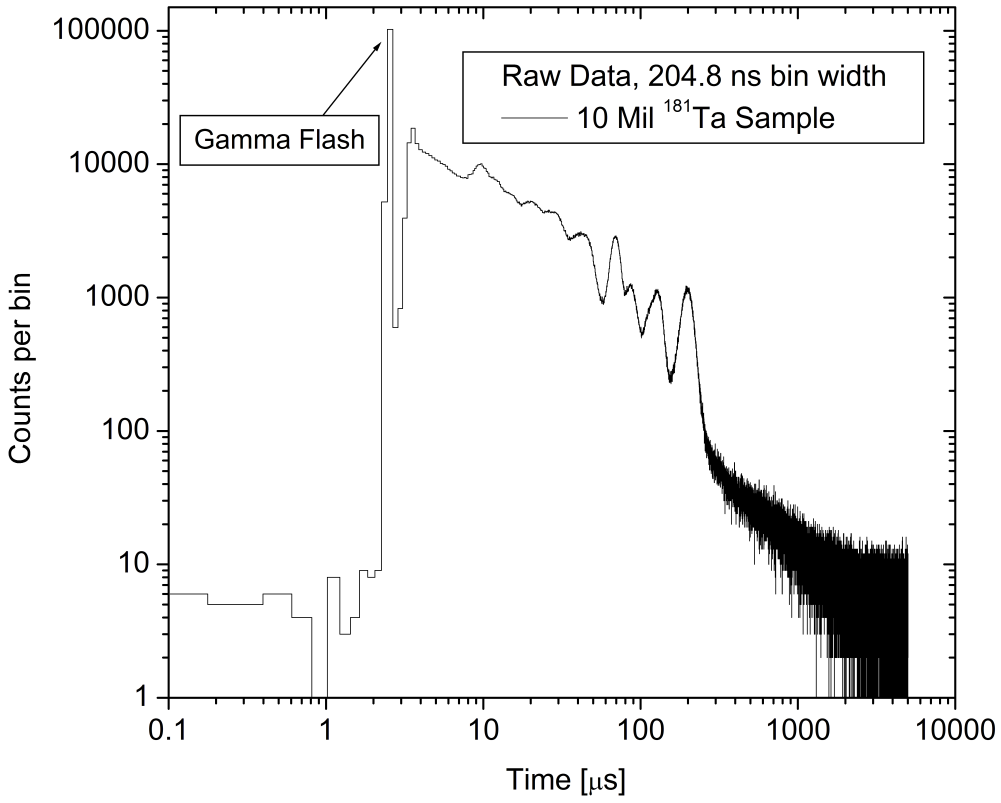

Figure 3.3: Raw data from a measurement of a 10 mil tantalum sample, one 2mm YAP detector, one 600 second (ten minute) run.

The digital system worked in the similar way. The same LINAC pre-trigger signal was also sent to the Acqiris board, which would begin data collection. Detector signals would be collected by the software if the signal rose above a certain voltage threshold, which would be determined before the experiment. If the signal voltage rose above the threshold, the system would save 200 nanoseconds of data in 1 nanosecond increments. These files are much larger, often well over 1 GB in size. Data was written in binary and included the time of the pulse, the pulse shape, and which channel the signal originated from. The advantage of collecting digital data on pulse shapes is it allows for the researchers to re-analyze the data after the experiment.

Even when data were collected with the digital system, the analog system was also used, as the ^{235}U fission chamber data for measuring neutron flux was collected with the analog system. Additionally, during most measurements, other detectors were tested in other LSDS measurement channels, and this data would be collected using the analog system.

3.3 Data Analysis

Once a measurement was completed, it was compared to an MCNP simulation of the same conditions. The MCNP simulation was set up to provide capture gamma data (F6 gamma energy deposition in the sample) and capture rate data (F4 neutron flux in the sample, with a FM/flux multiplier card to simulate the capture rate) as a function of time, and the measurements were also taken as a function of time. However, before comparisons could be done, a number of steps needed to be done to correct and adjust the data. For example, recording on the data acquisition systems began with a pre-trigger signal that would fire at a set time before the LINAC fired; and once the LINAC fired, there was a short period of time (Gamma Flash) where electrical noise and gammas from the LINAC would cause the detectors to be effectively "dead". The timing of the Gamma Flash in the data also provided another check to verify the timing of the data collection was consistent. In the data, the pre-trigger timing was corrected to match simulations.

Data was also summed from multiple runs, grouped into bins, converted to count rate, corrected for deadtime, decay corrected (for samples which were becoming activated), and background subtracted (where the background was scaled by the neutron flux in the LSDS). Below is this process represented as Equation 3.1:

$$C_{net,i} = S_i - B_S - (B_i - B_0)\frac{F_S}{F_B} \tag{3.1}$$

where $C_{net,i}$ is the background subtracted measurement, S_i is the sample measurement (deadtime corrected), B_S is the activity of the sample, B_i is the background measurement (deadtime corrected), B_0 is the constant background, F_S is the flux monitor measurement from the sample runs, and F_B is the flux monitor measurement from the background runs. B_S and B_0 were determined by calculating the average

count rate in the region before the gamma flash. There are little to no neutrons in the LSDS at this point, so only gammas from background and radioactive decay are measured. B_0 is calculated from the background measurement (measurement with no sample) and B_S is calculated from the sample measurement.

The data analysis was done using a combination of tools including RPIXDR (for summing and deadtime correction) and custom made python and C programs (the code for analyzing digital pulses is shown in Appendix B.). Simulation results were normally reported from MCNP as a function of capture events in the sample over time, per incident neutron (or as energy deposited in the detector over time, per incident neutron). Simulation results were normalized to count rate (with a normalization factor) before they were compared against measurements. Note: one of the assumptions being made in comparing measurement results against MCNP simulations of capture rates is that MCNP is accurately simulating interactions with the sample - not only capture, but also scattering and any other interactions that may occur in the sample. It's quite possible that the scattering cross section for a material could be incorrect, and this could show up as a discrepancy in the neutron capture rate results. For an example of where the scattering cross section may be impacting simulation results between nuclear data libraries, read Section 4.1.5.

Error was calculated by assuming that the deadtime corrected number of counts in each bin followed a Poisson distribution, where the error (standard deviation) could be estimated to be the square root of the counts. In this particular case, each of the variables in Equation 3.1 has an associated error, and that error needs to be propagated. Equation 3.2 shows the equation used to calculated the error in each bin:

$$\sigma_{C_{net,i}}(T) = \sqrt{\begin{array}{l} S_i(T) + B_S(T) + \left(\frac{F_S}{F_B}\right)^2 B_i(T) + \left(\frac{F_S}{F_B}\right)^2 B_0(T) + \\ \left(\frac{B_i(T) - B_0(T)}{F_B}\right)^2 F_S + \left(\frac{\big(B_i(T) - B_0(T)\big)F_S}{F_B^2}\right)^2 F_B \end{array}} \tag{3.2}$$

where $\sigma_{C_{net,i}}$(T) is the error in the background subtracted measurement.

3.3.1 Comparison Between Data Acquisition Systems

As was explained earlier, both an analog Time-of-Flight clock and a digital data acquisition system were used in these measurements. However, while the analog system had been used before with LSDS measurements, the digital data acquisition system hadn't been used with the LSDS or these particular detectors before. So to ensure that the data collected was in fact correct, the analog system was used to verify that the digital system was working properly. During measurements, the discriminator set point on the analog system for the detectors would be recorded, and the digital system would be set with a slightly lower set point, as ensure that all pulses collected by the analog system would also be collected by the digital system. Then, in post-processing the data from the digital system, the correct discriminator set point would be used to see if the two systems collected the same number of pulses. Figure 3.4 shows a comparison between two measurements (one with a tantalum sample and one without).

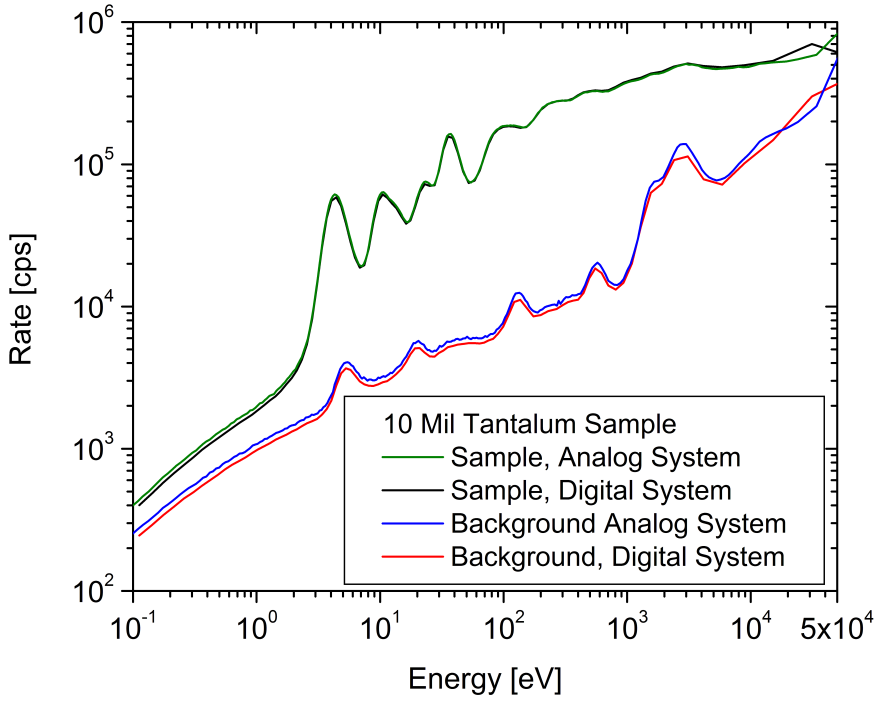

Figure 3.4: Comparison between the measurement results between the analog and digital data acquisition systems.

These measurements verified that the digital system was working properly and

could measure the same response as the analog system.

3.3.2 Impacts of Changing the Discriminator Level

Simulations and measurements were performed to simulate the impacts of changing the discriminator level of the measurement. Using MCNP-PoliMi, a simulation of the measurement was performed (simulating a 10 mil Ta sample), and a time-of-flight spectra was generated from on the list mode data, where only energy deposition above a discriminator setting were counted. By changing this discriminator level, multiple time-of-flight spectra were generated, as is shown in Figure 3.5.

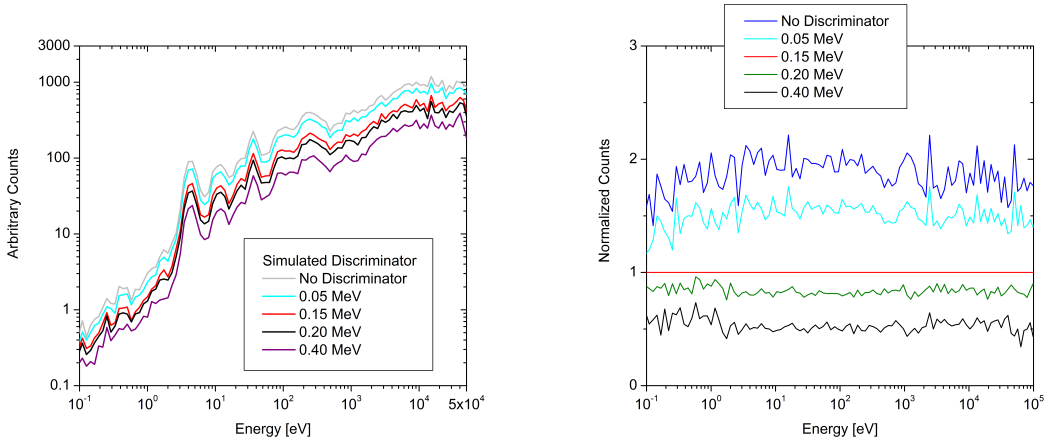

Figure 3.5: Left: Comparison between MCNP-PoliMi generate spectra using different discriminator setpoints. Right: Same data, normalized to a simulated 150 keV discriminator setpoint.

This simulation demonstrated that the pulse height spectra is not varying much over this energy region, and so the discriminator level chosen is not biasing the results. If there were significant changes in the gamma cascade, some of these spectra would have different slopes or large differences, instead, the lines are virtually parallel to each other.

This test was also performed with measurement data as well, and the results of this test can be found in Figure 3.6. The left plot of Figure 3.6 shows the same 10 mil tantalum sample measurement results using different discriminator setpoints, and as was demonstrated with the MCNP-PoliMi simulation, all of the measurements

seem parallel to each other, meaning that changing the discriminator setpoint is not biasing the results. To test how parallel the results actually were to each other, in the right plot of Figure 3.6, the results have been normalized to the 125 keV discriminator setpoint used in the experiment. As can be seen in the plot, after 2 μs, each of the plots is relatively flat, indicating that the capture gamma cascade and multiplicity is not varying over this region.

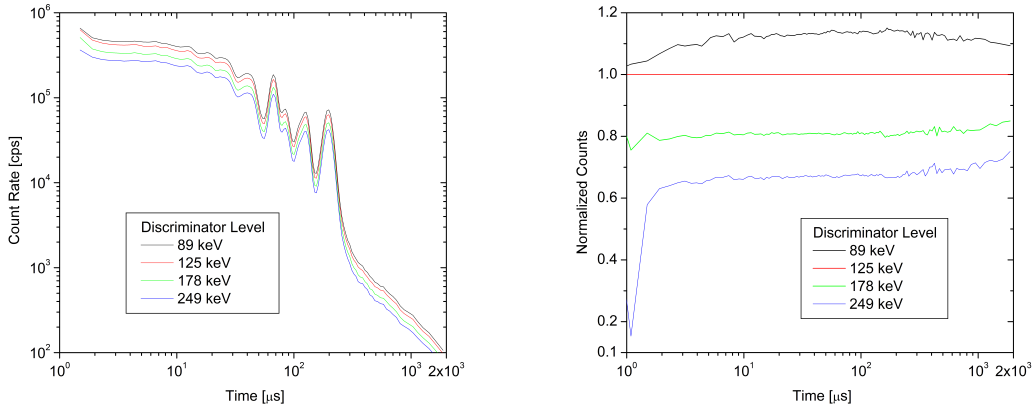

Figure 3.6: Left: Comparison between measurement data using different discriminator setpoints. Right: Same data, normalized to the 125 keV discriminator setpoint used in the experiment.

3.3.3 Generating Cross Sections

As was explained in Section 1.3, the neutron energy resolution of the LSDS is quite poor in comparison to time-of-flight methods, and because of this, resonances are smoothed, or broadened. In order to compare these measurements to actual cross sections, the data must first be divided by the neutron flux, and then translated into a capture cross section through Equation 3.3:

$$\sigma_\gamma(E) = \frac{Y(E)\sigma_t(E)k}{(1 - e^{-N\sigma_t(E)x})} \tag{3.3}$$

where σ_γ is the capture cross section, Y is the capture yield (for this measurement, capture rate divided by neutron flux), σ_t is the total cross section, k is a normalization constant, N is the number density, and x is the sample thickness. The

exponential term on the bottom is also known as the transmission (T). Normally, the normalization constant k would not be needed, but as these measurements do not measure an absolute capture yield, k is needed to normalize the result.

For this analysis, the neutron flux used was taken from an MCNP simulation of the neutron flux at the sample location. And due to the neutron energy resolution of the LSDS, a broadened total neutron cross section must be used in Equation 3.3. Note: one of the assumptions being made here is that the total cross section of the material being analyzed is well known; this may not always be a good assumption, especially in cases where there is large disagreement between nuclear data libraries and/or the experimental results.

One additional note: for beam measurements where neutrons are only traveling in one direction, the distance the neutrons travel through the sample is the sample thickness. However, in these measurements, neutrons are scattering in every direction, and can enter the sample at any angle. Because of this, the average distance neutrons travel through the sample is actually larger than the sample thickness, and an 'effective thickness' must be calculated. For these measurements, the effective sample thickness was calculated by comparing two simulations, one where the neutrons enter the sample in a beam, and one where neutrons enter the sample from all directions, and comparing the capture probability. If this 'effective thickness' is not accounted for, the cross section results will not be correct.

After calculating the capture cross section from Equation 3.3, this cross section can be compared with a broadened capture cross section. In order to broaden a cross section, the product of the point-wise cross section and the LSDS resolution function (Equation 1.4) must be integrated over the energy region of interest. This can be done using Equation 3.4[41]:

$$\bar{\sigma}_\gamma(E_i) = \frac{1}{\sqrt{E_i}} \int_{E_{min}}^{E_{max}} G(E, E_i)\sqrt{E}\sigma_\gamma(E)dE \tag{3.4}$$

where $\bar{\sigma}_\gamma(E_i)$ is the broadened capture cross section at E_i, G(E,E_i) is the Gaussian resolution function of the LSDS, and σ_γ(E) is the pointwise capture cross section[5].

[5]This same formula can be used to calculated the broadened total cross section, which is an input to Equation 3.3 by substituting the capture cross section (σ_γ(E)) for the total cross section

3.3.4 Pulse Shape Analysis and Pulse Height Weighting

Since individual pulse shapes were also collected with the digital data acquisition system, pulse shape analysis could be performed on the pulses. One type of pulse shape analysis is called Pulse Height Weighting. As mentioned earlier, Pulse Height Weighting[6] can be used to correct for differences in detector efficiency, since the Total Energy Detection method (see Section 1.2) of measuring capture cross sections requires that the detector efficiency be proportional to the energy of the incident gamma. As can be seen in Figure 3.7, the detector efficiency of the YAP detectors is not proportional to gamma energy.

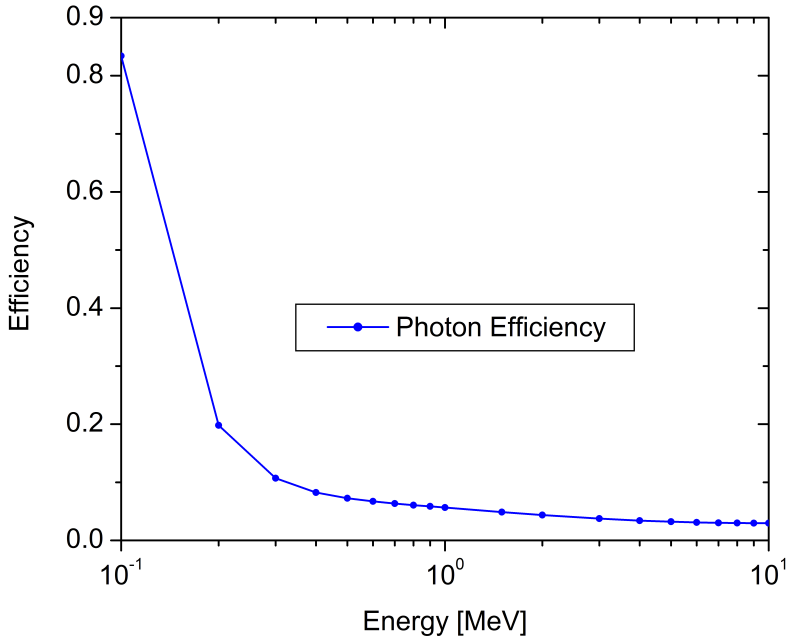

Figure 3.7: Plot of the detector efficiency, based on MCNP simulations.

The basic idea behind Pulse Height weighting is that if the total decay energy of a capture is known (or is not varying), and the response of the detector to incident gammas is known, then detector responses can be weighted such that the weighted

(σ_t(E)).

[6] In this particular work, Pulse Height Weighting is a little bit of a misnomer; instead of weighting the pulse height, the pulse integral (which is less noisy and more proportional to gamma energy deposited) is weighted, so the more accurate term would be "Pulse Integral Weighting". However, since "Pulse Height Weighting" is the commonly accepted name of the technique, this text will continue to refer to it by that name.

detector efficiency is proportional to the energy of the incident gamma, as shown in equation Equation 3.5[24][7]:

$$\eta_{\gamma,i} = kE_{\gamma,i} \tag{3.5}$$

where k is a normalization factor, $E_{\gamma,i}$ is the energy of the incident gamma, and $\eta_{\gamma,i}$ is the efficiency to detect that gamma. This method assumes that the detector has a low efficiency, and only one gamma ray per gamma cascade is detected at a time. In this case, the efficiency to detect a capture event becomes Equation 3.6[24]:

$$\eta_C = 1 - \prod_i (1 - \eta_{\gamma,i}) \approx \sum_i \eta_{\gamma,i} \tag{3.6}$$

where η_C is the efficiency to detect a capture event. If the detector efficiency is proportional to the incident neutron energy (Equation 3.5), then the efficiency to detect a capture event becomes approximately proportional to the total excitation energy (the neutron energy plus the binding energy). This is important, because if the detector efficiency is proportional to the total excitation energy, then the measurement is insensitive to changes in the capture gamma cascade and/or multiplicity[8]. This proportionality is shown in Equation 3.7[24]:

$$\eta_C \approx k \sum_i E_{\gamma,i} \approx kE_{ex} = k(S_n + E_n) \tag{3.7}$$

where E_{ex} is the total excitation energy, S_n is the neutron binding energy, and E_n is the energy of the neutron. As the efficiency of many detectors is not proportional to the incident gamma energy, the Pulse Height Weighting technique corrects for this by multiplying the pulse height (or in this case pulse integral, see footnote 6, which is calibrated to a certain energy gamma, by an energy dependent weighting function; this weighting function is based on the detector response to detect that incident gamma. Equation 3.8 is the formula the weighting function must satisfy:

[7]For those interested, this derivation is spelled out in more detail in [24].

[8]Just to hammer this point home, if the detector efficiency is proportional to incident gamma energy, then the detector will have the same efficiency to detect a capture gamma cascade where only one 5 MeV gamma is emitted as it is to detect a capture gamma cascade where five 1 MeV gammas are emitted.

$$\int_0^\infty R_d(E_d, E_\gamma) W(E_d) dE_d = kE_\gamma \tag{3.8}$$

where $R_d(E_d, E_\gamma)$ is a detector response matrix containing the detector energy deposition (E_d) for many incident gamma energies (E_γ), and $W(E_d)$ is the weighting function. In this work, the response matrix was based on simulations of Gaussian energy broadened F8 detector response tallies in MCNP, and the Gaussian energy broadening function that fit the measured detector response for ^{136}Cs and ^{60}Co sources was used. Figure 3.8 is a plot of some of the detector responses generated from MCNP that were used to generate the weighting function. More detail about Pulse Height Weighting can be found in McDermott et al.[42].

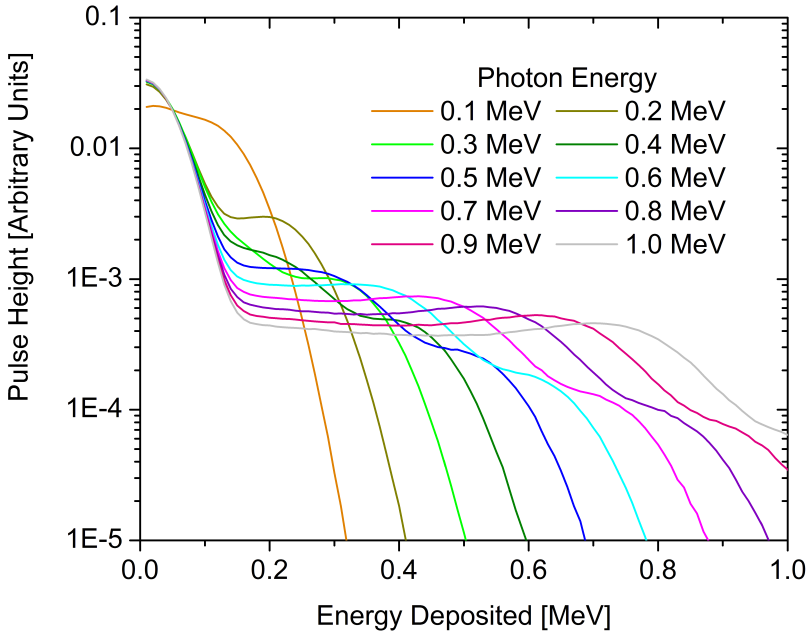

Figure 3.8: Plot of detector responses to various energy gammas, generated by MCNP. The large spread in energies is due to the Gaussian Energy Broadening card used with the F8 tally.

Based on the response matrix, a weighting function was generated, modeled as a fifth order polynomial, and reproduced below as Equation 3.9:

$$W(E) = -12.349 + 96.654E + -27.923E^2 + 25.853E^3 - 4.417E^4 + 0.322E^5; \quad (3.9)$$

where W(E) is the weighting function. Figure 3.9 is a plot of the weighting function as a function of energy.

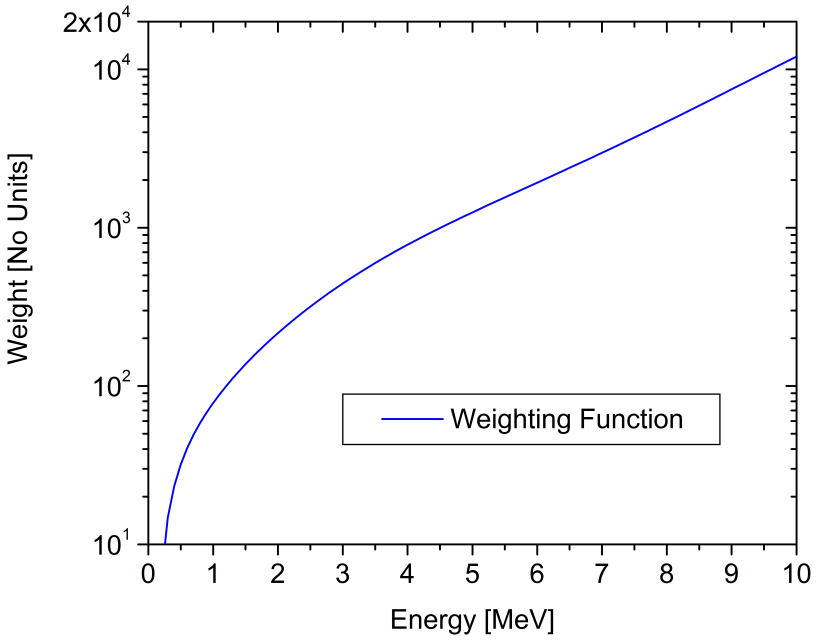

Figure 3.9: Plot of weighting function as a function of energy. Note that the Y axis is a log scale; large pulses are weighted much more than small pulses.

A weighted Time-of-Flight spectrum can be created by applying the weighting function to the data. Borella et al. described this process in Equation 3.10[24]:

$$C_W(T_n) = \int C(T_n, E_d) W(E_d) dE_d \quad (3.10)$$

where $C(T_n,E_d)$ is the measured count rate as at each Time-of-Flight and energy deposition and $C_W(T_n)$ is the weighted count rate as a function of Time-of-Flight. This same process can be used to create a weighted background count rate, and the two can be subtracted from each other (after being normalized and dead time

corrected).

To ensure that the background was subtracted correctly, this work used a slightly different method than Borella et al., by creating a Time-of-Flight/Energy matrix. Figure 3.10 shows an example of what this matrix looks like for a Ta sample measurement.

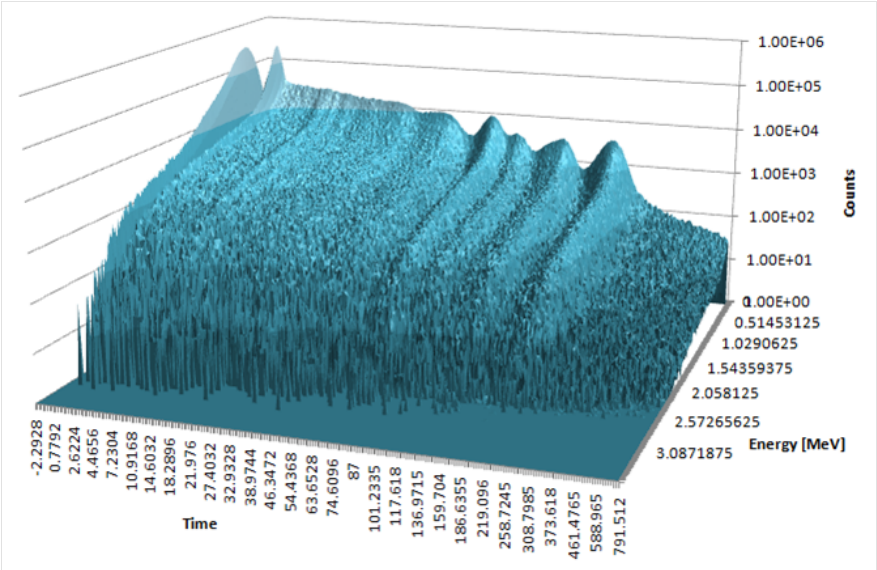

Figure 3.10: Plot of Time-of-Flight/Energy matrix.

This Time-of-Flight/Energy matrix was then weighted, as is shown in 3.11:

$$C_W(T_n, E_d) = C(T_n, E_d)W(E_d) \tag{3.11}$$

where $C_W(T_n,E_d)$ is the weighted Time-of-Flight/Energy matrix. Figure 3.11 shows an example of what this weighted matrix looks like for the same Ta sample measurement.

A similar weighted matrix can be created for the background, and the two matrices can be converted to count rate, corrected for deadtime, and subtracted from each other. If the weighted matrix is integrated over energy deposited, then the weighted Time-of-Flight is identical to one obtained using the Borella et al. method. However, by keeping all the data in matrix form, it's must easier to determine if the background has been subtracted properly, particularly if the background has a different energy distribution than the sample.

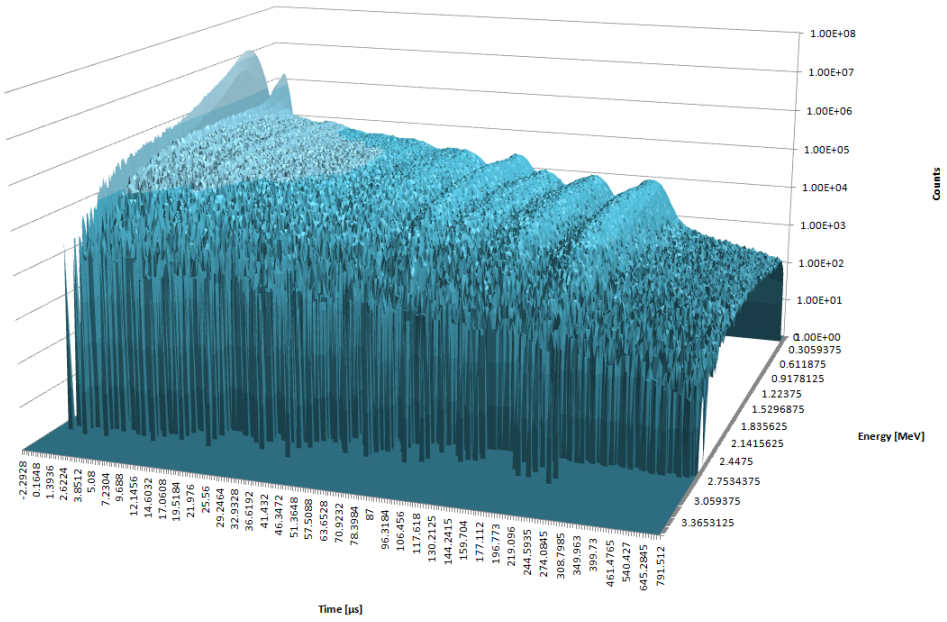

Figure 3.11: Plot of Time-of-Flight/Energy matrix after weighting.

CHAPTER 4
RESULTS

For this work, measurements of detectors and samples were taken at the RPI LSDS. The details of some of the results of these measurements will be outlined below.

4.1 Validating Nuclear Data

In 2003, Perrot et al.[29] demonstrated that an LSDS can be a useful tool for validating nuclear data. This was accomplished by making measurements using an LSDS and scintillator, and comparing the measured capture rate as a function of time to an MCNP simulation of the experiment. Two of the goals of this work were to replicate some of the results of Perrot et. al. and make new validation measurements.

Measurements of many samples were taken throughout the course of this project; information about those samples can be found in Table 4.1. Note, tantalum appears twice in the table as two different tantalum samples were measured (40 mils and 10 mils).

When comparing MCNP simulation results and measurement results, the MCNP simulation results were normalized to the measurement results. In most cases, the 1/v region was used for normalization, but in some cases where there were few or widely varying counts in the 1/v region, the first resonance was used for normalization. Appendix D contains tables of the background subtracted count rate data for these measurements, and Appendix E contains tables of the MCNP results for ENDF/B-VII.1, JEFF 3.2, and JENDL 4.0 normalized to the measurement results.

Portions of this chapter previously appeared as: N.W. Thompson et al. "Progress On Using a Lead Slowing-Down Spectrometer to Measure Neutron Capture Cross Section," in *12th Int. Topical Meeting on Nucl. Applicat. of Accelerators*, Washington D.C., 2015, pp. 351-354[1].

Portions of this chapter are to appear in: N.W. Thompson et al. "Measurements and Analysis of Neutron Capture Cross Sections Using A Lead Slowing-Down Spectrometer," *Nucl. Sci. Eng.*, to be published.

Table 4.1: Sample Information

Sample	Sample Thickness		Mass [g] ± 0.01 g
	[mm]	[mils]	
Ag - Silver	0.6	23.6	1.60
Au - Gold	0.4	15.7	1.34
C - Carbon	2	78.7	1.01
Co - Cobalt	0.6	23.6	1.58
Fe - Iron	1.0	39.4	2.07
In - Indium	0.6	23.6	1.23
Mo - Molybdenum	1	39.4	3.96
Nb - Niobium	1.27	50	1.71
Ni - Nickel	3	118.2	17.20
Sn - Tin	1	39.4	1.84
Ta - Tantalum	1.016	40	1.70
Ta - Tantalum	0.254	10	1.03
Zr - Zirconium	1	39.4	1.60

4.1.1 Tantalum Measurements

The first round of measurements demonstrated that the system developed was indeed functioning as intended, although, as was shown in Section 2.3, not to the neutron energy desired due to deadtime issues (see Figure 2.7). By the second round of measurements, using thinner scintillators (2mm and 5mm thick instead of 15mm), measurements of tantalum were made that showed very good agreement with simulations, shown in Figure 4.1. These measurements also used a thinner and smaller sample of tantalum (10 mil, 0.424 grams) which helped to reduce self-shielding in the sample. This demonstrated that the measurements were providing accurate results and the simulations and data processing were being performed correctly. Additionally, these measurements agree well with those made by Perrot et. al.[29]. Note: the measurements are being compared to simulations of the capture rate in the sample, using an F4 tally with an FM card to simulate the capture rate.

A third set of measurements of tantalum were made using the same system, and again, there was good agreement between the measurements and simulations. However, when comparing simulations using ENDF/B-VII.1, JEFF 3.2, and JENDL 4.0 libraries, differences between the libraries were found above 100 eV. These dif-

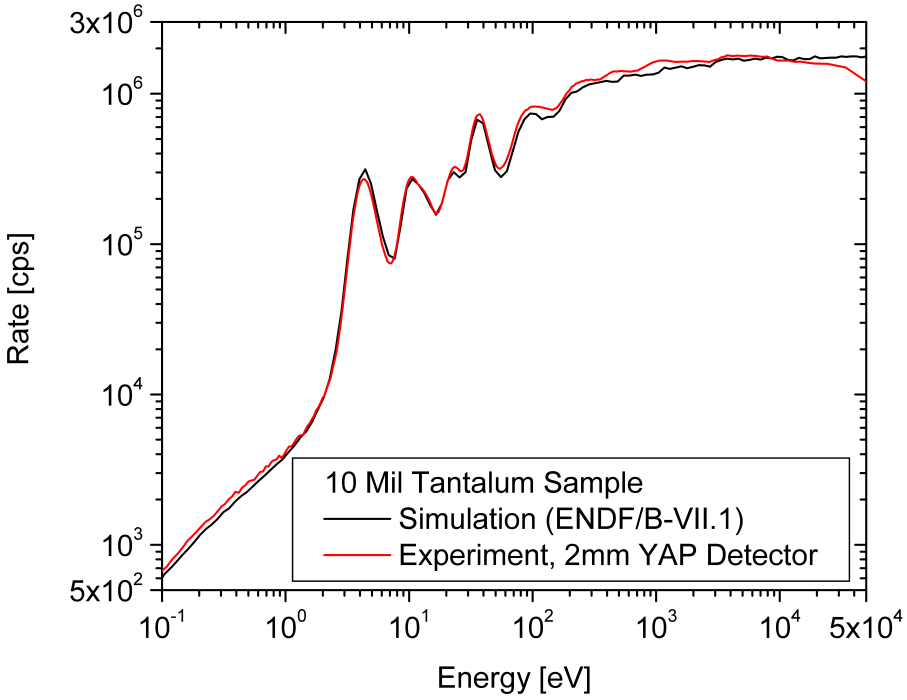

Figure 4.1: Measurement and Simulation of a 10 mil tantalum sample, one 2mm YAP detector (Second round of measurements).

ferences stem from the fact that the unresolved resonance region for tantalum in ENDF/B-VII.1 begins at 330 eV, and whereas for JEFF 3.2 and JENDL 4.0, the unresolved resonance region begins at 2.4 keV. Figure 4.2 shows the differences between the measurement and simulations using ENDF/B-VII.1, JEFF 3.2, and JENDL 4.0 libraries.

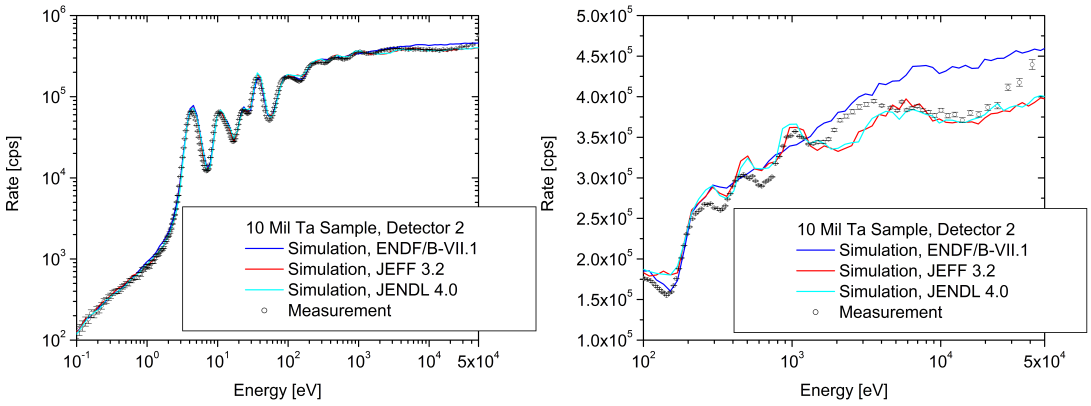

Figure 4.2: Left: Measurement of 10 mil tantalum sample, compared to MCNP simulations using ENDF/B-VII.1, JEFF 3.2, and JENDL 4.0 libraries. Right: Same data, zoomed in, with a linear y-axis. Note that above 330 eV, the ENDF/B-VII.1 result becomes linear, missing features present in the measurement, JEFF 3.2, and JENDL 4.0 results.

4.1.2 Nickel Measurements

In addition to measurements of tantalum, measurements of nickel were also made. While tantalum has many low energy capture resonances with high neutron capture cross sections, the neutron capture cross section of nickel is much lower, and does not have large resonances (for example, the cross section of natural nickel at 1 keV is 20 mB). This makes nickel much more of a stress test on the lower bounds of what cross sections/materials can be measured with this particular setup. For this measurement, a much larger sample was used (3 mm, 17.2 grams) so that a larger signal could be collected. Even with the larger sample though, the difference in count rate between the nickel sample and background was small, as can be see in Figure 4.3. However, even with this poor signal to background ratio, the results matched well with the MCNP simulation.

This nickel sample was natural Nickel of 99.6 % purity. However, some of the impurities in the sample were materials that have very high neutrons capture cross sections (eg. Co-59, Mn-55). To see the difference between the captures in the nickel sample (including impurities) and the captures in only the nickel, two simulations were performed, one simulating just a natural nickel sample, and one including the

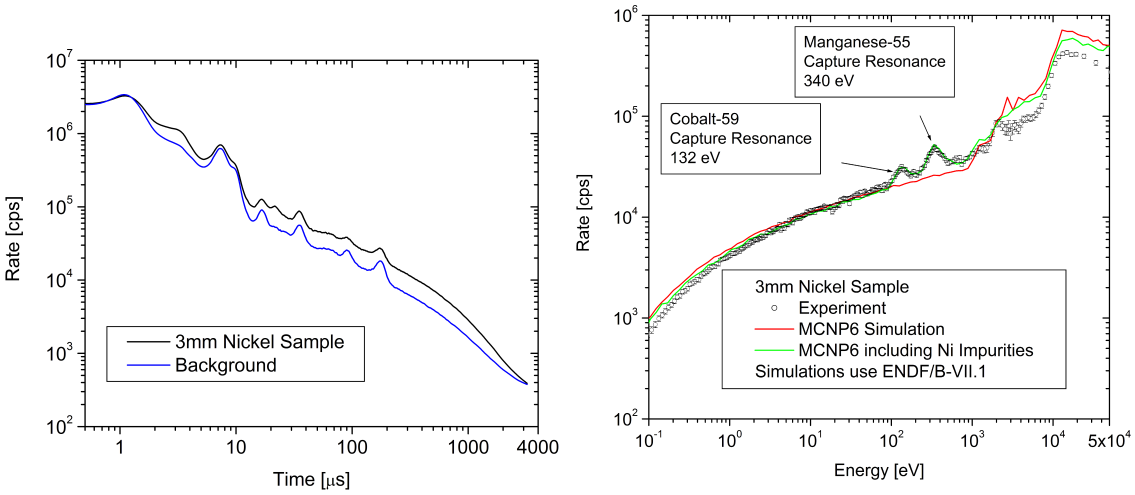

Figure 4.3: Left: Experimental results from a measurement with nickel and without a sample, as a function of time. Right: Simulations and experimental data from a measurement with a nickel sample plotted as a function of energy. One simulation simulated a pure natural nickel sample, the other simulated the nickel sample and all impurities.

impurities. As can be seen in Figure 4.3, the two peaks at 132 eV and 340 eV are not resonances in Nickel, but resonances in impurities.

There are two differences between the simulation and measurement: 1) the low energy tail does not exactly match as well as the tantalum measurements did, 2) above 2 keV, there is a seemingly systematic difference between the simulation and measurement. This could indicate that the capture cross section for nickel might be systematically low above 2 keV. However, it's also possible that these two effects could be explained by differences in efficiency to detect gammas between the multiple isotopes of nickel (nickel has five stable isotopes).

It should be noted that Kapchigashev and Popov [43] in 1962 also published results from measuring capture cross sections of nickel in an LSDS, and when converting their measurement results into cross sections, they needed to correct their data up to 70 percent above 15 keV to account for multiple scattering, they started their multiple scattering correction at 2 keV. That said, using this method, multiple scattering is already taken into account by simulating the entire system and sample.

4.1.3 Silver Measurements

Measurements of silver were also made and are presented in Figure 4.4. While silver has two stable isotopes (^{107}Ag and ^{109}Ag), the measurement still does a reasonably good job at matching the simulations, up until 100 eV. Above 100 eV, the simulations of the different libraries start to disagree with each other, and the simulations do not agree with the experiment. Figure 4.4 also contains a zoomed in plot to show the differences in the 100 eV to 10 keV region better. JENDL 4.0 seems to do the best job at matching the experimental results from 100 eV to 300 eV; above 300 eV the disagreements become more stark. The capture cross section in ENDF-B/VII.1 seems too low between 1 keV and 10 keV, this difference is most likely due the fact that the resolved resonance region in ENDF extends much further than in JEFF or JENDL. High detector deadtime may be biasing the results at high energies (above 10 keV).

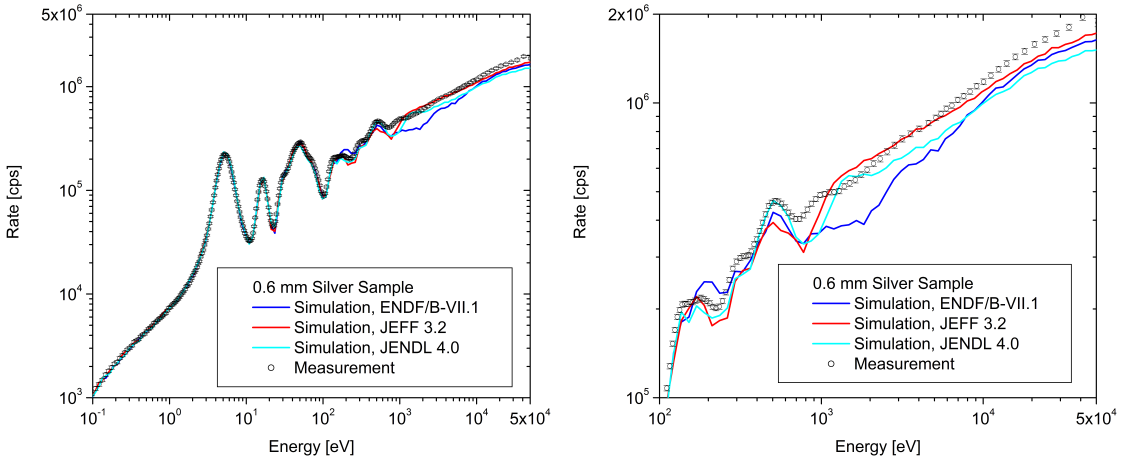

Figure 4.4: Left: Measurement of a 0.6 mm silver sample, one 2mm YAP detector and MCNP simulations using ENDF/B-VII.1, JEFF 3.2, and JENDL 4.0 libraries. Right: Same data, zoomed in to better show discrepancies between 100 eV to 10 keV.

There are a few discrepancies that stand out between the ENDF/B-VII.1, JEFF 3.2, and JENDL 4.0 simulation results, and they both seem to stem from differences in those cross sections libraries. The first discrepancy is near 200 eV, where ENDF/B-VII.1 estimates a capture rate much higher than the experimental results and simulations of JEFF 3.2, and JENDL 4.0. Looking into those three

libraries, it's clear that this discrepancy is caused by differences in ^{107}Ag, namely a resonance at 202.5 eV, where ENDF/B-VII.1 has a wide resonance with a peak cross section (at 300K) of 2515 barns, whereas that resonance in JEFF 3.2 has a peak cross section of 158 barns and in JENDL 4.0 the peak cross section is 265 barns - and the resonance is much more narrow than in ENDF/B-VII.1 (there are no large differences between the three libraries in this region for ^{109}Ag). Figure 4.5 is a plot of these libraries in this energy region. As can be seen in 4.2 the Γ_n (neutron resonance width) value for that 202.5 eV resonance in ENDF/B-VII.1 is also over ten times larger than in JENDL 4.0 and JEFF 3.2. This looked like a mistake in the nuclear data, possibly a transcription error (that the Γ_n value was supposed to be 0.01793333). Reviewing previous ENDF versions, the ENDF/B-VI.8 library seems to match JEFF 3.2 library nearly exactly; further evidence that this was a transcription error.

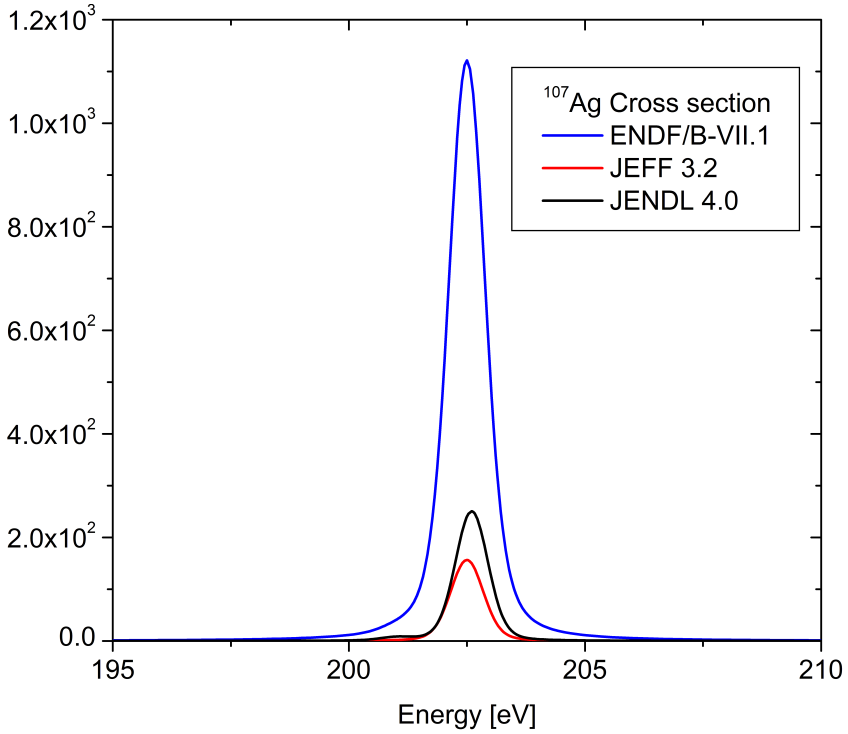

Figure 4.5: Neutron capture cross section from the ENDF/B-VII.1, JEFF 3.2, and JENDL 4.0 libraries for ^{107}Ag, 202.5 eV resonance.

This potential error was brought to Dr. Vladimir Sobes, a nuclear data expert

Table 4.2: ^{107}Ag Resonance Parameters, 202.5 eV, T=300 K

Library	Γ [meV]	Γ_n [meV]	Γ_γ [meV]	$\sigma(T)$[b]
ENDF/B-VII.1	0.3333333	0.1793333	0.1540000	2515.49
JEFF 3.2	0.1642670	0.01026700	0.1540000	158.21
JENDL 4.0	0.1572000	0.01720000	0.1400000	265.60
ENDF/B-VI.8	0.1642700	0.01026700	0.1540000	158.21

at Oak Ridge National Laboratory who works on evaluations, and the discrepancy was traced back to the *Atlas of Neutron Resonances*[44], where ENDF/B-VII.1 took the resonance data from. After communicating with Dr. Said Mughabghab, the author of the *Atlas of Neutron Resonances*[44], it was determined that this was in fact a transcription error; the $2g\Gamma_n$ value should have been 26.9 meV instead of 269 meV, which would change the Γ_n value to 0.01793333 meV instead of 0.1793333 meV. This issue has been submitted to the ENDF GForge Issue Tracker and Dr. David Brown has been notified; the fix will be implemented after ENDF/B-VIII.0 is released and will be incorporated in the next version of the *Atlas of Neutron Resonances*[44].

A much less visible discrepancy was also found in JEFF 3.2. Just below 200 eV (at roughly 173 eV), the JEFF 3.2 library has a higher cross section than the JENDL 4.0 library and the experiment results. Digging into the data further, it seems to be that the value had been taken from *Neutron Cross Sections*[45], authored by Dr. Mughabgahb, Dr. Divadeenam, and Dr. Holden, published in 1981. ENDF/B-VII.1 used values from the *Atlas of Neutron Resonances*[44] (*Atlas*), the next update of the same book, and JENDL 4.0 used values from many of the same measurements the value in the *Atlas*[44] is based on. As is shown in Table 4.3 the Γ_n value for this resonance is almost six times lower in the *Atlas*[44] than it was in *Neutron Cross Sections*[45], resulting in a much higher capture cross section for JEFF 3.2 at that energy. This issue has been submitted to the OECD-NEA JEFF 3.2 feedback portal.

Another discrepancy relates to neutron energies between 1 keV and 10 keV. Above 1 keV, the measurement and simulations differ significantly. As can be seen

Table 4.3: ^{107}Ag Resonance Parameters, 173.7 eV, T=300 K

Library	Energy [eV]	Γ [meV]	Γ_n [meV]	Γ_γ [meV]	$\sigma(T)$[b]
ENDF/B-VII.1	173.7	0.149333	0.007333	0.142	142.42
JEFF 3.2	173.5	0.185933	0.043933	0.142	839.94
JENDL 4.0	173.7	0.147333	0.007333	0.140	142.54

in the left plot in Figure 4.6, a plot of the ^{107}Ag capture cross section, each library also models this region differently, so none of the libraries agree with each other either. JEFF 3.2 begins the unresolved resonance region at 1.06 keV, above which the cross section is modeled as linear. Based on the simulations, this approach tends to estimate the capture rate relatively well. ENDF/B-VII.1 starts the unresolved resonance region at 6.5 keV for ^{107}Ag and 7 keV for ^{109}Ag, so below 6.5 keV, resonances are modeled explicitly. However, ENDF/B-VII.1 seems to under-predict the capture rate in this region, meaning resonances may be incorrect or may be missing. JENDL 4.0 evaluators ran into a similar issue, and added artificial p-wave resonances between 1.28 keV and 2.64 keV to better reproduce the capture rate found by Macklin[46]. Based on these results, the JENDL 4.0 library produces results similar to the JEFF library. As shown in the right plot of Figure 4.6, ^{109}Ag was modeled the same way in this region, with JEFF 3.2 starting the unresolved resonance region earlier than JENDL 4.0 and ENDF/B-VII.1, and JENDL 4.0 adding artificial resonances from 1.25 keV to 2.59 keV to help match Macklin's data[46]. Based on these measurements, the discrepancies between the three libraries, and the high probability of missing resonances for these two isotopes, it might be useful to make another high accuracy resonance region capture cross section measurement of both ^{107}Ag and ^{109}Ag, specifically targeting the 100 eV - 20 keV region.

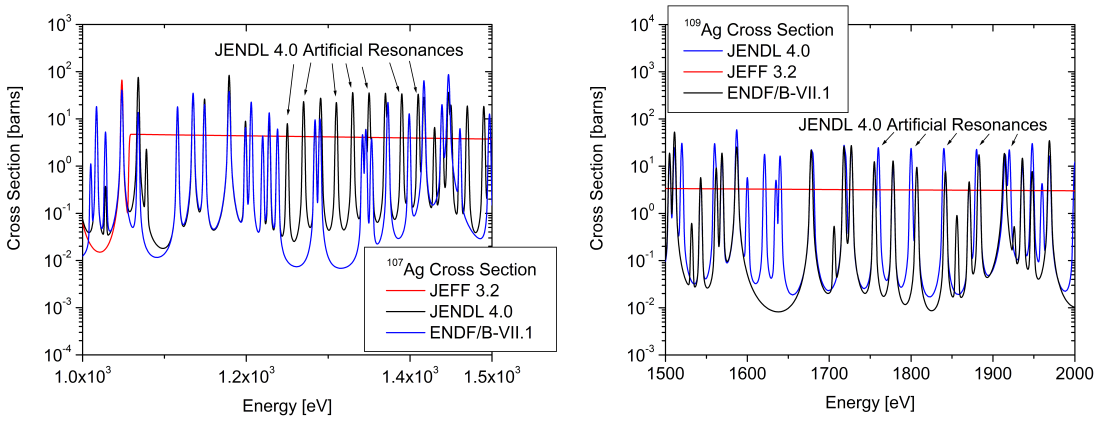

Figure 4.6: Left: Neutron capture cross section from the ENDF/B-VII.1, JEFF 3.2, and JENDL 4.0 libraries for ^{107}Ag from 1 keV to 1.5 keV. Right: Neutron capture cross section from the ENDF/B-VII.1, JEFF 3.2, and JENDL 4.0 libraries for ^{109}Ag from 1.5 keV to 2 keV.

4.1.4 Gold Measurements

Measurements of gold are presented in Figure 4.7. Simulations and experimental results match reasonably well. However, there is a large discrepancy from roughly 15 eV to 40 eV - this is mostly due to two reasons: room return of epithermal neutrons causing more captures at this time filling in this region and a low signal to background ratio in this region. Additionally, due to differences in modeling between the three libraries, there are discrepancies in expected capture rate between the libraries in the region of 2 keV to 5 keV. Each library begins the unresolved resonance region at a different energy (5 keV for ENDF/B-VII.1, 2 keV for JEFF 3.2, and 2.3 keV for JENDL 4.0), as is shown in Figure 4.8. In this region, JEFF 3.2 seems to perform the best, followed by ENDF/B-VII.1. However, JENDL 4.0 and JEFF 3.2 are nearly identical after 2.3 keV, and JENDL 4.0 is similar to ENDF/B-VII.1 from 2 keV to 2.3 keV. This likely means that the cross sections for ENDF/B-VII.1 and JENDL 4.0 are too high in the 2 keV - 2.3 keV region, and from 2.3 keV to 5 keV, the ENDF/B-VII.1 cross section is too low (particularly right before 5 keV, where the cross section is near zero for a wide region). An accurate resonance region measurement from 1 keV - 10 keV may help to fix these discrepancies.

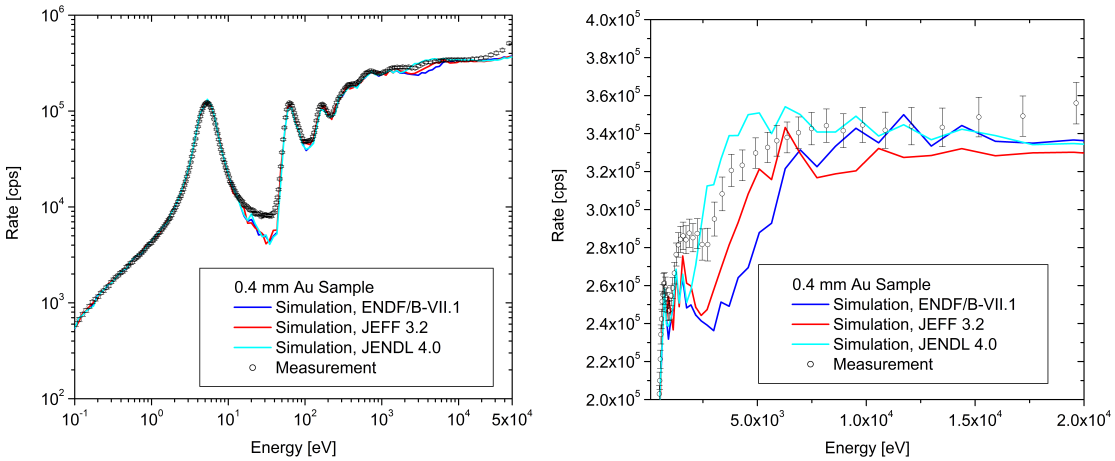

Figure 4.7: Left: Measurement of a 0.4 mm gold sample, one 2mm YAP detector and MCNP simulations using ENDF/B-VII.1, JEFF 3.2, and JENDL 4.0 libraries. Right: Same data, zoomed in to highlight discrepancies.

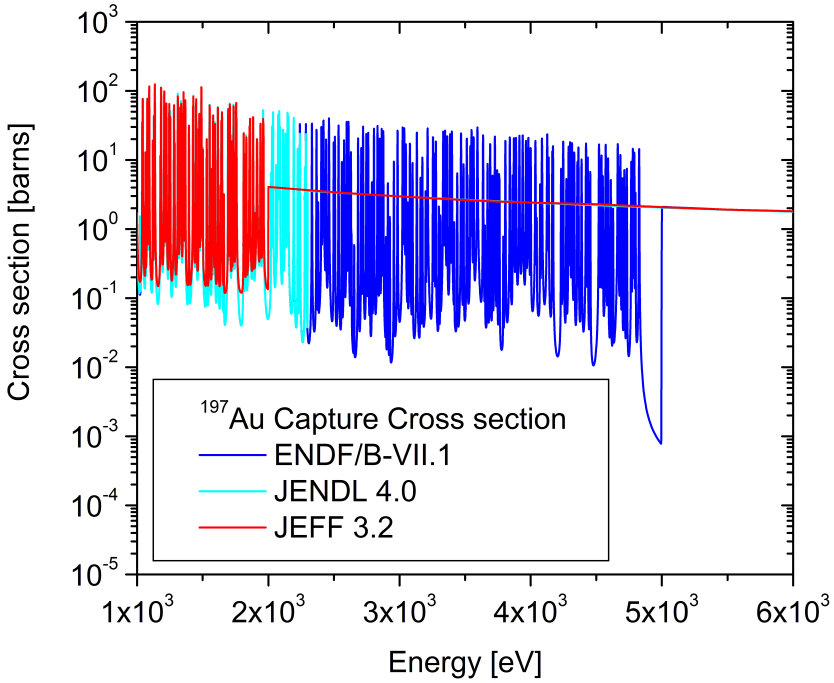

Figure 4.8: Neutron capture cross section from the ENDF/B-VII.1, JEFF 3.2, and JENDL 4.0 libraries for ^{197}Au.

4.1.5 Niobium Measurements

Measurements of niobium are shown in Figure 4.9. Niobium has one stable isotope (^{93}Nb) with a very low capture cross section in the thermal region. Niobium is also used in some zirconium alloys (including ZIRLO [47] and M5[48]) which are used in nuclear reactors for cladding materials and structural components. In many ways, this was a stress test on how low of a capture cross section could be accurately measured with this method. It's easy to see that at 70 eV and below 20 eV, the measurement does not accurately follow the simulated response, this is due to small difference in the count rate between the sample and background measurements in those region. In regions where the cross section is higher though, the experiment and simulation agree quite well (up until a few keV). If this measurement (and background measurement) were taken for a longer amount of time (or at a higher current, or with a larger scintillator), it might be possible to make a more accurate measurement of the low energy/low capture cross section region of niobium.

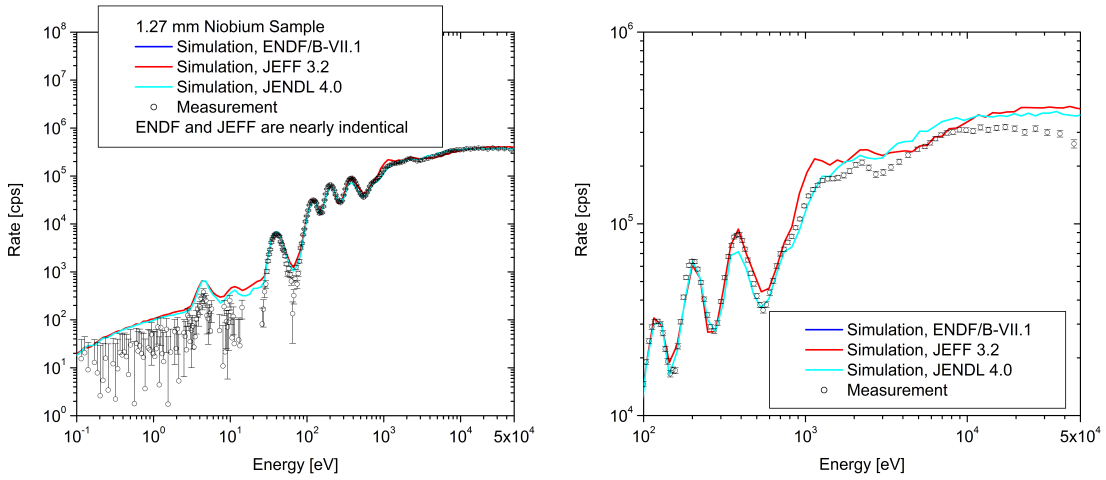

Figure 4.9: Left: Measurement of a 1.27 mm niobium sample, one 2mm YAP detector and MCNP simulations using ENDF/B-VII.1, JEFF 3.2, and JENDL 4.0 libraries. Right: Same data, zoomed in. Note: ENDF/B-VII.1 and JEFF 3.2 are identical.

At higher energies, there are some discrepancies between JENDL 4.0 and ENDF/B-VII.1 (JEFF 3.2 is identical to ENDF/B-VII.1). In the range of 100 eV to 1 keV, there is a strange phenomena, where the measurement seems to track

the expected capture rate from the JENDL 4.0 simulations where the JENDL 4.0 cross section is low - and it tracks ENDF/B-VII.1 when the capture cross section is high (eg. where there is a resonance). This seems to be caused by differences in the JENDL 4.0 and ENDF/B-VII.1 capture cross sections; in this region, the capture resonances are higher in ENDF/B-VII.1 than in JENDL 4.0, and the valley between resonances is lower in JENDL 4.0 than in ENDF/B-VII.1, as shown in Figure 4.10. The right side plot of Figure 4.10 shows just the 378.47 eV resonance in JENDL 4.0 and ENDF/B-VII.1, and it's easy to see that JENDL 4.0 has a much larger scattering cross section in this resonance (nearly 150 barns larger than ENDF/B-VII.1) and JENDL 4.0 has a smaller capture cross section (roughly 25 barns smaller). These two differences drastically lower the expected capture rate in the simulation at this resonance in JENDL 4.0. There are similar differences between ENDF/B-VII.1 and JENDL 4.0 at other resonances (eg. near 1010 eV). Above 1 keV, the data still matches relatively well, but may not be accurate above 10 keV.

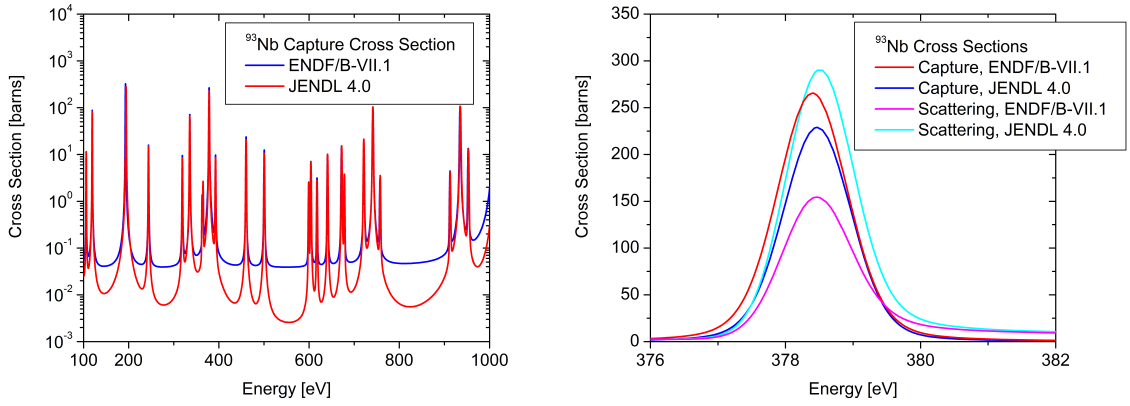

Figure 4.10: Left: ENDF/B-VII.1 and JENDL 4.0 capture cross section libraries for ^{93}Nb. Right: ENDF/B-VII.1 and JENDL 4.0 capture and scattering neutron cross section libraries at the 378.47 eV resonance of ^{93}Nb.

ENDF/B-VIII.b4 seems to have copied the JENDL 4.0 evaluation, but based on this data, ENDF/B-VII.1 does a better job estimating certain resonances in ^{93}Nb. A new evaluation of ^{93}Nb could be performed to reconcile the differences between JENDL 4.0 and ENDF/B-VII.1 and bring them in alignment with these measurements.

4.1.6 Tin Measurements

Tin was also measured and the result of this measurement can be found in Figure 4.11. Tin, like molybdenum, has many stable isotopes. This is may be the explanation for the difference near 60 eV between the experiment and simulation. The resonance near 40 eV is from ^{117}Sn, and the resonance near 60 eV is from ^{124}Sn; since these resonances are from two seperate isotopes, it's possible that the difference in efficiency between the two explains this discrepancy. The resonance near 110 ev is from ^{116}Sn, and the resonance near 200 eV is from ^{117}Sn (which the measurement greatly over-predicts the simulations). There is a large resonance in ^{118}Sn near 360 eV which is significantly different between ENDF/B-VII.1 and JEFF 3.2/JENDL 4.0. JEFF and JENDL model this capture cross section as nearly 550 barns, whereas ENDF models it closer to 330 barns. The difference stems from a large discrepancy in the Γ_γ value for the resonance, JEFF and JENDL have a value of 0.085 eV and ENDF has a value of 0.045 eV. This difference can be seen clearly in Figure 4.11, however, the measurement is lower than all three libraries.

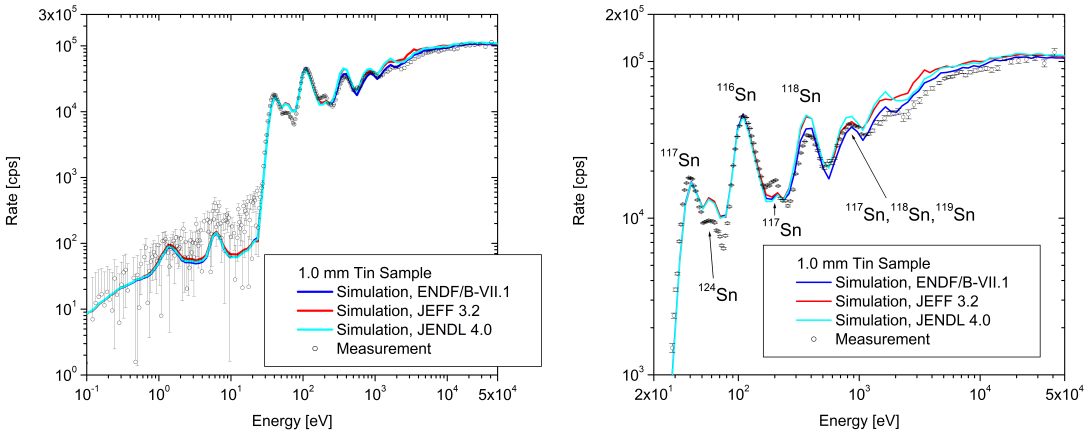

Figure 4.11: Left: Measurement of 1.0 mm tin sample compared to MCNP simulations using ENDF/B-VII.1, JEFF 3.2, and JENDL 4.0 libraries. Right: Zoomed in to highlight differences.

Near 800 eV, there is another discrepancy between the various libraries: in ENDF/B-VII.1, ^{118}Sn's capture cross section at the 771 eV resonance is 96 barns, whereas in JEFF 3.2 and JENDL 4.0, the cross section is over 170 barns. JEFF and JENDL also have an additional 30 barn resonance in ^{118}Sn at 784 eV which is

not present in ENDF. But due to the resolution of the LSDS, there are also other overlapping resonances: ^{117}Sn has a resonance at 813 eV, which in JENDL and ENDF is 103 and 94 barns respectively, but in JEFF, this resonance is 36 barns. To make things a little more complicated, there is also a resonance in ^{119}Sn which ENDF and JENDL model as 95 barns, but JEFF models as 44 barns. When these resonances are effectively broadened due to the LSDS resolution function, the result is JENDL modeling the largest capture rate, followed by JEFF and ENDF, with the measurement fitting between the JEFF and ENDF capture rates.

Because tin has so many isotopes, and the efficiency to detect each of them likely varies widely, it's not possible to draw definitive conclusions from this measurement about which library performs the best and where improvements could be made. However, if samples of separated isotopes were available to be measured, this technique could be used to find and correct some of the discrepancies between nuclear data libraries.

Also, like niobium, tin has a low thermal capture cross section. Because of this, the low energy region has a significant amount of statistical noise. That said, there is relatively good agreement between the simulation and experiment for tin.

4.1.7 Zirconium Measurements

Zirconium was also measured and the result of this measurement can be found in Figure 4.12. Zirconium also has a low thermal capture cross section and many isotopes. And so, like tin, the low energy region has a significant amount of noise. However, above 120 eV, the experiment and simulation match well.

At roughly 180 eV, the experiment capture rate is much higher than the simulated capture rate for all three nuclear data libraries - although it's hard to tell from the simulations, there is a resonance in ^{91}Zr at 182 eV of close to 120 barns. Like the ^{117}Sn resonances in tin, it's possible that the efficiency to detect this isotope is much higher than the efficiency to detect other isotopes, and that's the cause of the discrepancy.

There is some disagreement between the three nuclear data libraries at 681 eV, which can be seen in the right plot of Figure 4.12. ENDF/B-VII.1 and JEFF

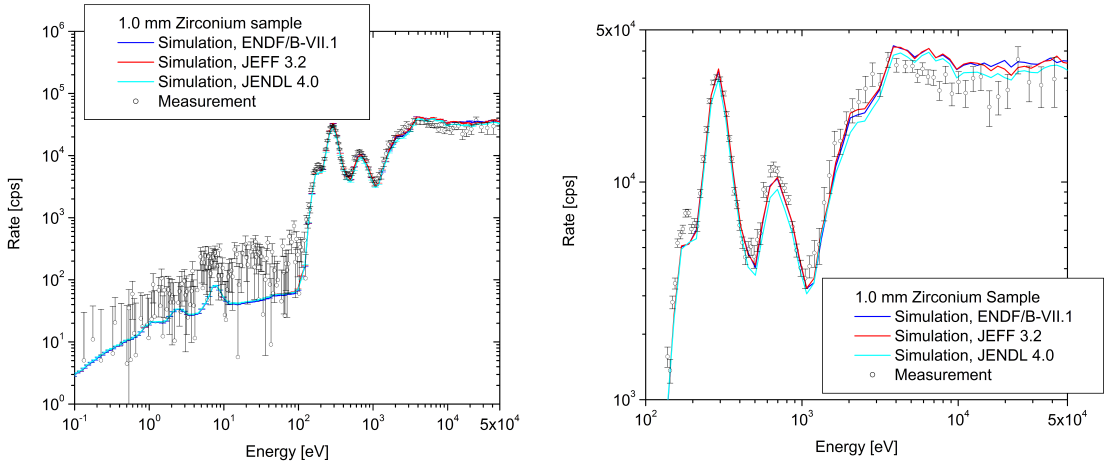

Figure 4.12: Left: Measurement of a 1.0 mm zirconium sample, one 2mm YAP detector compared to simulations using ENDF/B-VII.1, JEFF 3.2, and JENDL 4.0 libraries. Right: Zoomed in to highlight differences.

3.2 model a resonance in ^{91}Zr as 145 barns, and JENDL 4.0 models it as 131 barns (ENDF and JEFF have the same Γ_γ and Γ_n values for this resonance, both values are lower in JENDL). If the efficiency to detect captures from ^{91}Zr is indeed higher than it is for other isotopes of Zr, then this measurement can not say which library is more accurate for this resonance. Again, measurements of separated isotopes may be able to answer this question.

4.1.8 Indium Measurements

A 0.6 mm indium sample was also measured, and the results of these measurements are shown in Figure 4.13 and Figure 4.14. Indium has two stable isotopes, ^{113}In (4.28% abundance) and ^{115}In (95.72% abundance). Because it only has two isotopes which are close together, the efficiencies to detect those two isotopes should be quite similar, and inferences should be able to be drawn from these measurements.

Starting from the bottom of the energy spectrum, there is a difference in the thermal region. This could be explained by an incorrect subtraction of constant background due to the activity of the sample - indium becomes activated when exposed to neutrons, and was highly activated at the end of the LSDS measurement. That said, the silver sample was also highly activated and the same method was used

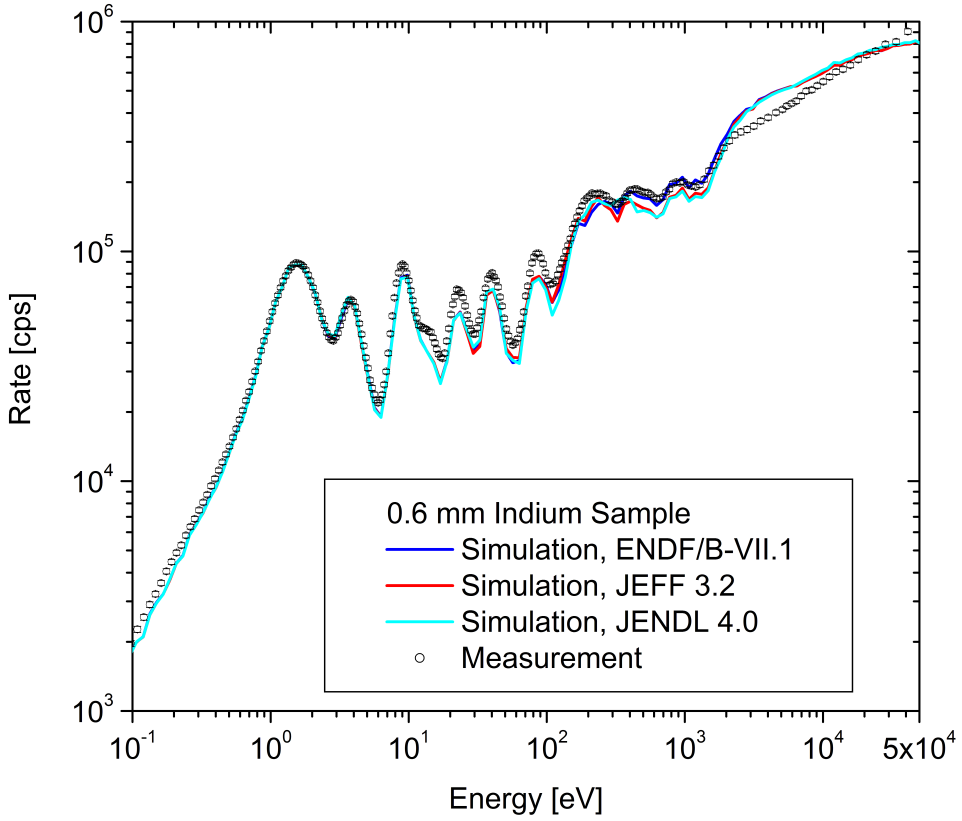

Figure 4.13: Measurement of a 0.6 mm indium sample, one 2mm YAP detector, compared to MCNP simulations using ENDF/B-VII.1, JEFF 3.2, and JENDL 4.0 libraries.

to subtract out the activation for silver, and this method seemed to work well. Since thermal cross sections are well known for most materials, this is not likely a mistake in the nuclear data.

Moving to higher energies, as is shown in Figure 4.14, the measurement and MCNP agree very well for the first (1.4 eV) and second (3.8 eV) large resonances in indium (these two are predominantly resonances in ^{115}In). For the next few resonances though (9 eV, 14.5 eV, 21-25 eV, 40 eV, 83 eV), the measurement has a higher capture rate than the simulations. One theory that would help explain this anomaly is that there is more moderation in the physical LSDS than there is in the simulation, and even if a few extra percent of neutrons are lower energy, these neutrons would be absorbed in the large first resonance of indium - increasing the

detected capture rate at these higher energies. This particular measurement would be extremely sensitive to changes in moderation, and extra moderation would also help explain the additional captures in the gold measurement (Figure 4.7) in the valley just before the large resonance.

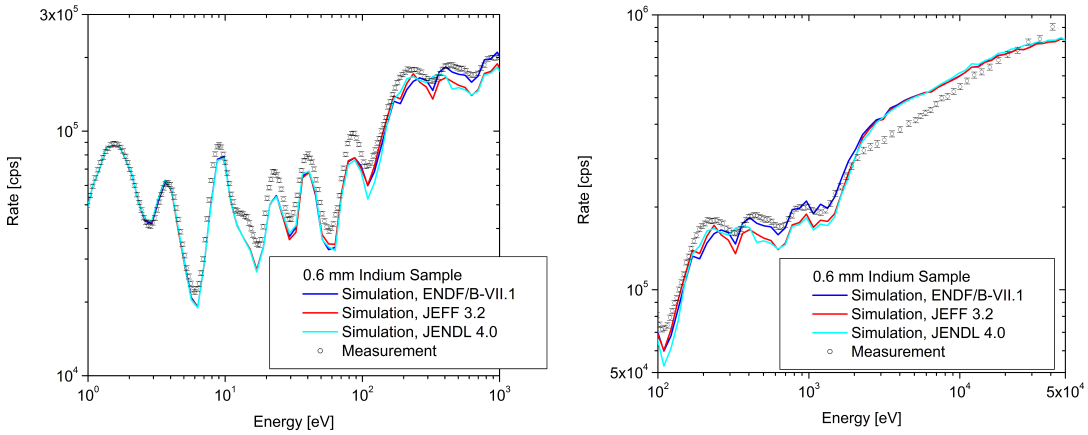

Figure 4.14: Measurement of 0.6 mm indium sample compared to MCNP simulations using ENDF/B-VII.1, JEFF 3.2, and JENDL 4.0 libraries. Left: Zoomed in to show differences in the eV region. Right: Zoomed in to show differences in the keV region.

To test this theory, an additional simulation was performed using the JEFF 3.2 library and increasing the hydrogen content of the lead in the LSDS to 2 part per million (ppm), from 1 ppm, the results of which are shown in Figure 4.15. Original value of 1 ppm was taken from a chemical analysis of one of the lead bricks which was performed in 2012 (see Section A.1 in Appendix A for more information). However, in Becker et al.[33], it was found that by modifying the hydrogen content of the LSDS to 1.8 ppm of hydrogen, better agreement was found between the measurements and simulations[9].

As is shown in shown in Figure 4.15, moving to 2 ppm of hydrogen has a significant impact on the resolution of the system. The 2 ppm simulation no longer agrees with the measurement in the first two resonances, but has better agreement

[9]In Becker et al., measurements were of nondestructive assay of fissile materials, using the LSDS flux to induce fissions in the fissile material and then measuring the prompt neutrons emitted from those fissions. While this is a different measurement, the hydrogen content of the LSDS, and therefore the neutron energy resolution of the LSDS should be similar between the two measurements.

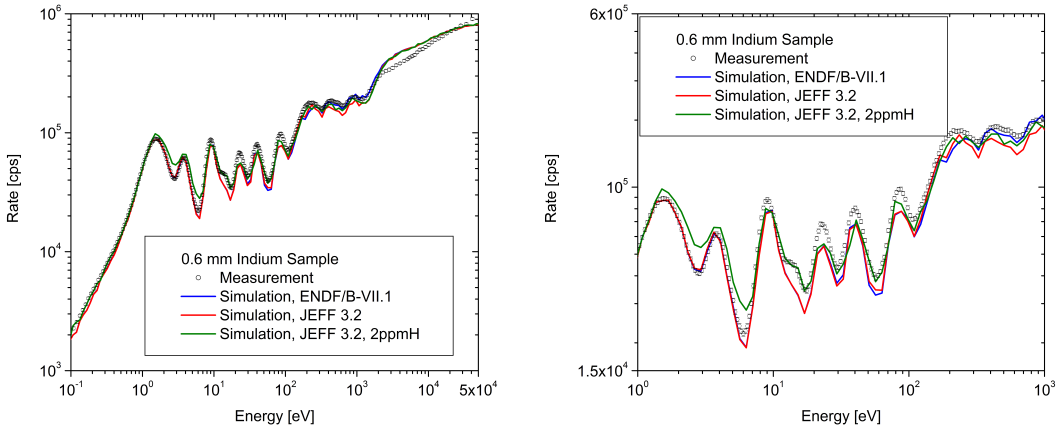

Figure 4.15: Comparison between measurement of 0.6 mm indium sample and to MCNP simulations using 1 ppm of hydrogen and 2 ppm of hydrogen in the LSDS. Right: Zoomed in to show differences in the eV region.

in other regions, particularly between 10 and 18 eV and in the valleys between the 21-25 eV, 40 eV, 83 eV resonances. But even adding this much hydrogen to the LSDS does not make the simulation match at the peaks of these resonances. So it's likely that extra moderation is the cause of these discrepancies, but that the extra moderation is coming from a different source, for example, additional Teflon tape near the sample or additional room return. This issue should be looked at in the future if additional measurements are performed. It should be noted that the change in hydrogen concentration made only minor impacts above 1 keV and below 1 eV, and the difference in above 2 keV between the simulations and measurement still persist in the 2 ppm hydrogen simulation.

At higher energies (above 100 eV), the measurement and simulations begin to agree again, with ENDF/B-VII.1 agreeing the best in most regions, although there are significant differences between the three neutron cross section libraries. Above 2 keV however, there is a large discrepancy between the simulations and the experimental results - this happens to coincide with the beginning of the unresolved resonance region. This seems to be evidence that the cross section in the unresolved resonance region of indium may be too high.

4.1.9 Iron Measurements

A 1.0 mm indium sample was also measured, and the results of these measurements are shown in Figure 4.16. Iron has four stable isotopes and relatively low capture cross section; at 100 eV, the capture cross section of natural Iron is just 38 millibarns. So aside from the 63 barn resonance in ^{56}Fe at 1.15 keV, iron is one of the test cases for measuring small cross sections.

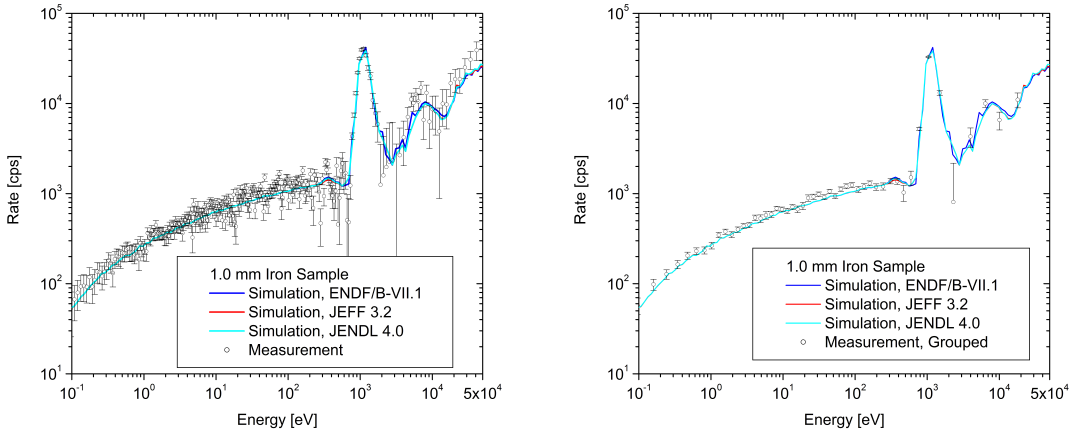

Figure 4.16: Left: Measurement of a 1.0 mm iron sample, one 2mm YAP detector compared to simulations using ENDF/B-VII.1, JEFF 3.2, and JENDL 4.0 libraries. Right: Same data, but more aggressively grouped to smooth out the low energy region.

As expected, there is a considerable amount of noise in the measurements, so to try to smooth out the data, the data was grouped more agressively, and the results of this can be seen in the right plot of Figure 4.16. With the extra grouping, the measurement data fits the simulation very well. This demonstrates that the method for measuring capture cross sections is working, even for samples with very small cross sections. Additionally, with more data (either with longer run times, higher fluxes, a thicker sample, or larger detectors), it would be possible to make a more accurate measurement of the small capture cross section of iron with the LSDS.

4.1.10 Cobalt Measurements

An 0.6 mm cobalt sample was also measured, and the results of these measurements are shown in Figure 4.17. Cobalt has one stable isotope, ^{59}Co with a rather large cross section. The measurement of cobalt also has the valley between the first and second resonance filled in, similar to gold. At the higher energy region (ie. above 10 keV), the measurement results are substantially higher than the simulated capture rate for JEFF 3.2, and the measurement results are also higher than the simulated capture rate for JENDL 4.0 and ENDF/B-VII.1, indicating that the capture cross section in this region might be too low for all three libraries.

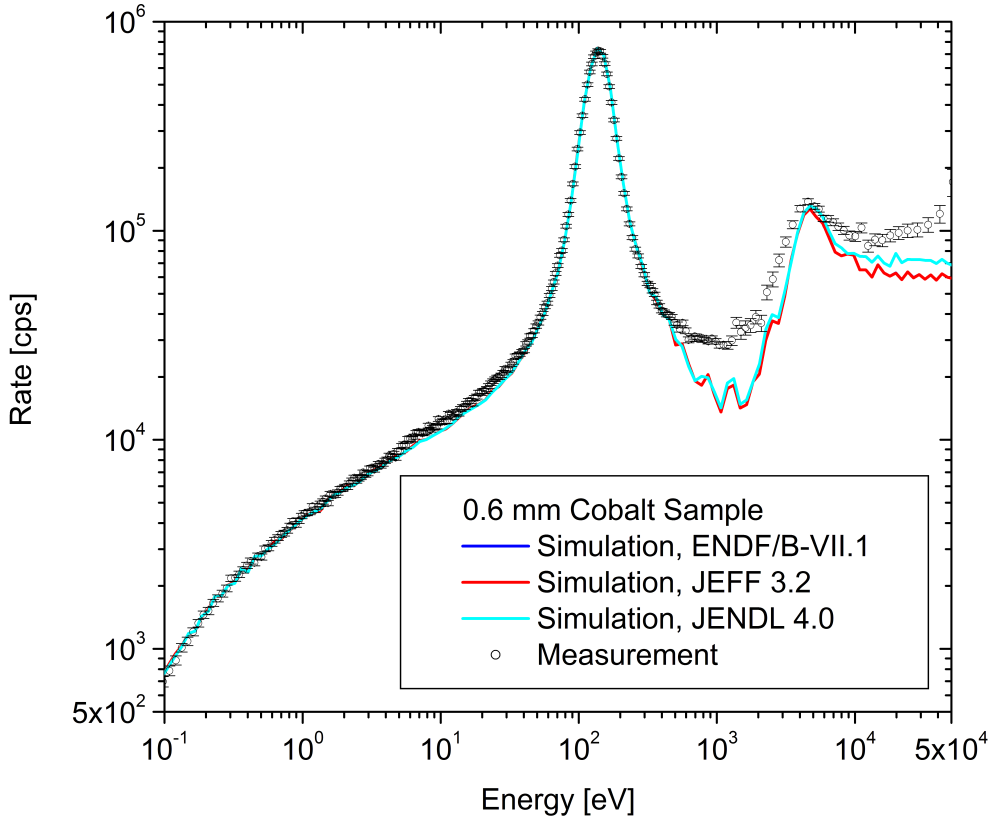

Figure 4.17: Measurement of a 0.6 mm cobalt sample, one 2mm YAP detector, compared to MCNP simulations using ENDF/B-VII.1, JEFF 3.2, and JENDL 4.0 libraries. ENDF/B-VII.1 and JEFF 3.2 are nearly identical.

4.1.11 Molybdenum Measurements

A 1.0 mm molybdenum sample was also measured, and the results of these measurements are shown in Figure 4.18 and Figure 4.19. Molybdenum has seven stable isotopes (92, 94, 95, 96, 97, 98, 100), each with their own binding energy and therefore, their own efficiency to be detected. This can be seen easily in the left plot of Figure 4.19, where each of the first few large resonances comes from a different isotope. Because of this, the experiment and simulation differ slightly on each of these resonances; for some the measurement is too high, and for others, the measurement is too low.

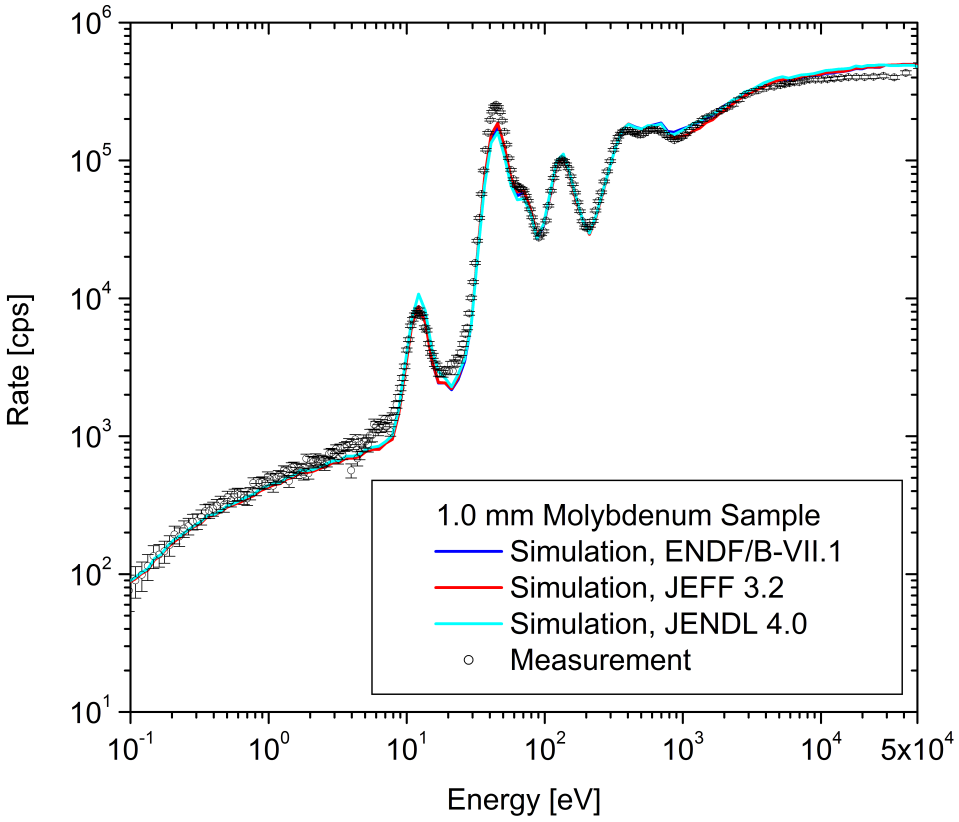

Figure 4.18: Measurement of a 1.0 mm molybdenum sample, one 2mm YAP detector, compared to MCNP simulations using ENDF/B-VII.1, JEFF 3.2, and JENDL 4.0 libraries.

In the high energy region, plotted in the right plot of Figure 4.19, the measurement and simulation follow each other closely even into the keV region. The resolved resonance region for ^{97}Mo ends at 2 keV, ^{95}Mo ends at 2.15 keV, ^{96}Mo ends

at 19 keV, ^{94}Mo ends at 20 keV, ^{100}Mo ends at 26 keV, ^{92}Mo ends at 40 keV. It's possible that the differences between the measurement and simulations above 3 keV is due to differences in efficiency to detector the various isotopes, but the widening of the gap above that is not easily explainable.

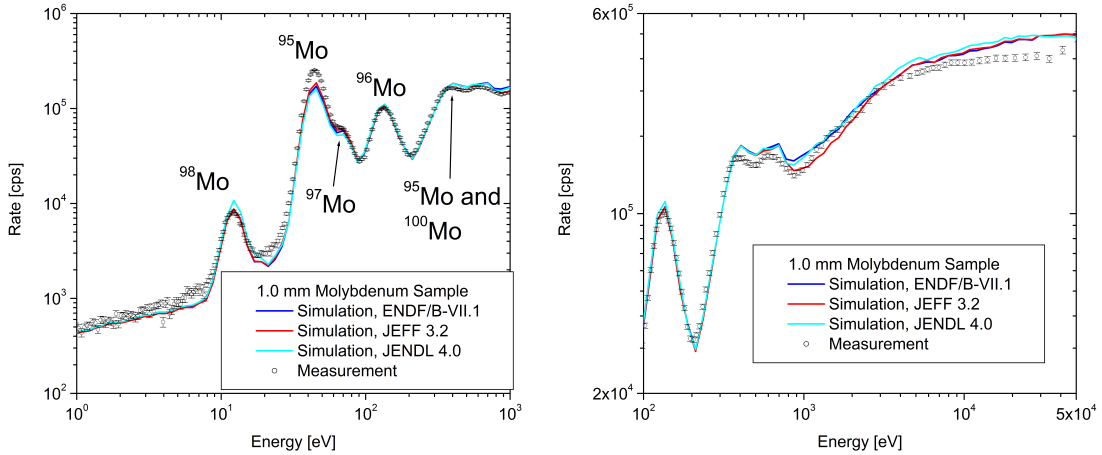

Figure 4.19: Measurement of a 1.0 mm molybdenum sample, one 2mm YAP detector compared to simulations using ENDF/B-VII.1, JEFF 3.2, and JENDL 4.0 libraries. Left: Zoomed in on the eV region. Right: Same data, highlighting the keV region.

4.1.12 Carbon Measurements

The sample with the absolute lowest capture cross section that was measured was carbon. Over the energy region investigated, the capture cross section of carbon varies from 2 mb to 11 μb. Unsurprisingly, the measurement was unsuccessful because the background count rate was orders of magnitude higher than the number of expected captures in the carbon sample. Because of this, the background subtracted spectra is near zero for most of the energy region. For the sake of completeness, the results of this measurement are included and are shown in Figure 4.20.

For many of the measurements of samples with small cross sections (eg. low energy regions of tin, zirconium, nickel, niobium), it's plausible that with larger samples and/or longer collection times, accurate data could be collected. The same can not be said for carbon, the capture cross section is simply too low to be measured using this method. There is more discussion of this topic in Section 4.3.1.

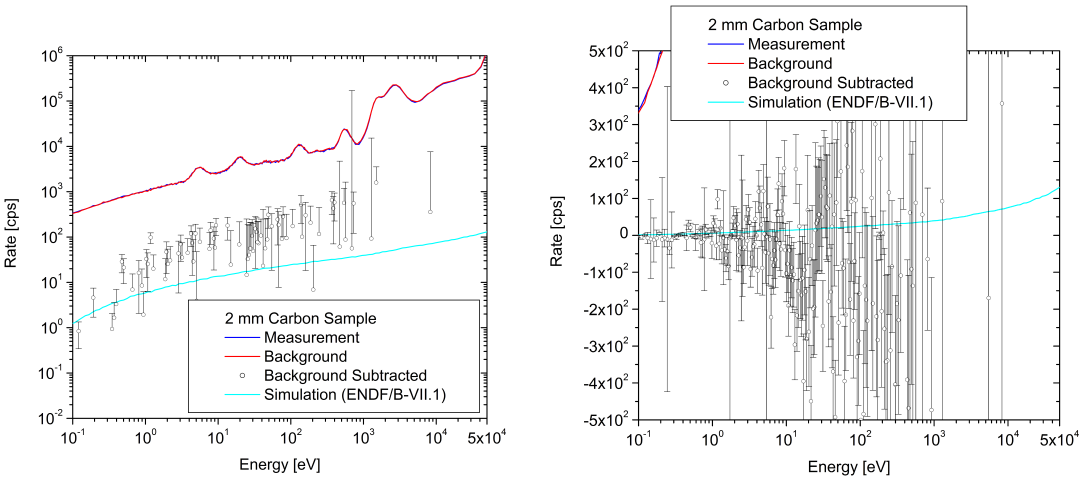

Figure 4.20: Measurement of 2.0 mm carbon sample compared to an MCNP simulation using ENDF/B-VII.1. Left: Log-Log plot showing the entire energy region. Note, the capture rate in carbon is so low that the sample and background measurements are nearly identical. Also note that in this figure, if there are no error bars below the data point, that means the error bar is a negative value and can could not be plotted. Right: The same plot, but with a linear Y-axis, to show that most of the data points are near zero.

4.2 Coincidence Measurements

As was stated before, coincidence measurements were taken as part of this project, with the goal of getting a significantly better signal to noise ratio for more accurate measurements of samples with low cross sections. This was indeed the case, and Figure 4.21 shows the improvement in signal to background ratio (roughly a factor of four improvement).

However, the count rate also dropped significantly (as the coincidence rate was much smaller that the single detector rate). This can be seen in Figure 4.22, where the count rate is roughly an order of magnitude lower. This low count rate, coupled with other difficulties in repeatability of measurements, made coincidence measurements unfavorable for later measurements. The coincidence timing window was 15 ns, Figure 4.23 is an example coincidence timing plot with a ^{60}Co source.

Due to the much improved signal to background ratio, this means that small samples and samples with smaller cross sections could be measured using an LSDS

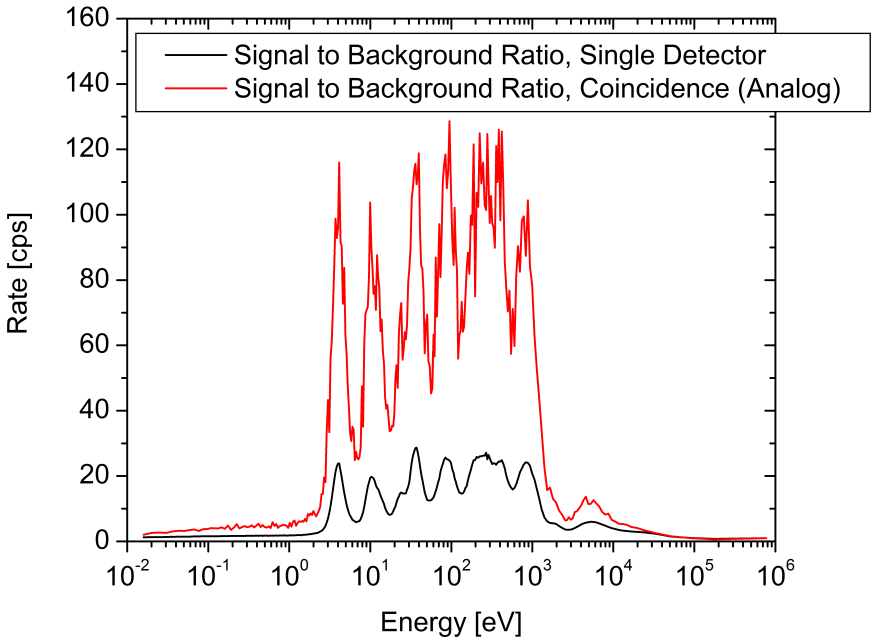

Figure 4.21: Comparison between the signal to background ratio for coincidence measurements and single detector measurements (same data as Figure 4.22).

with coincidence, but since the count rate was much lower, these measurements would take significantly more time, on the order of ten times longer (a measurement which took 30 minutes without coincidence would take 5 hours using coincidence).

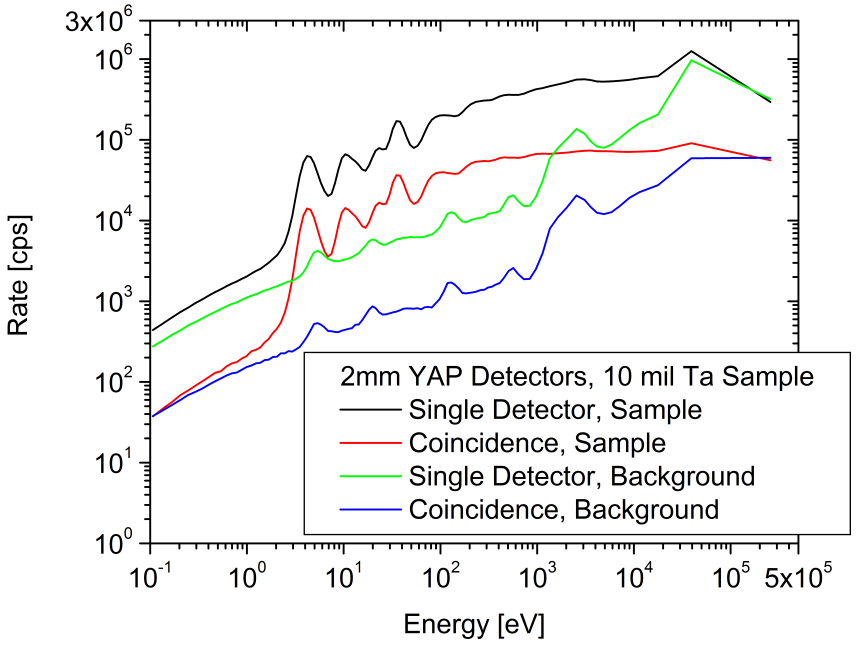

Figure 4.22: Measurement of a tantalum sample and background, comparing the single detector count rate and coincidence count rate.

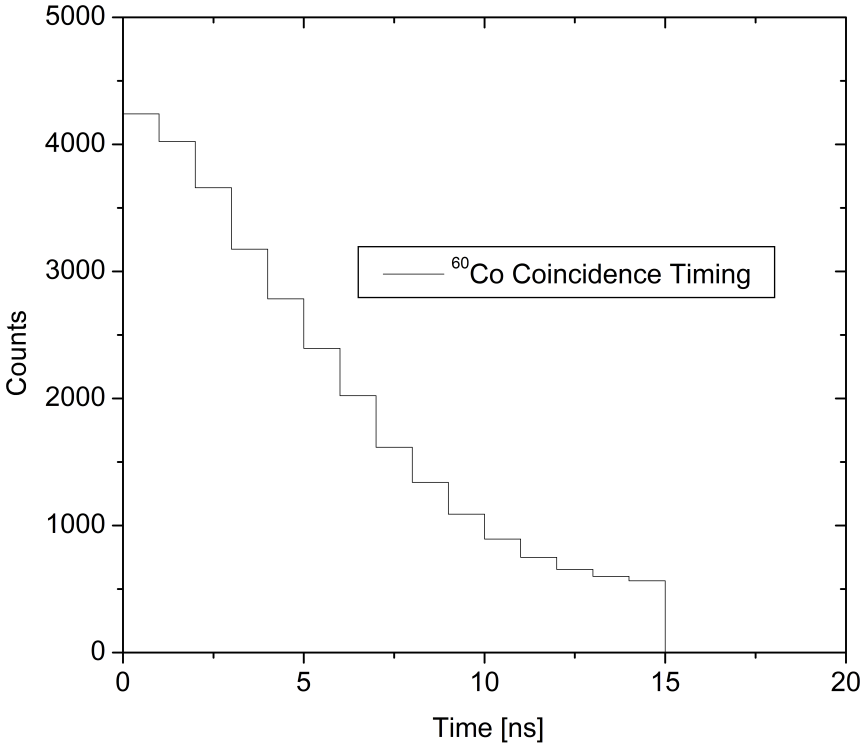

Figure 4.23: Measurement of a tantalum sample and background, comparing the single detector count rate and coincidence count rate.

4.3 Cross Section Results

In addition to comparing measurement capture rates to simulations, measurement data were also converted to cross sections (see Section 3.3.3 for more information on this process).

4.3.1 Minimum Cross Section

The technique of using Lead Slowing-Down Spectrometers to measure neutron capture cross sections was originally pioneered (almost exclusively) by a number of researchers in Russia (then the USSR) in the 1950's and 1960's. Two of those researchers, Popov and Shapiro in 1961 proposed a minimum cross section that could be measured using this method[25], reproduced below as Equation 4.1:

$$\begin{aligned} \sigma_\gamma &> 0.2E^{-\frac{1}{2}} \text{ barn for E} < 1\text{keV}, \\ \sigma_\gamma &> E^{-\frac{1}{2}} \text{ barn for E} > 1 \text{ keV}. \end{aligned} \tag{4.1}$$

This set of measurements pushes beyond these limits by attempting to measure multiple materials with cross sections lower than Equation 4.1. Figure 4.24 compares the minimum cross section from 4.1 to the ENDF/B-VII.1 broadened capture cross sections for zirconium, tin, niobium[10], nickel, and iron. Each of these materials have capture cross sections that are near or below the Popov and Shapiro limit.

Figure 4.25 shows the broadened cross section calculated of natural tin, based on a measurement of a 1.0 mm sample of tin (see capture rate measurement in Section 4.1.6). The error bars in this plot were calculated based on the relative error in the capture rate, and are most likely much larger as multiple effects are not being accounted for (eg. multiple scattering, resonance self shielding). That said, given there were significant disagreements between the measured and simulated capture rate, the calculated broadened cross section does a reasonably good job at matching the ENDF/B-VII.1 broadened cross section.

[10]Popov and Shapiro[25] did measure niobium, but could not resolve and did not report cross sections for niobium below 15 eV, their minimum measurable cross section formula is partially based on that measurement.

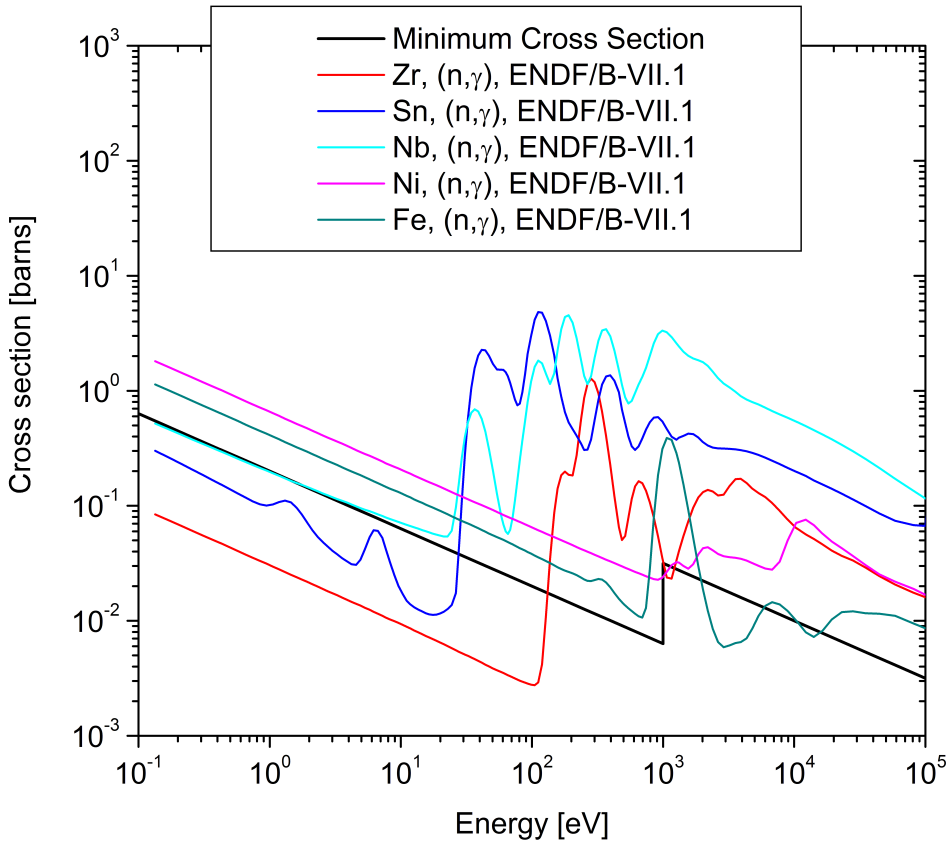

Figure 4.24: The minimum cross section from 4.1 compared to broadened ENDF/B-VII.1 cross sections of zirconium (Zr), tin, (Sn), niobium (Nb), nickel (Ni), and iron (Fe).

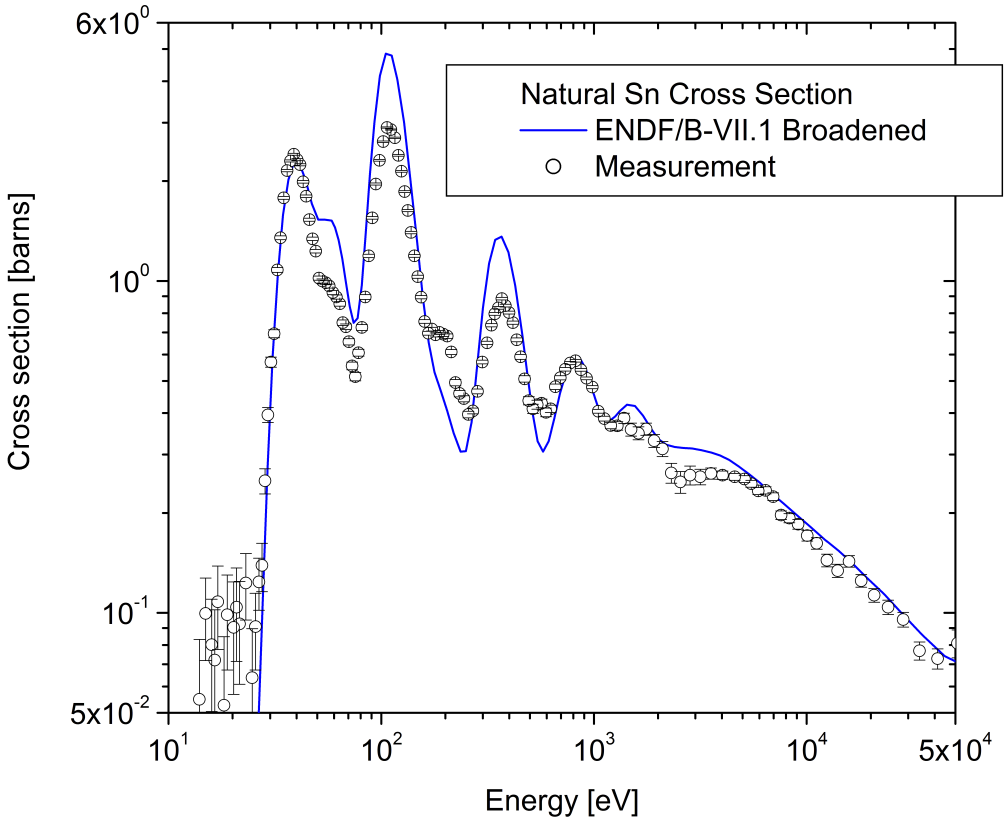

Figure 4.25: Broadened capture cross section of tin calculated from measurement of 1.0 mm tin sample compared to ENDF/B-VII.1 natural broadened capture cross section.

4.3.2 Limitations

While some of the above results agree very well, for samples with larger cross sections, disagreements were found between the broadened cross section found via measurement and broadened cross section libraries. For example, Figure 4.26 is a plot of the calculated and measurement generated broadened cross section for silver. While the high energy region (above 1 keV), the low energy region (below 1 eV), and the first large resonance (5 eV) agree very well, in regions where there are multiple resonances (10 eV to 1 keV), resonance self shielding is occurring, artificially bringing down the calculated cross section. In fact, the same process used to generate the measurement broadened cross section can be applied to the simulation result (resonance self shielding between 10 eV and 1 keV), which should not be surprising, because the simulation and measurement agree very well in this region. This further demonstrates that MCNP is accurately simulating these interactions.

In future measurements, it would be useful to select sample thicknesses by calculating the expected transmission (T(E) = $e^{-N\sigma_t(E)x}$, see Section 3.3.3) through the sample using MCNP - as a best practice, if the transmission falls below 0.8, a thinner sample should be selected. As can be seen in Figure 4.26, the transmission falls well below this value in the region where resonance self shielding is occurring. This may mean that measurements of different sample thicknesses are needed to measure different energy regions.

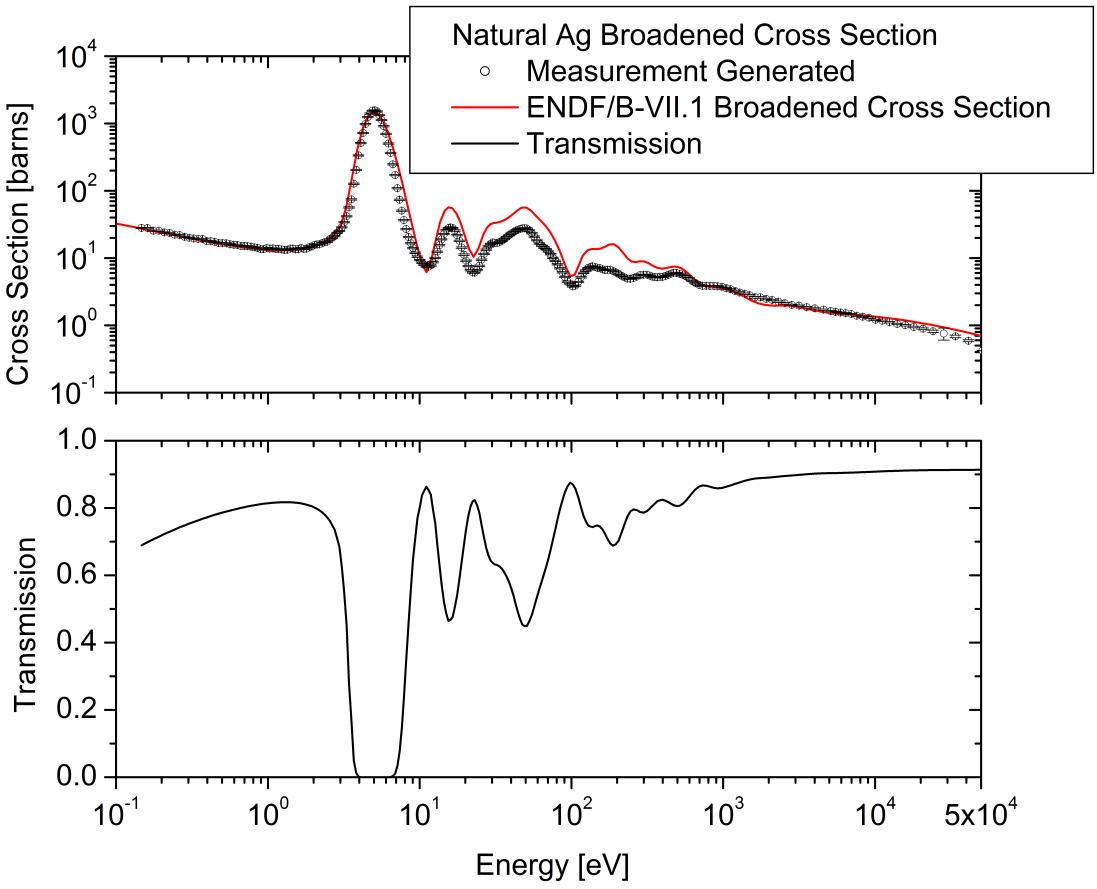

Figure 4.26: Top: Natural silver broadened capture cross section generated from measurement results compared to ENDF/B-VII.1 broadened cross section. Bottom: Plot of transmission through the sample. Note that the first resonance is a "black" resonance, meaning the transmission effectively falls to zero as nearly all neutrons are interacting with the sample.

4.4 Pulse Height Weighting Results

As explained in Section 3.3.4, this work attempted to use Pulse Height Weighting to analyze measurement results. In theory, this should make the detector efficiency proportional to the incoming gamma energy, and it has been used successfully in the past[42],[49]. However, when implemented, the results changed very little, aside from the high energy region, as is seen in Figure 4.27.

Since the results changed very little in the materials studied, this means that

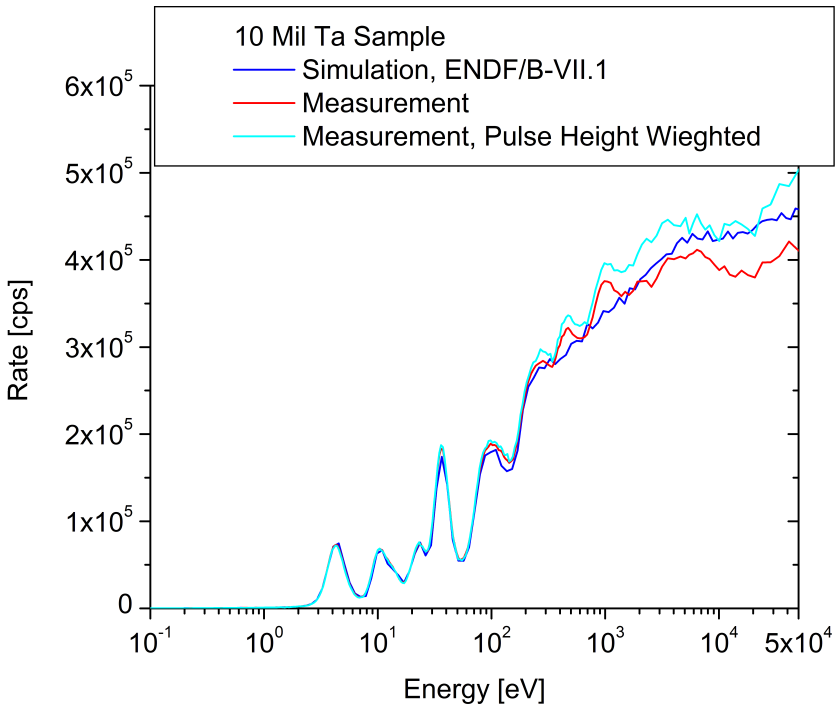

Figure 4.27: Measured capture rate, comparing analysis using pulse height weighting to not using pulse height weighting, and comparing against simulated ENDF/B-VII.1 cross section library.

there are not large changes in the gamma cascades/multiplicity over the energy region studied. This also might be partially due to the poor energy resolution of the detector, and a detector with better energy resolution might be able to distinguish small changes in gamma cascades and multiplicities.

The one region where Pulse Height Weighting did have an impact was in the high energy region. Additionally, the impact of Pulse Height Weighting seems to be proportional to the count rate. This is a sign that at high energies, there may be double pulses, where two gammas from two separate capture events interact with the detector within the same detection window (200 ns). Based on the high count rates seen, this is very likely, however, detector deadtime is already corrected for using the standard nonparalyzable formula [50]. Figure 4.28 shows the expected pileup of pulses (defined as two detector pulses in the same 200 ns window based on the count rate) and at the highest count rates, there is a large amount of pileup of pulses.

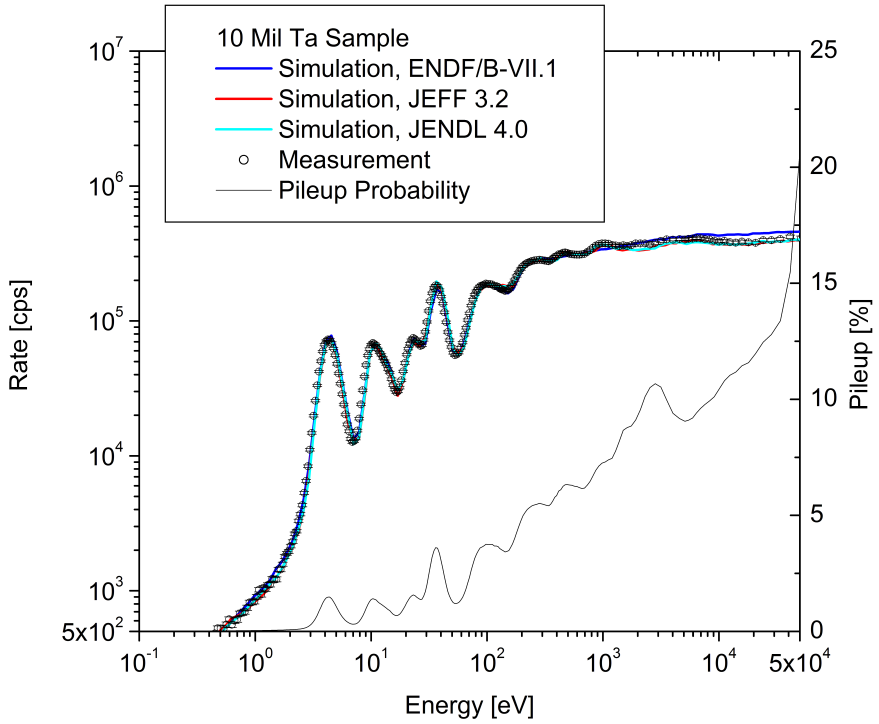

Figure 4.28: Measured capture rate, Simulations, and the expected percentage of pileup.

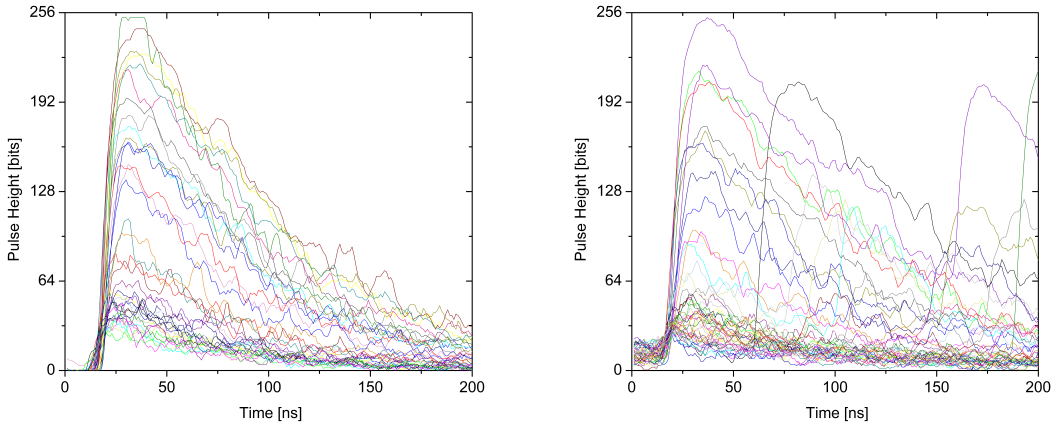

Figure 4.29: Left: 40 pulses from 97.4-99.4 μs, roughly 17 eV. Right: 40 pulses from 1.15-1.40 μs, roughly 60 keV. Note the double pulses in the graph on the right.

Giving these pulses additional weight and also correcting the data for dead-

time would be double counting these pulses, artificially bringing the count rate up. Because of this, and because there were no noticeable changes in gamma cascades and multiplicities, Pulse Height Weighting was not used.

CHAPTER 5
CONCLUSIONS AND FUTURE WORK

5.1 Conclusions

This work is important and new for a few reasons:

- based on an exhaustive survey of the literature, this was the first time that neutron capture measurements were performed with a LSDS in the United States.
- these measurements confirmed previous studies which showed that the LSDS can be a useful tool for validating capture cross sections in nuclear data libraries[29].
- these measurements can be made quickly (often in under one hour), and so many samples can be measured in a very short amount of time.
- these measurements showed that activated and radioactive samples, which may be difficult to measure using other methods, can be measured using the LSDS[11]
- this was also the first time LSDS capture data has been collected with a digital data acquisition system to collect pulse shape data, and the first time pulse height weighting has been used with LSDS capture data.
- while success was limited, this was also the first time that coincidence measurements had been performed in an LSDS while measuring capture cross sections.

[11]Two samples, silver and indium, were activated in the process of being in the LSDS neutron flux, and were quite radioactive during the measurement. The maximum radioactivity that a sample can be is related to the cross section of the material, the lower the cross section of the sample, the lower the maximum level of radioactivity that would permit a measurement. It should be easy to measure samples in the μCi range, samples in the mCi range would be tougher and might require a different/faster detection system.

- results of these measurements are already having an impact on the nuclear data, most notably with silver, where an incorrect cross section was identified and is in the process of being corrected. Additionally, differences and discrepancies between nuclear data libraries which may be hard to detect using other methods, have been identified.

To do this, an experimental system was designed from scratch. Detectors were modeled, built, and tested, a new digital data acquisition was set up, and the system was modified and optimized with each set of experiments. Once everything was working properly, measurements of twelve different materials with a wide variety of uses and characteristics were performed. In short, modern and new techniques were applied to an old and rarely used method, resulting in new and impactful data. Additionally, the impacts of varying capture gamma cascades and multiplicities were determined through the use of Pulse Height Weighting.

5.2 Future Work

An enormous number of lessons have been learned from these measurements, and with minimal work, additional measurements could be performed. Additionally, the analysis and data processing codes created have greatly streamlined the data analysis process, to the point that initial results of even large numbers of measurements can be calculated in just a few hours.

Future work on this topic should focus on measuring multiple thicknesses of different samples (especially when the cross section is very small or very large), further optimizing sample sizes and measurement times to obtain the best possible measurements, taking another look at other detectors (using the information gained from these measurements) and measurements of radioactive samples. For example, it might be possible to make an even smaller detector or segmented detector and measure cross sections to even higher neutron energies.

Additionally, these measurements showed that it might be possible to measure even smaller cross sections by using coincidence to improve the signal to background ratio. This possibility should be explored further, and needs further development. Any future coincidence system should ensure that the distance between detectors

remains constant and that the sample is held perfectly in the middle of the detectors. Additionally, this system also relies on the detectors being placed in the exact same location in the LSDS to ensure that the flux is the same.

The author would like to thank the NNSA's Stewardship Science Academic Alliance for supporting this research under grant numbers: DE-NA0002906 and DE-NA0001814.

REFERENCES

[1] N.W. Thompson et al. "Progress on using a lead slowing-down spectrometer to measure neutron capture cross section," in *12th Int. Topical Meeting on Nucl. Applicat. of Accelerators*, Washington D.C., 2015, pp. 351-354.

[2] J.J. Duderstadt and L.J. Hamilton, *Nuclear Reactor Analysis.* New York: Wiley, 1976.

[3] L. Shroeder and E. Lusk, "Report of the nuclear physics and related computational science R&D for advanced fuel cycles workshop", Office of Nuclear Physics, Office of Advanced Scientific Computing Research, US Department of Energy Office of Science, Bethesda, MD, 2006.

[4] M.B. Chadwick et al. "ENDF/B-VII.0: Next generation evaluated nuclear data library for nuclear science and technology," *Nucl. Data Sheets*, vol. 107, no. 12, pp. 2931-3060, Dec, 2006.

[5] "Computer simulations help design new nuclear reactors", Nucl. Eng. Division, Argonne National Laboratory, 2008 Available: http://www.ne.anl.gov/About/headlines/new_nuclear_age.shtml. Date Last Accessed 07/26/2017.

[6] T.K. Scheber and J.R. Harvey, "Assessment of U.S. readiness to design, develop, and produce nuclear warheads: current status and some remedial steps", National Institute for Public Policy, National Institute Press, Fairfax, VA, 2015.

[7] G. Palmiotti et al. "Requirements for advanced simulation of nuclear reactor and chemical separation plants", Nucl. Eng. Division, Argonne National Laboratory, Argonne, Illinois, ANL-AFCI-168, May, 2005.

[8] L. Bernstein et al. "Nuclear data needs and capabilities for applications," Lawrence Berkeley National Laboratory and the Nuclear Science and Security

Consortium at U.C. Berkeley. Berkeley, CA, 2015.
Available:http://arxiv.org/pdf/1511.07772. Date Last Accessed 07/26/2017.

[9] R. Bahran et al. "A survey of nuclear data deficiencies affecting nuclear non-proliferation," *2014 Inst. Nucl. Materials Manag. Annu. Meeting*, Atlanta, GA, LANL Report LA-UR-14-26531, 2014.

[10] T.A. Taiwo and H.S. Khalil, "Nuclear data needs for generation iv nuclear energy systems - summary of U.S. workshop," Nucl. Data Needs For Generation IV Nucl. Energy Syst., Proc. of the Int. Workshop, Antwerpen, Belgium, 2005.

[11] D.G. Cacuci, *Handbook of Nuclear Engineering*. New York: Springer, 2010.

[12] M.B. Chadwick et al. "ENDF/B-VII.1 Nuclear data for science and technology: cross sections, covariances, fission product yields and decay data," *Nucl. Data Sheets*, vol 112, no. 12, pp. 2887-2996, Dec, 2011.

[13] OECD/NEA. (2014). *JEFF-3.2 evaluated data library - neutron data*. [Online]. Available: https://www.oecd-nea.org/dbforms/data/eva/evatapes/jeff_32/. Date Last Accessed 07/26/2017.

[14] K. Shibata et al. "JENDL-4.0: A new library for nuclear science and engineering," *J. Nucl. Sci. Tech.*, vo. 48, no. 1, pp. 1-30, 2011.

[15] S. Glasstone and A. Sesonske, *Nuclear Reactor Engineering*. Princeton, NJ: D. Van Nostrand Company Inc., 1963.

[16] A. Vertes et al. *Handbook of Nuclear Chemistry, Volume 4: Radiochemistry and Radiopharmaceutical Chemistry in Life Sciences.* Norwell, MA: Kluwer Academic Publishers, 2003.

[17] K. Krane, *Introductory Nuclear Physics*, New York: John Wiley & Sons (1988).

[18] F. Bečvář, "Simulation of cascades in complex nuclei with emphasis on assessment of uncertainties of cascade-related quantities," *Nucl. Instruments and Methods Physics Res. A*, vol. 417, pp. 434-449, 1998.

[19] "Proceedings of the Oak Ridge Electron Linear Accelerator (ORELA) workshop," Oak Ridge National Laboratory, ORNL/TM-2005/272 Available: web.ornl.gov/~webworks/cppr/y2006/rpt/124460.pdf, 2006. Date Last Accessed 07/22/2016.

[20] S. Mosby et al. "Improved neutron capture cross section of ^{239}Pu," *Phys. Rev. C* vol. 89, no. 034610, Mar. 2014.

[21] C. Guerrero et al., "The n_TOF total absorption calorimeter for neutron capture measurements at CERN," *Nucl. Instruments and Methods Physics Res. A*, vol. 608, pp. 424-433, 2009.

[22] D. Williams et al. "A new method for the measurement of the neutron capture and fission cross sections of ^{235}U," *Proc. Tenth Int. Topical Meeting Nucl. Appl. Accelerators (AccApp 2011)*, Knoxville, TN, 2011.

[23] B. McDermott et al. "Capture cross sections in nat-Fe and 181-Ta from 1 to 2000 keV using a new C_6D_6 detector array," *Int. Conf. Nucl. Criticality Safety*, Charlotte, NC, Sep. 2015.

[24] A. Borella et al. "The use of C_6D_6 detector for neutron induced capture cross-section measurements in the resonance region," *Nucl. Instruments and Methods in Physics Res. A*, vol. 577, pp. 626-640, 2007.

[25] Y. Popov and F. Shapiro, "Energy dependence of cross sections for (n,γ) reactions on a number of odd-z nuclei," *J. Exptl. Theoret. Phys. (U.S.S.R.)* vol. 42, pp. 988-1000, 1962.

[26] R. Pouriamani et al. "Resonance capture γ-ray spectrometry at lead slowing-down neutron spectrometer," *Nucl. Instruments and Methods in Physics Res. A*, vol. 488, pp. 226-239, 2002.

[27] L. Perrot et al. "Precise validation of neutron cross section data bases using a lead slowing down spectrometer and simulation from 0.1 eV to 40 keV. Methodology and data on thin and thick targets and data bases adjustment", arXiv:nucl-ex/0201004v1 (2008). Date Last Accessed 07/26/2017.

[28] K. Kobayashi et al. "Measurement of neutron capture cross section of ^{237}Np and with linac-driven lead slowing-down spectrometer," *J. Nucl. Sci. and Tech.*, 39:2, 111-119, DOI: http://dx.doi.org/10.1080/18811248.2002.9715164 (2002). Date Last Accessed 07/26/2017.

[29] L. Perrot et al. "Precise validation of database (n,γ) cross sections using a lead-slowing-down-spectrometer and simulation from 0.1 eV to 30 keV: methodology and data for a few elements," *Nucl. Sci. and Eng.*, vol. 144, pp. 1-15, 2003.

[30] M. Yeater, "Neutron physics," *Proc. Symp. held May 5-6, 1961, Rensselaer Polytechnic Inst., Troy, New York*. Academic Press, NY, 1962.

[31] N. Abdurrahman, "System performance and monte carlo analysis of light water reactor spent fuel assay using neutron slowing down time," Ph.D. dissertation, Dept. of Nucl. Eng. and Sci., Rensselaer Polytechnic Inst., Troy, NY, 1991.

[32] H.M. Fisher, "MCNP analysis of the LSTDS system to determine its feasibility as a spent fuel assay device," Ph.D. dissertation, Dept. of Nucl. Eng., Rensselaer Polytechnic Inst., Troy, NY, 1985.

[33] B. Becker et al. "Nondestructive assay measurements using the RPI Lead Slowing-Down Spectrometer," *Nucl. Sci. and Eng.*, vol. 175, pp. 124-134, 2013; dx.doi.org/10.13182/NSE12-66. Date Last Accessed 07/26/2017.

[34] J. Thompson, "A method for (n,alpha) and (n,p) cross section measurements using a lead slowing-down spectrometer", Ph.D. dissertation, Gaerttner LINAC Center, Mech., Aerospace, and Nucl. Eng. Dept., Rensselaer Polytechnic Inst., NY, 2012.

[35] X.-5. Monte Carlo Team, "MCNP - A general monte carlo n-particle transport code, version 5," LA-UR-03-1987, Los Alamos National Laboratory, 2003.

[36] J. Goorley et al., "Initial MCNP6 release overview - MCNP6 version 1.0," LA-UR 13-22934, Los Alamos National Laboratory, 2013.

[37] S. A. Pozzi et al. "MCNP-PoliMi: A monte carlo code for correlation measurements," *Nucl. Instruments and Methods in Physics Res. A*, vol. 513, no. 3, pp. 550-558, Nov. 2003.

[38] S.W. Mosher et al., "ADVANTG-An automated variance reduction parameter generator," ORNL/TM 2013/416 Rev. 1, Oak Ridge National Laboratory (2015).

[39] N.W. Thompson et al. "Neutron capture cross section measurements using a lead slowing-down spectrometer," *Trans. of the American Nuclear Society*, vol. 111, Anaheim, California, Nov. 9-13, 2014.

[40] N.W. Thompson and Y. Danon, "Neutron capture cross section measurements using a lead slowing-down spectrometer," 2016 Stewardship Science Academic Programs Annual, DOE/NA-0038, National Nuclear Security Administration, 2016. Date Last Accessed 07/26/2017.

[41] Y. Danon et al. "Fission cross-section measurements of ^{247}Cm, ^{254}Es, and ^{250}Cf from 0.1 eV to 80 keV," *Nucl. Sci. Eng.*, vol. 109, pp. 341-349, Jun. 1991.

[42] B.J. McDermott et al., "New (n,γ) measurements on elemental iron from 850 to 2500 keV," AccApp 15, Washington, DC, pp. 374-379, Nov. 2015.

[43] S. V. Kapchigashev and Yu. P. Popov, "Capture cross sections in construction materials for neutrons with energies up to 50 keV," *Atomnaya Énergiya*, vol. 15, no. 2, pp. 120-126, 1963.

[44] S. Mughabghab, *Atlas of Neutron Resonances*. Amsterdam: Elsevier, 2006.

[45] S. Mughabghab, et. al., *Neutron Cross Sections, Volume 1: Neutron Resonance Parameters and Thermal Cross Sections*. New York: Academic Press, Inc., 1981.

[46] R.L. Macklin, "Neutron Capture cross sections of the silver isotopes ^{107}Ag and ^{109}Ag from 2.6 to 2000 keV," *Nucl. Sci. Eng.*, vol. 82, pp. 400-407, Jul. 1982.

[47] J. P. Foster et al. "Zirlo material for light water reactor applications," U.S. Patent 5112573, Westinghouse Electric Corporation, May 12 1992.

[48] D. B. Mitchell and B. M. Dunn, "Evaluation of advanced cladding and structural material (M5) in PWR reactor fuel," Framatome Cogema Fules, BAW-10227-A, Feb. 2000. Available: https://www.nrc.gov/docs/ML0036/ML003686365.pdf. Date Last Accessed 07/26/2017.

[49] B.J. McDermott et al. "Iron-56 capture cross section experiments at the RPI LINAC center," *ND 2016 Int. Conf. Nucl. Data Science and Technol.*, Bruges, Belgium, 2016.

[50] G.F. Knoll, *Radiation Detection and Measurement, Third Edition*, New York: John Wiley & Sons Inc., 2000.

[51] A.D. Weltz, "Benchmarking and characterization of the RPI LSDS for spent fuel assay," M.S. thesis, Mech., Aerospace and Nucl. Eng. Dept., Rensselaer Polytechnic Inst., Troy, NY, 2017.

APPENDIX A
Material Impurities

A.1 LSDS Impurities

Below are the impurities in the LSDS lead, determined by chemical analysis performed in 2012[51].

Table A.1: LSDS Impurities Table

Impurity	Weight Fraction (g/g)
C	20.0
H	1.0
Ag	1.31
B	0.0
Cu	4.52
As	0.04
Sb	0.11
Ni	0.15
Zn	0.03
Cd	0.01
Fe	1.0
Sn	0.03
Te	0.19
Gd	0.01
Sm	0.01
Tl	2.54
Bi	11.53

A.2 Sample Materials

This section details all the sample impurities as reported from the sample vendor, Alfa-Aesar.

A.2.1 Silver Sample

Product No.: 12126

Silver foil, 0.1 mm thick, hard - 1.60 g ± 0.01 g sample

Premion, 99.998 % (metals basis)

Lot No.: X20A030

Ag	99.999 % (by difference)				
Al	< 1	As	< 1	Au	< 1
B	< 1	Bi	3	Cd	< 1
Cr	< 1	Cu	2	Fe	< 1
Ge	< 1	Hg	< 1	In	< 1
Mg	< 1	Mn	< 1	Mo	< 1
Ni	< 1	Pb	1	Pd	< 1
Pt	< 1	S	< 1	Sb	< 1
Se	< 1	Si	< 1	Sn	< 1
Te	< 1	Ti	< 1	Zn	< 1

Values given in ppm unless otherwise noted
ND: Not detected

A.2.2 Gold Sample

Product No.: 14721

Gold foil, 0.1 mm thick, hard - 1.34 g ± 0.01 g sample

Premion, 99.95 % (metals basis)

Lot No.: K07Y035

Purity	99.999+ %				
Ag	1.8	Al	ND	As	ND
Bi	ND	Cr	ND	Cu	ND
Fe	ND	In	ND	Mg	ND
Mn	ND	Ni	ND	Pb	ND
Pd	ND	Pt	ND	Sn	ND
Si	ND	Ti	ND	Zn	ND
Zr	ND				

Values given in ppm unless otherwise noted
ND: Not detected

A.2.3 Cobalt Sample

Product No.: 42658

Cobalt foil, 0.1 mm thick, 99.95 % (metals basis) - 1.58 g ± 0.01 g sample

Lot No.: T17B032

Co 99.98 %

Ag	< 0.01	Al	0.61	As	< 0.5	Au	< 0.05
B	< 0.005	Ba	< 0.01	Be	< 0.005	Bi	< 0.005
Br	< 0.01	C	< 50	Ca	< 0.05	Cd	< 0.05
Ce	< 0.01	Cl	< 0.01	Cr	1	Cs	< 0.01
Cu	3.3	Dy	< 0.01	Er	< 0.01	Eu	< 0.01
F	< 0.5	Fe	5	Ga	0.33	Gd	< 0.01
Ge	< 0.05	H	< 10	Hf	< 0.01	Hg	< 0.05
Ho	< 0.01	I	< 0.05	In	< 0.05	Ir	0.04
K	< 0.01	La	< 0.05	Li	< 0.005	Lu	< 0.01
Mg	0.03	Mn	0.91	Mo	0.08	N	< 10
Na	0.03	Nb	< 0.01	Nd	< 0.01	Ni	84
O	86	Os	0.3	P	0.24	Pb	< 0.01
Pd	< 0.01	Pr	< 0.01	Pt	< 0.05	Rb	< 0.005
Re	0.13	Rh	< 0.01	Ru	0.01	S	0.18
Sb	2.5	Sc	< 0.005	Se	< 0.02	Si	0.53
Sm	< 0.01	Sn	0.02	Sr	< 0.01	Ta	< 1
Tb	< 0.01	Te	< 0.05	Th	<0.001	Ti	0.09
Tl	< 0.01	Tm	< 0.01	U	< 0.001	V	0.02
W	0.35	Y	< 0.005	Yb	< 0.01	Zn	< 0.01
Zr	0.01						

Values given in ppm unless otherwise noted
Carbon determined by combustion
Hydrogen and Nitrogen determined by IGF-TC
Oxygen determined with IGF-NDIR
All other elements determined by GDMS

A.2.4 Iron Sample

Product No.: 40496

Iron foil, 1.0 mm thick - 2.07 g $\pm$ 0.01 g sample

99.99 % (metals basis)

Lot No.: R22B027

Iron 99.991 %

Ag	< 0.01	Al	1.6	As	0.08	Au	< 0.05
B	0.77	Ba	< 0.05	Be	< 0.005	Bi	< 0.01
Br	< 0.05	C	< 100	Ca	0.07	Cd	< 0.05
Ce	< 0.05	Cl	0.12	Co	12	Cr	6.6
Cs	< 0.01	Cu	2.1	Dy	< 0.01	Er	< 0.01
Eu	< 0.01	F	< 0.05	Ga	0.07	Gd	< 0.01
Ge	6.2	Hf	< 0.01	Hg	< 0.05	Ho	< 0.01
I	< 0.01	In	< 0.01	Ir	< 0.05	K	0.08
La	< 0.01	Li	< 0.005	Lu	< 0.01	Mg	0.02
Mn	4.1	Mo	0.36	N	< 100	Na	0.48
Nb	0.03	Nd	< 0.01	Ni	2.8	O	200
Os	< 0.01	P	7.2	Pb	0.03	Pd	< 0.05
Pr	< 0.01	Pt	< 0.05	Rb	< 0.01	Re	0.01
Rh	< 0.05	Ru	< 0.05	S	5.3	Sb	< 0.05
Sc	< 0.01	Se	< 0.05	Si	45	Sm	< 0.01
Sn	0.15	Sr	< 0.05	Ta	< 1	Tb	< 0.01
Te	< 0.05	Th	< 0.001	Ti	1.4	Tl	< 0.01
Tm	< 0.01	U	< 0.001	V	0.06	W	0.15
Y	< 0.005	Yb	< 0.01	Zn	0.3	Zr	< 0.05

Values given in ppm unless otherwise noted
Carbon determined with IR
Hydrogen and Nitrogen determined with IGF-TC
Oxygen determined with IGF-NDIR
All other elements determined by GDMS

A.2.5 Indium Sample

Product No.: 11385

Indium foil, 0.1 mm thick - 1.23 g ± 0.01 g sample

Puratronic, 99.9975 % (metals basis)

Lot No.: N19A065

In 99.998 %

Al	< 1	As	< 1
Bi	< 1	Cd	< 1
Cu	< 1	Fe	< 1
Ga	< 1	Hg	< 1
Ni	< 1	Pb	2
Sb	< 1	Sn	1.2
Tl	< 1	Zn	< 1

Values given in ppm unless otherwise stated

A.2.6 Niobium Sample

Product No.: 00236

Niobium foil, 0.127 mm thick - 1.71 g ± 0.01 g sample

99.97 % (metals basis excluding Ta), Ta ¡0.06%

Lot No.: 062585

C	20	N	10	Ta	465	Ti	< 10
Mn	< 10	Sn	< 10	Cr	< 10	Na	ND
Mo	< 10	Zr	< 10	Mg	< 10	W	< 100
O	< 50	H	10	Nb	Balance	Fe	< 10
Si	15	Ni	< 10	Ca	< 10	Al	< 10
Cu	< 10	Co	< 10	B	< 10		

Values given in ppm unless otherwise noted

A.2.7 Nickel Sample

Product No.: 44824

Nickel foil, 1.0 mm thick - 17.2 g ± 0.1 g sample

99.5 % (metals basis)

Lot No.: P19B031

Ni 99.6 %

Al	170	C	150
Co	350	Cu	70
Fe	120	Mg	50
Mn	1120	S	40
Si	740	Ti	940

Values given in ppm unless otherwise noted

A.2.8 Molybdenum Sample

Product No.: 10043

Molybdenum foil, 0.1 mm thick - 3.96 g ± 0.01 g sample

99.95 % (metals basis)

Lot No.: S25A004

Mo	> 99.95 %		
Al	< 0.001 %	Mn	< 0.001 %
C	< 0.003 %	Ni	< 0.001 %
Ca	< 0.001 %	Pb	< 0.001 %
Cr	< 0.001 %	Si	< 0.001 %
Cu	< 0.001 %	Sn	< 0.001 %
Fe	0.0010 %	Ti	< 0.001 %
Mg	< 0.001 %		

A.2.9 Tin Sample

Product No.: 43235

Tin foil, 1.0 mm thick, 99.8 % (metals basis) - 1.84 g ± 0.01 g sample

Lot No.: B21T003

Ag	< 1	Al	< 1
As	8	Bi	6
Cd	< 1	Co	< 1
Cu	< 3	Fe	1
In	10	Ni	< 1
Pb	9	Sb	52
Zn	< 1		

Values given in ppm unless otherwise noted

A.2.10 Tantalum Sample

Product No.: 10353

Tantalum foil, 0.254 mm thick, annealed - 1.03 g ± 0.01 g sample

99.95 % (metals basis)

Lot No.: L21J17

Analysis in ppm unless otherwise indicated

C	<10	Ti	<5	Cr	<5	Zr	<5
O	25	Fe	<5	Ca	<5	Co	<5
N	<10	Mn	<5	Na	NR	Mg	<5
H	<5	Si	<5	Al	<5	B	<1
Ta	99.98%	Sn	<5	Mo	<5	W	<25
Nb	65	Ni	<5	Cu	<5	O_2	NR
N_2	NR	H_2	NR				

NR - Not reported

A.2.11 Zirconium Sample

Product No.: 10591

Zirconium foil, 0.25mm thick, annealed - 1.60 g ± 0.01 g sample

99.8% (metals basis excluding Hf), Hf nominal 2%

Lot No.: K18U008

Zr	99.94 %
C	80
Fe + Cr	600
H	4
Hf	< 25
N	20
O	700

Values given in ppm unless otherwise noted

APPENDIX B
Event by Event Analysis Code

C code, filename: SimplePSA_3.2.1.cpp

```
#include <math.h>
#include <fstream>
#include <vector>
#include <algorithm>
#include <iostream>


const int detectorNum = 2;                          // # Of Detectors
const int TimeOfFlight = 2000000;
const int pSIZE = 200;
const int pLEN = pSIZE + 28;
const int GaussSize = 15;
const int ex = 2;
//const int intervalMax = 5000;


//int Ranges = {{500,1100},{100000,200000},{10000000,20000000}};
//int numRange;
//numRange = Ranges::size();


const float BoardOffset = 128.0 - 2.45*(256.0/5.0);      // Default
    Board Offset

int gTOF[detectorNum][TimeOfFlight];                    // Events in TOF
int COIN[TimeOfFlight];                               // Coincidence Array in
    TOF
float intTOF[detectorNum][TimeOfFlight];
float centTOF[detectorNum][TimeOfFlight];

using namespace std;

void ConvertPulse(char Array[], float *pulseArray, int &P, float &TOT,
    float &HT, bool &SAT)
{
  int i;
  float sum;
  sum = 0.0;

  float sum20;
  sum20 = 0.0;

  int sat_counter;
```

```
41    sat_counter = 0;
42    float sum10;
43    sum10 = 0.0;
44    float max = 0.0;
45
46    TOT = 0.0;
47    HT=0.0;
48    for(i=0; i<10; i++)
49    {
50      sum10 += 128.0 + (float)(signed char)Array[i+pLEN-pSIZE-1];
51    }
52    sum10 = (sum10/10.0);
53
54    for(i=0; i<pSIZE; i++)
55    {
56      pulseArray[i] = 128.0 + (float)(signed char)Array[i+pLEN-pSIZE-1] -
            BoardOffset;
57      if (pulseArray[i]>max)
58      {
59        max=pulseArray[i];
60      }
61      if(128 + (int)(signed char)Array[i+pLEN-pSIZE-1] == 255)
62      {
63        sat_counter++;
64      }
65      sum += pulseArray[i];
66
67    }
68    TOT = sum;
69    HT=max;
70 //   if (TOT>max)
71 //   {
72 //     max = TOT;
73 //   }
74
75    if(sat_counter > 2)
76    {
77      SAT = true;
78    }
79
80    for(i=0; i<pSIZE; i++)
81    {
82      if(sum*0.2 > sum20)
83      {
84        sum20 += pulseArray[i];
85        P++;
86      }
87    }
88
89 }
90
91 struct Pulse
```

```
92 {
93   int DET;
94   float INT;
95   long long int TOF;
96   long long int GLOB;
97 };
98
99 struct By_GLOB
100 {
101   bool operator()(Pulse const &a, Pulse const &b)
102   {
103     if(a.GLOB == b.GLOB)
104     {
105       return a.TOF < b.TOF;
106     }
107         return a.GLOB < b.GLOB;
108     }
109 };
110
111 void DoCoin(std::vector<Pulse> *P, int *CoinArr, int *GausArr, int
      MCArr[][30000])
112 {
113   int i, j, k;
114
115   int MIN_DET;
116   long long int TMP_GLOB;
117   long long int TMP_TOF;
118   float TMP_INT;
119
120   bool setTMP;
121
122   int d[detectorNum];
123   int e[detectorNum];
124
125   for(i=0;i<detectorNum;i++)
126   {
127     d[i] = P[i].size()-1;                    // Number of Events For
          Each Detector
128     e[i] = 0;                              // Number of Processed Events For
          Each Detector
129   }
130
131   vector<int> NEW_DET_VEC;
132   vector<long long int> NEW_TOF_VEC;
133   vector<long long int> NEW_GLOB_VEC;
134   vector<float> NEW_INT_VEC;
135
136
137   while((e[0]<d[0]) && (e[1]<d[1]))
138   {
139     i = 0;
140     setTMP = true;
```

```
141     TMP_GLOB = 0;
142     MIN_DET = 0;
143     TMP_TOF = 0;
144     TMP_INT = 0.0;
145     while(i < detectorNum)
146     {
147       if((setTMP) && (e[i] < d[i]))                                    //
            Set TMP values only first time through detector iteration
148       {
149         TMP_GLOB = P[i][e[i]].GLOB;
150         TMP_TOF = P[i][e[i]].TOF;
151         TMP_INT = P[i][e[i]].INT;
152         MIN_DET = i;
153         setTMP = false;
154       }
155
156       if(i == 1)
157       {
158         break;
159       }
160
161       if((TMP_GLOB == P[i+1][e[i+1]].GLOB) && (!setTMP) && (e[i+1] < d[
            i+1]))              // If Both Detectors Have ~ Same Global
            Time Stamp (0.001)
162       {
163         if(P[i+1][e[i+1]].TOF < TMP_TOF)
              // If Next Detector Has LOWER TOF
164         {
165           TMP_TOF = P[i+1][e[i+1]].TOF;
166           TMP_GLOB = P[i+1][e[i+1]].GLOB;
167           TMP_GLOB = P[i+1][e[i+1]].INT;
168           MIN_DET = i+1;
169         }
170       }
171       else if((TMP_GLOB > P[i+1][e[i+1]].GLOB) && (!setTMP) && (e[i+1]
            < d[i+1]))            // If The Current Detector Has A LOWER
            Global Time Stamp
172       {
173         TMP_TOF = P[i+1][e[i+1]].TOF;
174         TMP_GLOB = P[i+1][e[i+1]].GLOB;
175         TMP_INT =  P[i+1][e[i+1]].INT;
176         MIN_DET = i+1;
177       }
178       i++;
179
180       if(e[MIN_DET] < d[MIN_DET])
181       {
182         NEW_DET_VEC.push_back(P[MIN_DET][e[MIN_DET]].DET);
183         NEW_TOF_VEC.push_back(P[MIN_DET][e[MIN_DET]].TOF);
184         NEW_GLOB_VEC.push_back(P[MIN_DET][e[MIN_DET]].GLOB);
185         NEW_INT_VEC.push_back(P[MIN_DET][e[MIN_DET]].INT);
186         e[MIN_DET]++;
```

```
187         }
188       }
189     }
190
191     i = 0;
192     while(i < NEW_DET_VEC.size()-1)
193     {
194       if(NEW_GLOB_VEC[i] != NEW_GLOB_VEC[i+1])
195       {
196         i++;
197         continue;
198       }
199       if(NEW_DET_VEC[i] == NEW_DET_VEC[i+1])
200       {
201         i++;
202         continue;
203       }
204       if(abs(NEW_TOF_VEC[i]-NEW_TOF_VEC[i+1]) < GaussSize)
205       {
206         GausArr[abs(NEW_TOF_VEC[i]-NEW_TOF_VEC[i+1])]++;
207         if(abs(NEW_TOF_VEC[i]-NEW_TOF_VEC[i+1]) == 0)
208         {
209           GausArr[abs(NEW_TOF_VEC[i]-NEW_TOF_VEC[i+1])]++;
210         }
211         CoinArr[(NEW_TOF_VEC[i]+NEW_TOF_VEC[i+1])/2]++;
212         if(
213           ((int)round(((int)NEW_INT_VEC[i]+(int)NEW_INT_VEC[i+1])/2)>0)
214         &&
215           ((int)round(((int)NEW_INT_VEC[i]+(int)NEW_INT_VEC[i+1])/2)
                <30000)
216         )
217         {
218           MCArr[2][(int)round(((int)NEW_INT_VEC[i]+(int)NEW_INT_VEC[i+1])
                /2)]++;
219         }
220       }
221       i++;
222     }
223     if(NEW_DET_VEC.size() > 0)
224     {
225       NEW_DET_VEC.clear();
226       NEW_TOF_VEC.clear();
227       NEW_INT_VEC.clear();
228       NEW_GLOB_VEC.clear();
229     }
230     return;
231 }
232
233 float PulseCent(float *pulseArray, int expo, int integral)
234 {
235   int i;
236
```

```
237   float Top, Bot;
238   Top = 0.0;
239   Bot = 0.0;
240
241   for(i=0;i<pSIZE;i++)
242   {
243     Top += (pulseArray[i] * pow(i ,expo));
244     Bot += pow(i,expo);
245   }
246
247   return Top/(Bot*integral);
248 }
249
250
251 int main()
252 {
253   int i, j, k;
254
255   int detector;                    // Used to store detector number
256   int fine_time;                     // 1 ns resolution finder
257   int gFlashLoc = 0;                     // Used to eliminate gamma flash
          pulses from analysis
258   int gFlashBuf = 0;                     // Used to add extra no
          collection time after gamma flash
259   int intCut = 0;
260   int htCut=250;
261   float cntCut=0.0;
262   float centroid=0.0;
263
264   int intMCA = 30000;                  // Default length of MCA
265
266   int GAUS[GaussSize*2 + 1];
267
268
269   long long int T1, T2, T3, T4;          // Used to get the TOF
270   long long int totalTOF;                // Used to store TOF
271   long long int P1, P2, P3, P4, P5;        // Used to get the Global
          Time Stamp
272   long long int GTS;                   // Used to store Global Time Stamp
273
274   bool saturated;
275   bool saturatedOn = false;
276   bool CoinOn = true;
277
278   char getDetector[1];                 // Used to read the detector number
279   char buffer[pLEN-1];
280
281   float pulseArray[pSIZE];
282   float pulseInt;                    // pulse integral
283   float pulseCent;                   // Pulse Centroid
284   float pulseHt;                     // Pulse height
285
```

```
286   vector<Pulse> P[detectorNum];
287
288   ifstream fileIn;
289   string file;                    // String For The File Name
290   string sv;                      // String for line of input file
291   string rawFileName;                 // String For Line Of File
292 /*=============================================================
293 =============================================================*/
294   file = "SimplePSA.amd";
295   fileIn.open(file.c_str());
296   if(fileIn.is_open())
297   {
298     while(fileIn.good())
299     {
300       getline(fileIn, sv);
301       if(sv[0] == '#')
302       {
303         continue;
304       }
305       else if(sv.substr(0,6) == "gflash")
306       {
307         gFlashLoc = atof(sv.substr(9,6).c_str());
308       }
309       else if(sv.substr(0,6) == "sat_on")
310       {
311         saturatedOn = true;
312       }
313       else if(sv.substr(0,6) == "buffer")
314       {
315         gFlashBuf = atof(sv.substr(9,6).c_str());
316       }
317       else if(sv.substr(0,6) == "intCut")
318       {
319         intCut = atof(sv.substr(9,4).c_str());
320       }
321       else if(sv.substr(0,5) == "htCut")
322       {
323         htCut = atof(sv.substr(9,4).c_str());
324       }
325       else if(sv.substr(0,6) == "cntCut")
326       {
327         cntCut=atof(sv.substr(9,4).c_str());
328       }
329       else if (sv.substr(0,7) == "CoinOff")
330       {
331         CoinOn = false;
332       }
333     }
334   }
335   else                                          // If you can not
        open "DATAFILE.txt"
336   {
```

```
337     cout << "Could not open file: " << file << ".  Error Exit #1.
            Exiting Program.\n";   // Output to user
338     return 0;                                          // Exit Program
339   }
340   fileIn.close();
341
342   int MCA[detectorNum+1][30000];           // An MCA for each detector +
          1 for coincidence
343
344 /*=============================================================
345 =============================================================*/
346
347   int NumOfFiles;                    // File Increment Integer
348   char rawDataFileName[1000][1000];
349
350 /*=============================================================
351 =============================================================*/
352   file = "DATAFILE.txt";                                    // This
          file is made by the Python Script
353   fileIn.open(file.c_str());                                  // Open
          file "DATAFILE.txt"
354   if(fileIn.is_open())                                     // If file "
          DATAFILE.txt" is Open
355   {
356     NumOfFiles = 0;                                      // Counts the
          number of files (technically lines but one file per line)
357     while(fileIn.good())                                   // While "
          DATAFILE.txt" is open
358     {
359       getline(fileIn, rawFileName);                            // Using
            getline because the code uses paths with "/" not "\" which
            could break string
360       for(i=0;i<1000;i++)                                  // Problem if
            path length + file name is over 1000 chars long
361       {
362         if((rawFileName[i]=='\n')||(rawFileName[i]=='\r'))
                // Find the end of the line
363         {
364           break;                                       // Stop
                incrementing i
365         }
366         rawDataFileName[NumOfFiles][i] = rawFileName[i];
                // Save string into char array
367       }
368       NumOfFiles++;                                     // Increment
            Number of Files
369     }
370   }
371   else                                               // If you can not
          open "DATAFILE.txt"
372   {
373     cout << "Could not open file: " << file << ".  Error Exit #2.
```

```
        Exiting Program.\n";    // Output to user
374     return 0;                                           // Exit Program
375   }
376   fileIn.close();                                       // Close file "
        DATAFILE.txt"
377
378 /*=================================================
379 =================================================*/
380   int fSize;
381   int NumOfFilesCounter = 0;
382
383
384   //  string Names[numRange];
385 //  Names[0] = "CentTOF"
386
387
388 //  ofstream fOUT;
389 //  string file2;
390 //  file2 = "MOOOOO.txt";
391
392
393   int Range[2];
394   Range[0] = 0;
395   Range[1] = 2000000;
396   int Z = 0;
397   int Y = 0;
398
399 //  ofstream fP, fOUT;
400   ofstream fP;
401 //  fP.open("CentHist.txt");
402 //  fOUT.open("PulsesROI_1.txt");
403
404   while(NumOfFilesCounter<NumOfFiles)
405   {
406     file = rawDataFileName[NumOfFilesCounter];
407     fileIn.open(file.c_str(), ios::in | ios::binary);
408 //    fOUT.open(file2.c_str(), ios::out);
409
410     fileIn.seekg(0,ios::end);
411     fSize = fileIn.tellg();
412     fileIn.seekg(0,ios::beg);
413
414     if(fSize == 0)
415     {
416       NumOfFilesCounter++;
417       continue;
418     }
419     cout << "Opening:\t" << file << "\nCounts: \t" << fSize/pLEN <<"\n"
         ;
420
421     if(fileIn.is_open())                // If file "DATAFILE.txt" is Open
422     {
```

```
423 //      cout<< "\t Start While\n";
424       int Counter = 0;
425       while(fileIn.good())
426       {
427         pulseHt=0;
428         saturated = false;
429         fileIn.read(getDetector, 1);
430         detector = (int)(unsigned char)getDetector[0];
431         fileIn.read(buffer, pLEN-1);
432 
433         T1 = (int)(unsigned char)buffer[pLEN - pSIZE - 5]*pow(256,0);
434         T2 = (int)(unsigned char)buffer[pLEN - pSIZE - 4]*pow(256,1);
435         T3 = (int)(unsigned char)buffer[pLEN - pSIZE - 3]*pow(256,2);
436         T4 = (int)(unsigned char)buffer[pLEN - pSIZE - 2]*pow(256,3);
437         totalTOF = T1 + T2 + T3 + T4;
438         if(T1 + T2 + T3 + T4 < gFlashLoc + gFlashBuf)          // Skip
              Pulse if before Gamma Flash and Buffer Location
439         {
440           continue;
441         }
442 
443         fine_time = 0;
444 
445         P1 = (int)(unsigned char)buffer[pLEN - pSIZE - 25];
446         P2 = (int)(unsigned char)buffer[pLEN - pSIZE - 21];
447         P3 = (int)(unsigned char)buffer[pLEN - pSIZE - 17];
448         P4 = (int)(unsigned char)buffer[pLEN - pSIZE - 13];
449         P5 = (int)(unsigned char)buffer[pLEN - pSIZE -  9];
450 //        GTS = P1*pow(256,0) + P2*pow(256,1) + P3*pow(256,2) + P4*pow
        (256,3) +P5*pow(256,4);
451         GTS = P3*pow(256,2) + P4*pow(256,3) +P5*pow(256,4);
452 //        fOUT << detector << "\t" << GTS << "\n";
453 
454         ConvertPulse(buffer, pulseArray, fine_time, pulseInt, pulseHt,
              saturated);
455 //        cout<< pulseHt<<"\t"<<int(pulseHt)<<"\t"<<htCut<<"\n";
456         if((saturated) && (saturatedOn))
457         {
458           continue;
459         }
460         totalTOF += fine_time - gFlashLoc;                  // All times
              are gamma flash adjusted
461         centroid=PulseCent(pulseArray,ex,pulseInt);
462 //        centroid = 0;
463         if(centroid<cntCut)
464         {
465           continue;
466         }
467         if(totalTOF > TimeOfFlight)
468         {
469           continue;
470         }
```

```
471         if(intCut > (int)round(pulseInt+0.05))
472         {
473           continue;
474         }
475         if((htCut > (int)pulseHt)) //||((int)pulseHt>195))          //
              pulses above 195 are cut to get rid of ringing pulses
476         {
477 //            cout<<"\t Skipped pulse\n";
478           continue;
479         }
480 //        cout<< "\t Kept Pulse\n";
481
482
483 /*        if(((totalTOF > Range[0]) && (totalTOF < Range[1])))
484         {
485           for(Y=0;Y<pSIZE-1;Y++)
486           {
487             fOUT << pulseArray[Y] << "\t";
488           }
489           fOUT << pulseArray[pSIZE-1] << "\n";
490           Z++;
491         }
492 */
493         P[detector-1].push_back(Pulse());
494         P[detector-1][P[detector-1].size()-1].DET = detector-1;
495         P[detector-1][P[detector-1].size()-1].TOF = totalTOF;
496         P[detector-1][P[detector-1].size()-1].GLOB = GTS;
497         P[detector-1][P[detector-1].size()-1].INT = pulseInt;
498
499         gTOF[detector-1][totalTOF]++;
500         intTOF[detector-1][totalTOF]+= pulseInt;
501         if((pulseInt < 30000) &&(pulseInt>0))
502         {
503           MCA[detector-1][(int)pulseInt]++;
504         }
505 //        pulseCent = PulseCent(pulseArray,ex);
506 //        fP << PulseCent(pulseArray,ex,pulseInt) << "\n";
507 //        centTOF[detector-1][totalTOF]+= PulseCent(pulseArray,ex,
    pulseInt);
508 //        cout<< "End of Read File Loop\n";
509 //        if(Counter%1000 == 0)
510 //        {
511 //          cout<< Counter << "\n";
512 //        }
513 //        Counter = Counter + 1;
514       }
515 //      cout<< "End of File\n";
516       //=================================================
517       // COINCIDENCE AREA
518       //=================================================
519       //=================================================
520       if(CoinOn)
```

```
521         {
522 //          cout<< "Start of ifCoinon\n";
523           for(j=0;j<detectorNum;j++)
524           {
525             sort(P[j].begin(), P[j].end(), By_GLOB());
526           }
527 //          cout<< "Start of DoCoin\n";
528           DoCoin(P, COIN, GAUS, MCA);
529 //          cout<< "End of DoCoin\n";
530           //=============================================================
531           // DELETE VECTORS TO CLEAR MEMORY
532           //=============================================================
533           for(j=0;j<detectorNum;j++)
534           {
535             P[j].clear();
536           }
537         }
538       }
539       fileIn.close();
540       NumOfFilesCounter++;
541 //      cout<< "End of Num Files Counter\n";
542     }
543     cout<<"\nFinished File";
544 //    fP.close();
545 //    fOUT.close();
546 //=================================================================
547 //    TIME OF FLIGHT OUTPUT
548 //=================================================================
549     fP.open("TOF.txt");
550     for(i=0;i<TimeOfFlight;i++)
551     {
552       fP << gTOF[0][i] << "\t" << gTOF[1][i] << "\n";
553     }
554     fP.close();
555 //=================================================================
556 //    PULSE INT IN TIME OF FLIGHT OUTPUT
557 //=================================================================
558 /*( fP.open("intTOF.txt");
559     float Amanda1, Amanda2;
560     for(i=0;i<TimeOfFlight;i++)
561     {
562       Amanda1 = intTOF[0][i]/gTOF[0][i];
563       Amanda2 = intTOF[1][i]/gTOF[1][i];
564       fP << Amanda1 << "\t" << Amanda2 << "\n";
565     }
566     fP.close();
567 */
568 //=================================================================
569 //    CENTROID IN TIME OF FLIGHT OUTPUT
570 //=================================================================
571 /*    fP.open("centTOF.txt");
572     for(i=0;i<TimeOfFlight;i++)
```

```
573    {
574      Amanda1 = centTOF[0][i]/gTOF[0][i];
575      Amanda2 = centTOF[1][i]/gTOF[1][i];
576      fP << Amanda1 << "\t" << Amanda2 << "\n";
577    }
578    fP.close();
579  */
580  //=============================================================
581  // COINCIDENCE TOF OUTPUT
582  //=============================================================
583    fP.open("Coin.txt");
584    for(i=0;i<TimeOfFlight;i++)
585    {
586      fP << COIN[i] << "\n";
587    }
588    fP.close();
589  //=============================================================
590  // GAUSSING ARRAY OUTPUT
591  //=============================================================
592    fP.open("Gauss.txt");
593    for(i=0;i<GaussSize*2+1;i++)
594    {
595      fP << GAUS[i] << "\n";
596    }
597    fP.close();
598  //=============================================================
599  // MCA ARRAY OUTPUT
600  //=============================================================
601    fP.open("MCA.txt");
602    for(i=0;i<30000;i++)
603    {
604      fP << MCA[0][i] << "\t" << MCA[1][i] << "\t" << MCA[2][i] << "\n";
605    }
606    fP.close();
607
608    return 0;
609  }
```

Input file for SimplePSA, filename: SimplePSA.amd

```
1  #  This is an input file
2     #  use '#' for comments
3     #
4     #
5     #
6     # Use the command 'gflash' and place the value at column 10
7     # Example (remove the '#' to see proper locations)
8     # Current Max Value 999999
9     #         HERE
10    #gflash    100000
11    #         HERE
12    gflash    0000
13    # buffer used to extend 'no collection region' beyond peak of gamma
```

```
        flash
#buffer    2000
#
#
#
# To turn on the saturated filter the following command is needed:
#sat_on
 sat_off
#         HERE (Integral cut of pulse interval, 0-9999)
intCut    0000
#
#         HERE (Pulse Height cut)
htCut     0
# htCut     50
#
#         HERE (Centroid Cut)
cntCut    0.0
# cntCut    0.7
# Coincidence Off
# CoinOff
```

Additional thanks to Dr. Adam Matthew Daskalakis for his help writing and modifying this code.

APPENDIX C
Example MCNP6 Simulation Input

MCNP6 input file, filename: newh_Ta10mil_ENDF_impENDF.txt

```
N THOMPSON A LEWIS
c
c Basic LSDS structure uses cells 1-161, surfaces 1-131
c
c Simulation is for the small hole on the right side of the LSDS
c
c Cells
c
1 0 2 3 4 5 6 7 8 $ Void
2 2 -2.30 -2 8 $ Front Wall
3 2 -2.30 -3 8 $ Right Side Wall
4 2 -2.30 -4 8 $ Left Side Wall
5 2 -2.30 -5 8 9 $ Back Wall
6 2 -2.30 -6 8 $ Floor
7 2 -2.30 -7 8 $ Ceiling
9 1 -0.001124 -9 16 $ Hole in back wall
39 8 -2.11 -9 -16 $ Li in hole in back wall
c
10 4 -0.64 -10 $ Wood Layer
11 3 -7.82 -11 12 $ Steel Layer
15 3 -7.82 -15 -2016 2020 $ Steel plate below LSDS Shells
16 3 -7.82 -15 -2012 2016
17 3 -7.82 -15 2012 -2005
18 3 -7.82 -15 2005 -2000
8 3 -7.82 -15 2000
c
19 5 -11.34 -19 2000 $ Lead Shell (furthest)
2000 5 -11.34 -2000 2001 -19 50 56 $ Lead Shell
2001 5 -11.34 -2001 2002 -19 50 56 $ Lead Shell
2002 5 -11.34 -2002 2003 -19 14 50 56 $ Lead Shell
2003 5 -11.34 -2003 2004 -19 14 50 56 $ Lead Shell
2004 5 -11.34 -2004 2005 -19 50 56 $ Lead Shell
2005 5 -11.34 -2005 2006 -19 50 56 $ Lead Shell
2006 5 -11.34 -2006 2007 -19 50 56 $ Lead Shell
2007 5 -11.34 -2007 2008 -19 50 56 $ Lead Shell
2008 5 -11.34 -2008 2009 -19 50 56 $ Lead Shell
2009 5 -11.34 -2009 2010 -19 50 56 $ Lead Shell
2010 5 -11.34 -2010 2011 -19 50 56 $ Lead Shell
2011 5 -11.34 -2011 2012 -19 50 56 $ Lead Shell
2012 5 -11.34 -2012 2013 -19 50 56 $ Lead Shell
2013 5 -11.34 -2013 2014 -19 50 56 $ Lead Shell
2014 5 -11.34 -2014 2015 -19 50 56
2015 5 -11.34 -2015 2016 -19 50 56
2016 5 -11.34 -2016 2017 -19 50 56
2017 5 -11.34 -2017 2018 -19 50 56
2018 5 -11.34 -2018 2019 -19 50 56
```

```
2019 5 -11.34 -2019 2020 -19 50 56
2020 5 -11.34 -2020 2021 -19 50 56
2021 5 -11.34 -2021 2022 -19 50 56
2022 5 -11.34 -2022 2023 -19 50 56
2023 5 -11.34 -2023 2024 -19 50 56
2024 5 -11.34 -2024 2025 -19 50 56
2025 5 -11.34 -2025 2026 -19 50 56
2026 5 -11.34 -2026 2027 -19 50 56
2027 5 -11.34 -2027 2028 -19 50 56
2028 5 -11.34 -2028 2029 -19 50 56
2029 5 -11.34 -2029 2030 -19 50 56
2030 5 -11.34 -2030 2031 -19 50 56
2031 5 -11.34 -2031 2032 -19 50 56
2032 5 -11.34 -2032 -19 50 56 $ Lead Shell (closest)
c
30 1 -0.001124 -8 2000 18 10 11 12 13 14 15 $ Air Shells
31 1 -0.001124 -2000 2005 18 -8 10 11 12 13 14 15 #90
32 1 -0.001124 -2005 2012 18 10 11 12 13 14 15 93 95 #86 #95 #90 #98
33 1 -0.001124 -2012 2016 18 15 14 13 90 91 92 12 93 95 96 #86
34 1 -0.001124 -2016 2020 18 15 14 13 90 91 92 93 96 95 94
35 1 -0.001124 -2020 2026 18 14 13 90 91 92 93 94 95 96
36 1 -0.001124 -2026 2027 18 14 13 93 94 95 96
37 1 -0.001124 -2027 2029 18 14 13 93 94 95 96
38 1 -0.001124 -2029 2031 18 14 13 94 95 96
c
40 6 -8.65 -18 19 2000 $ Cd cover shells
41 6 -8.65 -18 19 -2000 2005
42 6 -8.65 -18 19 -2005 2012
43 6 -8.65 -18 19 -2012 2016 #15
44 6 -8.65 -18 19 -2016 2020
45 6 -8.65 -18 19 -2020 2026
46 6 -8.65 -18 19 -2026 2027
47 6 -8.65 -18 19 -2027 2029
48 6 -8.65 -18 19 -2029
c $ Measurement Port
50 5 -11.34 51 -50 #51 #450 #451 #300 #301 #402 #303 #304 #305
#306 #307 #308 #311 #312 #313 $ Back Lead Bricks (meas port)
#320 #321 #422 #323 #324 #325 #326 #327 #328
#331 #332 #333 #309 #329
51 1 -0.001124 -52 51 -50 #300 #301 #402 #303 #304 #305
#306 #307 #308 #311 #312 #313 $ Hole (sq) in Back Bricks
#320 #321 #422 #323 #324 #325 #326 #327 #328
#331 #332 #333 #450 #451 #309 #329
52 5 -11.34 -50 53 -51 #53 #54 #313 #333 $ Middle Lead Bricks (meas port)
53 1 -0.001124 54 -51 -52 53 #313 #333 $ Hole (sq) in Middle Bricks
54 1 -0.001124 -55 -54 -51 53 #313 #333 $ Hole (cyl) in Middle Bricks
55 5 -11.34 -50 -53 55 #313 #333
56 1 -0.001124 -55 -50 -53 #313 #333 $ Hole (cyl) in Front Bricks
c $ Fuel Assay Port
57 1 -0.001124 -56 2012 -2005 -58 57 $ Back Section Shells (Air)
58 5 -11.34 -56 2012 -2005 58 57 $ Back Section Shells (Pb)
59 1 -0.001124 -56 -2012 2016 -58
```

```
60 5 -11.34 -56 -2012 2016 58 57
61 1 -0.001124 -56 -2016 2020 -58
62 5 -11.34 -56 -2016 2020 58 57
63 1 -0.001124 -56 -2020 2026 -58
64 5 -11.34 -56 -2020 2026 58 57
65 1 -0.001124 -56 -2026 2027 -58
88 1 -0.001124 -56 -2027 -58
66 5 -11.34 -56 -2026 2027 58 57
67 1 -0.001124 -2026 2027 -59 -57 51 $ Middle Back Section Shells
68 5 -11.34 -56 -57 51 59 -2026 2027
69 1 -0.001124 -2020 2026 -59 -57 51
70 5 -11.34 -56 -57 51 59 -2019 2026 60
71 5 -11.34 -56 -57 51 59 -2027 2029
72 5 -11.34 -56 -57 51 59 -2029 2031
73 5 -11.34 -56 53 60 -51 -2019 2026 $ Middle Front Section Shells
74 5 -11.34 -56 53 60 -51 -2026 2027
75 5 -11.34 -56 53 60 -51 -2027 2029
76 5 -11.34 -56 53 60 -51 -2029
77 1 -0.001124 -60 2026 -2020
78 1 -0.001124 -60 -2026 2027
79 5 -11.34 -56 -53 61 62 2026 $ Front Section Shells
80 5 -11.34 -56 -53 61 62 -2026 2027
81 5 -11.34 -56 -53 61 62 -2027 2029
82 1 -0.001124 -61 #73
83 1 -0.001124 -62 #73
84 5 -11.34 -56 -5 61 62 -2029
85 5 -11.34 -56 -2023 58 57 2029
87 5 -11.34 -56 -2029 58 57
c $ Lead Bricks outside m. port
90 5 -11.34 -90 2016 $ revised
91 5 -11.34 -90 -2016 2020
92 5 -11.34 -90 -2020 2026
93 4 -0.64 -91 -2020 2026 $ Wood Plate
94 4 -0.64 -91 2020 -2016
95 4 -0.64 -91 2016 $ revised
96 1 -0.001124 -92 -2020 2026 $ revised $ Short Lead Block
97 8 -2.11 -92 -2016 2020
98 8 -2.11 -92 2016
99 8 -2.11 -93 -2020 2026 $ revised
100 8 -2.11 -93 -2005 2020
101 8 -2.11 -93 -2026 2027
102 8 -2.11 -93 -2027 2029
86 8 -2.11 -94 2020 $ revised
103 8 -2.11 -94 -2020 2026
104 8 -2.11 -94 -2026 2027
105 8 -2.11 -94 -2027 2029
106 8 -2.11 -94 -2029 2031
107 8 -2.11 -95 -2027 2029 $ revised $ Lower Li Brick
108 8 -2.11 -95 -2026 2027
109 8 -2.11 -95 -2020 2026
110 8 -2.11 -95 2031 -2029
111 8 -2.11 -96 -2029 2031 $ Upper Li Brick
```

```
112 8 -2.11 -96 -2027 2029
113 8 -2.11 -96 -2026 2027
114 8 -2.11 -96 2025 -2012
115 8 -2.11 -95 2020
c
116 3 -7.82 -116 -117:-118:-119 u=2 $ I-Beam for bottom, no Li
117 1 -0.001124 -116 117 118 119 u=2 $ Air around I-Beam
118 0 116 u=2 $ Outside of Universe
c
119 3 -7.82 -116 -117:-118:-119 u=3 $ I-Beam for bottom, with Li
120 1 -0.001124 -116 117 118 119 120 121 u=3 $ Air
121 8 -2.11 -120 u=3 $ Li on left
122 8 -2.11 -121 u=3 $ Li on right
123 0 116 u=3 $ Outside universe
c
124 3 -7.82 -122 -123:-124:-125 u=4 $ I-Beam for middle, no Li
125 1 -0.001124 -122 123 124 125 u=4 $ Air around I-Beam
126 0 122 u=4 $ Outside of Universe
c
127 3 -7.82 -122 -123:-124:-125 u=5 $ I-Beam for middle, with Li
128 1 -0.001124 -122 123 124 125 126 127 u=5 $ Air
129 8 -2.11 -126 u=5 $ Li on left
130 8 -2.11 -127 u=5 $ Li on right
131 0 122 u=5 $ Outside universe
c
132 3 -7.82 -128 -117:-118:-119 u=6 $ I-Beam for top, no Li
133 1 -0.001124 -128 117 118 119 u=6 $ Air
134 0 128 u=6 $ Outside universe
c
135 3 -7.82 -128 -117:-118:-119 u=7 $ I-Beam for top, with Li
136 1 -0.001124 -128 117 118 119 129 130 u=7 $ Air
137 8 -2.11 -129 u=7 $ Li on left
138 8 -2.11 -130 u=7 $ Li on right
139 0 128 u=7 $ Outside universe
c
c
140 3 -7.82 -128 -117:-118:-119 u=8 $ I-Beam for top, with Li (full)
141 1 -0.001124 -128 117 118 119 131 u=8 $ Air
142 8 -2.11 -131 u=8 $ Li blocks
143 0 128 u=8 $ Outside universe
c
158 3 -7.82 -122 -123:-124:-125 u=11 $ I-Beam for middle, with Li (full)
159 1 -0.001124 -122 123 124 125 132 u=11 $ Air
160 8 -2.11 -132 u=11 $ Li
161 0 122 u=11 $ Outside universe
c
144 0 -116 lat=1 u=9 trcl=(-105.20 -155.40 -152.86) $ I-Beam Shells for bottom base
fill=0:4 0:0 0:0 2 3 2 2 2
145 0 -12 -2005 2012 fill=9
146 0 -12 -2000 2005 fill=9
147 0 -12 2000 fill=9
c
```

```
148 0 -122 lat=1 u=10 trcl=(-105.20 -155.40 -132.54) $ I-Beam Shells for middle base
fill=0:0 0:7 0:0 11 5 11 11 11 11 11 4
149 0 -13 2000 fill=10
150 0 -13 -2000 2005 fill=10
151 0 -13 -2005 2012 fill=10
152 0 -13 -2012 2016 fill=10
c
153 0 -128 lat=1 u=12 trcl=(-93.35 -155.40 -112.22) $ I-Beam Shells for top base
fill=0:4 0:0 0:0 8 7 6 6 8
154 0 -14 2000 fill=12
155 0 -14 -2000 2005 fill=12
156 0 -14 -2005 2012 fill=12
157 0 -14 -2012 fill=12
c New Cells
300 1 -0.001124 -200 #450 #451 #422 #331 #321 #332 trcl=(26.5 -54.44 34.12) $ Inner PMT
301 1 -0.001124 -201 trcl=(26.5 -54.44 34.12) $ Quartz
402 1 -0.001124 -202 trcl=(26.5 -54.44 34.12) $ 5mm scintillator
303 1 -0.001124 -203 trcl=(26.5 -54.44 34.12) $ Wires
304 1 -0.001124 -204 trcl=(26.5 -54.44 34.12)
305 1 -0.001124 -205 trcl=(26.5 -54.44 34.12)
306 1 -0.001124 -206 203 trcl=(26.5 -54.44 34.12) $ Wire insulation
307 1 -0.001124 -207 204 trcl=(26.5 -54.44 34.12)
308 1 -0.001124 -208 205 trcl=(26.5 -54.44 34.12)
309 1 -0.001124 -209 210 -211 212 #450 #451 #329 trcl=(26.5 -54.44 34.12) $ Kapton Walls
311 1 -0.001124 -214 202 trcl=(26.5 -54.44 34.12) $ Teflon wrap around Sc
312 1 -0.001124 -215 200 201 trcl=(26.5 -54.44 34.12) $ Teflon wrap around pmt, qz
313 1 -0.001124 -216 206 207 208 214 215 200 #309 #422 #331 #332 #329 #450 #451
trcl=(26.5 -54.44 34.12)
c
320 1 -0.001124 -220 trcl=(26.5 -64.31172 34.12) $ Outer PMT
321 9 -2.6 -221 trcl=(26.5 -54.73972 34.12) $ Quartz
422 10 -5.37 -222 trcl=(26.5 -54.73972 34.12) $ 5mm scintillator
323 11 -8.96 -223 trcl=(26.5 -64.31172 34.12) $ Wires
324 11 -8.96 -224 trcl=(26.5 -64.31172 34.12)
325 11 -8.96 -225 trcl=(26.5 -64.31172 34.12)
326 12 -1.406 -226 223 trcl=(26.5 -64.31172 34.12) $ Wire insulation
327 12 -1.406 -227 224 trcl=(26.5 -64.31172 34.12)
328 12 -1.406 -228 225 trcl=(26.5 -64.31172 34.12)
329 18 -1.42 -229 230 231 -233 trcl=(26.5 -54.73972 34.12) $ Kapton Walls
331 13 -2.25 -234 222 trcl=(26.5 -54.73972 34.12) $ Teflon wrap around Sc
332 13 -2.25 -235 220 221 trcl=(26.5 -54.73972 34.12) $ Teflon wrap around pmt, qz
333 1 -0.001124 -236 226 227 228 234 235 220 #329
trcl=(26.5 -64.31172 34.12)
c
450 15 -16.69 -450 trcl=(26.5 -54.48 34.12)
451 20 -2.700 -451 450 trcl=(26.5 -54.48 34.12)
c
c Surfaces
2 BOX 208.75 -585.30 -154.14 91.44 0 0 0 1170.60 0 0 0 600.00 $ Back Wall
3 BOX -208.75 -585.30 -154.14 417.50 0 0 0 91.44 0 0 0 600.00 $ Right side wall (side of port)
4 BOX -208.75 493.86 -154.14 417.50 0 0 0 91.44 0 0 0 600.00 $ Left side wall
5 BOX -208.75 -585.30 -154.14 -579.12 0 0 0 1170.60 0 0 0 600.00 $ Front wall
```

```
6 BOX -787.87 -585.30 -245.58 1088.06 0 0 0 1170.60 0 0 0 091.44 $ Floor
7 BOX -787.87 -585.30 445.86 1088.06 0 0 0 1170.60 0 0 0 091.44 $ Ceiling
8 BOX -208.75 -493.86 -154.14 417.50 0 0 0 987.72 0 0 0 600.00 $ Air Inside Room
9 RCC -208.75 0.00 -1.74 -487.68 0 0 91.44 $ Hole in back wall
16 PZ -32.22 $ Height of Lithium in back wall
c
10 BOX -105.20 -155.40 -154.14 210.40 0 0 0 310.80 0 0 0 0.64 $ Wood layer
11 BOX -105.20 -155.40 -153.50 210.40 0 0 0 310.80 0 0 0 0.64 $ Steel layer
12 BOX -105.20 -155.40 -152.86 210.40 0 0 0 310.80 0 0 0 20.32 $ Lower base cell
13 BOX -105.20 -155.40 -132.54 210.40 0 0 0 310.80 0 0 0 20.32 $ Middle base cell
14 BOX -93.35 -155.40 -112.22 186.70 0 0 0 310.80 0 0 0 20.32 $ Upper base cell
15 BOX -93.35 -155.40 -91.90 186.70 0 0 0 310.80 0 0 0 1.80 $ Sheet of Steel below LSDS
c
18 BOX -90.10 -90.10 -90.10 180.20 0 0 0 180.20 0 0 0 180.20 $ Cadmium Cover (outside)
19 BOX -90.00 -90.00 -90.00 180.00 0 0 0 180.00 0 0 0 180.00 $ Cadmium Cover (inside)
2000 S 26.5 -64.34 34.12 175.00 $ Lead Shell (furthest)
2001 S 26.5 -64.34 34.12 170.00 $ Lead Shell
2002 S 26.5 -64.34 34.12 165.00 $ Lead Shell
2003 S 26.5 -64.34 34.12 160.00 $ Lead Shell
2004 S 26.5 -64.34 34.12 155.00 $ Lead Shell
2005 S 26.5 -64.34 34.12 150.00 $ Lead Shell
2006 S 26.5 -64.34 34.12 145.00 $ Lead Shell
2007 S 26.5 -64.34 34.12 140.00 $ Lead Shell
2008 S 26.5 -64.34 34.12 135.00 $ Lead Shell
2009 S 26.5 -64.34 34.12 130.00 $ Lead Shell
2010 S 26.5 -64.34 34.12 125.00 $ Lead Shell
2011 S 26.5 -64.34 34.12 120.00 $ Lead Shell
2012 S 26.5 -64.34 34.12 115.00 $ Lead Shell
2013 S 26.5 -64.34 34.12 110.00 $ Lead Shell
2014 S 26.5 -64.34 34.12 105.00 $ Lead Shell
2015 S 26.5 -64.34 34.12 100.00 $ Lead Shell
2016 S 26.5 -64.34 34.12 95.00 $ Lead Shell
2017 S 26.5 -64.34 34.12 90.00 $ Lead Shell
2018 S 26.5 -64.34 34.12 85.00 $ Lead Shell
2019 S 26.5 -64.34 34.12 80.00 $ Lead Shell
2020 S 26.5 -64.34 34.12 75.00 $ Lead Shell
2021 S 26.5 -64.34 34.12 70.00 $ Lead Shell
2022 S 26.5 -64.34 34.12 65.00 $ Lead Shell
2023 S 26.5 -64.34 34.12 60.00 $ Lead Shell
2024 S 26.5 -64.34 34.12 55.00 $ Lead Shell
2025 S 26.5 -64.34 34.12 50.00 $ Lead Shell
2026 S 26.5 -64.34 34.12 46.00 $ Lead Shell
2027 S 26.5 -64.34 34.12 38.00 $ Lead Shell
2028 S 26.5 -64.34 34.12 35.00 $ Lead Shell
2029 S 26.5 -64.34 34.12 30.00 $ Lead Shell
2030 S 26.5 -64.34 34.12 25.00 $ Lead Shell
2031 S 26.5 -64.34 34.12 22.00 $ Lead Shell
2032 S 26.5 -64.34 34.12 14.00 $ Lead Shell (closest)
c
1020 S -49.36 -59.26 0.00 175.00 $ Lead Shell (furthest)
1021 S -49.36 -59.26 0.00 150.00 $ Lead Shell
1022 S -49.36 -59.26 0.00 115.00 $ Lead Shell
```

```
1023 S -49.36 -59.26 0.00 95.00 $ Lead Shell
1024 S -49.36 -59.26 0.00 75.00 $ Lead Shell
1025 S -49.36 -59.26 0.00 46.00 $ Lead Shell
1026 S -49.36 -59.26 0.00 38.00 $ Lead Shell
1027 S -49.36 -59.26 0.00 30.00 $ Lead Shell
1028 S -49.36 -59.26 0.00 22.00 $ Lead Shell
1029 S -49.36 -59.26 0.00 14.00 $ Lead Shell (closest)
c
50 BOX 19.00 -90.00 26.62 15.00 0 0 0 35.56 0 0 0 15.00 $ Assay Port
51 PY -74.76 $ Plane for back bricks
52 BOX 25.23 -90.00 32.85 2.54 0 0 0 40.64 0 0 0 2.54 $ Sq Hole in bricks
53 PY -84.92 $ Plane for middle bricks
54 PZ 34.12 $ Plane for middle brick hole
55 C/Y 26.50 34.12 1.27 $ Cylinder hole in bricks
c
56 BOX -49.36 -90.00 23.96 25.40 0 0 0 147.32 0 0 0 25.40 $ Fuel Assay Port
57 PY -49.36 $ Plane for Back Section
58 BOX -44.28 -49.36 34.12 15.24 0 0 0 106.68 0 0 0 15.24 $ Air in Back Section
59 BOX -44.28 -69.68 44.28 10.16 0 0 0 20.32 0 0 0 5.08 $ Air for back middle section
60 BOX -44.28 -79.84 44.28 5.08 0 0 0 10.16 0 0 0 5.08 $ Air for middle front section
61 BOX -49.36 -90.00 44.28 5.08 0 0 0 10.16 0 0 0 5.08 $ Air for front section, left
62 BOX -34.12 -90.00 44.28 5.08 0 0 0 10.16 0 0 0 5.08 $ Air for front section, right
c
90 BOX -69.68 -90.10 -90.00 60.96 0 0 0 -30.48 0 0 0 40.64 $ Bottom set of Lead Bricks
91 BOX -69.68 -90.10 -49.36 81.28 0 0 0 -35.56 0 0 0 2.54 $ Wood Layer
92 BOX -69.68 -90.10 -46.82 81.28 0 0 0 -30.48 0 0 0 5.08 $ Short Lead Brick
93 BOX -64.60 -90.10 -41.74 60.09 0 0 0 -30.48 0 0 0 15.24 $ Lead Brick below Li
94 BOX -64.60 -94.50 -26.50 60.09 0 0 0 -26.40 0 0 0 30.48 $ Lead Brick in front Li
95 BOX -92.64 -90.10 -26.50 124.46 0 0 0 -4.40 0 0 0 25.40 $ Lower Li Bricks
96 BOX -76.13 -90.10 -1.10 63.50 0 0 0 -4.40 0 0 0 12.7 $ Upper Li Brick
c
116 BOX 0.00 0.00 0.00 42.08 0 0 0 310.80 0 0 0 20.32 $ I-Beam Box (bottom)
117 BOX 0.00 0.00 0.00 13.34 0 0 0 310.80 0 0 0 0.64 $ Bottom of I-Beam
118 BOX 6.35 0.00 0.64 0.64 0 0 0 310.80 0 0 0 19.05 $ Middle of I-Beam
119 BOX 0.00 0.00 19.69 13.34 0 0 0 310.80 0 0 0 0.64 $ Top of I-Beam
120 BOX 13.34 0.00 0.00 2.94 0 0 0 310.80 0 0 0 20.32 $ Li left of cylinder
121 BOX 39.14 0.00 0.00 2.94 0 0 0 310.80 0 0 0 20.32 $ Li right of cylinder
c
122 BOX 0.00 0.00 0.00 310.80 0 0 0 42.08 0 0 0 20.32 $ I-Beam Box (middle)
123 BOX 0.00 0.00 0.00 310.80 0 0 0 13.34 0 0 0 0.64 $ Bottom of I-Beam
124 BOX 0.00 6.35 0.64 310.80 0 0 0 0.64 0 0 0 19.05 $ Middle of I-Beam
125 BOX 0.00 0.00 19.69 310.80 0 0 0 13.34 0 0 0 0.64 $ Top of I-Beam
126 BOX 0.00 13.34 0.00 310.80 0 0 0 2.94 0 0 0 20.32 $ Li left of cylinder
127 BOX 0.00 39.14 0.00 310.80 0 0 0 2.94 0 0 0 20.32 $ Li right of cylinder
132 BOX 0.00 13.34 0.00 310.80 0 0 0 28.74 0 0 0 20.32 $ Li full
c
128 BOX 0.00 0.00 0.00 37.34 0 0 0 310.80 0 0 0 20.32 $ I-Beam Box (top)
129 BOX 13.34 124.46 0.00 0.57 0 0 0 186.34 0 0 0 20.32 $ Li left of cylinder
130 BOX 36.77 124.46 0.00 0.57 0 0 0 186.34 0 0 0 20.32 $ Li right of cylinder
131 BOX 13.34 0.00 0.00 24.00 0 0 0 310.80 0 0 0 20.32 $ Li full
c
c New Surfaces
```

```
200 RCC 0.00 0.000 0.00 0 -9.172 0 0.916 $ Inner detector PMT
201 RCC 0.00 -9.172 0.00 0 -0.2 0 0.916 $ Quartz
202 RCC 0.00 -9.372 0.00 0 -0.2 0 0.9525 $ 2mm crystal
203 RCC 0.8062 0.000 1.1096 0 -9.87172 0 0.06096 $ Wires
204 RCC 0.9699 0.000 0.970 0 -9.87172 0 0.06096
205 RCC 1.1096 0.000 0.8062 0 -9.87172 0 0.06096
206 RCC 0.8062 0.000 1.1096 0 -9.87172 0 0.1016 $ Wire insulation
207 RCC 0.9699 0.000 0.970 0 -9.87172 0 0.1016
208 RCC 1.1096 0.000 0.8062 0 -9.87172 0 0.1016
209 C/Y 0.00 0.00 0.992 $ Outer Kapton cylinder
210 C/Y 0.00 0.00 .980 $ Inner Kapton cylinder
211 PY 0.00 $ Outer end of Kapton
212 PY -9.572 $ Inner end of kapton
214 RCC 0.00 -9.372 0.00 0 -0.2 0 0.9789 $ Teflon tape around Sc
215 RCC 0.00 -7.032 0.00 0 -2.34 0 0.9415 $ Teflon tape around pmt, qz
216 BOX -1.265 0.000 -1.265 2.53 0 0 0 -9.572 0 0 0 2.53 $ Total det
c
220 RCC 0.00 -0.4 0.00 0 -9.172 0 0.916 $ Outer detector PMT
221 RCC 0.00 -0.2 0.00 0 -0.2 0 0.916 $ Qz
222 RCC 0.00 -0.0 0.00 0 -0.2 0 0.9525 $ Crystal
223 RCC 0.8062 0.0 1.1096 0 -9.572 0 0.06096 $ Wires
224 RCC 0.9699 0.0 0.970 0 -9.572 0 0.06096
225 RCC 1.1096 0.0 0.8062 0 -9.572 0 0.06096
226 RCC 0.8062 0.0 1.1096 0 -9.572 0 0.1016 $ Wire Insulation
227 RCC 0.9699 0.0 0.970 0 -9.572 0 0.1016
228 RCC 1.1096 0.0 0.8062 0 -9.572 0 0.1016
229 C/Y 0.00 0.00 0.992
230 C/Y 0.00 0.00 .980
231 PY -9.572
233 PY 0.0
234 RCC 0.00 -0.0 0.00 0 -0.2 0 0.9789 $ Teflon Tape around sc
235 RCC 0.00 -0.2 0.00 0 -2.34 0 0.9415 $ Teflon tape around pmt, qz
236 BOX -1.265 0.00 -1.265 2.53 0 0 0 -9.572 0 0 0 2.53
c
450 BOX -0.625 0.00 -.925 1.25 0 0 0 -0.0254 0 0 0 1.85 $ Sample (118 mils)
451 BOX -0.645 0.02 -.945 1.29 0 0 0 -0.0654 0 0 0 1.89 $ Aluminum Foil
c

c Materials (Switching to two columns to save space)
c Air (-0.001124)
M1 6000 0.000125
7014 0.6869
8016 0.301248
18000 0.011717
c
c Concrete (-2.30)
M2 1001 -0.010000
8016 -0.532000
11023 -0.029000
13027 -0.034000
14000 -0.337000
20000 -0.044000
26000 -0.014000
c
c Steel (-7.82)
M3 6000 -0.005000
26000 -0.995000
c
c Wood (southern pine) (-0.64)
M4 1001 -0.059642
6000 -0.497018
7014 -0.004970
8016 -0.427435
12000 -0.001988
16000 -0.004970
```

```
19000 -0.001988
20000 -0.001988
c
c Lead (-11.34)
M5 82204 -1.3779E-02
82206 -2.3953E-01
82207 -2.2072E-01
82208 -5.2587E-01
1001 -1.0000E-6
6000 -2.0000E-05
47107 -6.791E-07
47109 -6.309E-07
29063 -3.126E-06
29065 -1.394E-06
33075 -4.000E-08
c 51000 -1.1E-07
51121 -6.293E-08
51123 -4.707E-08
28058 -1.021E-07
28060 -3.933E-08
28061 -1.710E-09
28062 -5.452E-09
28064 -1.388E-09
c 30000 -3.0E-08
30064.80c -0.00000001458
30066.80c -0.00000000837
30067.80c -0.00000000123
30068.80c -0.00000000564
30070.80c -0.00000000018
c 48000 -1.0E-08
48106 -1.250E-10
48108 -8.900E-11
48110 -1.249E-09
48111 -1.280E-09
48113 -1.222E-09
48114 -2.873E-09
48116 -7.490E-10
26054 -5.845E-08
26056 -9.175E-07
26057 -2.119E-08
26058 -2.820E-09
c 50000 -3.0E-08
50112 -2.910E-10
50114 -1.980E-10
50115 -1.020E-10
50116 -4.362E-09
50117 -2.304E-09
50118 -7.266E-09
50119 -2.577E-09
50120 -9.774E-09
50122 -1.389E-09
50124 -1.737E-09
52120 -1.710E-10
52122 -4.845E-09
52123 -1.691E-09
52124 -9.006E-09
52125 -1.343E-08
52126 -3.580E-08
52128 -6.031E-08
52130 -6.475E-08
64152 -2.000E-11
64154 -2.180E-10
64155 -1.480E-09
64156 -2.047E-09
64157 -1.565E-09
64158 -2.484E-09
64160 -2.186E-09
62144 -3.070E-10
62147 -1.499E-09
62148 -1.124E-09
62149 -1.382E-09
62150 -7.380E-10
62152 -2.675E-09
62153 -2.275E-09
83209 -1.153E-5
c
c Cadmium (-8.65)
M6 48106 -1.25
48108 -0.89
48110 -12.49
48111 -12.80
48112 -24.13
48113 -12.22
48114 -28.73
48116 -7.49
c Bismuth (-9.78)
M7 83209 1
c
c LiCO3 (-2.11)
M8 3006 0.15
3007 1.85
6000 1
8016 3
c
c Quartz (-2.6 )
M9 14000 1
8016 2
c nlib=70c
c YAP:Ce (-5.37)
M10 39089 0.1988
13027 0.1988
8016 0.5964
58136 0.0000111
58138 0.00001506
```

```
58140.86c 0.005307
58142.86c 0.000066684
c
c Tinned Copper (assumed) (-8.96)
M11 29000 -0.89
50000 -0.11
c
c PVC (-1.406)
M12 1001 -0.048382
6000 -0.384361
17000 -0.567257
c
c Teflon (-2.25)
M13 6000 -0.240182
9019 -0.759818
c
c Carbon Fiber (assumed) (-1.61)
M14 6000 -0.975258
1001 -0.004914
8016 -0.009829
c
c Tantalum 181 (-16.69)
M15 73180.80c -0.000119974200334803
73181.80c -0.999665028589691
13027.80c -4.99992499894992E-06
5010.80c -1.99996999957997E-07
5011.80c -7.99987999831987E-07
6000.80c -0.00001
20040.80c -4.84697729323204E-06
20042.80c -3.2349514743206E-08
20043.80c -6.74989874858239E-09
20044.80c -1.04298435478095E-07
20046.80c -1.99996999957997E-10
20048.80c -9.34985974803635E-09
24050.80c -2.17246741204374E-07
24052.80c -4.18938715737015E-06
24053.80c -4.75042874150232E-07
24054.80c -1.18248226225166E-07
29063.80c -3.45744813677387E-06
29065.80c -1.54247686217605E-06
26054.80c -2.9249561243857E-07
26056.80c -4.58743118653655E-06
26057.80c -1.05998409977738E-07
26058.80c -1.39997899970598E-08
1001.80c -0.000004999
1002.80c -0.000000001
12024.80c -3.94994074917044E-06
12025.80c -4.99992499894992E-07
12026.80c -5.49991749884491E-07
25055.80c -4.99992499894992E-06
42092.80c -7.32489012346163E-07
42094.80c -4.59493107403498E-07
42095.80c -7.93488097333352E-07
42096.80c -8.33487497324952E-07
42097.80c -4.78992814899402E-07
42098.80c -1.21448178224494E-06
42100.80c -4.86992694897722E-07
7014.80c -0.000018924
7015.80c -0.000000076
41093.80c -0.000064999024986349
28058.80c -3.40379894153514E-06
28060.80c -1.31113033247464E-06
28061.80c -5.69991449880291E-08
28062.80c -1.8174727371183E-07
28064.80c -4.62993054902763E-08
8016.80c -0.00002499
8017.80c -0.00000001
14028.80c -4.60993084903183E-06
14029.80c -2.34996474950646E-07
14030.80c -1.54997674967448E-07
50112.80c -4.84992724898142E-08
50114.80c -3.29995049930695E-08
50115.80c -1.69997449964297E-08
50116.80c -7.26989094847318E-07
50117.80c -3.83994239919354E-07
50118.80c -1.21098183474567E-06
50119.80c -4.29493557409798E-07
50120.80c -1.62897556465788E-06
50122.80c -2.31496527451381E-07
50124.80c -2.894956574392E-07
22046.80c -4.12493812413368E-07
22047.80c -3.71994419921874E-07
22048.80c -3.68594470922588E-06
22049.80c -2.70495942443191E-07
22050.80c -2.58996114945606E-07
74180.80c -2.99995499936995E-08
74182.80c -6.62490062360864E-06
74183.80c -3.57744633674867E-06
74184.80c -7.65988509839128E-06
74186.80c -7.10739338600731E-06
40090.80c -2.57246141195973E-06
40091.80c -5.60991584882181E-07
40092.80c -8.57487137319912E-07
40094.80c -8.68986964817496E-07
40096.80c -1.39997899970598E-07
c
c Molybdenum
M16 42000 -1.0
c
c Nickel
M17 28058 0.6807
28060 0.2622
28061 0.0114
28062 0.0363
```

```
28064 0.0093
c
c Kapton
M18 1001 0.256399
6000 0.564114
7014 0.051282
8016 0.128205
c
c Uranium
M19 92234 0.000050
92235 0.007200
92238 0.992740
M995 92235.70c 1
c
c Aluminum (-2.70)
M20 13027 1
c
c Source Specification
MODE N
NPS 799995
CUT:N 400000
print -128
sdef ERG=D1 tme=d2
SP1 -5 0.46
si2 -4.9 4.9
sp2 0 1
c
IMP:N,P
0.000E+00 $1
1.000E+00 $2
1.000E+00 $3
1.000E+00 $4
1.000E+00 $5
1.000E+00 $6
1.000E+00 $7
1.000E+00 $9
1.000E+00 $39
1.000E+00 $10
1.000E+00 $11
0.000E+00 $15
0.000E+00 $16
1.000E+00 $17
1.000E+00 $18
1.000E+00 $8
1.000E+00 $19
1.000E+00 $2000
1.000E+00 $2001
1.000E+00 $2002
1.000E+00 $2003
1.000E+00 $2004
1.000E+00 $2005
1.000E+00 $2006
1.000E+00 $2007
1.000E+00 $2008
1.000E+00 $2009
1.000E+00 $2010
1.000E+00 $2011
1.000E+00 $2012
1.000E+00 $2013
1.000E+00 $2014
1.000E+00 $2015
1.000E+00 $2016
1.000E+00 $2017
1.000E+00 $2018
1.000E+00 $2019
2.000E+00 $2020
4.000E+00 $2021
8.000E+00 $2022
1.600E+01 $2023
3.200E+01 $2024
6.400E+01 $2025
1.280E+02 $2026
2.560E+02 $2027
5.120E+02 $2028
1.024E+03 $2029
2.048E+03 $2030
4.096E+03 $2031
8.192E+03 $2032
1.000E+00 $30
1.000E+00 $31
1.000E+00 $32
1.000E+00 $33
2.000E+00 $34
8.000E+00 $35
3.200E+01 $36
1.280E+02 $37
5.120E+02 $38
1.000E+00 $40
1.000E+00 $41
1.000E+00 $42
2.000E+00 $43
8.000E+00 $44
3.200E+01 $45
1.280E+02 $46
5.120E+02 $47
2.048E+03 $48
8.192E+03 $50
8.192E+03 $51
4.096E+03 $52
4.096E+03 $53
8.192E+03 $54
2.048E+03 $55
4.096E+03 $56
4.000E+00 $57
```

4.000E+00 $58
4.000E+00 $59
4.000E+00 $60
4.000E+00 $61
4.000E+00 $62
4.000E+00 $63
4.000E+00 $64
0.000E+00 $65
0.000E+00 $88
0.000E+00 $66
0.000E+00 $67
0.000E+00 $68
4.000E+00 $69
4.000E+00 $70
0.000E+00 $71
0.000E+00 $72
4.000E+00 $73
0.000E+00 $74
0.000E+00 $75
0.000E+00 $76
4.000E+00 $77
0.000E+00 $78
4.000E+00 $79
0.000E+00 $80
0.000E+00 $81
4.000E+00 $82
4.000E+00 $83
0.000E+00 $84
0.000E+00 $85
0.000E+00 $87
1.000E+00 $90
0.000E+00 $91
0.000E+00 $92
0.000E+00 $93
1.000E+00 $94
1.000E+00 $95
0.000E+00 $96
1.000E+00 $97
1.000E+00 $98
1.000E+00 $99
1.000E+00 $100
0.000E+00 $101
0.000E+00 $102
1.000E+00 $86
1.000E+00 $103
0.000E+00 $104
0.000E+00 $105
0.000E+00 $106
0.000E+00 $107
1.000E+00 $108
1.000E+00 $109
0.000E+00 $110
0.000E+00 $111
0.000E+00 $112
0.000E+00 $113
1.000E+00 $114
1.000E+00 $115
1.000E+00 $116
1.000E+00 $117
0.000E+00 $118
1.000E+00 $119
1.000E+00 $120
1.000E+00 $121
1.000E+00 $122
0.000E+00 $123
1.000E+00 $124
1.000E+00 $125
0.000E+00 $126
1.000E+00 $127
1.000E+00 $128
1.000E+00 $129
1.000E+00 $130
0.000E+00 $131
1.000E+00 $132
1.000E+00 $133
0.000E+00 $134
1.000E+00 $135
1.000E+00 $136
1.000E+00 $137
1.000E+00 $138
0.000E+00 $139
1.000E+00 $140
1.000E+00 $141
1.000E+00 $142
0.000E+00 $143
1.000E+00 $158
1.000E+00 $159
1.000E+00 $160
0.000E+00 $161
0.000E+00 $144
0.000E+00 $145
0.000E+00 $146
0.000E+00 $147
0.000E+00 $148
0.000E+00 $149
0.000E+00 $150
0.000E+00 $151
0.000E+00 $152
0.000E+00 $153
0.000E+00 $154
0.000E+00 $155
0.000E+00 $156
0.000E+00 $157
8.192E+03 $300

```
8.192E+03 $301
8.192E+03 $402
8.192E+03 $303
8.192E+03 $304
8.192E+03 $305
8.192E+03 $306
8.192E+03 $307
8.192E+03 $308
8.192E+03 $309
8.192E+03 $311
8.192E+03 $312
8.192E+03 $313
8.192E+03 $320
8.192E+03 $321
8.192E+03 $422
8.192E+03 $323
8.192E+03 $324
8.192E+03 $325
8.192E+03 $326
8.192E+03 $327
8.192E+03 $328
8.192E+03 $329
8.192E+03 $331
8.192E+03 $332
8.192E+03 $333
8.192E+03 $450
8.192E+03 $451
c
c Tallies
c
FC4 (n,g) Sample
F4:N 450
fq4 t e
T4 100 300iLOG 400000
c
FC14 (n,g) Sample FM
F14:N 450
FM14 -1 15 -2
fq14 t e
T14 100 300iLOG 400000
c
c Gamma tallies:
FC204 g,det
F204:P 402 422 T
fq204 t e
T204 100 300iLOG 400000
c
FC314 (n,g) det
F314:N 402 422 T
FM314 1 8 -2
fq314 t e
T314 100 300iLOG 400000
c
FC404 g,det Total
F404:P 402 422 T
FM404 -1 8 -5
fq404 t e
T404 100 300iLOG 400000
c
FC414 g,det Heating
F414:P 402 422 T
FM414 -1 8 -6
fq414 t e
T414 100 300iLOG 400000
c
FC424 g,det Total * Heating
F424:P 402 422 T
FM424 -1 8 -5 -6
fq424 t e
T424 100 300iLOG 400000
c
F6:P 422
fq6 t e
T6 100 300iLOG 400000
c
```

APPENDIX D
Measurement Results Tables

Below are tables of measurement results as a function of time. One note, D1 stands for Detector 1, which was placed in the back middle measurement port, location (-49.36 -49.36 0.00) in MCNP. D2 stands for Detector 2, which was placed in the forward top quadrant measurement port, location (26.5 -54.44 34.12) in MCNP. All measurement numbers represent the detected count rate in counts per second, numbers in parentheses represent the associated statistical uncertainty.

Table D.1: Measurement Results: Ta, Ag, Au.

Time [μs]	**0.254mm Ta (D1)**	**0.6mm Ag (D1)**	**0.4mm Au (D1)**
0.2672	4720000 (130000)	4530000 (140000)	20000 (120000)
0.472	-1444000 (62000)	-2193000 (68000)	-121000 (56000)
0.6768	2000 (62000)	-6000 (68000)	0 (56000)
0.8816	-39000 (1100)	-70600 (1100)	-18100 (1000)
1.0864	-1170000 (42000)	-1983000 (42000)	-485000 (38000)
1.2912	492000 (51000)	-49000 (54000)	475000 (45000)
1.496	749000 (18000)	1981000 (19000)	602000 (16000)
1.7008	586200 (8200)	1910300 (8800)	485500 (7300)
1.9056	524700 (5900)	1798900 (6400)	426000 (5300)
2.1104	506100 (5400)	1727300 (5800)	402000 (4800)
2.3152	500600 (5000)	1646800 (5400)	385800 (4500)
2.52	473400 (4700)	1589200 (5000)	362200 (4200)
2.7248	470400 (4300)	1498800 (4600)	356700 (3800)
2.9296	474500 (4000)	1439100 (4300)	349900 (3600)
3.1344	462600 (3900)	1361800 (4100)	350200 (3500)
3.3392	463300 (3700)	1306300 (3900)	343900 (3300)
3.544	470500 (3300)	1239700 (3500)	344400 (3000)
3.7488	460900 (3000)	1181800 (3200)	342300 (2700)
3.9536	463100 (2600)	1141200 (2800)	345000 (2300)
4.1584	467500 (2300)	1096200 (2500)	342200 (2100)
4.3632	468100 (2100)	1057000 (2300)	345000 (1900)
4.568	472400 (1900)	1026100 (2000)	342900 (1700)
4.7728	471900 (1700)	982200 (1800)	340900 (1500)
4.9776	464800 (1500)	958300 (1700)	338600 (1400)
5.1824	462000 (1500)	920200 (1600)	336800 (1300)

Continued on next page

Table D.1 – continued from previous page

Time [μs]	0.254mm Ta (D1)	0.6mm Ag (D1)	0.4mm Au (D1)
5.3872	456900 (1500)	893600 (1600)	333700 (1300)
5.6944	460800 (1600)	858500 (1700)	330600 (1400)
6.104	460400 (1800)	820400 (2000)	324500 (1600)
6.5136	469100 (2300)	790300 (2600)	321900 (2100)
6.9232	466200 (3000)	759800 (3200)	309800 (2700)
7.3328	453400 (3400)	721700 (3700)	295900 (3000)
7.7424	440800 (3400)	685600 (3600)	282200 (3000)
8.152	443000 (2900)	647000 (3100)	282000 (2600)
8.5616	435400 (2300)	624300 (2500)	288100 (2100)
8.9712	429900 (1900)	594200 (2100)	285700 (1700)
9.3808	415900 (1900)	572500 (2000)	288400 (1700)
9.7904	410000 (1900)	549900 (2000)	284700 (1700)
10.2	412600 (1700)	535700 (1900)	286700 (1500)
10.6096	402200 (1400)	521600 (1400)	284600 (1200)
11.0192	402340 (910)	503090 (990)	281600 (810)
11.4288	401400 (610)	499170 (640)	276500 (540)
11.8384	409360 (430)	498650 (430)	266700 (380)
12.248	409800 (330)	492450 (360)	258920 (290)
12.6576	409890 (270)	487860 (290)	254920 (250)
13.0672	404400 (230)	472640 (240)	247280 (210)
13.4768	392480 (220)	455990 (230)	246940 (190)
13.8864	376860 (200)	435440 (220)	251580 (180)
14.296	360180 (210)	416050 (220)	253950 (190)
14.7056	348670 (220)	404820 (240)	259490 (200)
15.1152	338300 (260)	404890 (270)	261780 (230)
15.5248	335100 (290)	413550 (320)	261310 (260)
15.9344	334300 (340)	426090 (380)	255560 (300)
16.344	334490 (380)	443780 (390)	252010 (340)
16.7536	335080 (380)	456750 (410)	242690 (340)
17.1632	337470 (390)	464130 (430)	234430 (350)
17.5728	339790 (360)	465770 (390)	221330 (330)
17.9824	344090 (320)	459490 (360)	210050 (290)
18.392	347210 (270)	448010 (310)	203110 (240)
18.8016	344790 (230)	419240 (250)	198330 (210)
19.2112	337250 (210)	392970 (220)	191490 (190)
19.6208	334470 (190)	367850 (200)	192810 (170)
20.0304	323460 (170)	344950 (190)	191200 (150)
20.44	318710 (160)	331880 (180)	191830 (150)
20.8496	307840 (160)	313810 (190)	188430 (150)
21.2592	300250 (160)	305400 (180)	189190 (150)
21.6688	295150 (170)	302330 (180)	187500 (150)

Continued on next page

Table D.1 – continued from previous page

Time [μs]	0.254mm Ta (D1)	0.6mm Ag (D1)	0.4mm Au (D1)
22.0784	296130 (170)	302590 (180)	178930 (150)
22.5904	298180 (160)	298420 (180)	174760 (150)
23.2048	300730 (160)	290020 (170)	163190 (140)
23.8192	302910 (160)	274220 (170)	154330 (140)
24.4336	300700 (150)	251290 (160)	142190 (140)
25.048	298810 (150)	227840 (160)	134270 (140)
25.6624	296540 (150)	212890 (160)	123140 (130)
26.2768	291510 (160)	203950 (160)	110560 (140)
26.8912	286330 (160)	201530 (160)	100190 (140)
27.5056	278430 (150)	203720 (160)	92190 (130)
28.12	269420 (150)	209380 (160)	89070 (130)
28.7344	255860 (140)	212950 (150)	89170 (130)
29.3488	240780 (140)	216460 (150)	94260 (130)
29.9632	225810 (140)	218640 (150)	101850 (130)
30.5776	210200 (140)	215380 (150)	107860 (130)
31.192	196520 (150)	213740 (160)	115360 (140)
31.8064	186960 (160)	211240 (170)	117640 (140)
32.4208	177560 (170)	211550 (170)	116910 (160)
33.0352	175470 (180)	208060 (190)	112890 (160)
33.6496	173750 (180)	208490 (200)	103530 (170)
34.264	176570 (190)	207320 (210)	91500 (170)
34.8784	178450 (200)	198470 (210)	79160 (180)
35.4928	181310 (200)	188050 (220)	67450 (180)
36.1072	186520 (190)	169790 (210)	59360 (170)
36.7216	188770 (180)	152570 (200)	54330 (160)
37.4384	189380 (170)	127960 (190)	50320 (160)
38.2576	194200 (160)	107740 (170)	48950 (150)
39.0768	195520 (140)	93010 (160)	49150 (130)
39.896	195350 (140)	88000 (150)	48530 (120)
40.7152	197190 (120)	92520 (140)	48250 (110)
41.5344	193430 (120)	98030 (130)	47790 (110)
42.3536	190650 (120)	112030 (120)	48210 (110)
43.1728	188400 (110)	125680 (120)	51940 (100)
43.992	181740 (110)	137310 (120)	56098 (99)
44.8112	172750 (110)	150530 (120)	62196 (96)
45.6304	162640 (100)	164340 (120)	67778 (94)
46.4496	148280 (110)	175790 (110)	74469 (96)
47.2688	133720 (110)	188870 (110)	80127 (97)
48.088	116960 (100)	196800 (120)	88464 (94)
48.9072	103975 (98)	203440 (110)	96109 (89)
49.7264	90750 (100)	209470 (110)	105504 (91)

Continued on next page

Table D.1 – continued from previous page

Time [μs]	0.254mm Ta (D1)	0.6mm Ag (D1)	0.4mm Au (D1)
50.5456	80380 (100)	215920 (110)	114080 (94)
51.4672	70330 (100)	224030 (110)	120015 (94)
52.4912	64150 (100)	237020 (110)	121772 (92)
53.5152	59040 (100)	255210 (110)	116529 (91)
54.5392	57280 (97)	271390 (110)	103462 (88)
55.5632	56520 (100)	286850 (110)	85489 (94)
56.5872	58820 (100)	292250 (110)	66871 (93)
57.6112	65097 (98)	288870 (110)	50552 (88)
58.6352	73318 (99)	283590 (110)	37190 (90)
59.6592	84330 (110)	274960 (110)	26426 (96)
60.6832	100220 (100)	263320 (110)	19578 (91)
61.7072	119110 (100)	254690 (110)	15156 (94)
62.7312	138637 (99)	241610 (110)	12620 (89)
63.7552	156808 (95)	231040 (100)	11127 (86)
64.8816	176129 (95)	211690 (100)	9804 (86)
66.1104	189171 (95)	193940 (100)	8749 (86)
67.3392	190700 (91)	176570 (100)	8585 (82)
68.568	182691 (91)	162291 (100)	8042 (83)
69.7968	166418 (92)	152865 (99)	8259 (83)
71.0256	144625 (90)	146596 (100)	8027 (81)
72.2544	121856 (92)	141837 (97)	8173 (83)
73.4832	100450 (90)	138108 (98)	8153 (81)
74.712	84567 (90)	130110 (100)	8264 (82)
75.9408	73564 (91)	118500 (100)	8325 (83)
77.1696	67048 (94)	103890 (100)	8108 (85)
78.5008	66387 (93)	89190 (100)	8204 (84)
79.9344	68576 (97)	73790 (100)	7927 (87)
81.368	71471 (97)	59040 (110)	8639 (88)
82.8016	74720 (100)	49990 (110)	8364 (94)
84.2352	75980 (110)	45450 (110)	8409 (97)
85.6688	73300 (110)	44460 (120)	8625 (99)
87.1024	69000 (120)	46490 (130)	8410 (110)
88.536	63330 (120)	50930 (130)	8640 (110)
89.9696	57100 (120)	58600 (130)	9060 (110)
91.5056	49400 (120)	68640 (130)	9320 (110)
93.144	42750 (120)	82650 (130)	9290 (110)
94.7824	36650 (110)	97570 (120)	9280 (100)
96.4208	32370 (110)	109900 (120)	9592 (97)
98.0592	30330 (100)	121470 (110)	9877 (93)
99.6976	29921 (97)	126510 (100)	10144 (88)
101.336	31295 (94)	126757 (98)	10394 (85)

Continued on next page

Table D.1 – continued from previous page

Time [μs]	0.254mm Ta (D1)	0.6mm Ag (D1)	0.4mm Au (D1)
102.9744	33688 (89)	121300 (97)	10406 (81)
104.7152	37410 (87)	111417 (93)	10742 (78)
106.5584	41927 (85)	96471 (90)	11396 (77)
108.4016	44514 (82)	81009 (87)	11696 (74)
110.2448	48471 (76)	66677 (86)	12080 (69)
112.088	50937 (78)	54322 (82)	12410 (70)
113.9312	53780 (76)	45102 (78)	12939 (69)
115.7744	56761 (74)	38776 (82)	13312 (67)
117.72	59188 (73)	34484 (76)	14184 (66)
119.768	62548 (73)	32779 (76)	14913 (66)
121.816	66690 (70)	32484 (75)	15786 (64)
123.864	68479 (71)	32789 (76)	16752 (64)
125.912	69695 (69)	34123 (73)	17680 (63)
128.0624	67843 (70)	35866 (75)	18319 (63)
130.3152	62771 (67)	38309 (72)	20502 (61)
132.568	56223 (66)	41208 (74)	22137 (60)
134.8208	47696 (67)	45343 (73)	23959 (61)
137.0736	39077 (66)	49751 (74)	26067 (60)
139.4288	30839 (68)	55231 (74)	28903 (62)
141.8864	24239 (67)	61926 (72)	31493 (61)
144.344	18993 (66)	69856 (73)	36177 (60)
146.8016	15487 (68)	78790 (75)	39783 (61)
149.2592	13525 (69)	89717 (76)	44618 (62)
151.8192	12935 (71)	102310 (77)	50598 (65)
154.4816	12749 (71)	118677 (79)	57972 (65)
157.144	13441 (74)	134180 (79)	64839 (67)
159.8064	15300 (76)	150535 (83)	73322 (69)
162.5712	17203 (80)	169250 (82)	82588 (72)
165.4384	20403 (79)	188188 (85)	92317 (72)
168.3056	24216 (83)	202140 (88)	101043 (75)
171.1728	28878 (81)	214242 (88)	108695 (74)
174.1424	34555 (81)	220255 (88)	115619 (73)
177.2144	41280 (80)	223935 (87)	120451 (73)
180.2864	48612 (79)	220597 (85)	122288 (71)
183.4608	56495 (76)	211461 (82)	121726 (69)
186.7376	63520 (73)	198137 (80)	118781 (66)
190.0144	69813 (69)	181328 (75)	113034 (63)
193.3936	73661 (66)	162073 (73)	106500 (60)
196.8752	74091 (62)	141947 (69)	97322 (56)
200.3568	72200 (62)	123650 (65)	87874 (56)
203.9408	67603 (57)	106184 (64)	78525 (52)

Continued on next page

Table D.1 – continued from previous page

Time [μs]	0.254mm Ta (D1)	0.6mm Ag (D1)	0.4mm Au (D1)
207.6272	60156 (56)	89805 (62)	68686 (51)
211.416	50946 (56)	76664 (59)	59576 (50)
215.3072	42556 (53)	64718 (58)	51216 (48)
219.1984	33518 (53)	55795 (58)	44663 (48)
223.192	25824 (52)	48134 (57)	38517 (47)
227.288	19913 (51)	42395 (55)	33643 (47)
231.4864	14838 (51)	36985 (54)	29391 (46)
235.7872	11146 (51)	32969 (54)	25762 (47)
240.1904	8401 (50)	29774 (55)	23104 (46)
244.696	6544 (50)	26586 (54)	20669 (45)
249.304	5338 (49)	24778 (54)	18591 (45)
254.0144	4326 (49)	22832 (52)	16877 (45)
258.8272	3708 (48)	20633 (53)	15309 (44)
263.8448	3309 (48)	19654 (53)	14122 (44)
268.9648	2784 (49)	18139 (52)	12949 (45)
274.1872	2663 (48)	16907 (51)	12244 (43)
279.6144	2326 (47)	16180 (52)	11313 (43)
285.144	2158 (47)	15196 (50)	10562 (43)
290.776	1971 (46)	14248 (50)	9815 (42)
296.6128	1903 (46)	13559 (49)	9258 (42)
302.6544	1805 (46)	12616 (50)	8830 (41)
308.9008	1586 (45)	12019 (49)	8144 (41)
315.352	1448 (46)	11884 (49)	7652 (42)
321.9056	1451 (44)	11083 (49)	7376 (40)
328.5616	1226 (45)	10542 (49)	6978 (41)
335.4224	1219 (44)	10220 (47)	6668 (40)
342.5904	1237 (43)	9787 (46)	6342 (39)
350.0656	1123 (43)	9284 (47)	6040 (39)
357.7456	1111 (42)	8948 (46)	5770 (39)
365.6304	1040 (42)	8628 (46)	5458 (38)
373.72	1061 (41)	8315 (44)	5347 (37)
382.1168	948 (41)	8058 (44)	5034 (38)
390.8208	1027 (40)	7827 (44)	4824 (36)
399.832	912 (40)	7476 (44)	4604 (36)
409.2528	844 (40)	7339 (43)	4429 (36)
418.9808	829 (39)	6922 (43)	4180 (36)
429.016	828 (38)	6539 (43)	4128 (35)
439.4608	758 (39)	6404 (42)	3956 (35)
450.3152	710 (38)	6179 (41)	3804 (34)
461.5792	697 (38)	5932 (41)	3590 (35)
473.3552	687 (38)	5786 (41)	3427 (34)

Continued on next page

Table D.1 – continued from previous page

Time [μs]	0.254mm Ta (D1)	0.6mm Ag (D1)	0.4mm Au (D1)
485.6432	621 (37)	5578 (40)	3299 (34)
498.4432	609 (37)	5346 (40)	3164 (33)
511.8576	569 (36)	5247 (39)	3034 (33)
525.8864	623 (36)	4950 (39)	2931 (32)
540.5296	571 (35)	4739 (38)	2827 (32)
555.8896	533 (35)	4600 (38)	2649 (32)
572.0688	534 (34)	4381 (38)	2588 (31)
589.0672	536 (34)	4147 (38)	2447 (31)
606.8848	491 (34)	4056 (37)	2358 (31)
625.624	452 (33)	3891 (36)	2201 (30)
645.3872	438 (33)	3653 (36)	2111 (30)
666.2768	430 (32)	3555 (35)	2037 (29)
688.3952	411 (32)	3442 (35)	1929 (29)
711.8448	381 (31)	3181 (34)	1844 (28)
736.728	357 (30)	3028 (33)	1752 (28)
763.2496	349 (30)	2914 (33)	1640 (28)
791.6144	290 (30)	2729 (32)	1499 (28)
821.9248	291 (29)	2560 (32)	1441 (27)
854.3856	270 (28)	2406 (32)	1339 (26)
889.2016	235 (28)	2196 (30)	1270 (26)
926.68	244 (28)	2124 (30)	1161 (25)
967.2304	220 (27)	1956 (30)	1090 (25)
1011.2624	214 (26)	1809 (29)	1020 (24)
1059.1856	195 (26)	1668 (28)	918 (24)
1111.4096	170 (25)	1481 (28)	834 (23)
1168.6512	155 (24)	1345 (27)	760 (22)
1231.7296	136 (24)	1226 (27)	669 (22)
1301.464	115 (24)	1091 (26)	602 (22)
1378.9808	107 (23)	964 (25)	527 (21)
1465.7136	93 (22)	835 (25)	464 (21)
1563.4032	75 (22)	708 (24)	393 (20)
1674.2	58 (21)	586 (24)	331 (20)
1800.8688	52 (21)	491 (23)	278 (19)

Table D.2: Measurement Results: Nb, In, Mo.

Time [μs]	1.27mm Nb (D1)	0.6mm In (D2)	1.0mm Mo (D2)
0.2672	-4180000 (130000)	264000 (41000)	293000 (39000)
0.472	3191000 (59000)	-2830000 (170000)	-1260000 (160000)
0.6768	0 (59000)	-15590 (210)	-10880 (200)
0.8816	126100 (1100)	-244200 (6700)	-44400 (6300)

Continued on next page

Table D.2 – continued from previous page

Time [μs]	1.27mm Nb (D1)	0.6mm In (D2)	1.0mm Mo (D2)
1.0864	701000 (40000)	-751000 (52000)	107000 (49000)
1.2912	-110000 (48000)	1061000 (36000)	426000 (33000)
1.496	251000 (17000)	1021000 (13000)	464000 (12000)
1.7008	347200 (7800)	880100 (6300)	421300 (5900)
1.9056	370800 (5600)	814300 (5000)	400200 (4700)
2.1104	371200 (5100)	799300 (4400)	411900 (4100)
2.3152	384900 (4800)	744500 (4200)	406800 (4000)
2.52	366000 (4500)	718500 (3900)	403500 (3600)
2.7248	377700 (4100)	685500 (3500)	403500 (3300)
2.9296	383300 (3900)	646700 (3400)	403900 (3200)
3.1344	377100 (3700)	622300 (3400)	397400 (3100)
3.3392	366100 (3500)	605600 (3100)	394000 (2900)
3.544	373600 (3200)	575600 (2900)	389100 (2700)
3.7488	353500 (2900)	548500 (2600)	386400 (2400)
3.9536	353200 (2500)	526800 (2300)	386800 (2100)
4.1584	353000 (2200)	505600 (2100)	387400 (2000)
4.3632	340600 (2000)	499600 (1900)	379300 (1800)
4.568	334600 (1800)	474600 (1700)	370100 (1600)
4.7728	323200 (1600)	451300 (1500)	369300 (1400)
4.9776	307800 (1500)	440900 (1400)	364700 (1300)
5.1824	291200 (1400)	430000 (1300)	357700 (1300)
5.3872	278400 (1400)	415400 (1300)	352700 (1300)
5.6944	269200 (1500)	403500 (1400)	344100 (1300)
6.104	251800 (1700)	383800 (1700)	338500 (1600)
6.5136	235100 (2200)	371100 (2100)	325000 (2000)
6.9232	223500 (2900)	352700 (2700)	314800 (2500)
7.3328	212100 (3200)	341100 (3000)	298900 (2900)
7.7424	206700 (3200)	332500 (3000)	276800 (2800)
8.152	221100 (2700)	321700 (2600)	255200 (2500)
8.5616	232700 (2200)	303100 (2100)	243000 (2000)
8.9712	223900 (1800)	282300 (1800)	232600 (1700)
9.3808	206000 (1800)	259700 (1700)	223600 (1600)
9.7904	195600 (1800)	237700 (1700)	212600 (1600)
10.2	189300 (1600)	224400 (1500)	205600 (1400)
10.6096	185400 (1300)	206000 (1200)	196700 (1100)
11.0192	182310 (870)	195220 (820)	183820 (770)
11.4288	176890 (580)	191140 (540)	177350 (510)
11.8384	166370 (410)	193060 (370)	164270 (350)
12.248	156700 (310)	195610 (290)	154680 (270)
12.6576	144820 (260)	201190 (240)	147590 (220)
13.0672	127950 (220)	199460 (220)	144390 (210)

Continued on next page

Table D.2 – continued from previous page

Time [μs]	1.27mm Nb (D1)	0.6mm In (D2)	1.0mm Mo (D2)
13.4768	108850 (210)	200530 (210)	140640 (200)
13.8864	97720 (190)	197840 (210)	145220 (200)
14.296	87960 (200)	186670 (230)	149870 (220)
14.7056	81910 (210)	181680 (250)	156780 (240)
15.1152	75290 (250)	172860 (300)	162130 (280)
15.5248	71190 (280)	170440 (360)	166290 (340)
15.9344	61570 (320)	170120 (420)	166820 (390)
16.344	51400 (370)	172550 (470)	168560 (440)
16.7536	44610 (360)	177410 (490)	166020 (460)
17.1632	38500 (370)	180970 (490)	160910 (460)
17.5728	36030 (350)	180470 (470)	155270 (440)
17.9824	38300 (300)	182310 (410)	154410 (390)
18.392	42650 (260)	184350 (340)	154410 (320)
18.8016	49410 (220)	186860 (290)	157710 (270)
19.2112	56090 (200)	187210 (230)	159360 (220)
19.6208	65890 (180)	185330 (190)	164510 (180)
20.0304	75190 (160)	184840 (180)	163710 (170)
20.44	83730 (160)	179430 (170)	165010 (160)
20.8496	89710 (160)	172600 (150)	162900 (140)
21.2592	89190 (160)	166870 (150)	156880 (150)
21.6688	87130 (160)	163320 (150)	148700 (140)
22.0784	78900 (160)	160840 (150)	135720 (140)
22.5904	68640 (160)	161090 (150)	119410 (140)
23.2048	53060 (150)	164870 (150)	99090 (140)
23.8192	39790 (150)	167560 (150)	83380 (140)
24.4336	30620 (150)	174800 (160)	70400 (150)
25.048	27840 (150)	176560 (170)	58710 (160)
25.6624	29320 (140)	179430 (170)	50720 (160)
26.2768	33810 (150)	178950 (180)	43420 (170)
26.8912	40930 (150)	178040 (190)	36520 (180)
27.5056	50170 (140)	179770 (180)	33710 (170)
28.12	58940 (140)	174670 (170)	32380 (160)
28.7344	64500 (140)	170820 (150)	32650 (140)
29.3488	64790 (130)	166430 (140)	36300 (130)
29.9632	61750 (130)	158130 (130)	42870 (120)
30.5776	53240 (140)	150600 (120)	49780 (110)
31.192	41930 (150)	141490 (120)	58570 (110)
31.8064	31140 (150)	132420 (120)	67350 (110)
32.4208	23130 (170)	126040 (120)	76990 (110)
33.0352	17230 (170)	114030 (120)	87630 (120)
33.6496	17400 (180)	106690 (130)	93990 (120)

Continued on next page

Table D.2 – continued from previous page

Time [μs]	1.27mm Nb (D1)	0.6mm In (D2)	1.0mm Mo (D2)
34.264	16610 (180)	100510 (130)	99450 (120)
34.8784	19340 (190)	93470 (130)	101700 (120)
35.4928	22450 (190)	89790 (130)	98830 (130)
36.1072	27100 (180)	84070 (130)	93630 (130)
36.7216	30250 (170)	79510 (130)	86830 (120)
37.4384	31280 (170)	74470 (130)	74710 (120)
38.2576	31230 (150)	72770 (130)	60250 (120)
39.0768	29190 (130)	72080 (120)	46980 (120)
39.896	24640 (130)	75000 (130)	36690 (120)
40.7152	19130 (120)	81070 (130)	30670 (120)
41.5344	14640 (120)	88610 (130)	29240 (120)
42.3536	11280 (110)	94050 (130)	27600 (120)
43.1728	7800 (110)	98320 (120)	30510 (120)
43.992	5940 (100)	98150 (130)	33840 (120)
44.8112	3970 (100)	95000 (120)	38750 (120)
45.6304	3153 (99)	89330 (120)	44230 (110)
46.4496	1660 (100)	80630 (120)	51070 (110)
47.2688	920 (100)	70790 (110)	55620 (110)
48.088	558 (99)	64230 (100)	60811 (96)
48.9072	1252 (94)	54820 (100)	62579 (94)
49.7264	725 (96)	48719 (99)	63400 (93)
50.5456	320 (99)	45831 (96)	65110 (91)
51.4672	134 (99)	42020 (92)	66549 (87)
52.4912	639 (98)	40363 (91)	73267 (86)
53.5152	873 (96)	39400 (89)	85661 (84)
54.5392	1184 (93)	40874 (89)	104174 (84)
55.5632	916 (99)	43206 (91)	130624 (86)
56.5872	1468 (99)	46264 (91)	161653 (86)
57.6112	2127 (94)	51383 (89)	195183 (84)
58.6352	2744 (95)	58013 (91)	224564 (85)
59.6592	2950 (100)	63586 (95)	245416 (89)
60.6832	3792 (97)	70271 (91)	254430 (86)
61.7072	4241 (100)	75012 (92)	247430 (87)
62.7312	5482 (95)	77781 (87)	226025 (82)
63.7552	5797 (91)	80886 (88)	197148 (83)
64.8816	6150 (91)	78940 (86)	158841 (81)
66.1104	6161 (91)	76119 (85)	119530 (80)
67.3392	6096 (87)	69378 (86)	84662 (81)
68.568	5475 (88)	63235 (87)	57091 (82)
69.7968	4897 (88)	54948 (88)	38291 (83)
71.0256	4136 (86)	50369 (87)	26169 (82)

Continued on next page

Table D.2 – continued from previous page

Time [μs]	1.27mm Nb (D1)	0.6mm In (D2)	1.0mm Mo (D2)
72.2544	2919 (88)	46713 (89)	18043 (84)
73.4832	2325 (86)	43937 (87)	13120 (82)
74.712	1676 (86)	44069 (88)	10077 (84)
75.9408	1022 (87)	45512 (93)	7784 (88)
77.1696	556 (90)	48853 (95)	6133 (90)
78.5008	387 (89)	53045 (95)	5513 (89)
79.9344	167 (93)	58176 (99)	4669 (94)
81.368	82 (93)	63210 (100)	4032 (99)
82.8016	-210 (100)	66500 (110)	3570 (100)
84.2352	-270 (100)	68210 (110)	3690 (100)
85.6688	-10 (110)	68600 (120)	3400 (110)
87.1024	-590 (110)	63800 (120)	2970 (110)
88.536	-440 (110)	59070 (120)	3320 (110)
89.9696	-280 (120)	53400 (120)	2960 (110)
91.5056	-90 (110)	46420 (120)	2970 (110)
93.144	-360 (110)	41000 (110)	3030 (110)
94.7824	-490 (110)	36300 (110)	2840 (100)
96.4208	-210 (100)	34500 (100)	2852 (98)
98.0592	-258 (99)	34900 (97)	2875 (92)
99.6976	-300 (93)	35925 (93)	3246 (87)
101.336	-387 (90)	37854 (91)	3354 (86)
102.9744	-292 (85)	40246 (87)	3835 (82)
104.7152	-216 (83)	42439 (84)	4034 (79)
106.5584	-289 (82)	44853 (84)	4703 (79)
108.4016	-83 (78)	45084 (78)	5893 (74)
110.2448	180 (73)	46080 (75)	6136 (71)
112.088	-162 (75)	46482 (71)	7367 (67)
113.9312	29 (73)	46478 (68)	7710 (64)
115.7744	38 (71)	47435 (67)	8294 (63)
117.72	-61 (70)	47971 (69)	7955 (65)
119.768	-12 (70)	51612 (65)	7623 (61)
121.816	1 (68)	55483 (64)	7044 (60)
123.864	32 (68)	61434 (65)	6330 (61)
125.912	117 (66)	67738 (62)	5025 (59)
128.0624	42 (67)	74904 (62)	4222 (59)
130.3152	148 (64)	80784 (63)	3213 (60)
132.568	253 (63)	86413 (62)	2651 (59)
134.8208	89 (64)	88193 (62)	2240 (59)
137.0736	71 (64)	86614 (61)	1910 (57)
139.4288	92 (65)	80877 (61)	1690 (58)
141.8864	21 (65)	73037 (64)	1528 (61)

Continued on next page

Table D.2 – continued from previous page

Time [μs]	1.27mm Nb (D1)	0.6mm In (D2)	1.0mm Mo (D2)
144.344	189 (63)	63191 (64)	1390 (60)
146.8016	11 (65)	52628 (67)	1086 (63)
149.2592	-49 (66)	44094 (70)	1319 (66)
151.8192	-68 (68)	36307 (72)	1169 (68)
154.4816	60 (68)	30266 (73)	1325 (69)
157.144	-71 (71)	26594 (79)	1226 (74)
159.8064	-40 (73)	24055 (82)	1165 (77)
162.5712	-185 (76)	22874 (85)	1111 (81)
165.4384	-65 (76)	22235 (88)	1176 (83)
168.3056	-48 (79)	22807 (91)	1221 (86)
171.1728	-4 (78)	24096 (91)	1018 (86)
174.1424	169 (78)	25721 (93)	1013 (88)
177.2144	59 (77)	27777 (92)	872 (87)
180.2864	131 (76)	31288 (89)	921 (84)
183.4608	106 (73)	34716 (85)	925 (80)
186.7376	123 (70)	39085 (81)	873 (76)
190.0144	253 (66)	43848 (76)	762 (72)
193.3936	289 (64)	48827 (71)	690 (67)
196.8752	377 (59)	54008 (63)	949 (60)
200.3568	225 (59)	57642 (61)	874 (57)
203.9408	284 (55)	60814 (58)	564 (55)
207.6272	187 (54)	61961 (52)	895 (50)
211.416	130 (53)	61088 (51)	852 (48)
215.3072	167 (51)	58897 (49)	837 (46)
219.1984	103 (51)	55431 (48)	735 (45)
223.192	44 (50)	51550 (46)	817 (44)
227.288	27 (49)	47926 (47)	686 (45)
231.4864	75 (48)	44413 (46)	808 (43)
235.7872	61 (49)	42457 (45)	740 (43)
240.1904	35 (48)	41133 (45)	760 (42)
244.696	110 (48)	41468 (44)	748 (42)
249.304	124 (47)	42596 (45)	654 (42)
254.0144	24 (47)	44561 (44)	618 (42)
258.8272	45 (46)	47885 (44)	664 (41)
263.8448	54 (46)	51290 (43)	676 (40)
268.9648	-28 (47)	55275 (43)	642 (41)
274.1872	-27 (46)	60342 (42)	693 (39)
279.6144	-15 (45)	64798 (43)	653 (40)
285.144	5 (45)	69941 (41)	663 (39)
290.776	65 (45)	74712 (41)	538 (39)
296.6128	25 (44)	79234 (41)	689 (39)

Continued on next page

Table D.2 – continued from previous page

Time [μs]	1.27mm Nb (D1)	0.6mm In (D2)	1.0mm Mo (D2)
302.6544	57 (44)	83360 (41)	530 (39)
308.9008	-1 (43)	86212 (40)	573 (38)
315.352	-56 (44)	88105 (41)	585 (39)
321.9056	21 (43)	88972 (40)	543 (38)
328.5616	-17 (43)	89312 (40)	600 (37)
335.4224	2 (43)	88134 (39)	593 (37)
342.5904	63 (41)	85437 (39)	473 (37)
350.0656	-42 (42)	82785 (38)	552 (36)
357.7456	13 (41)	78455 (38)	562 (36)
365.6304	20 (40)	74709 (38)	509 (36)
373.72	69 (39)	69793 (37)	518 (35)
382.1168	4 (40)	64667 (37)	494 (35)
390.8208	71 (38)	59841 (37)	436 (36)
399.832	25 (38)	54911 (37)	486 (35)
409.2528	17 (38)	49998 (36)	507 (34)
418.9808	20 (38)	45194 (36)	454 (34)
429.016	49 (37)	41054 (36)	465 (34)
439.4608	24 (37)	37245 (35)	460 (33)
450.3152	26 (36)	33411 (35)	412 (33)
461.5792	-20 (37)	30328 (34)	457 (33)
473.3552	4 (36)	27381 (34)	385 (32)
485.6432	17 (36)	24765 (34)	354 (33)
498.4432	20 (35)	22688 (33)	359 (31)
511.8576	29 (35)	20572 (33)	378 (31)
525.8864	22 (34)	18789 (33)	380 (31)
540.5296	33 (34)	17159 (32)	375 (30)
555.8896	2 (34)	15772 (32)	345 (31)
572.0688	-17 (33)	14424 (32)	361 (30)
589.0672	30 (32)	13343 (31)	317 (30)
606.8848	7 (32)	12356 (31)	331 (29)
625.624	17 (32)	11407 (31)	312 (29)
645.3872	21 (31)	10514 (30)	298 (29)
666.2768	19 (31)	9793 (30)	288 (28)
688.3952	21 (30)	8997 (29)	285 (27)
711.8448	10 (30)	8347 (29)	259 (27)
736.728	2 (29)	7741 (28)	242 (27)
763.2496	12 (29)	7120 (28)	240 (26)
791.6144	-7 (29)	6602 (27)	223 (26)
821.9248	3 (28)	6070 (27)	214 (25)
854.3856	16 (27)	5524 (26)	187 (25)
889.2016	5 (27)	5144 (26)	194 (25)

Continued on next page

Table D.2 – continued from previous page

Time [μs]	1.27mm Nb (D1)	0.6mm In (D2)	1.0mm Mo (D2)
926.68	3 (27)	4718 (26)	162 (24)
967.2304	8 (26)	4315 (25)	147 (24)
1011.2624	13 (25)	3867 (24)	138 (23)
1059.1856	-1 (25)	3490 (24)	135 (23)
1111.4096	9 (24)	3168 (23)	114 (22)
1168.6512	21 (24)	2820 (23)	99 (22)
1231.7296	15 (23)	2530 (22)	90 (21)
1301.464	0 (23)	2228 (22)	76 (21)
1378.9808	13 (22)	1977 (21)	71 (20)
1465.7136	13 (22)	1738 (21)	59 (20)
1563.4032	4 (21)	1482 (20)	32 (19)
1674.2	3 (21)	1227 (20)	36 (19)
1800.8688	5 (20)	1030 (19)	15 (19)

Table D.3: Measurement Results: Sn, Zr.

Time [μs]	1.0mm Sn (D2)	1.0mm Zr (D2)
0.2672	421000 (42000)	310000 (48000)
0.472	-3000000 (180000)	-1090000 (160000)
0.6768	-13450 (220)	-1161 (57)
0.8816	-240100 (6800)	-14000 (4800)
1.0864	-407000 (53000)	-137000 (55000)
1.2912	231000 (36000)	-112000 (42000)
1.496	164000 (13000)	19000 (14000)
1.7008	109500 (6400)	29300 (6800)
1.9056	97000 (5000)	27600 (5300)
2.1104	106100 (4400)	28800 (4800)
2.3152	103100 (4300)	36900 (4500)
2.52	101300 (3900)	26200 (4200)
2.7248	100000 (3600)	24500 (3800)
2.9296	104900 (3400)	22100 (3700)
3.1344	90400 (3400)	30800 (3500)
3.3392	88500 (3200)	30000 (3300)
3.544	90500 (2900)	25600 (3100)
3.7488	89200 (2600)	28800 (2800)
3.9536	87500 (2300)	25400 (2500)
4.1584	85400 (2100)	31300 (2200)
4.3632	81600 (1900)	26300 (2100)
4.568	86100 (1700)	30300 (1800)
4.7728	84100 (1600)	30500 (1700)
4.9776	80100 (1400)	33100 (1500)

Continued on next page

Table D.3 – continued from previous page

Time [μs]	1.0mm Sn (D2)	1.0mm Zr (D2)
5.1824	79500 (1300)	30800 (1500)
5.3872	77900 (1300)	34200 (1400)
5.6944	73000 (1400)	34000 (1500)
6.104	67500 (1700)	34500 (1800)
6.5136	63300 (2100)	36700 (2200)
6.9232	56700 (2700)	28100 (2900)
7.3328	53200 (3100)	31500 (3200)
7.7424	46100 (3100)	26900 (3200)
8.152	44200 (2700)	23300 (2800)
8.5616	47900 (2100)	21400 (2300)
8.9712	46800 (1800)	18700 (1900)
9.3808	46600 (1700)	15500 (1700)
9.7904	43500 (1700)	15100 (1700)
10.2	40500 (1500)	10700 (1600)
10.6096	40900 (1200)	8100 (1200)
11.0192	36190 (830)	5150 (870)
11.4288	34460 (550)	4720 (570)
11.8384	33940 (370)	4100 (390)
12.248	34350 (290)	3610 (300)
12.6576	38160 (240)	4030 (260)
13.0672	38770 (220)	4860 (240)
13.4768	39300 (210)	6230 (240)
13.8864	39840 (220)	8270 (230)
14.296	37440 (230)	9380 (250)
14.7056	34920 (250)	10010 (290)
15.1152	31960 (300)	11180 (340)
15.5248	29050 (360)	11740 (390)
15.9344	24030 (420)	11240 (460)
16.344	22480 (470)	8830 (510)
16.7536	23230 (500)	9230 (550)
17.1632	22270 (490)	5810 (550)
17.5728	20980 (480)	5430 (520)
17.9824	21400 (410)	4560 (450)
18.392	23990 (350)	5060 (370)
18.8016	27060 (290)	4910 (310)
19.2112	29500 (240)	4520 (260)
19.6208	32240 (200)	5270 (220)
20.0304	33300 (180)	6330 (190)
20.44	33550 (170)	7870 (180)
20.8496	33900 (150)	9060 (170)
21.2592	30870 (160)	12740 (160)

Continued on next page

Table D.3 – continued from previous page

Time [μs]	1.0mm Sn (D2)	1.0mm Zr (D2)
21.6688	28950 (150)	15880 (160)
22.0784	26110 (150)	20580 (150)
22.5904	22320 (150)	25540 (160)
23.2048	19220 (150)	29660 (160)
23.8192	15200 (150)	30300 (170)
24.4336	12860 (160)	28690 (170)
25.048	11970 (170)	23530 (190)
25.6624	12920 (170)	17410 (190)
26.2768	12920 (190)	12740 (190)
26.8912	13410 (190)	8860 (200)
27.5056	16040 (180)	6270 (200)
28.12	17510 (170)	6480 (180)
28.7344	17250 (150)	6090 (170)
29.3488	16910 (140)	7210 (150)
29.9632	16100 (130)	7190 (140)
30.5776	16310 (120)	6080 (140)
31.192	15650 (120)	5720 (130)
31.8064	16270 (120)	5240 (130)
32.4208	18450 (120)	3420 (130)
33.0352	20610 (120)	2800 (130)
33.6496	23200 (130)	1360 (140)
34.264	26540 (130)	1580 (140)
34.8784	30070 (130)	840 (140)
35.4928	33520 (130)	930 (140)
36.1072	37470 (130)	110 (150)
36.7216	40300 (130)	430 (150)
37.4384	43930 (130)	0 (140)
38.2576	44880 (130)	300 (140)
39.0768	44290 (120)	340 (140)
39.896	38870 (130)	60 (140)
40.7152	33210 (130)	250 (140)
41.5344	27600 (130)	450 (130)
42.3536	21680 (130)	190 (140)
43.1728	16220 (130)	740 (130)
43.992	11840 (130)	-50 (140)
44.8112	9300 (130)	400 (130)
45.6304	7720 (120)	-70 (130)
46.4496	6400 (120)	500 (120)
47.2688	6690 (110)	180 (120)
48.088	7630 (100)	140 (120)
48.9072	8220 (100)	180 (110)

Continued on next page

Table D.3 – continued from previous page

Time [μs]	1.0mm Sn (D2)	1.0mm Zr (D2)
49.7264	8355 (100)	30 (100)
50.5456	9361 (97)	130 (100)
51.4672	9576 (93)	347 (99)
52.4912	9557 (91)	45 (97)
53.5152	9658 (90)	-199 (100)
54.5392	9542 (90)	-30 (99)
55.5632	9424 (92)	100 (98)
56.5872	9312 (92)	82 (99)
57.6112	10956 (90)	-110 (100)
58.6352	11741 (91)	142 (96)
59.6592	13088 (95)	60 (100)
60.6832	14881 (91)	281 (95)
61.7072	16127 (93)	9 (95)
62.7312	17762 (88)	85 (94)
63.7552	18012 (88)	-21 (97)
64.8816	18128 (87)	395 (92)
66.1104	16727 (85)	221 (93)
67.3392	15123 (87)	101 (93)
68.568	12246 (88)	-138 (96)
69.7968	9121 (89)	28 (93)
71.0256	7112 (87)	234 (94)
72.2544	4429 (89)	239 (96)
73.4832	3497 (88)	272 (94)
74.712	2390 (89)	48 (99)
75.9408	1488 (94)	284 (100)
77.1696	802 (96)	230 (100)
78.5008	694 (95)	410 (100)
79.9344	500 (100)	160 (110)
81.368	340 (110)	340 (110)
82.8016	170 (110)	-10 (120)
84.2352	630 (110)	280 (120)
85.6688	190 (120)	-210 (130)
87.1024	450 (120)	-50 (130)
88.536	490 (120)	170 (130)
89.9696	420 (120)	230 (130)
91.5056	60 (120)	380 (130)
93.144	430 (110)	-300 (130)
94.7824	230 (110)	-80 (120)
96.4208	20 (110)	270 (110)
98.0592	433 (98)	170 (110)
99.6976	283 (93)	-200 (100)

Continued on next page

Table D.3 – continued from previous page

Time [μs]	1.0mm Sn (D2)	1.0mm Zr (D2)
101.336	311 (91)	83 (99)
102.9744	149 (88)	6 (96)
104.7152	367 (85)	258 (90)
106.5584	21 (84)	-107 (89)
108.4016	189 (79)	307 (83)
110.2448	167 (76)	-25 (83)
112.088	210 (72)	112 (78)
113.9312	331 (68)	141 (75)
115.7744	121 (68)	-52 (74)
117.72	-9 (70)	137 (71)
119.768	28 (65)	112 (70)
121.816	143 (64)	69 (70)
123.864	-17 (65)	23 (70)
125.912	182 (63)	27 (67)
128.0624	126 (63)	-11 (69)
130.3152	65 (64)	155 (67)
132.568	244 (62)	117 (67)
134.8208	209 (63)	58 (68)
137.0736	273 (61)	306 (66)
139.4288	222 (62)	116 (66)
141.8864	77 (65)	165 (68)
144.344	220 (64)	235 (70)
146.8016	-32 (68)	273 (71)
149.2592	121 (70)	223 (74)
151.8192	200 (73)	233 (78)
154.4816	370 (74)	192 (80)
157.144	195 (79)	127 (84)
159.8064	310 (83)	158 (90)
162.5712	177 (86)	242 (92)
165.4384	411 (89)	47 (98)
168.3056	231 (91)	161 (100)
171.1728	311 (92)	243 (99)
174.1424	139 (94)	188 (99)
177.2144	37 (93)	73 (99)
180.2864	208 (90)	188 (96)
183.4608	149 (86)	236 (89)
186.7376	229 (81)	-41 (87)
190.0144	-115 (76)	-34 (81)
193.3936	-21 (72)	68 (74)
196.8752	216 (64)	-6 (69)
200.3568	-37 (61)	12 (65)

Continued on next page

Table D.3 – continued from previous page

Time [μs]	1.0mm Sn (D2)	1.0mm Zr (D2)
203.9408	37 (58)	39 (60)
207.6272	159 (53)	138 (56)
211.416	110 (51)	66 (55)
215.3072	91 (49)	40 (53)
219.1984	110 (48)	-7 (53)
223.192	197 (47)	25 (51)
227.288	101 (48)	64 (50)
231.4864	62 (46)	57 (49)
235.7872	103 (46)	96 (48)
240.1904	73 (45)	-19 (48)
244.696	110 (44)	87 (48)
249.304	42 (45)	31 (48)
254.0144	61 (45)	66 (46)
258.8272	20 (44)	43 (47)
263.8448	105 (43)	-39 (47)
268.9648	61 (43)	-17 (46)
274.1872	167 (42)	10 (46)
279.6144	56 (43)	44 (45)
285.144	118 (42)	55 (45)
290.776	87 (41)	44 (45)
296.6128	83 (41)	59 (45)
302.6544	91 (41)	69 (44)
308.9008	123 (41)	34 (43)
315.352	65 (41)	1 (43)
321.9056	109 (40)	68 (42)
328.5616	96 (40)	12 (43)
335.4224	83 (39)	106 (41)
342.5904	44 (40)	38 (42)
350.0656	72 (39)	68 (41)
357.7456	95 (39)	-11 (41)
365.6304	116 (38)	-21 (41)
373.72	110 (38)	26 (41)
382.1168	108 (37)	84 (40)
390.8208	8 (38)	23 (40)
399.832	60 (37)	-3 (40)
409.2528	94 (36)	12 (39)
418.9808	53 (36)	19 (39)
429.016	65 (36)	-25 (39)
439.4608	74 (35)	-2 (39)
450.3152	62 (35)	18 (38)
461.5792	53 (35)	24 (37)

Continued on next page

Table D.3 – continued from previous page

Time [μs]	1.0mm Sn (D2)	1.0mm Zr (D2)
473.3552	38 (34)	-16 (37)
485.6432	12 (35)	-2 (36)
498.4432	86 (33)	6 (36)
511.8576	62 (33)	14 (36)
525.8864	-5 (33)	59 (35)
540.5296	49 (32)	5 (35)
555.8896	11 (33)	35 (34)
572.0688	33 (32)	4 (34)
589.0672	2 (32)	-3 (34)
606.8848	30 (31)	1 (33)
625.624	-2 (31)	9 (32)
645.3872	-2 (31)	-9 (33)
666.2768	19 (30)	-31 (32)
688.3952	40 (29)	21 (31)
711.8448	36 (29)	7 (31)
736.728	24 (28)	-7 (31)
763.2496	6 (28)	-11 (30)
791.6144	17 (28)	-15 (30)
821.9248	29 (27)	-7 (29)
854.3856	10 (27)	5 (28)
889.2016	14 (26)	-13 (28)
926.68	18 (26)	-21 (28)
967.2304	11 (25)	11 (27)
1011.2624	17 (24)	-3 (26)
1059.1856	15 (24)	-9 (26)
1111.4096	12 (24)	5 (25)
1168.6512	7 (23)	-13 (25)
1231.7296	-3 (23)	-13 (24)
1301.464	2 (22)	-8 (24)
1378.9808	3 (21)	-14 (23)
1465.7136	5 (21)	-21 (23)
1563.4032	-6 (21)	-15 (22)
1674.2	-5 (20)	-17 (22)
1800.8688	-7 (20)	-16 (21)

Table D.4: Measurement Results: Fe, Co.

Time [μs]	1.0mm Fe (D2)	0.6mm Co (D1)
0.2672	1170000 (56000)	11950000 (380000)
0.472	-5700000 (190000)	-2920000 (130000)
0.6768	-2178 (65)	#DIV/0!

Continued on next page

Table D.4 – continued from previous page

Time [μs]	1.0mm Fe (D2)	0.6mm Co (D1)
0.8816	-262500 (5700)	-57300 (2200)
1.0864	-1473000 (65000)	-1176000 (66000)
1.2912	-55000 (49000)	32000 (55000)
1.496	51000 (17000)	141000 (22000)
1.7008	34900 (8100)	113000 (11000)
1.9056	30200 (6300)	105900 (8600)
2.1104	24800 (5600)	101200 (7800)
2.3152	18500 (5300)	100200 (7400)
2.52	18600 (4900)	97700 (6900)
2.7248	16800 (4500)	95300 (6500)
2.9296	9500 (4300)	89900 (6100)
3.1344	10100 (4100)	90900 (5900)
3.3392	4700 (3900)	84500 (5600)
3.544	8500 (3600)	104200 (5600)
3.7488	8600 (3300)	93900 (5100)
3.9536	6200 (3000)	95000 (4700)
4.1584	13100 (2600)	100600 (4500)
4.3632	6500 (2500)	104800 (4400)
4.568	15100 (2200)	110200 (4200)
4.7728	10500 (2000)	114100 (4100)
4.9776	12700 (1800)	114700 (3900)
5.1824	10100 (1700)	127500 (4100)
5.3872	11200 (1700)	131400 (4200)
5.6944	7100 (1800)	138200 (4500)
6.104	4200 (2100)	128000 (4500)
6.5136	2700 (2600)	107200 (4700)
6.9232	200 (3400)	88700 (5000)
7.3328	2400 (3800)	72500 (5100)
7.7424	2300 (3800)	58600 (4800)
8.152	2000 (3300)	50700 (4100)
8.5616	1600 (2700)	36100 (3200)
8.9712	1200 (2300)	38700 (2900)
9.3808	6000 (2000)	35400 (2700)
9.7904	7800 (2000)	34400 (2700)
10.2	10900 (1900)	32800 (2500)
10.6096	20200 (1500)	36400 (2200)
11.0192	24800 (1000)	29800 (1600)
11.4288	34190 (670)	28300 (1200)
11.8384	40520 (460)	28500 (1000)
12.248	39370 (350)	28370 (920)
12.6576	31510 (310)	29600 (880)

Continued on next page

Table D.4 – continued from previous page

Time [μs]	1.0mm Fe (D2)	0.6mm Co (D1)
13.0672	21990 (280)	30540 (850)
13.4768	12980 (280)	29580 (820)
13.8864	7430 (270)	30070 (820)
14.296	4330 (290)	30820 (840)
14.7056	1220 (340)	30380 (850)
15.1152	480 (390)	31240 (900)
15.5248	510 (460)	30580 (930)
15.9344	1690 (540)	30090 (980)
16.344	1640 (600)	33300 (1100)
16.7536	2170 (640)	36300 (1100)
17.1632	1790 (650)	33800 (1100)
17.5728	900 (610)	35500 (1100)
17.9824	450 (530)	36500 (1100)
18.392	2040 (430)	38700 (1100)
18.8016	1070 (360)	39600 (1000)
19.2112	820 (300)	39800 (1000)
19.6208	950 (250)	40800 (1000)
20.0304	1240 (220)	41500 (1000)
20.44	1090 (210)	43800 (1100)
20.8496	1460 (200)	45400 (1100)
21.2592	2150 (180)	49700 (1200)
21.6688	1840 (190)	51600 (1200)
22.0784	2230 (170)	54700 (1300)
22.5904	940 (190)	56100 (1300)
23.2048	1460 (180)	61700 (1400)
23.8192	470 (200)	67600 (1500)
24.4336	1040 (200)	75900 (1700)
25.048	1280 (220)	81700 (1800)
25.6624	1450 (220)	92800 (2000)
26.2768	1610 (230)	108100 (2300)
26.8912	690 (230)	127400 (2700)
27.5056	900 (230)	151400 (3200)
28.12	1640 (210)	181500 (3800)
28.7344	1150 (200)	222300 (4600)
29.3488	1250 (170)	277300 (5700)
29.9632	1010 (170)	339900 (6900)
30.5776	950 (160)	412800 (8400)
31.192	1250 (150)	492000 (10000)
31.8064	1800 (140)	566000 (11000)
32.4208	1370 (150)	634000 (13000)
33.0352	1170 (150)	687000 (14000)

Continued on next page

Table D.4 – continued from previous page

Time [μs]	1.0mm Fe (D2)	0.6mm Co (D1)
33.6496	870 (170)	726000 (15000)
34.264	1420 (160)	730000 (15000)
34.8784	1330 (160)	712000 (14000)
35.4928	1350 (170)	682000 (14000)
36.1072	1070 (170)	629000 (13000)
36.7216	1250 (170)	576000 (12000)
37.4384	970 (170)	501000 (10000)
38.2576	1190 (160)	425500 (8700)
39.0768	1340 (160)	355300 (7300)
39.896	840 (160)	295200 (6100)
40.7152	1430 (160)	246200 (5100)
41.5344	1440 (150)	202900 (4200)
42.3536	1270 (160)	167600 (3500)
43.1728	1220 (160)	139600 (2900)
43.992	900 (160)	119700 (2500)
44.8112	680 (160)	105300 (2200)
45.6304	1060 (150)	90500 (1900)
46.4496	1640 (140)	80500 (1700)
47.2688	1440 (140)	76400 (1600)
48.088	1240 (130)	68200 (1500)
48.9072	1110 (130)	62600 (1400)
49.7264	1190 (120)	56900 (1200)
50.5456	1270 (120)	53000 (1200)
51.4672	1030 (110)	49000 (1100)
52.4912	1020 (110)	45100 (1000)
53.5152	1140 (110)	43350 (970)
54.5392	1010 (110)	40250 (910)
55.5632	730 (110)	38640 (880)
56.5872	960 (110)	36260 (830)
57.6112	880 (120)	35030 (810)
58.6352	1510 (110)	33240 (780)
59.6592	630 (110)	31610 (740)
60.6832	940 (110)	31400 (730)
61.7072	1020 (110)	29420 (700)
62.7312	1190 (110)	28780 (680)
63.7552	950 (110)	26720 (640)
64.8816	1030 (110)	26460 (630)
66.1104	930 (110)	25710 (620)
67.3392	1030 (110)	25290 (610)
68.568	650 (110)	25150 (600)
69.7968	1160 (110)	23610 (570)

Continued on next page

Table D.4 – continued from previous page

Time [μs]	1.0mm Fe (D2)	0.6mm Co (D1)
71.0256	1100 (110)	22980 (560)
72.2544	960 (110)	21900 (540)
73.4832	1050 (110)	21580 (530)
74.712	660 (110)	21870 (540)
75.9408	750 (110)	20970 (520)
77.1696	750 (120)	20360 (510)
78.5008	1150 (120)	19970 (500)
79.9344	870 (120)	19890 (500)
81.368	1110 (130)	19480 (500)
82.8016	970 (140)	19080 (490)
84.2352	940 (140)	18660 (490)
85.6688	800 (150)	18080 (480)
87.1024	1060 (150)	17500 (480)
88.536	730 (150)	17160 (470)
89.9696	810 (150)	17110 (470)
91.5056	990 (150)	16780 (460)
93.144	430 (150)	16800 (460)
94.7824	480 (140)	16120 (440)
96.4208	970 (130)	15860 (430)
98.0592	570 (120)	14930 (410)
99.6976	610 (120)	15360 (410)
101.336	750 (110)	15370 (410)
102.9744	570 (110)	14890 (390)
104.7152	870 (100)	14320 (380)
106.5584	670 (100)	14350 (380)
108.4016	825 (96)	14050 (370)
110.2448	496 (95)	13350 (350)
112.088	836 (89)	13610 (350)
113.9312	736 (87)	13410 (350)
115.7744	505 (85)	12880 (340)
117.72	763 (81)	13180 (340)
119.768	671 (80)	13340 (340)
121.816	710 (80)	12310 (320)
123.864	578 (80)	12230 (320)
125.912	791 (77)	12290 (320)
128.0624	521 (79)	12130 (320)
130.3152	664 (77)	12580 (320)
132.568	751 (77)	11590 (310)
134.8208	623 (77)	11520 (300)
137.0736	775 (75)	11430 (300)
139.4288	806 (75)	11190 (300)

Continued on next page

Table D.4 – continued from previous page

Time [μs]	1.0mm Fe (D2)	0.6mm Co (D1)
141.8864	775 (78)	11700 (310)
144.344	570 (80)	10980 (290)
146.8016	503 (82)	10840 (290)
149.2592	674 (85)	10750 (290)
151.8192	474 (90)	10840 (290)
154.4816	706 (92)	10910 (300)
157.144	584 (97)	10780 (290)
159.8064	520 (100)	10360 (290)
162.5712	560 (110)	10050 (280)
165.4384	500 (110)	10160 (290)
168.3056	550 (120)	10100 (290)
171.1728	690 (110)	9350 (280)
174.1424	580 (110)	9500 (280)
177.2144	490 (110)	9320 (270)
180.2864	600 (110)	8830 (260)
183.4608	760 (100)	8830 (260)
186.7376	326 (100)	8230 (240)
190.0144	471 (93)	8570 (250)
193.3936	612 (85)	8300 (240)
196.8752	536 (79)	8390 (240)
200.3568	499 (75)	8050 (230)
203.9408	544 (69)	7940 (220)
207.6272	512 (64)	7700 (220)
211.416	513 (62)	7530 (210)
215.3072	457 (60)	7670 (210)
219.1984	365 (60)	7440 (210)
223.192	485 (58)	7200 (200)
227.288	424 (57)	7340 (200)
231.4864	459 (55)	7290 (200)
235.7872	428 (55)	6930 (190)
240.1904	434 (55)	6820 (190)
244.696	494 (54)	6980 (190)
249.304	373 (54)	6640 (190)
254.0144	425 (53)	6540 (180)
258.8272	446 (53)	6380 (180)
263.8448	370 (54)	6590 (180)
268.9648	422 (52)	6390 (180)
274.1872	336 (52)	6190 (170)
279.6144	382 (52)	5960 (170)
285.144	321 (51)	5960 (170)
290.776	323 (51)	5840 (170)

Continued on next page

Table D.4 – continued from previous page

Time [μs]	1.0mm Fe (D2)	0.6mm Co (D1)
296.6128	365 (51)	5810 (170)
302.6544	366 (50)	5600 (160)
308.9008	369 (49)	5450 (160)
315.352	358 (49)	5440 (160)
321.9056	365 (48)	5520 (160)
328.5616	358 (48)	4990 (150)
335.4224	447 (46)	5240 (150)
342.5904	359 (47)	5070 (150)
350.0656	352 (47)	4940 (150)
357.7456	387 (47)	4810 (140)
365.6304	315 (47)	4620 (140)
373.72	325 (46)	4810 (140)
382.1168	364 (45)	4520 (130)
390.8208	228 (46)	4470 (130)
399.832	261 (45)	4450 (130)
409.2528	228 (44)	4320 (130)
418.9808	247 (44)	4110 (130)
429.016	285 (44)	3940 (120)
439.4608	187 (44)	4080 (120)
450.3152	261 (43)	3870 (120)
461.5792	230 (42)	3690 (120)
473.3552	212 (42)	3580 (110)
485.6432	225 (41)	3530 (110)
498.4432	221 (41)	3410 (110)
511.8576	222 (41)	3310 (100)
525.8864	246 (39)	3200 (100)
540.5296	239 (39)	3044 (99)
555.8896	217 (39)	3011 (98)
572.0688	220 (38)	2752 (93)
589.0672	189 (38)	2779 (93)
606.8848	198 (38)	2583 (88)
625.624	203 (37)	2634 (88)
645.3872	188 (37)	2507 (86)
666.2768	131 (36)	2386 (83)
688.3952	170 (35)	2274 (80)
711.8448	182 (35)	2185 (77)
736.728	148 (34)	2174 (77)
763.2496	135 (34)	1948 (72)
791.6144	121 (34)	1839 (69)
821.9248	135 (33)	1746 (67)
854.3856	136 (32)	1662 (65)

Continued on next page

Table D.4 – continued from previous page

Time [μs]	**1.0mm Fe (D2)**	**0.6mm Co (D1)**
889.2016	110 (32)	1519 (61)
926.68	93 (31)	1458 (59)
967.2304	119 (30)	1327 (56)
1011.2624	93 (30)	1207 (53)
1059.1856	95 (29)	1087 (50)
1111.4096	93 (28)	1013 (48)
1168.6512	80 (28)	882 (45)
1231.7296	67 (27)	786 (42)
1301.464	53 (27)	697 (40)
1378.9808	51 (26)	616 (38)
1465.7136	36 (25)	534 (35)
1563.4032	37 (25)	432 (33)
1674.2	28 (24)	329 (30)
1800.8688	30 (23)	262 (28)

APPENDIX E
Simulation Results Tables

Below are tables of simulation results as a function of time for each associated measurement, for ENDF/B-VII.1, JEFF 3.2 and JENDL 4.0 libraries (in order to save space, in the tables, ENDF will refer to ENDF/B-VII.1, JEFF will refer to JEFF 3.2, and JENDL will refer to JENDL 4.0). All simulation numbers have been normalized to measurement count rate in counts per second. Time is reported in μs. Associated uncertainty for each bin ranged from under 1 % to 6 % between 1 keV and 0.2 eV in each simulation. Above 1 keV and below 0.2 eV, uncertainties were generally higher.

Table E.1: Simulation Results: Ta, Ag.

	0.254mm Ta (D1)			**0.6mm Ag (D1)**		
Time[μs]	**ENDF**	**JEFF**	**JENDL**	**ENDF**	**JEFF**	**JENDL**
1.01	4.14E+05	3.88E+05	3.81E+05	1.50E+06	1.67E+06	1.45E+06
1.07	4.48E+05	4.10E+05	4.03E+05	1.66E+06	1.79E+06	1.59E+06
1.13	4.41E+05	4.10E+05	4.01E+05	1.64E+06	1.79E+06	1.55E+06
1.2	4.51E+05	4.13E+05	4.06E+05	1.65E+06	1.77E+06	1.55E+06
1.26	4.46E+05	4.09E+05	4.03E+05	1.69E+06	1.80E+06	1.58E+06
1.34	4.57E+05	4.06E+05	4.04E+05	1.67E+06	1.78E+06	1.56E+06
1.41	4.52E+05	3.96E+05	3.94E+05	1.62E+06	1.76E+06	1.52E+06
1.49	4.61E+05	3.97E+05	4.00E+05	1.65E+06	1.73E+06	1.52E+06
1.58	4.57E+05	3.98E+05	4.01E+05	1.62E+06	1.70E+06	1.50E+06
1.67	4.59E+05	3.93E+05	3.99E+05	1.61E+06	1.70E+06	1.50E+06
1.76	4.56E+05	3.89E+05	3.91E+05	1.58E+06	1.64E+06	1.46E+06
1.86	4.54E+05	3.93E+05	3.87E+05	1.54E+06	1.60E+06	1.44E+06
1.96	4.57E+05	3.89E+05	3.89E+05	1.51E+06	1.58E+06	1.39E+06
2.08	4.52E+05	3.82E+05	3.87E+05	1.49E+06	1.54E+06	1.39E+06
2.19	4.47E+05	3.83E+05	3.83E+05	1.46E+06	1.54E+06	1.36E+06
2.32	4.47E+05	3.80E+05	3.91E+05	1.40E+06	1.46E+06	1.32E+06
2.45	4.45E+05	3.79E+05	3.85E+05	1.40E+06	1.44E+06	1.31E+06
2.59	4.46E+05	3.74E+05	3.78E+05	1.34E+06	1.38E+06	1.27E+06
2.73	4.35E+05	3.66E+05	3.74E+05	1.31E+06	1.36E+06	1.24E+06
2.89	4.35E+05	3.69E+05	3.72E+05	1.25E+06	1.29E+06	1.18E+06
3.05	4.39E+05	3.68E+05	3.68E+05	1.19E+06	1.26E+06	1.12E+06
3.23	4.35E+05	3.69E+05	3.69E+05	1.13E+06	1.21E+06	1.09E+06
3.41	4.37E+05	3.68E+05	3.71E+05	1.12E+06	1.18E+06	1.07E+06
3.6	4.32E+05	3.68E+05	3.71E+05	1.06E+06	1.13E+06	1.03E+06
3.81	4.29E+05	3.73E+05	3.68E+05	1.00E+06	1.09E+06	9.87E+05
4.02	4.36E+05	3.70E+05	3.76E+05	9.43E+05	1.04E+06	9.40E+05

Continued on next page

Table E.1 – continued from previous page

	0.254mm Ta (D1)			0.6mm Ag (D1)		
Time[μs]	**ENDF**	**JEFF**	**JENDL**	**ENDF**	**JEFF**	**JENDL**
4.25	4.38E+05	3.82E+05	3.78E+05	9.10E+05	1.02E+06	9.01E+05
4.49	4.38E+05	3.91E+05	3.82E+05	8.37E+05	9.68E+05	8.59E+05
4.74	4.37E+05	3.88E+05	3.84E+05	7.87E+05	9.40E+05	8.39E+05
5.01	4.26E+05	3.97E+05	3.82E+05	7.56E+05	9.07E+05	8.05E+05
5.3	4.20E+05	3.85E+05	3.72E+05	6.87E+05	8.85E+05	7.57E+05
5.6	4.19E+05	3.90E+05	3.81E+05	6.93E+05	8.55E+05	7.44E+05
5.91	4.15E+05	3.76E+05	3.82E+05	6.43E+05	8.18E+05	7.06E+05
6.25	4.16E+05	3.78E+05	3.78E+05	6.21E+05	8.15E+05	7.07E+05
6.6	4.02E+05	3.64E+05	3.73E+05	6.16E+05	7.72E+05	6.74E+05
6.98	4.03E+05	3.60E+05	3.62E+05	5.88E+05	7.52E+05	6.49E+05
7.37	4.00E+05	3.57E+05	3.44E+05	5.50E+05	7.17E+05	6.39E+05
7.79	3.92E+05	3.40E+05	3.43E+05	4.99E+05	6.94E+05	6.03E+05
8.23	3.82E+05	3.36E+05	3.41E+05	4.50E+05	6.73E+05	5.81E+05
8.7	3.81E+05	3.33E+05	3.37E+05	4.31E+05	6.47E+05	5.67E+05
9.19	3.70E+05	3.36E+05	3.36E+05	3.87E+05	6.37E+05	5.73E+05
9.71	3.68E+05	3.39E+05	3.42E+05	3.99E+05	6.05E+05	5.63E+05
10.26	3.62E+05	3.34E+05	3.46E+05	3.86E+05	5.89E+05	5.67E+05
10.84	3.51E+05	3.39E+05	3.42E+05	3.83E+05	5.65E+05	5.41E+05
11.46	3.46E+05	3.59E+05	3.50E+05	3.74E+05	5.35E+05	4.71E+05
12.11	3.41E+05	3.62E+05	3.66E+05	3.81E+05	4.82E+05	4.11E+05
12.79	3.39E+05	3.62E+05	3.66E+05	3.61E+05	4.15E+05	3.59E+05
13.52	3.32E+05	3.33E+05	3.61E+05	3.60E+05	3.64E+05	3.40E+05
14.28	3.29E+05	3.20E+05	3.21E+05	3.33E+05	3.11E+05	3.32E+05
15.09	3.21E+05	3.18E+05	3.12E+05	3.40E+05	3.43E+05	3.51E+05
15.95	3.10E+05	3.09E+05	3.11E+05	3.75E+05	3.62E+05	4.11E+05
16.85	3.11E+05	3.11E+05	3.12E+05	4.13E+05	3.69E+05	4.48E+05
17.81	3.05E+05	3.27E+05	3.24E+05	4.25E+05	3.93E+05	4.66E+05
18.82	3.00E+05	3.21E+05	3.12E+05	3.65E+05	3.73E+05	4.11E+05
19.88	2.94E+05	2.93E+05	2.84E+05	3.32E+05	3.24E+05	3.46E+05
21.01	2.87E+05	2.77E+05	2.75E+05	2.92E+05	2.75E+05	2.73E+05
22.2	2.89E+05	2.81E+05	2.78E+05	2.67E+05	2.70E+05	2.62E+05
23.46	2.91E+05	2.88E+05	2.91E+05	2.68E+05	2.48E+05	2.53E+05
24.79	2.77E+05	2.77E+05	2.85E+05	2.28E+05	1.86E+05	2.01E+05
26.19	2.68E+05	2.69E+05	2.74E+05	2.26E+05	1.83E+05	1.90E+05
27.67	2.57E+05	2.60E+05	2.57E+05	2.47E+05	1.76E+05	1.86E+05
29.24	2.13E+05	2.22E+05	2.21E+05	2.47E+05	2.06E+05	1.94E+05
30.9	1.73E+05	1.83E+05	1.91E+05	2.29E+05	2.20E+05	2.05E+05
32.65	1.60E+05	1.80E+05	1.80E+05	1.88E+05	2.01E+05	1.80E+05
34.5	1.69E+05	1.85E+05	1.81E+05	1.81E+05	1.83E+05	1.96E+05
36.45	1.74E+05	1.80E+05	1.82E+05	1.42E+05	1.32E+05	1.41E+05

Continued on next page

Table E.1 – continued from previous page

	0.254mm Ta (D1)			0.6mm Ag (D1)		
Time[μs]	**ENDF**	**JEFF**	**JENDL**	**ENDF**	**JEFF**	**JENDL**
38.52	1.85E+05	1.79E+05	1.85E+05	8.66E+04	9.25E+04	8.69E+04
40.7	1.85E+05	1.84E+05	1.88E+05	8.90E+04	8.24E+04	8.29E+04
43.01	1.77E+05	1.69E+05	1.70E+05	1.17E+05	1.19E+05	1.02E+05
45.44	1.39E+05	1.41E+05	1.39E+05	1.56E+05	1.48E+05	1.45E+05
48.02	1.00E+05	9.61E+04	9.59E+04	1.87E+05	1.89E+05	1.80E+05
50.74	6.96E+04	6.52E+04	6.38E+04	2.07E+05	2.06E+05	1.97E+05
53.61	5.57E+04	5.79E+04	5.53E+04	2.55E+05	2.62E+05	2.29E+05
56.65	6.03E+04	6.29E+04	6.26E+04	2.97E+05	2.80E+05	2.66E+05
59.86	9.63E+04	1.04E+05	1.10E+05	2.70E+05	2.67E+05	2.66E+05
63.25	1.61E+05	1.67E+05	1.76E+05	2.36E+05	2.43E+05	2.22E+05
66.84	1.71E+05	1.91E+05	1.96E+05	1.80E+05	1.85E+05	1.75E+05
70.62	1.19E+05	1.31E+05	1.28E+05	1.53E+05	1.46E+05	1.46E+05
74.62	6.78E+04	7.64E+04	7.19E+04	1.30E+05	1.20E+05	1.27E+05
78.85	6.54E+04	6.53E+04	6.90E+04	7.30E+04	8.07E+04	7.16E+04
83.32	7.49E+04	6.81E+04	7.21E+04	3.87E+04	4.03E+04	4.47E+04
88.04	5.88E+04	5.78E+04	5.63E+04	4.61E+04	4.22E+04	4.85E+04
93.03	3.67E+04	3.62E+04	3.68E+04	7.96E+04	8.40E+04	7.89E+04
98.3	2.91E+04	2.80E+04	3.04E+04	1.31E+05	1.26E+05	1.33E+05
103.87	4.02E+04	3.74E+04	3.98E+04	1.19E+05	1.11E+05	1.17E+05
109.75	5.00E+04	4.59E+04	4.71E+04	6.58E+04	6.04E+04	6.46E+04
115.97	5.67E+04	5.61E+04	6.14E+04	3.57E+04	3.54E+04	3.59E+04
122.54	6.66E+04	6.92E+04	6.88E+04	3.11E+04	3.03E+04	3.03E+04
129.49	5.80E+04	5.71E+04	5.75E+04	3.78E+04	4.00E+04	3.88E+04
136.82	2.92E+04	2.67E+04	2.78E+04	4.70E+04	5.08E+04	4.94E+04
144.57	1.50E+04	1.34E+04	1.36E+04	7.06E+04	6.98E+04	7.11E+04
152.77	1.33E+04	1.31E+04	1.22E+04	1.10E+05	1.15E+05	1.15E+05
161.42	2.09E+04	1.77E+04	2.00E+04	1.65E+05	1.72E+05	1.74E+05
170.56	3.53E+04	3.16E+04	3.41E+04	2.21E+05	2.17E+05	2.23E+05
180.23	6.00E+04	5.42E+04	5.62E+04	2.32E+05	2.33E+05	2.35E+05
190.44	7.79E+04	7.37E+04	7.27E+04	1.75E+05	1.84E+05	1.80E+05
201.23	7.11E+04	6.66E+04	6.75E+04	1.17E+05	1.23E+05	1.19E+05
212.63	4.25E+04	3.99E+04	4.13E+04	7.11E+04	7.13E+04	7.13E+04
224.68	1.95E+04	1.77E+04	1.76E+04	4.53E+04	4.60E+04	4.51E+04
237.4	8.67E+03	7.54E+03	6.92E+03	3.09E+04	3.31E+04	3.16E+04
250.86	4.77E+03	3.95E+03	3.97E+03	2.48E+04	2.54E+04	2.44E+04
265.07	3.17E+03	2.71E+03	2.79E+03	1.95E+04	1.98E+04	2.00E+04
280.09	2.34E+03	2.16E+03	2.12E+03	1.55E+04	1.59E+04	1.64E+04
295.96	1.93E+03	1.77E+03	1.73E+03	1.40E+04	1.42E+04	1.42E+04
312.72	1.63E+03	1.43E+03	1.44E+03	1.19E+04	1.21E+04	1.22E+04
330.44	1.45E+03	1.25E+03	1.25E+03	1.08E+04	1.06E+04	1.06E+04

Continued on next page

Table E.1 – continued from previous page

	0.254mm Ta (D1)			0.6mm Ag (D1)		
Time[μs]	**ENDF**	**JEFF**	**JENDL**	**ENDF**	**JEFF**	**JENDL**
349.16	1.22E+03	1.12E+03	1.13E+03	9.18E+03	9.25E+03	9.41E+03
368.94	1.08E+03	9.67E+02	1.01E+03	8.33E+03	8.44E+03	8.44E+03
389.85	9.83E+02	8.80E+02	9.24E+02	7.84E+03	7.89E+03	7.70E+03
411.94	9.04E+02	8.20E+02	8.33E+02	7.20E+03	7.23E+03	7.21E+03
435.27	8.08E+02	7.41E+02	7.60E+02	6.67E+03	6.88E+03	6.59E+03
459.94	7.30E+02	6.87E+02	6.77E+02	5.93E+03	6.18E+03	5.85E+03
485.99	6.57E+02	6.50E+02	6.30E+02	5.48E+03	5.49E+03	5.57E+03
513.53	6.03E+02	6.26E+02	5.85E+02	4.99E+03	5.14E+03	4.94E+03
542.62	5.39E+02	5.57E+02	5.40E+02	4.62E+03	4.70E+03	4.57E+03
573.36	4.97E+02	5.11E+02	4.76E+02	4.34E+03	4.48E+03	4.41E+03
605.85	4.53E+02	4.62E+02	4.40E+02	4.08E+03	4.08E+03	4.00E+03
640.17	4.07E+02	4.46E+02	4.06E+02	3.69E+03	3.58E+03	3.53E+03
676.44	3.88E+02	4.10E+02	3.83E+02	3.38E+03	3.46E+03	3.35E+03
714.77	3.60E+02	3.70E+02	3.58E+02	3.10E+03	3.22E+03	3.15E+03
755.27	3.34E+02	3.40E+02	3.26E+02	2.81E+03	2.79E+03	2.88E+03
798.06	3.01E+02	3.11E+02	3.11E+02	2.54E+03	2.74E+03	2.52E+03
843.27	2.73E+02	2.93E+02	2.69E+02	2.38E+03	2.47E+03	2.42E+03
891.05	2.51E+02	2.65E+02	2.41E+02	2.09E+03	2.11E+03	2.13E+03
941.53	2.31E+02	2.35E+02	2.27E+02	2.02E+03	1.97E+03	1.99E+03
994.89	2.06E+02	2.06E+02	2.09E+02	1.79E+03	1.82E+03	1.71E+03
1051.25	1.87E+02	1.93E+02	1.95E+02	1.55E+03	1.64E+03	1.64E+03
1110.8	1.80E+02	1.84E+02	1.70E+02	1.51E+03	1.47E+03	1.53E+03
1173.75	1.55E+02	1.54E+02	1.49E+02	1.29E+03	1.39E+03	1.27E+03
1240.25	1.33E+02	1.32E+02	1.28E+02	1.13E+03	1.14E+03	1.11E+03
1310.55	1.23E+02	1.26E+02	1.13E+02	9.77E+02	1.02E+03	9.98E+02
1384.75	1.06E+02	1.12E+02	1.05E+02	8.59E+02	9.27E+02	8.67E+02
1463.25	9.72E+01	9.70E+01	9.06E+01	7.58E+02	7.78E+02	7.54E+02
1546.1	8.16E+01	8.29E+01	7.96E+01	6.53E+02	6.92E+02	6.48E+02
1633.7	7.14E+01	7.29E+01	6.68E+01	6.20E+02	5.61E+02	5.88E+02
1726.3	6.04E+01	6.28E+01	5.88E+01	5.37E+02	5.08E+02	5.17E+02
1824.05	4.87E+01	4.73E+01	4.61E+01	4.29E+02	4.07E+02	4.07E+02
1927.45	4.10E+01	4.36E+01	3.94E+01	4.02E+02	3.60E+02	3.63E+02
2036.65	3.61E+01	3.86E+01	3.61E+01	2.99E+02	2.79E+02	2.80E+02
2152.05	3.07E+01	3.08E+01	2.65E+01	2.57E+02	2.77E+02	2.26E+02
2273.95	2.41E+01	2.33E+01	2.45E+01	2.17E+02	2.09E+02	1.84E+02
2402.8	1.93E+01	1.94E+01	2.30E+01	1.96E+02	1.87E+02	1.90E+02
2538.9	1.47E+01	1.65E+01	1.83E+01	1.51E+02	1.43E+02	1.44E+02
2682.75	1.43E+01	1.23E+01	1.26E+01	1.18E+02	1.18E+02	1.09E+02
2834.75	1.17E+01	9.67E+00	8.43E+00	8.78E+01	8.83E+01	9.15E+01
2995.35	9.35E+00	8.82E+00	7.65E+00	7.20E+01	8.33E+01	6.97E+01

Continued on next page

Table E.1 – continued from previous page

	0.254mm Ta (D1)			0.6mm Ag (D1)		
Time[μs]	**ENDF**	**JEFF**	**JENDL**	**ENDF**	**JEFF**	**JENDL**
3165.1	5.50E+00	5.66E+00	6.35E+00	6.37E+01	6.13E+01	5.47E+01
3344.4	4.64E+00	4.38E+00	5.63E+00	4.51E+01	5.13E+01	4.70E+01
3533.85	3.39E+00	3.71E+00	3.21E+00	3.36E+01	3.54E+01	2.76E+01
3734.05	2.24E+00	3.01E+00	2.03E+00	1.85E+01	1.92E+01	1.67E+01
3945.65	3.03E+00	3.45E+00	2.91E+00	2.76E+01	2.34E+01	3.15E+01

Table E.2: Simulation Results: Au, Nb.

	0.4mm Au (D1)			1.27mm Nb (D1)		
Time[μs]	**ENDF**	**JEFF**	**JENDL**	**ENDF**	**JEFF**	**JENDL**
1.01	3.83E+05	3.84E+05	3.79E+05	3.31E+05	3.31E+05	3.18E+05
1.07	4.05E+05	4.03E+05	4.03E+05	3.79E+05	3.79E+05	3.45E+05
1.13	3.96E+05	3.86E+05	3.92E+05	3.71E+05	3.71E+05	3.39E+05
1.2	3.94E+05	3.87E+05	3.89E+05	3.73E+05	3.73E+05	3.53E+05
1.26	3.86E+05	3.81E+05	3.81E+05	3.79E+05	3.79E+05	3.53E+05
1.34	3.86E+05	3.85E+05	3.79E+05	3.85E+05	3.85E+05	3.65E+05
1.41	3.82E+05	3.75E+05	3.73E+05	3.90E+05	3.90E+05	3.58E+05
1.49	3.73E+05	3.75E+05	3.67E+05	3.98E+05	3.98E+05	3.70E+05
1.58	3.74E+05	3.67E+05	3.67E+05	3.96E+05	3.96E+05	3.75E+05
1.67	3.72E+05	3.69E+05	3.64E+05	4.01E+05	4.01E+05	3.65E+05
1.76	3.64E+05	3.65E+05	3.55E+05	4.09E+05	4.09E+05	3.68E+05
1.86	3.66E+05	3.59E+05	3.58E+05	4.02E+05	4.02E+05	3.72E+05
1.96	3.54E+05	3.54E+05	3.46E+05	4.03E+05	4.03E+05	3.85E+05
2.08	3.50E+05	3.43E+05	3.39E+05	4.06E+05	4.06E+05	3.78E+05
2.19	3.50E+05	3.40E+05	3.41E+05	4.02E+05	4.02E+05	3.78E+05
2.32	3.45E+05	3.34E+05	3.36E+05	4.03E+05	4.03E+05	3.65E+05
2.45	3.45E+05	3.33E+05	3.38E+05	4.04E+05	4.04E+05	3.77E+05
2.59	3.35E+05	3.28E+05	3.33E+05	4.04E+05	4.04E+05	3.65E+05
2.73	3.37E+05	3.30E+05	3.35E+05	3.84E+05	3.84E+05	3.75E+05
2.89	3.35E+05	3.30E+05	3.34E+05	3.83E+05	3.83E+05	3.63E+05
3.05	3.36E+05	3.28E+05	3.39E+05	3.78E+05	3.78E+05	3.67E+05
3.23	3.44E+05	3.32E+05	3.42E+05	3.80E+05	3.80E+05	3.61E+05
3.41	3.33E+05	3.28E+05	3.37E+05	3.60E+05	3.60E+05	3.64E+05
3.6	3.50E+05	3.27E+05	3.45E+05	3.70E+05	3.70E+05	3.68E+05
3.81	3.35E+05	3.32E+05	3.39E+05	3.50E+05	3.50E+05	3.56E+05
4.02	3.43E+05	3.20E+05	3.49E+05	3.32E+05	3.32E+05	3.46E+05
4.25	3.33E+05	3.19E+05	3.41E+05	3.16E+05	3.16E+05	3.57E+05
4.49	3.23E+05	3.17E+05	3.41E+05	3.13E+05	3.14E+05	3.49E+05
4.74	3.31E+05	3.29E+05	3.50E+05	2.86E+05	2.86E+05	3.41E+05
5.01	3.22E+05	3.43E+05	3.54E+05	2.84E+05	2.84E+05	3.21E+05

Continued on next page

Table E.2 – continued from previous page

	0.4mm Au (D1)			1.27mm Nb (D1)		
Time[μs]	**ENDF**	**JEFF**	**JENDL**	**ENDF**	**JEFF**	**JENDL**
5.3	2.93E+05	3.16E+05	3.40E+05	2.57E+05	2.57E+05	3.04E+05
5.6	2.88E+05	3.21E+05	3.51E+05	2.55E+05	2.55E+05	3.04E+05
5.91	2.69E+05	3.08E+05	3.50E+05	2.38E+05	2.38E+05	2.70E+05
6.25	2.64E+05	2.93E+05	3.39E+05	2.40E+05	2.40E+05	2.68E+05
6.6	2.49E+05	2.81E+05	3.39E+05	2.38E+05	2.38E+05	2.63E+05
6.98	2.51E+05	2.69E+05	3.27E+05	2.35E+05	2.35E+05	2.42E+05
7.37	2.36E+05	2.58E+05	3.13E+05	2.27E+05	2.27E+05	2.21E+05
7.79	2.39E+05	2.47E+05	3.12E+05	2.33E+05	2.33E+05	2.18E+05
8.23	2.41E+05	2.44E+05	2.91E+05	2.43E+05	2.43E+05	2.20E+05
8.7	2.44E+05	2.49E+05	2.71E+05	2.43E+05	2.43E+05	2.27E+05
9.19	2.50E+05	2.60E+05	2.58E+05	2.25E+05	2.25E+05	2.14E+05
9.71	2.48E+05	2.61E+05	2.51E+05	2.08E+05	2.08E+05	2.11E+05
10.26	2.64E+05	2.76E+05	2.66E+05	2.15E+05	2.15E+05	1.95E+05
10.84	2.53E+05	2.49E+05	2.51E+05	2.03E+05	2.03E+05	1.76E+05
11.46	2.66E+05	2.67E+05	2.69E+05	2.13E+05	2.13E+05	1.77E+05
12.11	2.49E+05	2.37E+05	2.50E+05	2.18E+05	2.18E+05	1.50E+05
12.79	2.42E+05	2.46E+05	2.42E+05	1.86E+05	1.86E+05	1.23E+05
13.52	2.32E+05	2.54E+05	2.39E+05	1.44E+05	1.44E+05	9.28E+04
14.28	2.43E+05	2.42E+05	2.40E+05	9.62E+04	9.62E+04	7.56E+04
15.09	2.55E+05	2.54E+05	2.58E+05	8.00E+04	8.00E+04	7.16E+04
15.95	2.38E+05	2.43E+05	2.36E+05	5.93E+04	5.93E+04	5.50E+04
16.85	2.19E+05	2.22E+05	2.22E+05	4.60E+04	4.60E+04	4.07E+04
17.81	2.03E+05	1.97E+05	2.04E+05	4.42E+04	4.42E+04	3.64E+04
18.82	1.74E+05	1.88E+05	1.74E+05	5.58E+04	5.58E+04	4.28E+04
19.88	1.82E+05	1.76E+05	1.81E+05	7.05E+04	7.05E+04	5.89E+04
21.01	1.77E+05	1.71E+05	1.80E+05	9.38E+04	9.38E+04	7.15E+04
22.2	1.66E+05	1.77E+05	1.64E+05	7.71E+04	7.71E+04	6.83E+04
23.46	1.44E+05	1.52E+05	1.47E+05	4.45E+04	4.45E+04	3.83E+04
24.79	1.36E+05	1.29E+05	1.41E+05	2.75E+04	2.75E+04	2.74E+04
26.19	9.64E+04	1.10E+05	9.44E+04	2.72E+04	2.72E+04	3.15E+04
27.67	8.43E+04	8.18E+04	8.70E+04	5.20E+04	5.20E+04	5.22E+04
29.24	9.10E+04	9.30E+04	8.82E+04	6.08E+04	6.08E+04	6.38E+04
30.9	1.00E+05	1.11E+05	9.94E+04	3.86E+04	3.86E+04	3.92E+04
32.65	1.05E+05	1.05E+05	1.04E+05	2.32E+04	2.32E+04	2.15E+04
34.5	7.27E+04	7.84E+04	7.15E+04	1.89E+04	1.89E+04	1.63E+04
36.45	4.63E+04	5.12E+04	4.61E+04	2.95E+04	2.95E+04	3.04E+04
38.52	4.21E+04	4.47E+04	4.18E+04	3.23E+04	3.23E+04	2.99E+04
40.7	3.88E+04	4.61E+04	3.99E+04	1.84E+04	1.84E+04	1.82E+04
43.01	4.57E+04	4.87E+04	4.44E+04	7.99E+03	7.99E+03	7.07E+03
45.44	6.20E+04	6.02E+04	6.23E+04	3.03E+03	3.03E+03	2.38E+03

Continued on next page

Table E.2 – continued from previous page

	0.4mm Au (D1)			1.27mm Nb (D1)		
Time[μs]	**ENDF**	**JEFF**	**JENDL**	**ENDF**	**JEFF**	**JENDL**
48.02	7.57E+04	8.08E+04	7.51E+04	1.90E+03	1.90E+03	1.37E+03
50.74	1.09E+05	1.11E+05	1.10E+05	1.24E+03	1.24E+03	1.04E+03
53.61	1.07E+05	1.11E+05	1.04E+05	1.58E+03	1.58E+03	1.32E+03
56.65	5.70E+04	5.41E+04	5.69E+04	2.47E+03	2.47E+03	2.18E+03
59.86	1.76E+04	2.39E+04	1.74E+04	4.47E+03	4.47E+03	4.19E+03
63.25	5.42E+03	5.75E+03	5.24E+03	6.55E+03	6.55E+03	6.62E+03
66.84	4.95E+03	5.70E+03	4.85E+03	6.83E+03	6.83E+03	6.90E+03
70.62	4.26E+03	4.53E+03	4.07E+03	4.88E+03	4.88E+03	5.12E+03
74.62	4.89E+03	4.13E+03	5.10E+03	2.17E+03	2.17E+03	2.13E+03
78.85	5.22E+03	5.28E+03	4.88E+03	8.07E+02	8.07E+02	6.25E+02
83.32	5.10E+03	5.65E+03	5.76E+03	6.69E+02	6.69E+02	4.82E+02
88.04	6.47E+03	6.06E+03	6.72E+03	6.28E+02	6.28E+02	4.55E+02
93.03	7.40E+03	6.83E+03	8.46E+03	5.57E+02	5.56E+02	4.50E+02
98.3	7.07E+03	6.76E+03	7.22E+03	4.96E+02	4.96E+02	3.43E+02
103.87	8.06E+03	9.70E+03	8.24E+03	4.44E+02	4.44E+02	3.19E+02
109.75	1.02E+04	1.05E+04	1.02E+04	4.10E+02	4.10E+02	3.20E+02
115.97	1.32E+04	1.30E+04	1.32E+04	4.56E+02	4.56E+02	3.49E+02
122.54	1.63E+04	1.39E+04	1.58E+04	4.93E+02	4.93E+02	4.15E+02
129.49	2.01E+04	1.93E+04	2.00E+04	4.68E+02	4.68E+02	3.75E+02
136.82	2.73E+04	2.59E+04	2.72E+04	3.87E+02	3.87E+02	3.14E+02
144.57	3.78E+04	3.87E+04	3.75E+04	3.11E+02	3.11E+02	2.52E+02
152.77	5.52E+04	5.76E+04	5.55E+04	2.97E+02	2.97E+02	2.25E+02
161.42	8.53E+04	8.41E+04	8.62E+04	3.23E+02	3.23E+02	2.82E+02
170.56	1.15E+05	1.13E+05	1.15E+05	3.72E+02	3.72E+02	3.35E+02
180.23	1.32E+05	1.31E+05	1.33E+05	4.82E+02	4.82E+02	4.37E+02
190.44	1.11E+05	1.17E+05	1.12E+05	6.31E+02	6.31E+02	6.48E+02
201.23	9.13E+04	8.97E+04	9.35E+04	6.55E+02	6.55E+02	6.39E+02
212.63	6.08E+04	6.07E+04	6.04E+04	4.62E+02	4.62E+02	4.20E+02
224.68	3.86E+04	3.85E+04	3.88E+04	3.01E+02	3.01E+02	2.52E+02
237.4	2.60E+04	2.56E+04	2.60E+04	1.94E+02	1.94E+02	1.75E+02
250.86	1.89E+04	1.82E+04	1.93E+04	1.76E+02	1.76E+02	1.53E+02
265.07	1.48E+04	1.44E+04	1.47E+04	1.58E+02	1.58E+02	1.42E+02
280.09	1.18E+04	1.18E+04	1.18E+04	1.53E+02	1.53E+02	1.36E+02
295.96	9.69E+03	1.00E+04	9.79E+03	1.48E+02	1.48E+02	1.32E+02
312.72	8.56E+03	8.50E+03	8.44E+03	1.41E+02	1.41E+02	1.24E+02
330.44	6.90E+03	7.21E+03	6.87E+03	1.32E+02	1.32E+02	1.24E+02
349.16	6.23E+03	6.32E+03	6.33E+03	1.28E+02	1.28E+02	1.16E+02
368.94	5.47E+03	5.33E+03	5.54E+03	1.21E+02	1.21E+02	1.14E+02
389.85	5.09E+03	4.91E+03	5.05E+03	1.13E+02	1.13E+02	1.07E+02
411.94	4.51E+03	4.50E+03	4.54E+03	1.05E+02	1.05E+02	9.94E+01

Continued on next page

Table E.2 – continued from previous page

	0.4mm Au (D1)			1.27mm Nb (D1)		
Time[μs]	**ENDF**	**JEFF**	**JENDL**	**ENDF**	**JEFF**	**JENDL**
435.27	4.12E+03	4.16E+03	4.15E+03	1.03E+02	1.03E+02	9.26E+01
459.94	3.69E+03	3.84E+03	3.69E+03	9.41E+01	9.41E+01	9.00E+01
485.99	3.22E+03	3.35E+03	3.25E+03	9.32E+01	9.32E+01	8.81E+01
513.53	3.18E+03	3.18E+03	3.19E+03	8.10E+01	8.10E+01	8.13E+01
542.62	2.90E+03	3.00E+03	2.94E+03	8.21E+01	8.21E+01	7.76E+01
573.36	2.67E+03	2.62E+03	2.67E+03	7.31E+01	7.31E+01	7.19E+01
605.85	2.27E+03	2.30E+03	2.29E+03	7.04E+01	7.04E+01	6.86E+01
640.17	2.16E+03	2.23E+03	2.18E+03	6.66E+01	6.66E+01	6.42E+01
676.44	2.01E+03	2.03E+03	2.02E+03	6.01E+01	6.01E+01	6.00E+01
714.77	1.81E+03	1.83E+03	1.81E+03	5.78E+01	5.78E+01	5.39E+01
755.27	1.66E+03	1.68E+03	1.63E+03	5.33E+01	5.33E+01	5.17E+01
798.06	1.54E+03	1.58E+03	1.55E+03	4.85E+01	4.85E+01	4.56E+01
843.27	1.36E+03	1.36E+03	1.38E+03	4.48E+01	4.48E+01	4.22E+01
891.05	1.28E+03	1.31E+03	1.28E+03	4.26E+01	4.26E+01	4.11E+01
941.53	1.17E+03	1.09E+03	1.15E+03	3.72E+01	3.72E+01	3.55E+01
994.89	9.50E+02	1.01E+03	9.27E+02	3.27E+01	3.27E+01	2.99E+01
1051.25	8.77E+02	9.26E+02	8.78E+02	2.82E+01	2.82E+01	2.92E+01
1110.8	8.28E+02	8.30E+02	8.21E+02	2.61E+01	2.61E+01	2.89E+01
1173.75	7.47E+02	7.74E+02	7.39E+02	2.67E+01	2.67E+01	2.60E+01
1240.25	6.86E+02	6.35E+02	6.92E+02	2.23E+01	2.23E+01	2.15E+01
1310.55	5.44E+02	5.47E+02	5.51E+02	2.00E+01	2.00E+01	1.84E+01
1384.75	5.06E+02	5.25E+02	5.01E+02	1.84E+01	1.84E+01	1.66E+01
1463.25	4.49E+02	4.70E+02	4.47E+02	1.66E+01	1.66E+01	1.65E+01
1546.1	3.83E+02	4.06E+02	3.91E+02	1.56E+01	1.56E+01	1.36E+01
1633.7	3.31E+02	3.10E+02	3.35E+02	1.19E+01	1.19E+01	1.21E+01
1726.3	2.75E+02	2.96E+02	2.76E+02	1.03E+01	1.03E+01	9.87E+00
1824.05	2.44E+02	2.52E+02	2.45E+02	9.55E+00	9.55E+00	8.49E+00
1927.45	1.92E+02	2.11E+02	2.05E+02	7.20E+00	7.20E+00	7.53E+00
2036.65	1.96E+02	1.69E+02	1.95E+02	6.91E+00	6.91E+00	6.44E+00
2152.05	1.36E+02	1.46E+02	1.40E+02	5.18E+00	5.18E+00	6.05E+00
2273.95	1.12E+02	1.23E+02	1.11E+02	4.40E+00	4.40E+00	4.76E+00
2402.8	8.69E+01	1.00E+02	9.20E+01	3.76E+00	3.76E+00	3.67E+00
2538.9	8.53E+01	6.81E+01	8.44E+01	3.01E+00	3.01E+00	3.11E+00
2682.75	5.82E+01	6.50E+01	5.52E+01	2.16E+00	2.16E+00	2.38E+00
2834.75	6.54E+01	5.35E+01	6.23E+01	1.90E+00	1.90E+00	1.91E+00
2995.35	5.69E+01	6.19E+01	5.82E+01	1.80E+00	1.80E+00	1.64E+00
3165.1	2.46E+01	2.68E+01	2.43E+01	1.29E+00	1.29E+00	8.90E-01
3344.4	2.10E+01	2.02E+01	2.14E+01	8.65E-01	8.65E-01	7.34E-01
3533.85	1.36E+01	1.48E+01	1.29E+01	9.31E-01	9.31E-01	8.64E-01
3734.05	1.33E+01	1.10E+01	1.25E+01	4.43E-01	4.43E-01	5.99E-01

Continued on next page

Table E.2 – continued from previous page

	0.4mm Au (D1)			1.27mm Nb (D1)		
Time[μs]	**ENDF**	**JEFF**	**JENDL**	**ENDF**	**JEFF**	**JENDL**
3945.65	9.50E+00	1.21E+01	9.48E+00	3.45E-01	3.45E-01	3.37E-01

Table E.3: Simulation Results: In, Mo.

	0.6mm In (D2)			1.0mm Mo (D2)		
Time[μs]	**ENDF**	**JEFF**	**JENDL**	**ENDF**	**JEFF**	**JENDL**
1.01	8.23E+05	8.23E+05	8.11E+05	4.93E+05	4.92E+05	4.68E+05
1.07	8.58E+05	8.57E+05	8.50E+05	4.89E+05	4.88E+05	4.80E+05
1.13	8.41E+05	8.42E+05	8.38E+05	4.93E+05	4.90E+05	4.81E+05
1.2	8.33E+05	8.32E+05	8.28E+05	4.91E+05	4.86E+05	4.78E+05
1.26	8.21E+05	8.21E+05	8.18E+05	4.84E+05	4.85E+05	4.70E+05
1.34	8.28E+05	8.28E+05	8.18E+05	4.87E+05	4.84E+05	4.70E+05
1.41	8.49E+05	8.49E+05	8.43E+05	4.99E+05	4.97E+05	4.85E+05
1.49	8.06E+05	8.05E+05	8.01E+05	4.89E+05	4.89E+05	4.75E+05
1.58	8.19E+05	8.18E+05	8.27E+05	4.98E+05	4.97E+05	4.89E+05
1.67	8.00E+05	7.99E+05	8.09E+05	5.00E+05	4.99E+05	4.91E+05
1.76	7.96E+05	7.97E+05	8.09E+05	4.97E+05	4.96E+05	4.90E+05
1.86	7.88E+05	7.87E+05	7.94E+05	4.92E+05	4.93E+05	4.87E+05
1.96	7.86E+05	7.84E+05	7.95E+05	4.91E+05	4.92E+05	4.87E+05
2.08	7.64E+05	7.63E+05	7.80E+05	4.91E+05	4.92E+05	4.92E+05
2.19	7.47E+05	7.48E+05	7.74E+05	4.73E+05	4.75E+05	4.94E+05
2.32	7.50E+05	7.50E+05	7.55E+05	4.75E+05	4.76E+05	4.89E+05
2.45	7.32E+05	7.31E+05	7.51E+05	4.75E+05	4.77E+05	4.90E+05
2.59	7.19E+05	7.18E+05	7.31E+05	4.62E+05	4.68E+05	4.79E+05
2.73	7.12E+05	7.10E+05	7.24E+05	4.65E+05	4.67E+05	4.84E+05
2.89	6.84E+05	6.83E+05	6.96E+05	4.51E+05	4.55E+05	4.67E+05
3.05	6.77E+05	6.72E+05	6.81E+05	4.42E+05	4.44E+05	4.61E+05
3.23	6.49E+05	6.47E+05	6.61E+05	4.38E+05	4.41E+05	4.60E+05
3.41	6.46E+05	6.46E+05	6.64E+05	4.30E+05	4.38E+05	4.54E+05
3.6	6.17E+05	6.17E+05	6.28E+05	4.29E+05	4.34E+05	4.50E+05
3.81	5.96E+05	5.94E+05	6.12E+05	4.16E+05	4.20E+05	4.38E+05
4.02	5.79E+05	5.77E+05	5.89E+05	4.12E+05	4.16E+05	4.27E+05
4.25	5.61E+05	5.62E+05	5.71E+05	4.11E+05	4.12E+05	4.21E+05
4.49	5.45E+05	5.45E+05	5.52E+05	3.97E+05	4.03E+05	4.17E+05
4.74	5.27E+05	5.24E+05	5.33E+05	3.88E+05	3.87E+05	4.06E+05
5.01	5.21E+05	5.21E+05	5.16E+05	3.88E+05	3.93E+05	3.96E+05
5.3	5.11E+05	5.09E+05	5.07E+05	3.82E+05	3.84E+05	4.05E+05
5.6	5.00E+05	4.98E+05	4.95E+05	3.78E+05	3.77E+05	3.94E+05
5.91	4.87E+05	4.85E+05	4.80E+05	3.59E+05	3.60E+05	3.79E+05
6.25	4.70E+05	4.65E+05	4.63E+05	3.42E+05	3.40E+05	3.65E+05

Continued on next page

Table E.3 – continued from previous page

	0.6mm In (D2)			1.0mm Mo (D2)		
Time[μs]	**ENDF**	**JEFF**	**JENDL**	**ENDF**	**JEFF**	**JENDL**
6.6	4.58E+05	4.53E+05	4.46E+05	3.27E+05	3.28E+05	3.43E+05
6.98	4.23E+05	4.17E+05	4.24E+05	3.11E+05	3.12E+05	3.23E+05
7.37	4.15E+05	4.09E+05	4.05E+05	2.97E+05	2.93E+05	3.14E+05
7.79	3.92E+05	3.85E+05	3.73E+05	2.85E+05	2.76E+05	2.86E+05
8.23	3.67E+05	3.56E+05	3.47E+05	2.66E+05	2.53E+05	2.73E+05
8.7	3.25E+05	3.05E+05	3.07E+05	2.53E+05	2.33E+05	2.50E+05
9.19	2.94E+05	2.67E+05	2.56E+05	2.34E+05	2.17E+05	2.30E+05
9.71	2.54E+05	2.24E+05	2.22E+05	2.13E+05	1.97E+05	2.17E+05
10.26	2.17E+05	1.89E+05	1.84E+05	2.03E+05	1.88E+05	2.10E+05
10.84	1.98E+05	1.77E+05	1.71E+05	1.91E+05	1.72E+05	1.92E+05
11.46	2.05E+05	1.79E+05	1.73E+05	1.83E+05	1.64E+05	1.86E+05
12.11	1.89E+05	1.69E+05	1.65E+05	1.74E+05	1.53E+05	1.73E+05
12.79	2.10E+05	1.89E+05	1.83E+05	1.67E+05	1.49E+05	1.63E+05
13.52	1.98E+05	1.76E+05	1.73E+05	1.60E+05	1.47E+05	1.54E+05
14.28	1.96E+05	1.72E+05	1.70E+05	1.63E+05	1.58E+05	1.57E+05
15.09	1.68E+05	1.48E+05	1.46E+05	1.87E+05	1.84E+05	1.85E+05
15.95	1.59E+05	1.40E+05	1.41E+05	1.82E+05	1.77E+05	1.79E+05
16.85	1.69E+05	1.51E+05	1.47E+05	1.78E+05	1.75E+05	1.79E+05
17.81	1.71E+05	1.54E+05	1.51E+05	1.69E+05	1.68E+05	1.69E+05
18.82	1.74E+05	1.59E+05	1.49E+05	1.75E+05	1.73E+05	1.74E+05
19.88	1.83E+05	1.65E+05	1.68E+05	1.84E+05	1.84E+05	1.83E+05
21.01	1.74E+05	1.60E+05	1.72E+05	1.65E+05	1.67E+05	1.67E+05
22.2	1.47E+05	1.35E+05	1.67E+05	1.25E+05	1.24E+05	1.24E+05
23.46	1.61E+05	1.52E+05	1.58E+05	8.55E+04	8.56E+04	8.55E+04
24.79	1.65E+05	1.58E+05	1.61E+05	5.78E+04	5.75E+04	5.91E+04
26.19	1.60E+05	1.72E+05	1.67E+05	3.92E+04	3.89E+04	4.00E+04
27.67	1.48E+05	1.57E+05	1.64E+05	2.96E+04	2.91E+04	2.96E+04
29.24	1.30E+05	1.35E+05	1.44E+05	3.70E+04	3.67E+04	3.63E+04
30.9	1.32E+05	1.39E+05	1.35E+05	5.12E+04	5.03E+04	5.31E+04
32.65	1.07E+05	1.14E+05	1.08E+05	7.92E+04	7.87E+04	8.06E+04
34.5	8.55E+04	9.20E+04	7.73E+04	1.06E+05	1.06E+05	1.11E+05
36.45	6.81E+04	7.17E+04	6.13E+04	9.45E+04	9.48E+04	9.93E+04
38.52	5.99E+04	6.02E+04	5.28E+04	5.59E+04	5.64E+04	5.89E+04
40.7	7.19E+04	7.04E+04	6.80E+04	3.37E+04	3.41E+04	3.48E+04
43.01	7.78E+04	7.79E+04	7.61E+04	2.71E+04	2.85E+04	2.71E+04
45.44	7.50E+04	7.56E+04	7.27E+04	4.39E+04	4.43E+04	4.14E+04
48.02	5.54E+04	5.65E+04	5.45E+04	5.85E+04	6.04E+04	5.28E+04
50.74	3.35E+04	3.45E+04	3.25E+04	5.56E+04	5.92E+04	5.19E+04
53.61	3.28E+04	3.46E+04	3.36E+04	6.99E+04	7.58E+04	6.63E+04
56.65	3.63E+04	3.77E+04	3.61E+04	1.17E+05	1.27E+05	1.09E+05

Continued on next page

Table E.3 – continued from previous page

	0.6mm In (D2)			1.0mm Mo (D2)		
Time[μs]	**ENDF**	**JEFF**	**JENDL**	**ENDF**	**JEFF**	**JENDL**
59.86	5.47E+04	5.56E+04	5.69E+04	1.72E+05	1.86E+05	1.60E+05
63.25	6.85E+04	6.77E+04	6.86E+04	1.43E+05	1.54E+05	1.34E+05
66.84	6.57E+04	6.45E+04	6.67E+04	7.25E+04	7.48E+04	6.59E+04
70.62	4.04E+04	3.86E+04	4.11E+04	2.24E+04	2.24E+04	2.10E+04
74.62	3.70E+04	3.60E+04	3.83E+04	6.40E+03	6.44E+03	6.38E+03
78.85	4.56E+04	4.45E+04	4.56E+04	3.50E+03	3.79E+03	3.64E+03
83.32	5.45E+04	5.43E+04	5.39E+04	2.58E+03	2.65E+03	2.81E+03
88.04	5.03E+04	5.00E+04	5.03E+04	2.17E+03	2.21E+03	2.29E+03
93.03	3.35E+04	3.31E+04	3.32E+04	2.44E+03	2.44E+03	2.65E+03
98.3	2.71E+04	2.71E+04	2.66E+04	2.43E+03	2.46E+03	2.95E+03
103.87	3.27E+04	3.29E+04	3.25E+04	3.51E+03	3.54E+03	4.29E+03
109.75	3.65E+04	3.65E+04	3.64E+04	6.76E+03	6.66E+03	8.12E+03
115.97	4.13E+04	4.10E+04	4.11E+04	8.74E+03	8.73E+03	1.08E+04
122.54	5.24E+04	5.21E+04	5.27E+04	6.54E+03	6.50E+03	7.20E+03
129.49	7.88E+04	7.78E+04	7.73E+04	3.13E+03	3.12E+03	3.47E+03
136.82	7.68E+04	7.59E+04	7.60E+04	1.49E+03	1.47E+03	1.59E+03
144.57	4.98E+04	4.93E+04	4.88E+04	9.61E+02	9.48E+02	1.01E+03
152.77	2.91E+04	2.88E+04	2.92E+04	9.06E+02	8.90E+02	9.16E+02
161.42	1.91E+04	1.90E+04	1.89E+04	8.15E+02	8.01E+02	8.48E+02
170.56	2.09E+04	2.07E+04	2.05E+04	8.17E+02	8.01E+02	8.32E+02
180.23	2.90E+04	2.83E+04	2.87E+04	7.85E+02	7.73E+02	8.03E+02
190.44	4.01E+04	3.97E+04	4.06E+04	7.25E+02	7.11E+02	7.38E+02
201.23	5.79E+04	5.70E+04	5.77E+04	7.03E+02	6.91E+02	7.16E+02
212.63	6.18E+04	6.28E+04	6.32E+04	7.01E+02	6.94E+02	7.17E+02
224.68	5.17E+04	5.30E+04	5.34E+04	6.60E+02	6.48E+02	6.67E+02
237.4	4.20E+04	4.25E+04	4.29E+04	6.49E+02	6.42E+02	6.62E+02
250.86	4.28E+04	4.33E+04	4.38E+04	6.15E+02	6.05E+02	6.32E+02
265.07	5.08E+04	5.11E+04	5.06E+04	5.91E+02	5.83E+02	6.01E+02
280.09	6.59E+04	6.62E+04	6.63E+04	5.64E+02	5.57E+02	5.72E+02
295.96	7.68E+04	7.69E+04	7.70E+04	5.52E+02	5.45E+02	5.62E+02
312.72	8.73E+04	8.75E+04	8.73E+04	5.49E+02	5.43E+02	5.63E+02
330.44	8.69E+04	8.69E+04	8.74E+04	5.11E+02	5.05E+02	5.18E+02
349.16	8.53E+04	8.54E+04	8.49E+04	4.94E+02	4.89E+02	5.00E+02
368.94	6.98E+04	6.96E+04	6.99E+04	4.59E+02	4.53E+02	4.62E+02
389.85	6.01E+04	5.98E+04	6.00E+04	4.48E+02	4.43E+02	4.55E+02
411.94	4.63E+04	4.60E+04	4.62E+04	4.24E+02	4.22E+02	4.35E+02
435.27	3.87E+04	3.85E+04	3.87E+04	4.07E+02	4.02E+02	4.13E+02
459.94	2.88E+04	2.86E+04	2.86E+04	3.73E+02	3.71E+02	3.81E+02
485.99	2.31E+04	2.29E+04	2.29E+04	3.58E+02	3.54E+02	3.63E+02
513.53	1.87E+04	1.86E+04	1.85E+04	3.35E+02	3.33E+02	3.44E+02

Continued on next page

Table E.3 – continued from previous page

	0.6mm In (D2)			1.0mm Mo (D2)		
Time[μs]	**ENDF**	**JEFF**	**JENDL**	**ENDF**	**JEFF**	**JENDL**
542.62	1.62E+04	1.61E+04	1.60E+04	3.22E+02	3.20E+02	3.27E+02
573.36	1.33E+04	1.32E+04	1.33E+04	3.10E+02	3.06E+02	3.13E+02
605.85	1.11E+04	1.10E+04	1.10E+04	2.86E+02	2.83E+02	2.87E+02
640.17	9.47E+03	9.40E+03	9.45E+03	2.69E+02	2.67E+02	2.70E+02
676.44	8.41E+03	8.35E+03	8.32E+03	2.62E+02	2.61E+02	2.66E+02
714.77	7.29E+03	7.23E+03	7.27E+03	2.36E+02	2.33E+02	2.39E+02
755.27	6.52E+03	6.50E+03	6.43E+03	2.20E+02	2.20E+02	2.24E+02
798.06	5.86E+03	5.82E+03	5.82E+03	2.06E+02	2.04E+02	2.07E+02
843.27	4.75E+03	4.72E+03	4.72E+03	1.87E+02	1.87E+02	1.91E+02
891.05	4.40E+03	4.39E+03	4.39E+03	1.73E+02	1.72E+02	1.78E+02
941.53	3.71E+03	3.70E+03	3.74E+03	1.57E+02	1.56E+02	1.60E+02
994.89	3.22E+03	3.21E+03	3.22E+03	1.37E+02	1.37E+02	1.39E+02
1051.25	2.97E+03	2.95E+03	2.95E+03	1.28E+02	1.27E+02	1.30E+02
1110.8	2.65E+03	2.63E+03	2.63E+03	1.07E+02	1.07E+02	1.10E+02
1173.75	2.11E+03	2.10E+03	2.10E+03	1.01E+02	1.00E+02	1.02E+02
1240.25	1.99E+03	2.00E+03	2.00E+03	9.20E+01	9.16E+01	9.39E+01
1310.55	1.80E+03	1.78E+03	1.76E+03	8.64E+01	8.64E+01	8.74E+01
1384.75	1.52E+03	1.52E+03	1.54E+03	7.44E+01	7.40E+01	7.45E+01
1463.25	1.36E+03	1.34E+03	1.32E+03	6.77E+01	6.78E+01	6.81E+01
1546.1	1.13E+03	1.13E+03	1.11E+03	5.77E+01	5.73E+01	5.92E+01
1633.7	9.24E+02	9.23E+02	9.04E+02	4.56E+01	4.56E+01	4.70E+01
1726.3	8.61E+02	8.64E+02	8.75E+02	4.38E+01	4.37E+01	4.37E+01
1824.05	7.16E+02	7.11E+02	7.09E+02	3.69E+01	3.66E+01	3.72E+01
1927.45	4.89E+02	4.91E+02	4.83E+02	2.87E+01	2.81E+01	2.90E+01
2036.65	5.15E+02	5.12E+02	4.96E+02	2.83E+01	2.83E+01	2.81E+01
2152.05	4.04E+02	4.00E+02	4.01E+02	2.07E+01	2.07E+01	2.14E+01
2273.95	3.21E+02	3.19E+02	3.14E+02	1.70E+01	1.70E+01	1.74E+01
2402.8	2.77E+02	2.76E+02	2.80E+02	1.42E+01	1.40E+01	1.41E+01
2538.9	1.63E+02	1.64E+02	1.62E+02	1.28E+01	1.27E+01	1.30E+01
2682.75	1.62E+02	1.61E+02	1.58E+02	1.11E+01	1.11E+01	1.21E+01
2834.75	1.11E+02	1.10E+02	1.06E+02	6.50E+00	6.55E+00	6.60E+00
2995.35	8.09E+01	8.09E+01	8.18E+01	5.68E+00	5.67E+00	5.75E+00
3165.1	1.10E+02	1.11E+02	1.11E+02	5.81E+00	5.80E+00	5.89E+00
3344.4	6.29E+01	6.30E+01	6.42E+01	4.03E+00	3.99E+00	4.20E+00
3533.85	5.80E+01	5.85E+01	6.16E+01	3.06E+00	3.07E+00	3.22E+00
3734.05	2.88E+01	2.87E+01	3.09E+01	1.74E+00	1.81E+00	1.88E+00
3945.65	2.41E+01	2.40E+01	2.48E+01	1.65E+00	1.65E+00	1.53E+00

Table E.4: Simulation Results: Sn, Zr.

	1.0mm Sn (D2)			1.0mm Zr (D2)		
Time[μs]	**ENDF**	**JEFF**	**JENDL**	**ENDF**	**JEFF**	**JENDL**
1.01	1.14E+05	1.14E+05	1.15E+05	4.11E+04	3.93E+04	3.58E+04
1.07	1.10E+05	1.11E+05	1.13E+05	3.83E+04	3.81E+04	3.58E+04
1.13	1.09E+05	1.09E+05	1.11E+05	3.83E+04	3.78E+04	3.51E+04
1.2	1.08E+05	1.10E+05	1.11E+05	3.82E+04	3.69E+04	3.45E+04
1.26	1.06E+05	1.07E+05	1.08E+05	3.62E+04	3.48E+04	3.27E+04
1.34	1.07E+05	1.08E+05	1.09E+05	3.65E+04	3.61E+04	3.41E+04
1.41	1.08E+05	1.08E+05	1.12E+05	3.65E+04	3.60E+04	3.40E+04
1.49	1.04E+05	1.06E+05	1.08E+05	3.59E+04	3.50E+04	3.22E+04
1.58	1.05E+05	1.08E+05	1.10E+05	3.61E+04	3.54E+04	3.36E+04
1.67	1.05E+05	1.09E+05	1.10E+05	3.54E+04	3.79E+04	3.44E+04
1.76	1.06E+05	1.09E+05	1.11E+05	3.71E+04	3.62E+04	3.42E+04
1.86	1.05E+05	1.10E+05	1.10E+05	3.58E+04	3.59E+04	3.34E+04
1.96	1.06E+05	1.10E+05	1.12E+05	3.47E+04	3.45E+04	3.18E+04
2.08	1.07E+05	1.09E+05	1.12E+05	3.49E+04	3.33E+04	3.19E+04
2.19	1.05E+05	1.10E+05	1.10E+05	3.55E+04	3.40E+04	3.24E+04
2.32	1.07E+05	1.10E+05	1.11E+05	3.57E+04	3.35E+04	3.21E+04
2.45	1.07E+05	1.11E+05	1.12E+05	3.37E+04	3.09E+04	2.94E+04
2.59	1.07E+05	1.10E+05	1.12E+05	3.62E+04	3.31E+04	3.02E+04
2.73	1.04E+05	1.09E+05	1.10E+05	3.50E+04	3.41E+04	3.15E+04
2.89	1.02E+05	1.07E+05	1.08E+05	3.39E+04	3.25E+04	3.02E+04
3.05	1.01E+05	1.06E+05	1.07E+05	3.52E+04	3.44E+04	3.11E+04
3.23	1.02E+05	1.04E+05	1.05E+05	3.43E+04	3.51E+04	3.19E+04
3.41	9.94E+04	1.04E+05	1.06E+05	3.51E+04	3.55E+04	3.19E+04
3.6	9.55E+04	1.00E+05	9.96E+04	3.44E+04	3.48E+04	3.18E+04
3.81	9.27E+04	9.98E+04	9.68E+04	3.28E+04	3.30E+04	3.01E+04
4.02	9.39E+04	1.01E+05	9.83E+04	3.63E+04	3.68E+04	3.49E+04
4.25	9.09E+04	9.90E+04	9.61E+04	3.83E+04	3.87E+04	3.69E+04
4.49	9.16E+04	9.67E+04	9.55E+04	3.73E+04	3.72E+04	3.60E+04
4.74	8.84E+04	9.40E+04	9.36E+04	4.11E+04	4.10E+04	3.94E+04
5.01	8.65E+04	9.20E+04	9.29E+04	3.92E+04	3.95E+04	3.80E+04
5.3	8.52E+04	9.35E+04	9.18E+04	3.75E+04	3.69E+04	3.54E+04
5.6	8.47E+04	9.12E+04	9.06E+04	4.02E+04	4.00E+04	3.75E+04
5.91	7.86E+04	8.90E+04	8.55E+04	4.11E+04	4.15E+04	3.92E+04
6.25	7.56E+04	8.50E+04	8.04E+04	4.22E+04	4.17E+04	3.83E+04
6.6	7.30E+04	8.84E+04	7.76E+04	3.31E+04	3.32E+04	3.05E+04
6.98	6.50E+04	7.95E+04	6.74E+04	2.63E+04	2.67E+04	2.41E+04
7.37	6.09E+04	7.30E+04	6.34E+04	2.34E+04	2.41E+04	2.15E+04
7.79	5.51E+04	6.27E+04	5.73E+04	2.08E+04	2.17E+04	1.91E+04
8.23	5.22E+04	6.13E+04	5.64E+04	2.04E+04	2.15E+04	1.88E+04

Continued on next page

Table E.4 – continued from previous page

	1.0mm Sn (D2)			1.0mm Zr (D2)		
Time[μs]	**ENDF**	**JEFF**	**JENDL**	**ENDF**	**JEFF**	**JENDL**
8.7	4.76E+04	5.94E+04	5.62E+04	1.97E+04	2.07E+04	1.69E+04
9.19	4.80E+04	5.70E+04	5.88E+04	1.50E+04	1.57E+04	1.34E+04
9.71	5.14E+04	5.75E+04	6.42E+04	1.18E+04	1.23E+04	1.10E+04
10.26	4.72E+04	5.60E+04	5.87E+04	7.90E+03	8.11E+03	7.82E+03
10.84	4.21E+04	4.95E+04	5.26E+04	5.46E+03	5.87E+03	5.69E+03
11.46	3.55E+04	4.22E+04	4.34E+04	3.45E+03	3.61E+03	3.43E+03
12.11	3.14E+04	3.75E+04	3.64E+04	3.25E+03	3.26E+03	3.06E+03
12.79	3.57E+04	3.89E+04	4.08E+04	4.40E+03	4.47E+03	4.03E+03
13.52	3.82E+04	4.13E+04	4.47E+04	6.52E+03	6.55E+03	5.85E+03
14.28	3.49E+04	3.88E+04	4.37E+04	8.26E+03	8.33E+03	7.48E+03
15.09	2.89E+04	3.54E+04	3.73E+04	1.04E+04	1.05E+04	9.26E+03
15.95	2.29E+04	2.56E+04	2.74E+04	9.62E+03	9.50E+03	8.47E+03
16.85	1.78E+04	2.11E+04	2.09E+04	6.53E+03	6.66E+03	5.76E+03
17.81	2.08E+04	2.29E+04	2.28E+04	4.05E+03	4.16E+03	3.73E+03
18.82	2.75E+04	3.00E+04	3.09E+04	4.73E+03	4.64E+03	4.07E+03
19.88	3.75E+04	4.33E+04	4.33E+04	6.27E+03	6.28E+03	5.82E+03
21.01	3.71E+04	4.45E+04	4.55E+04	1.10E+04	1.09E+04	1.01E+04
22.2	3.10E+04	3.64E+04	3.81E+04	2.11E+04	2.12E+04	1.92E+04
23.46	1.97E+04	2.26E+04	2.29E+04	3.25E+04	3.31E+04	2.97E+04
24.79	1.43E+04	1.55E+04	1.52E+04	2.50E+04	2.50E+04	2.29E+04
26.19	1.30E+04	1.31E+04	1.30E+04	1.19E+04	1.19E+04	1.12E+04
27.67	1.45E+04	1.45E+04	1.41E+04	6.05E+03	5.95E+03	5.49E+03
29.24	1.32E+04	1.37E+04	1.28E+04	5.19E+03	5.19E+03	5.27E+03
30.9	1.34E+04	1.41E+04	1.28E+04	5.04E+03	5.09E+03	4.92E+03
32.65	1.82E+04	1.84E+04	1.72E+04	2.42E+03	2.47E+03	2.35E+03
34.5	2.55E+04	2.55E+04	2.42E+04	8.05E+02	8.18E+02	8.44E+02
36.45	3.60E+04	3.55E+04	3.46E+04	1.62E+02	1.69E+02	1.76E+02
38.52	4.62E+04	4.52E+04	4.48E+04	1.12E+02	1.16E+02	1.03E+02
40.7	3.69E+04	3.58E+04	3.60E+04	6.68E+01	7.13E+01	6.89E+01
43.01	1.77E+04	1.76E+04	1.74E+04	5.99E+01	6.41E+01	6.30E+01
45.44	1.05E+04	1.02E+04	1.03E+04	5.86E+01	6.26E+01	6.15E+01
48.02	1.03E+04	1.03E+04	1.00E+04	5.86E+01	6.19E+01	6.12E+01
50.74	1.28E+04	1.28E+04	1.24E+04	5.58E+01	5.91E+01	5.86E+01
53.61	1.34E+04	1.35E+04	1.32E+04	5.68E+01	6.01E+01	5.91E+01
56.65	1.16E+04	1.16E+04	1.14E+04	5.51E+01	5.82E+01	5.77E+01
59.86	1.42E+04	1.41E+04	1.41E+04	5.52E+01	5.79E+01	5.75E+01
63.25	1.70E+04	1.66E+04	1.68E+04	5.09E+01	5.36E+01	5.33E+01
66.84	1.27E+04	1.23E+04	1.24E+04	4.92E+01	5.17E+01	5.15E+01
70.62	5.51E+03	5.33E+03	5.42E+03	4.68E+01	4.90E+01	4.92E+01
74.62	1.50E+03	1.45E+03	1.45E+03	4.59E+01	4.78E+01	4.78E+01

Continued on next page

Table E.4 – continued from previous page

	1.0mm Sn (D2)			1.0mm Zr (D2)		
Time[μs]	**ENDF**	**JEFF**	**JENDL**	**ENDF**	**JEFF**	**JENDL**
78.85	4.02E+02	3.96E+02	3.91E+02	4.45E+01	4.67E+01	4.64E+01
83.32	1.21E+02	1.07E+02	1.16E+02	4.36E+01	4.55E+01	4.54E+01
88.04	1.12E+02	1.08E+02	1.08E+02	4.32E+01	4.47E+01	4.48E+01
93.03	9.34E+01	9.42E+01	9.05E+01	4.22E+01	4.36E+01	4.37E+01
98.3	8.04E+01	8.32E+01	7.79E+01	4.12E+01	4.27E+01	4.28E+01
103.87	7.63E+01	7.97E+01	7.46E+01	3.96E+01	4.07E+01	4.09E+01
109.75	6.82E+01	7.34E+01	6.73E+01	4.17E+01	4.31E+01	4.30E+01
115.97	6.17E+01	6.76E+01	6.13E+01	4.01E+01	4.13E+01	4.12E+01
122.54	6.22E+01	6.84E+01	6.22E+01	4.45E+01	4.58E+01	4.58E+01
129.49	6.12E+01	6.81E+01	6.14E+01	5.20E+01	5.28E+01	5.35E+01
136.82	6.85E+01	7.66E+01	6.92E+01	6.79E+01	6.89E+01	6.87E+01
144.57	8.49E+01	9.20E+01	8.60E+01	8.06E+01	8.15E+01	8.17E+01
152.77	1.19E+02	1.27E+02	1.21E+02	7.53E+01	7.62E+01	7.67E+01
161.42	1.42E+02	1.50E+02	1.45E+02	5.34E+01	5.40E+01	5.42E+01
170.56	1.28E+02	1.35E+02	1.30E+02	4.08E+01	4.15E+01	4.17E+01
180.23	8.89E+01	9.60E+01	9.16E+01	3.35E+01	3.42E+01	3.44E+01
190.44	6.03E+01	6.69E+01	6.25E+01	2.84E+01	2.90E+01	2.92E+01
201.23	5.29E+01	5.99E+01	5.52E+01	2.76E+01	2.83E+01	2.84E+01
212.63	5.04E+01	5.72E+01	5.27E+01	2.65E+01	2.72E+01	2.73E+01
224.68	4.95E+01	5.52E+01	5.20E+01	2.75E+01	2.81E+01	2.83E+01
237.4	5.08E+01	5.74E+01	5.33E+01	3.07E+01	3.13E+01	3.15E+01
250.86	5.15E+01	5.81E+01	5.39E+01	3.32E+01	3.39E+01	3.39E+01
265.07	5.16E+01	5.84E+01	5.38E+01	3.34E+01	3.38E+01	3.38E+01
280.09	5.58E+01	6.21E+01	5.79E+01	3.04E+01	3.09E+01	3.11E+01
295.96	6.52E+01	7.21E+01	6.73E+01	2.54E+01	2.60E+01	2.60E+01
312.72	7.61E+01	8.39E+01	7.76E+01	2.16E+01	2.20E+01	2.21E+01
330.44	8.50E+01	9.34E+01	8.70E+01	2.00E+01	2.06E+01	2.07E+01
349.16	8.74E+01	9.50E+01	8.93E+01	2.08E+01	2.14E+01	2.14E+01
368.94	7.24E+01	7.85E+01	7.40E+01	2.04E+01	2.07E+01	2.07E+01
389.85	6.03E+01	6.56E+01	6.15E+01	2.10E+01	2.13E+01	2.13E+01
411.94	4.75E+01	5.18E+01	4.84E+01	1.86E+01	1.88E+01	1.89E+01
435.27	4.01E+01	4.27E+01	4.10E+01	1.71E+01	1.73E+01	1.75E+01
459.94	3.45E+01	3.68E+01	3.54E+01	1.44E+01	1.47E+01	1.47E+01
485.99	3.13E+01	3.31E+01	3.21E+01	1.26E+01	1.28E+01	1.29E+01
513.53	3.03E+01	3.16E+01	3.10E+01	1.17E+01	1.19E+01	1.20E+01
542.62	2.84E+01	2.92E+01	2.90E+01	1.08E+01	1.11E+01	1.11E+01
573.36	2.80E+01	2.87E+01	2.86E+01	1.05E+01	1.07E+01	1.08E+01
605.85	2.59E+01	2.64E+01	2.63E+01	9.73E+00	1.00E+01	1.00E+01
640.17	2.43E+01	2.46E+01	2.47E+01	8.84E+00	9.00E+00	9.04E+00
676.44	2.29E+01	2.33E+01	2.32E+01	8.41E+00	8.59E+00	8.67E+00

Continued on next page

Table E.4 – continued from previous page

	1.0mm Sn (D2)			1.0mm Zr (D2)		
Time[μs]	**ENDF**	**JEFF**	**JENDL**	**ENDF**	**JEFF**	**JENDL**
714.77	2.15E+01	2.17E+01	2.18E+01	7.70E+00	7.91E+00	7.93E+00
755.27	2.06E+01	2.09E+01	2.10E+01	7.26E+00	7.47E+00	7.52E+00
798.06	1.90E+01	1.90E+01	1.92E+01	6.70E+00	6.88E+00	6.91E+00
843.27	1.71E+01	1.70E+01	1.73E+01	6.11E+00	6.24E+00	6.28E+00
891.05	1.60E+01	1.60E+01	1.62E+01	5.62E+00	5.76E+00	5.78E+00
941.53	1.44E+01	1.43E+01	1.45E+01	5.07E+00	5.18E+00	5.16E+00
994.89	1.32E+01	1.31E+01	1.33E+01	4.62E+00	4.74E+00	4.75E+00
1051.25	1.22E+01	1.20E+01	1.23E+01	4.21E+00	4.29E+00	4.33E+00
1110.8	1.07E+01	1.05E+01	1.08E+01	3.73E+00	3.82E+00	3.83E+00
1173.75	9.48E+00	9.38E+00	9.56E+00	3.34E+00	3.41E+00	3.45E+00
1240.25	9.02E+00	9.01E+00	9.06E+00	3.14E+00	3.20E+00	3.21E+00
1310.55	8.15E+00	7.99E+00	8.21E+00	2.76E+00	2.80E+00	2.81E+00
1384.75	7.39E+00	7.31E+00	7.41E+00	2.55E+00	2.62E+00	2.64E+00
1463.25	6.29E+00	6.13E+00	6.35E+00	2.13E+00	2.16E+00	2.18E+00
1546.1	5.50E+00	5.44E+00	5.53E+00	1.85E+00	1.88E+00	1.90E+00
1633.7	4.84E+00	4.68E+00	4.87E+00	1.66E+00	1.69E+00	1.71E+00
1726.3	4.32E+00	4.30E+00	4.40E+00	1.50E+00	1.53E+00	1.54E+00
1824.05	3.66E+00	3.60E+00	3.76E+00	1.27E+00	1.31E+00	1.31E+00
1927.45	2.85E+00	2.77E+00	2.86E+00	9.68E-01	9.77E-01	9.97E-01
2036.65	2.67E+00	2.57E+00	2.66E+00	9.31E-01	9.39E-01	9.51E-01
2152.05	2.31E+00	2.29E+00	2.29E+00	8.21E-01	8.27E-01	8.16E-01
2273.95	2.02E+00	2.00E+00	1.98E+00	6.93E-01	7.04E-01	7.05E-01
2402.8	1.46E+00	1.43E+00	1.50E+00	5.12E-01	5.33E-01	5.27E-01
2538.9	1.07E+00	1.05E+00	1.06E+00	3.72E-01	3.84E-01	3.91E-01
2682.75	1.00E+00	9.43E-01	1.00E+00	3.43E-01	3.50E-01	3.53E-01
2834.75	6.85E-01	6.87E-01	6.81E-01	2.43E-01	2.46E-01	2.49E-01
2995.35	4.83E-01	4.68E-01	4.99E-01	1.67E-01	1.73E-01	1.83E-01
3165.1	5.35E-01	4.97E-01	5.10E-01	1.76E-01	1.76E-01	1.76E-01
3344.4	4.28E-01	4.27E-01	4.23E-01	1.58E-01	1.61E-01	1.63E-01
3533.85	3.34E-01	3.28E-01	3.40E-01	1.10E-01	1.19E-01	1.17E-01
3734.05	4.30E-01	4.24E-01	4.33E-01	9.61E-02	9.90E-02	9.91E-02
3945.65	1.41E-01	1.32E-01	1.42E-01	4.74E-02	4.91E-02	4.80E-02

Table E.5: Simulation Results: Fe, Co.

	1.0mm Fe (D2)			0.6mm Co (D1)		
Time[μs]	**ENDF**	**JEFF**	**JENDL**	**ENDF**	**JEFF**	**JENDL**
1.01	2.99E+04	2.85E+04	2.94E+04	6.50E+04	6.49E+04	7.01E+04
1.07	3.53E+04	3.37E+04	3.43E+04	6.72E+04	6.72E+04	7.29E+04
1.13	2.91E+04	3.01E+04	3.03E+04	6.48E+04	6.48E+04	7.34E+04

Continued on next page

Table E.5 – continued from previous page

	1.0mm Fe (D2)			0.6mm Co (D1)		
Time[μs]	**ENDF**	**JEFF**	**JENDL**	**ENDF**	**JEFF**	**JENDL**
1.2	3.00E+04	2.87E+04	2.95E+04	6.53E+04	6.53E+04	7.25E+04
1.26	2.88E+04	2.86E+04	2.95E+04	6.22E+04	6.21E+04	7.35E+04
1.34	2.91E+04	2.91E+04	2.94E+04	6.06E+04	6.06E+04	6.88E+04
1.41	3.10E+04	3.14E+04	3.07E+04	6.10E+04	6.09E+04	7.21E+04
1.49	2.52E+04	2.52E+04	2.68E+04	5.91E+04	5.91E+04	6.81E+04
1.58	2.52E+04	2.60E+04	2.72E+04	5.99E+04	5.99E+04	6.98E+04
1.67	2.28E+04	2.35E+04	2.39E+04	6.23E+04	6.23E+04	7.30E+04
1.76	2.42E+04	2.35E+04	2.42E+04	5.81E+04	5.80E+04	6.97E+04
1.86	2.07E+04	2.13E+04	2.21E+04	6.16E+04	6.15E+04	7.21E+04
1.96	2.12E+04	2.10E+04	2.12E+04	5.87E+04	5.86E+04	7.22E+04
2.08	2.01E+04	2.16E+04	2.17E+04	6.17E+04	6.17E+04	7.29E+04
2.19	1.68E+04	1.75E+04	1.74E+04	5.96E+04	5.95E+04	7.27E+04
2.32	1.51E+04	1.55E+04	1.54E+04	6.36E+04	6.36E+04	7.30E+04
2.45	1.48E+04	1.59E+04	1.52E+04	5.83E+04	5.83E+04	7.03E+04
2.59	1.07E+04	1.12E+04	1.11E+04	6.28E+04	6.28E+04	7.79E+04
2.73	9.35E+03	9.04E+03	9.17E+03	6.07E+04	6.07E+04	6.77E+04
2.89	7.67E+03	7.31E+03	7.31E+03	6.28E+04	6.28E+04	7.01E+04
3.05	7.18E+03	6.82E+03	6.77E+03	6.88E+04	6.88E+04	7.58E+04
3.23	7.45E+03	6.80E+03	6.64E+03	6.01E+04	6.00E+04	7.07E+04
3.41	8.23E+03	7.62E+03	7.58E+03	6.50E+04	6.50E+04	7.52E+04
3.6	8.65E+03	8.03E+03	8.09E+03	6.50E+04	6.50E+04	7.55E+04
3.81	9.35E+03	9.11E+03	9.22E+03	7.65E+04	7.65E+04	7.81E+04
4.02	9.97E+03	9.58E+03	9.63E+03	7.74E+04	7.74E+04	7.78E+04
4.25	1.04E+04	9.98E+03	9.99E+03	7.59E+04	7.59E+04	8.29E+04
4.49	9.86E+03	9.05E+03	9.14E+03	7.91E+04	7.91E+04	8.68E+04
4.74	8.36E+03	8.13E+03	8.15E+03	9.29E+04	9.29E+04	9.97E+04
5.01	7.31E+03	6.94E+03	6.96E+03	1.09E+05	1.09E+05	1.17E+05
5.3	7.94E+03	5.54E+03	5.56E+03	1.16E+05	1.16E+05	1.28E+05
5.6	5.12E+03	4.39E+03	4.40E+03	1.27E+05	1.27E+05	1.32E+05
5.91	3.22E+03	2.95E+03	2.96E+03	1.19E+05	1.19E+05	1.22E+05
6.25	3.95E+03	3.44E+03	3.45E+03	9.68E+04	9.68E+04	9.81E+04
6.6	3.22E+03	3.01E+03	3.00E+03	7.23E+04	7.23E+04	7.06E+04
6.98	3.14E+03	2.68E+03	2.70E+03	4.90E+04	4.90E+04	5.15E+04
7.37	2.07E+03	2.07E+03	2.08E+03	3.61E+04	3.61E+04	3.84E+04
7.79	2.42E+03	2.71E+03	2.72E+03	3.71E+04	3.71E+04	3.97E+04
8.23	2.71E+03	3.33E+03	3.36E+03	3.00E+04	3.00E+04	3.38E+04
8.7	4.84E+03	4.09E+03	4.10E+03	2.06E+04	2.06E+04	2.30E+04
9.19	4.97E+03	4.90E+03	4.91E+03	1.90E+04	1.90E+04	1.90E+04
9.71	7.26E+03	8.47E+03	8.48E+03	1.47E+04	1.47E+04	1.55E+04
10.26	1.35E+04	1.39E+04	1.39E+04	1.42E+04	1.42E+04	1.48E+04

Continued on next page

Table E.5 – continued from previous page

	1.0mm Fe (D2)			0.6mm Co (D1)		
Time[μs]	**ENDF**	**JEFF**	**JENDL**	**ENDF**	**JEFF**	**JENDL**
10.84	2.53E+04	2.62E+04	2.62E+04	1.83E+04	1.83E+04	1.96E+04
11.46	4.19E+04	3.83E+04	3.84E+04	1.76E+04	1.76E+04	1.87E+04
12.11	3.42E+04	3.37E+04	3.37E+04	1.36E+04	1.36E+04	1.42E+04
12.79	2.73E+04	2.72E+04	2.72E+04	1.64E+04	1.64E+04	1.69E+04
13.52	8.23E+03	8.92E+03	8.93E+03	2.05E+04	2.05E+04	1.98E+04
14.28	4.32E+03	3.53E+03	3.54E+03	1.82E+04	1.82E+04	2.01E+04
15.09	1.29E+03	1.50E+03	1.51E+03	1.91E+04	1.91E+04	1.92E+04
15.95	1.24E+03	1.30E+03	1.31E+03	2.30E+04	2.30E+04	2.25E+04
16.85	1.21E+03	1.21E+03	1.22E+03	2.88E+04	2.88E+04	2.80E+04
17.81	1.33E+03	1.29E+03	1.30E+03	2.84E+04	2.84E+04	3.03E+04
18.82	1.35E+03	1.32E+03	1.34E+03	3.78E+04	3.78E+04	3.77E+04
19.88	1.46E+03	1.39E+03	1.43E+03	4.00E+04	4.00E+04	3.99E+04
21.01	1.52E+03	1.42E+03	1.48E+03	4.67E+04	4.67E+04	4.82E+04
22.2	1.47E+03	1.39E+03	1.43E+03	5.10E+04	5.10E+04	5.06E+04
23.46	1.33E+03	1.29E+03	1.32E+03	6.60E+04	6.60E+04	6.76E+04
24.79	1.28E+03	1.27E+03	1.27E+03	8.38E+04	8.38E+04	8.30E+04
26.19	1.23E+03	1.24E+03	1.23E+03	1.09E+05	1.09E+05	1.09E+05
27.67	1.22E+03	1.23E+03	1.22E+03	1.67E+05	1.67E+05	1.67E+05
29.24	1.19E+03	1.20E+03	1.19E+03	2.74E+05	2.75E+05	2.74E+05
30.9	1.16E+03	1.17E+03	1.17E+03	4.84E+05	4.84E+05	4.81E+05
32.65	1.17E+03	1.17E+03	1.18E+03	6.94E+05	6.94E+05	6.91E+05
34.5	1.14E+03	1.14E+03	1.14E+03	7.39E+05	7.39E+05	7.47E+05
36.45	1.13E+03	1.13E+03	1.13E+03	6.08E+05	6.08E+05	6.03E+05
38.52	1.08E+03	1.09E+03	1.09E+03	4.10E+05	4.10E+05	4.14E+05
40.7	1.05E+03	1.06E+03	1.06E+03	2.39E+05	2.39E+05	2.34E+05
43.01	1.04E+03	1.04E+03	1.05E+03	1.37E+05	1.37E+05	1.37E+05
45.44	1.02E+03	1.02E+03	1.03E+03	8.89E+04	8.89E+04	8.91E+04
48.02	9.94E+02	9.97E+02	9.98E+02	6.36E+04	6.36E+04	6.32E+04
50.74	9.61E+02	9.63E+02	9.64E+02	5.07E+04	5.07E+04	5.07E+04
53.61	9.46E+02	9.47E+02	9.48E+02	4.10E+04	4.10E+04	4.06E+04
56.65	9.40E+02	9.42E+02	9.45E+02	3.47E+04	3.47E+04	3.45E+04
59.86	9.39E+02	9.40E+02	9.42E+02	2.93E+04	2.93E+04	2.92E+04
63.25	8.87E+02	8.89E+02	8.91E+02	2.63E+04	2.63E+04	2.66E+04
66.84	8.72E+02	8.74E+02	8.74E+02	2.36E+04	2.36E+04	2.36E+04
70.62	8.38E+02	8.38E+02	8.40E+02	2.08E+04	2.08E+04	2.10E+04
74.62	8.24E+02	8.25E+02	8.28E+02	1.96E+04	1.96E+04	1.96E+04
78.85	8.08E+02	8.09E+02	8.10E+02	1.79E+04	1.79E+04	1.81E+04
83.32	7.68E+02	7.69E+02	7.70E+02	1.72E+04	1.72E+04	1.69E+04
88.04	7.49E+02	7.49E+02	7.51E+02	1.56E+04	1.56E+04	1.55E+04
93.03	7.33E+02	7.33E+02	7.34E+02	1.48E+04	1.48E+04	1.48E+04

Continued on next page

Table E.5 – continued from previous page

	1.0mm Fe (D2)			0.6mm Co (D1)		
Time[μs]	**ENDF**	**JEFF**	**JENDL**	**ENDF**	**JEFF**	**JENDL**
98.3	7.26E+02	7.26E+02	7.28E+02	1.44E+04	1.44E+04	1.41E+04
103.87	6.91E+02	6.91E+02	6.92E+02	1.37E+04	1.37E+04	1.36E+04
109.75	6.76E+02	6.77E+02	6.78E+02	1.28E+04	1.28E+04	1.29E+04
115.97	6.47E+02	6.47E+02	6.48E+02	1.20E+04	1.20E+04	1.20E+04
122.54	6.49E+02	6.50E+02	6.51E+02	1.13E+04	1.13E+04	1.14E+04
129.49	6.23E+02	6.24E+02	6.23E+02	1.09E+04	1.09E+04	1.09E+04
136.82	6.17E+02	6.16E+02	6.18E+02	1.05E+04	1.05E+04	1.05E+04
144.57	5.75E+02	5.75E+02	5.76E+02	1.00E+04	1.00E+04	1.00E+04
152.77	5.69E+02	5.68E+02	5.70E+02	9.92E+03	9.92E+03	9.81E+03
161.42	5.39E+02	5.39E+02	5.39E+02	9.38E+03	9.38E+03	9.21E+03
170.56	5.24E+02	5.23E+02	5.25E+02	8.80E+03	8.80E+03	8.88E+03
180.23	5.03E+02	5.04E+02	5.05E+02	8.43E+03	8.43E+03	8.37E+03
190.44	4.73E+02	4.73E+02	4.74E+02	8.25E+03	8.25E+03	8.12E+03
201.23	4.69E+02	4.69E+02	4.69E+02	7.81E+03	7.81E+03	7.76E+03
212.63	4.59E+02	4.60E+02	4.60E+02	7.44E+03	7.44E+03	7.31E+03
224.68	4.21E+02	4.19E+02	4.20E+02	7.14E+03	7.14E+03	7.05E+03
237.4	4.21E+02	4.20E+02	4.21E+02	6.83E+03	6.83E+03	6.81E+03
250.86	3.96E+02	3.96E+02	3.96E+02	6.37E+03	6.37E+03	6.34E+03
265.07	3.71E+02	3.71E+02	3.71E+02	6.02E+03	6.02E+03	6.05E+03
280.09	3.72E+02	3.71E+02	3.72E+02	6.04E+03	6.04E+03	5.92E+03
295.96	3.49E+02	3.49E+02	3.50E+02	5.67E+03	5.67E+03	5.62E+03
312.72	3.40E+02	3.40E+02	3.41E+02	5.47E+03	5.47E+03	5.46E+03
330.44	3.23E+02	3.23E+02	3.24E+02	5.16E+03	5.16E+03	5.09E+03
349.16	3.21E+02	3.20E+02	3.21E+02	4.61E+03	4.61E+03	4.69E+03
368.94	2.86E+02	2.87E+02	2.86E+02	4.50E+03	4.50E+03	4.52E+03
389.85	2.83E+02	2.83E+02	2.83E+02	4.38E+03	4.38E+03	4.35E+03
411.94	2.60E+02	2.60E+02	2.60E+02	4.16E+03	4.16E+03	4.14E+03
435.27	2.63E+02	2.63E+02	2.63E+02	3.83E+03	3.83E+03	3.87E+03
459.94	2.33E+02	2.32E+02	2.33E+02	3.63E+03	3.63E+03	3.64E+03
485.99	2.18E+02	2.18E+02	2.18E+02	3.34E+03	3.34E+03	3.40E+03
513.53	2.06E+02	2.06E+02	2.06E+02	3.27E+03	3.27E+03	3.15E+03
542.62	2.07E+02	2.08E+02	2.07E+02	2.98E+03	2.98E+03	3.01E+03
573.36	1.93E+02	1.93E+02	1.93E+02	2.80E+03	2.80E+03	2.78E+03
605.85	1.79E+02	1.79E+02	1.80E+02	2.74E+03	2.74E+03	2.77E+03
640.17	1.64E+02	1.63E+02	1.64E+02	2.40E+03	2.40E+03	2.33E+03
676.44	1.59E+02	1.59E+02	1.59E+02	2.40E+03	2.40E+03	2.42E+03
714.77	1.43E+02	1.43E+02	1.44E+02	2.10E+03	2.10E+03	2.06E+03
755.27	1.33E+02	1.32E+02	1.33E+02	2.02E+03	2.02E+03	2.01E+03
798.06	1.29E+02	1.29E+02	1.29E+02	1.79E+03	1.79E+03	1.80E+03
843.27	1.15E+02	1.15E+02	1.15E+02	1.79E+03	1.79E+03	1.79E+03

Continued on next page

Table E.5 – continued from previous page

	1.0mm Fe (D2)			0.6mm Co (D1)		
Time[μs]	**ENDF**	**JEFF**	**JENDL**	**ENDF**	**JEFF**	**JENDL**
891.05	1.05E+02	1.05E+02	1.05E+02	1.54E+03	1.54E+03	1.51E+03
941.53	9.67E+01	9.61E+01	9.66E+01	1.42E+03	1.42E+03	1.43E+03
994.89	8.69E+01	8.70E+01	8.71E+01	1.21E+03	1.21E+03	1.22E+03
1051.25	7.73E+01	7.73E+01	7.74E+01	1.18E+03	1.18E+03	1.18E+03
1110.8	7.14E+01	7.13E+01	7.16E+01	1.04E+03	1.04E+03	1.03E+03
1173.75	6.29E+01	6.29E+01	6.31E+01	9.45E+02	9.45E+02	9.24E+02
1240.25	5.60E+01	5.58E+01	5.62E+01	8.41E+02	8.41E+02	8.24E+02
1310.55	5.36E+01	5.37E+01	5.38E+01	7.26E+02	7.26E+02	7.36E+02
1384.75	4.52E+01	4.52E+01	4.52E+01	6.07E+02	6.07E+02	6.06E+02
1463.25	4.18E+01	4.14E+01	4.15E+01	5.64E+02	5.64E+02	5.52E+02
1546.1	3.38E+01	3.37E+01	3.35E+01	4.81E+02	4.81E+02	4.82E+02
1633.7	2.86E+01	2.85E+01	2.85E+01	3.83E+02	3.83E+02	3.74E+02
1726.3	2.68E+01	2.67E+01	2.68E+01	3.72E+02	3.72E+02	3.53E+02
1824.05	2.39E+01	2.38E+01	2.40E+01	2.90E+02	2.90E+02	2.75E+02
1927.45	1.71E+01	1.70E+01	1.71E+01	2.46E+02	2.46E+02	2.37E+02
2036.65	1.80E+01	1.80E+01	1.81E+01	2.36E+02	2.36E+02	2.33E+02
2152.05	1.40E+01	1.40E+01	1.40E+01	1.76E+02	1.76E+02	1.78E+02
2273.95	1.23E+01	1.23E+01	1.23E+01	1.52E+02	1.52E+02	1.51E+02
2402.8	8.90E+00	8.89E+00	8.91E+00	1.34E+02	1.34E+02	1.33E+02
2538.9	6.23E+00	6.23E+00	6.25E+00	9.70E+01	9.70E+01	9.13E+01
2682.75	6.81E+00	6.81E+00	6.82E+00	7.30E+01	7.30E+01	7.94E+01
2834.75	4.21E+00	4.20E+00	4.21E+00	7.06E+01	7.06E+01	6.96E+01
2995.35	3.12E+00	3.12E+00	3.12E+00	5.85E+01	5.85E+01	5.87E+01
3165.1	3.40E+00	3.40E+00	3.40E+00	3.06E+01	3.06E+01	3.12E+01
3344.4	2.62E+00	2.62E+00	2.62E+00	4.15E+01	4.15E+01	3.81E+01
3533.85	2.29E+00	2.29E+00	2.29E+00	2.32E+01	2.32E+01	2.24E+01
3734.05	1.15E+00	1.15E+00	1.15E+00	1.37E+01	1.37E+01	1.39E+01
3945.65	8.85E-01	8.84E-01	8.86E-01	2.86E+01	2.86E+01	2.57E+01

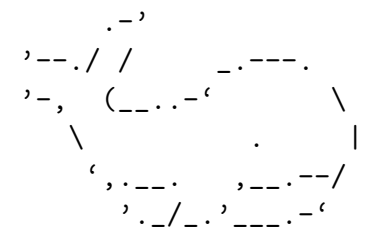

Figure E.1: Photograph of N. Thompson and A. Weltz setting up a measurement with the RPI LSDS.